1-1-1990

Structure, deformation behavior and properties in polyundecanamide (nylon 11) and high density polyethylene (HDPE) subjected to planar (equibiaxial) deformation by forging/

Jean-Philippe Autran
University of Massachusetts Amherst

STRUCTURE, DEFORMATION BEHAVIOR AND PROPERTIES IN POLYUNDECANAMIDE (NYLON 11) AND HIGH DENSITY POLYETHYLENE (HDPE) SUBJECTED TO PLANAR (EQUIBIAXIAL) DEFORMATION BY FORGING

A Dissertation Presented

by

JEAN-PHILIPPE AUTRAN

Submitted to the Graduate School of the
University of Massachusetts in partial fulfillment
of the requirements for the degree of

DOCTOR OF PHILOSOPHY

May 1990

Polymer Science and Engineering

STRUCTURE, DEFORMATION BEHAVIOR AND PROPERTIES IN POLYUNDECANAMIDE (NYLON 11) AND HIGH DENSITY POLYETHYLENE (HDPE) SUBJECTED TO PLANAR (EQUIBIAXIAL) DEFORMATION BY FORGING

A Dissertation Presented

by

JEAN-PHILIPPE AUTRAN

Approved in style and content by:

Roger S. Porter, Chairman

Richard J. Farris, Member

Edwin L. Thomas, Member

William J. MacKnight, Department Head
Polymer Science and Engineering

Dedicated

To the memory of my father, Jean Autran,
to my family for its patience and encouragement from overseas,
and to my wife Susan for her great love and spirit.

ACKNOWLEDGEMENTS

I would like to thank my advisor, Prof. Roger S. Porter, for his support and guidance throughout the course of my graduate studies and research and for inviting me to present my work at several meetings. Thanks also go to my committee members, Prof. Farris and Thomas, for their interest and assistance in the completion of this work.

Graduate studies require high personal dedication and commitment, as they represent a personal achievement. I feel however personally in debt of the friendly and supportive environment provided by many of my classmates, my research group and others, which has been very precious at times. Without ignoring others, I wish to extent special thanks to a few of my friends:

To the French "gang: Francois, Herve, Dom, Marc ..et les autres.." for bringing over the language and values which I grew up with.

To the american crew: Joe, Mike, Jerry, Kevin, Scott, Greg for their restless help and frienship.

To all the others: Olimpia, Sergio, Saroj, Shere, Osamu, Mrs Guan for giving another dimension to this experience.

To my dear friend Ravi, for introducing me to the delights of research and for providing constant encouragement in the project.

And finally to my beloved wife, Susan, who accompanied me through this work with her encouragements and made every day so special.

ABSTRACT

STRUCTURE ,DEFORMATION BEHAVIOR AND PROPERTIES IN POLYUNDECANAMIDE (NYLON 11) AND HIGH DENSITY POLYETHYLENE (HDPE) SUBJECTED TO PLANAR (EQUIBIAXIAL) DEFORMATION BY FORGING

MAY 1990

JEAN-PHILIPPE AUTRAN, B.S., E.N.S.C. PARIS

Ph.D., UNIVERSITY OF MASSACHUSETTS

Directed by: Professor Roger S. Porter

Cross-laminates composed of unidirectionally-reinforced composites are usually used to prepare polymeric materials with enhanced properties in a plane. In the present investigation, solid-state forging is considered as an alternate method to increase planar properties in semicrystalline flexible chain polymers by imparting equibiaxial orientation and extension of molecules in the deformation plane. Polyundecanamide (nylon 11) and High Density Polyethylene (HDPE) are chosen in this study to illustrate several aspects of forging on Polyamides and Polyolefins. They represent two families of polymers with already a large impact in the fiber technology.

First, novel aspects of the nature and origin of polymorphism in melt crystallized nylon 11 observed both prior and after forging are presented. Two distinct crystalline species (semidisordered smectic δ′-form and 3-dimensional crystal α-form) have been identified. Their respective content is highly dependent upon thermal history. The

smectic δ′-form is kinetically favored but does progressively transform into the thermodynamically preferred crystal form on heat treatment. Thermal analysis provides data on the thermodynamics and kinetics of melting and crystallization for each form. Also, new enthalpic measurements were obtained which correspond to the change of symmetry in the crystalline phase from the low-temperature α-form to the high-temperature δ-form. It exhibits a characteristic broad transition typical of crystal-condis crystal transition(introduced by Wunderlich). Differences in the mode of hydrogen-bonding are given as an explanation of polymorphism.

Both nylon 11 and HDPE exhibit alternate behaviors when forged to their maximum compression ratios over temperature ranges above and below about 100°C. Modifying the forging rate slightly shifts this temperature. For nylon 11, low temperature deformation favors the formation and/or stability of the smectic which is found to significantly inhibit large deformation without mechanical failure. Optimal forging conditions however are found over the high temperature range where the crystal forms (α- and δ-forms) are stable during the process. Accordingly, the in-plane modulus increases by an amount comparable to the one predicted by the composites theory. Inversely, for HDPE, optimal forging conditions are found at low temperatures where the stress-induced orthorhombic to monoclinic transformation is observed. Results are analysed in terms of differences in slip (or shear) mechanisms at the molecular scale with forging conditions.

TABLE OF CONTENTS

LIST OF TABLES

LIST OF FIGURES

C H A P T E R I

INTRODUCTION, BACKGROUND AND EXPERIMENTAL

1) Preamble.

It is well established that the structure and morphology of flexible chain polymers can be drastically altered by solid state processing. Since molecular relaxations are considerably hindered in the solid state, the material maintains much of its deformation-induced state. The state of anisotropy achieved by the molecular orientation and extension caused by any deformational field (in both crystalline and amorphous phases) usually impart significant differences in polymer properties with direction. Solid state deformation therefore offers an alternate means (to the preparation of composites, for example) for modifying the specific properties of a given polymer (in any given direction(s)).

Of a major concern for commercial applications, mechanical properties (modulus, impact, strength) of deformed semicrystalline polymers are strong functions of crystal orientation and chain extension. This has been largely demonstrated experimentally for many semicrystalline polymers in the particular case of uniaxial draw.

Several structural models[1-8] have been proposed to rationalize the remarkable enhancement in uniaxial mechanical properties and to describe the structure-properties relationships for flexible chain semicrystalline polymers drawn under various conditions. Despite some discrepancy in the terminology adopted by many authors, they all agree on the formation of structural elements of high aspect ratio with high molecular orientation and extension. These can be basically described as elongated crystallites tightly connected longitudinally in the direction of deformation. They exhibit high modulus and high strength because of the "alignment" of covalent bonds in "pseudo-continuous" crystals. It is also for this reason that uniaxially drawn flexible chain thermoplastics are often referred to as self-reinforced composites. State-of-the-art drawing processes, including crystallization/fiber spinning from dilute solutions[9] and from gels[10] and hydrostatic coextrusion of single crystal mats[11] or sintered native powders[12] have successfully been developped to prepare highly oriented polyethylene fibers for example. The tensile moduli experimentally measured could compare with theoretical predictions for perfectly extended continuous crystals in the chain direction[13]. On the other hand, such fibers exhibit poor lateral strength as they easily peel apart under lateral constraint. Molecular weight has been proved as a crucial factor: high molecular weight increases lateral cohesion (interfibrillar bridges) but impedes high draw (presence of entanglements); Low molecular weight however results in ease of creep because of lack of intercrystalline bridges.

These facts underscore some of the reasons why both scientific and commercial interests have motivated the research in the area of polymer deformation over the past decades. On a general basis, research objectives have centered around two poles:

i) A characterization of structural and morphological changes at all levels associated with molecular orientation. Such information is useful to understand the molecular mechanisms which control the deformation. Again, the current status of knowledge mainly comes from uniaxial deformation studies. Examples of uniaxial deformation processes are collected in Table 1.1[14]. Although the strain field varies with process, the following mechanisms are usually recognized as part of the general procedure for deforming bulk-crystallized semicrystalline polymers and illustrated in figure 1.1:

1) Initial breaking of spherulites by stack rotation, sliding of lamellae (interlamellar slip), possible phase changes and twinning of crystal lattice and significant orientation and extension of molecules in the compliant amorphous phase.

2) Further orientation and transformation of the crystallites by intralamellar slip into chain folded mosaic blocks, which reorganize into microfibrils.

3) Final plastic deformation of crystals within the fibrils by slip mechanisms to yield the ultimate orientational and extensional state for the molecules.

As noted above, all stages of the deformation process contributes to the orientation (and extension) of flexible molecular chains in the

Table 1.1 Characteristics and properties of the most common uniaxial processes. (After Shankernarayanan et al.)

	Tensile drawing [15]	Ram [16] or hydrostatic extrusion [17]	Die drawing [18]	Rolling [19]	Rolltrusion [20] and roller drawing [21]
Process mode	batch	batch	batch/ continuous	batch/ continuous	batch/ continous
Product form	thin films	films, fibers, etc.	rods, sheets tubes, fibers, etc.	rods, sheets, tapes, etc.	rods, sheets, tapes, etc.
Product dimension					
(1) length	limited	limited	unlimited	unlimited	unlimited
(2) width	narrow	limited by die shape	limited by die shape	limited by roller dimensions	limited by roller length
(3) thickness	thin	limited by die shape	limited by die shape	thin or thick adjustable	thin or thick (adjustable)
Applied load	uniaxial tension	multi-axial stresses with shear stress	multi-axial stresses with shear stress	multi-axial stresses with shear stress	multi-axial stresses with shear stress
Product morphology	uniaxial orientation	uniaxial orientation	uniaxial orientation	biaxial orientation	double orientation

Figure 1.1. Sequential stages in the drawing process for a flexible semicrystalline polymer.

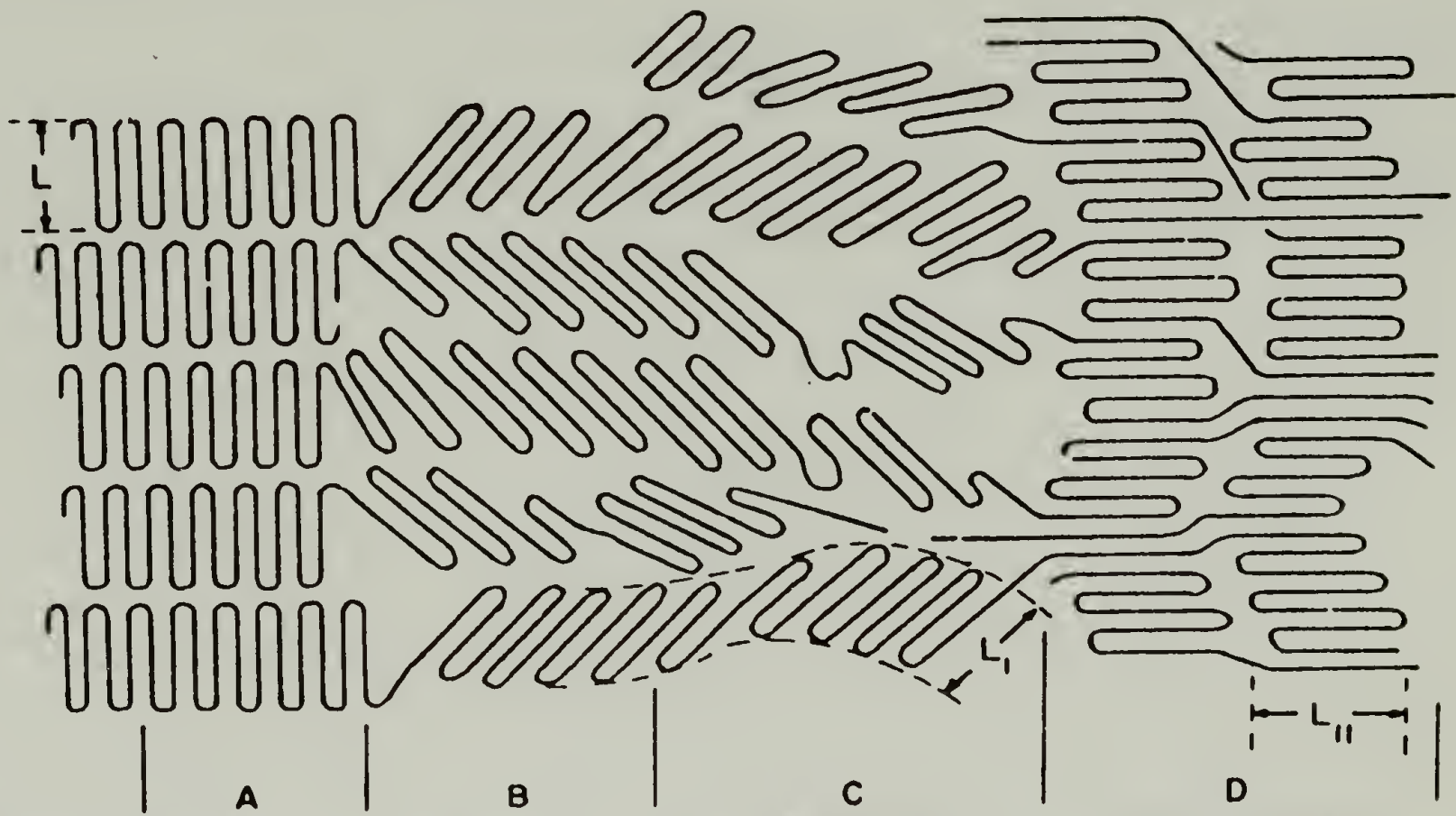

Increasing Deformation of Single Crystals

direction of stretching. Obviously, the extent of each process largely depends upon the polymer and deformation process chosen as well as the conditions of deformation (temperature, rate, initial morphology and deformation extent). In any case, slip mechanisms in the crystalline phase must play a major role in determining the behavior of the polymer at all stages of the deformation and hence have received considerable attention in the past.

ii) Evaluate the changes in physical properties of the deformed specimens and possibly correlate them with the structural aspects of the deformation. Mechanical properties (tensile strength, modulus, impact resistance and creep compliance), optical properties (transparency and haze), thermal properties (expansion, shrinkage or conductivity) or permeation to gazes or low molecular weight compounds are some of the most important properties which are significantly dependent upon molecular orientation[22,23]. Therefore, a thorough understanding of the process-structure-properties relationship is essential to help predict enhanced properties via deformation for new applications.

2)Motive for Biaxial Deformation.

As stated, earlier work has concentrated on uniaxial processes due mainly to their importance in the fiber manufacturing industry. These processes consist in a macroscopic increase of specimens size into one single direction referred to as the Machine Direction (MD), at the

expense of the two others. Concommitantly, chains tend to orient towards the Machine Direction (in both crystalline and amorphous phases) to accomodate the stress and the morphology changes from spherulitic to fibrillar. All phenomenologically possible modes of orientation for the crystalline phase have been reviewed earlier and classified with a uniform terminology by Heffelfinger and Burton[24] ,and are recalled in Table 1.2. According to the table, the last three types of orientation (axial, plan-axial, uniplanar-axial) were the only ones typically found for uniaxial deformation since they define the orientation of the crystals in reference to one unique axis (M) (the Machine Direction).

More recent investigators, however, have extended deformation studies to biaxial processes. This is essentially because structural elements are rarely required to carry simple uniaxial loads. Thus, fiberlike materials are often unacceptable for most engineering purpcses. Biaxial processes consist of increasing specimens dimensions in two directions (the Machine direction and the Transverse direction) defining the deformation plane, at the expense of the third direction (perpendicular to the deformation plane). Such biaxial deformation processes are relatively common in commercial applications (such as tubular extrusion[25], tentering[26], blow molding[27] or mandrel processes[28]) although most of them have been applied to melt processing instead of in the solid state. The idea beyond these processes is to induce preferred molecular orientation in a plane rather than in one direction. Morphological implications of such a molecular orientation are not

Table 1.2 Classification of possible orientation modes for crystals in deformed semicrystalline polymers (after Heffelfinger and Burton)

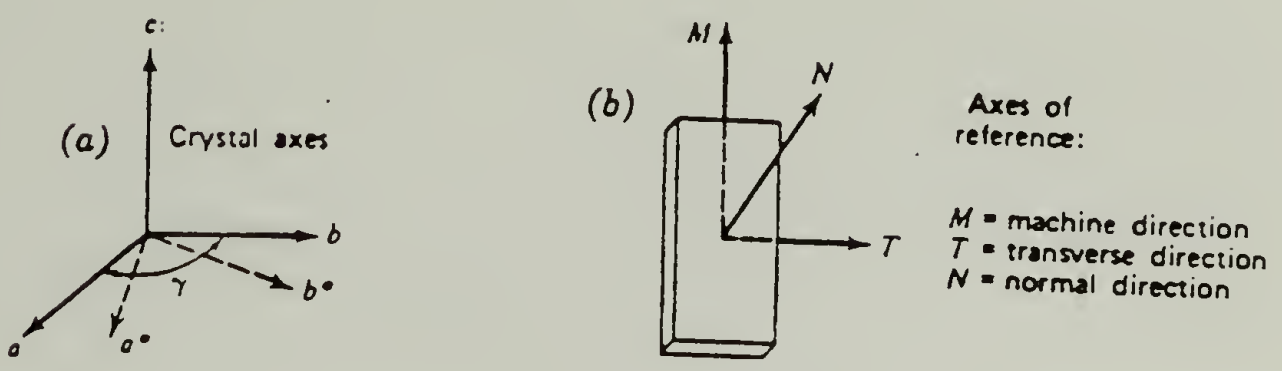

	ORIENTATION MODE		GEOMETRY			
	Heffelfinger – Burton	Sisson	Preferred Orientation	Crystal Operator Element	Reference Element	
1	Random	Random	None	None	None	
2	Planar	Uniplanar	A crystal axis *(c)* lying in a reference plane *(MT)*	Axis *c*	Plane *MT*	BIAXIAL
3	Uniplanar		A crystal plane (010) parallel to a reference plane *(MT)*	Plane (010)	Plane *MT*	BIAXIAL
4	Axial	Uniaxial	A crystal axis *(c)* parallel to a reference axis *(M)*	Axis *c*	Axis *M*	UNIAXIAL
5	Plan – axial		A crystal plane (010) parallel to a reference axis *(M)*	Plane (010)	Axis *M*	UNIAXIAL
6	Uniplanar-axial	Selective uniaxial	A given crystal axis *(c)* parallel to a reference axis *(M)* and a given plane (010) parallel to a reference plane *(MT)*	Axis *c* Plane (010)	Axis *M* Plane *MT*	UNIAXIAL

straightforward however as no simple equivalent of the fibrillar structure found in uniaxial orientation can be thought of in the case of biaxial. Nevertheless, enhancement of mechanical properties in the directions of orientation, i.e. in the plane, are then expected to reflect the state of biaxial orientation. By referring to the textures of Table 1.2, it appears that crystals can possibly adopt two different types of orientation in biaxial fields:

1) In the first case, the chain axis ($\underset{\sim}{c}$-axis) is the only crystal axis which orients in the directions of deformation during the process. This texture corresponds to the alignement of one crystal axis (c-axis) in the reference plane (MT) (plane of deformation) and thus has been called the "Planar" texture.

2) In the second case, another crystal axis also preferentially orients in the reference plane (MT) during the deformation (in addition to the $\underset{\sim}{c}$-axis). In this case, the crystallographic plane defined by these two axes align parallel to the deformation plane, which yields the so-called "Uniplanar" texture.

Prior investigations have demonstrated how Wide Angle X-Ray Diffraction Techniques can easily differentiate between these two types of crystal texture[29]. If the consider the orientation of a crystal by any of the reciprocal vectors $\underset{\sim}{R}(hkl)$ which correspond to reflections observable by X-ray, it can be easily defined by two angles (Euler angles) with respect to the reference frame (where X and Y correspond to the directions of deformation) (figure 1.2). In the particular case of equibiaxial orientation, only the angle ϕ is required as the crystal

Figure 1.2. Definition of crystal orientation with respect to the reference frame in biaxial orientation.

Crystal Orientation on Equibiaxial Deformation Field

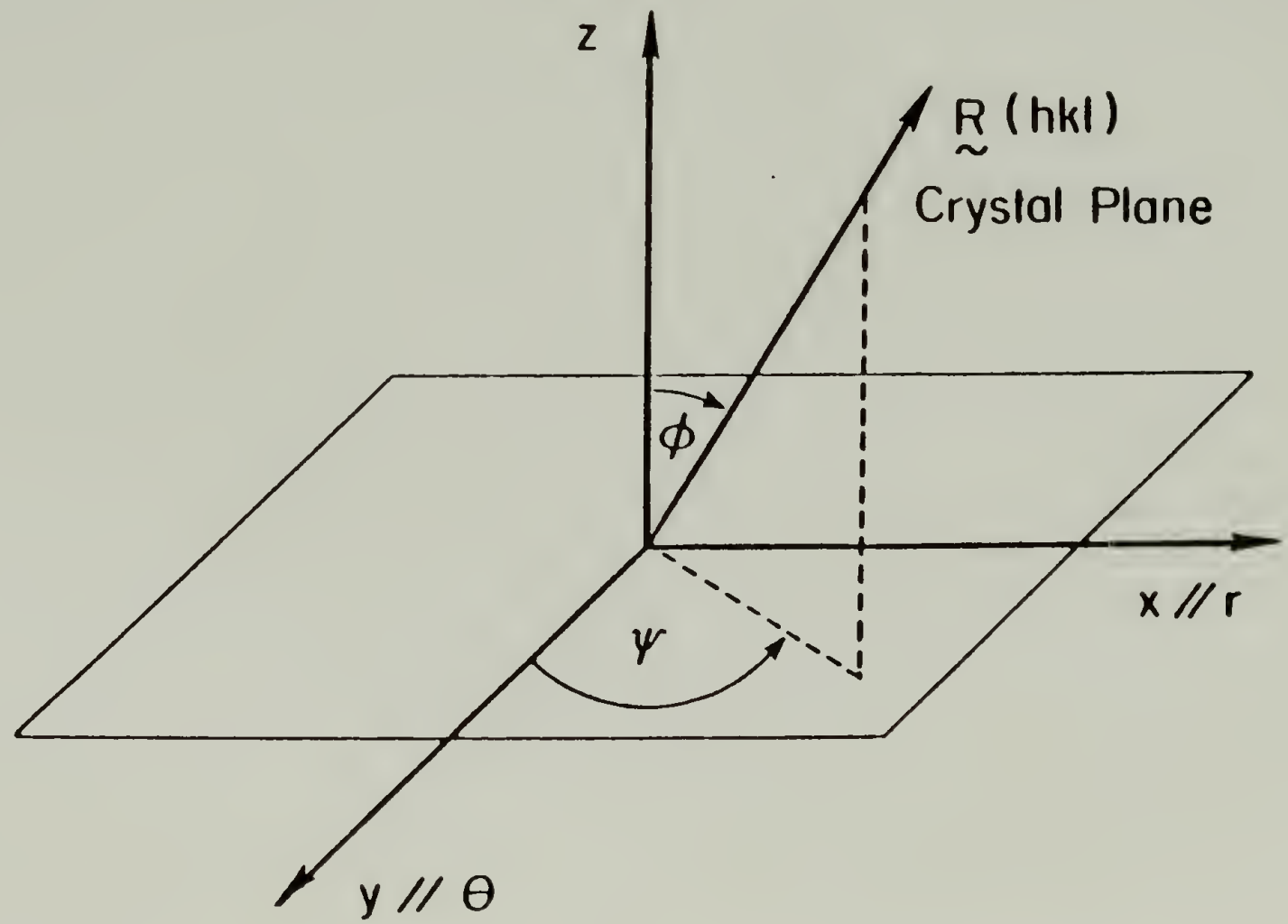

orientation becomes independent of ψ. It is possible to determine the azimuthal position for the intensity maxima (as a function of ϕ) for each reflection and for each of the above textures (Appendix A). A schematic example of the expected maximum Pole Density for $\underset{\sim}{R}(hkl)$ is given in Figure 1.3. The "Uniplanar" texture has also been referred to as the "Fiber" texture in the case of equibiaxial orientation[29].

It will be argued later how the ability of a semicrystalline polymer to biaxially deform may be connected to the type of texture which develops in the crystalline phase during the process. But first, the next sections are intended to present a general review of prior biaxial orientation studies and to define the main objectives of this contribution. The choice of materials and process studied will then be explained.

3) Review of Biaxial Deformation Studies.

Despite the limited amount of work published in the literature up to date on biaxial deformation, interesting conclusions have emerged. Most studies made best use of the experience and knowledge acquired from uniaxial studies in attempting to correlate results from both uni- and biaxial deformations.

Figure 1.3. Description of the pole density on a reciprocal sphere for any $\underset{\sim}{R}(hkl)$ for both Fiber and Planar textures. If $\underset{\sim}{R}(hkl)$ makes an angle α_1 with the $\underset{\sim}{c}$ chain axis ($\underset{\sim}{c}$-axis) and an angle α_2 with the normal to the crystallographic plane parallel to the deformation plane in the Fiber texture ($\underset{\sim}{b}$ in the figure), the maximum densities are found for $\phi=\pi/2+\alpha_1$, and $\phi=\alpha_2$, for the Planar and Fiber texture, respectively.

Maximum Pole Density for Plane $\underset{\sim}{R}$ (hkl)

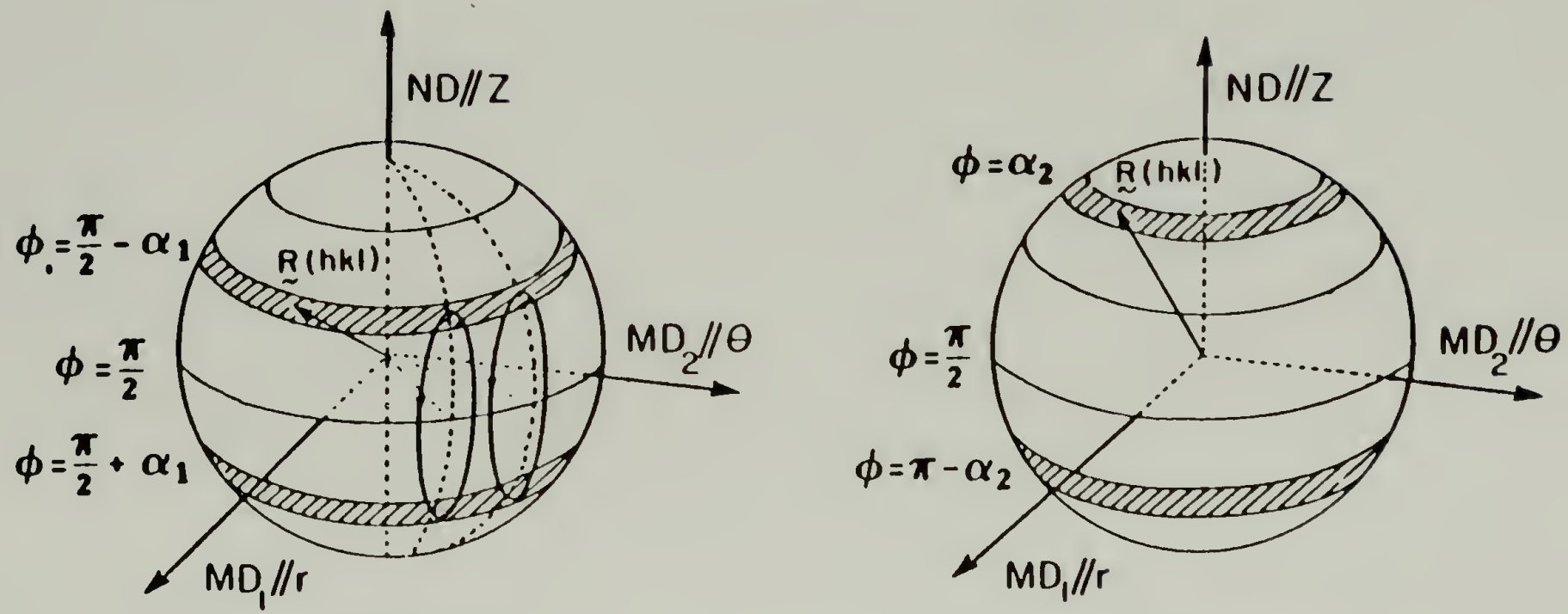

Planar Texture

Fiber Texture

α_1: Angle between chain axis ($\underset{\sim}{c}$) and $\underset{\sim}{R}$ (hkl)

α_2: Angle between $\underset{\sim}{b}^*$ and $\underset{\sim}{R}$ (hkl)

a) Solid State Biaxial Processes.

Difficulties encountered on biaxial deformation are generally a consequence of the process itself. Namely, many processes suffer from lack of simplicity, lack of control of the many variables involved, non-uniformity and/or inhomogeneity of the strain field, making any systematic study quite difficult. Most of these drawbacks ,however, could mostly be circumvent in the two processes studied in our laboratory over the last few years: Forging[30] and Tenterframing[31]. These processes present the advantage of producing equibiaxial deformation fields, which further simplify the crystal texture due to symmetry. In a comparative study of equibiaxial deformation of Polyethylene Terephtalate (PET)[32] by the two processes, hydrostatic deformation as produced by forging was shown to be more effective than free drawing deformation by tenterframing. Not only an increase of stress-induced crystallinity, but also a higher degree of uniplanar orientation ((100) plane parallel to the plane of deformation) were reported by forging. Moreover, a change of deformation temperature was found to have opposite effects on the degree of crystallinity in the two processes. In the case of isotactic Polypropylene (i-PP), deformation under hydrostatic pressure has been reported to stabilize the stress-induced smectic phase and consequently improve its drawability[33].

Our study will exclusively focus on the equibiaxial deformation by forging. A description of the experimental set up as well as the

rheology of the process (nature of the flow generated) have been given elsewhere[30] and will only be recalled briefly later on in this chapter.

b) Structure and Properties of Deformed Polymers.

Early publications confirm general expectations that common physical properties such as creep resistance, flexural strength, resistance to stress cracking and thermal shrinkage can be noticeably improved by biaxial orientation[34,35]. De Vries, Bonnebat and Beautemps investigated the biaxial stretching of initially amorphous polymers such as Polystyrene (PS) or Polyvinylchloride (PVC) and PET which partially crystallizes under constraints and/or heat setting[36]. Extent of molecular orientation was characterized by stress-optical methods. Part of the energy of deformation was found to be dissipated as internal stresses in oriented amorphous polymers, in addition to the recoverable entropic stresses typical of rubberlike network. A good correlation was found between internal entropic stress and birefringence for such films. According to their conclusions, the most ideal temperature for optimal deformation conditions of amorphous polymers is situated just around T_g, that is the lowest temperature where the material becomes ductile.

Unlike for uniaxial deformed specimens, there is no simple known expression relating the tensile properties of biaxially deformed semicrystalline polymers with the degree of crystallinity and the

orientation of both crystalline and amorphous phases (with the assumption of a two-phase model). Possible extensions of some of the models used in uniaxial studies to biaxial deformation are seeked. An example of such a model in uniaxial deformation has been given by Samuels for the axial compliance assuming the two phase series model and the additivity rule:

$$J^u = X(1-f_c)J_c^u + (1-X)(1-f_a)J_a^u \,, \qquad (1.1)$$

in which f_c and f_a are the orientation functions, J_c^u and J_a^u the compliances along the draw direction for the crystalline and amorphous phase respectively. The transverse compliance J^t of such anisotropic fiber is naturally much larger and may even exceed the compliance of the original isotropic material. The compliance of such a fiber at any angle θ to the fiber axis can be determined according to classical theory of elasticity in a continuous medium:

$$J^\theta = \cos^4\theta\ J^u + \sin^4\theta\ J^t + L \sin^2\theta \cos^2\theta, \qquad (1.2)$$

in which L is also function of the shear modulus and the Poisson's ratio. It is clear form this expression how the compliance dramatically increases as the angle θ increases. Accordingly, the increase in composite compliance caused by randomizing the orientation of the fibers in the plane would then be obtained by averaging out the compliance J^θ given in equation 1.2 over all values of the angle θ. Thus:

$$\langle J^\theta \rangle = \int_0^{\pi/2} J^\theta d\theta \,/ \int_0^{\pi/2} d\theta\,; \qquad (1.3)$$

This model will be reconsidered further on with some necessary approximations in order to make some predictions for the moduli of

equibiaxially deformed specimens. These will be compared with experimental results.

For semicrystalline polymers, a comprehensive determination of the degree of orientation in both phases requires WAXD and density measurements to be combined with refractive index measurements (in all directions) . A recent study recorded the WAXD and SAXD pole figures of simultaneously biaxially stretched PET to both equal and unequal draw ratios (in each direction)[37]. The WAXD results confirmed the rapid alignment of the phenyl rings (which are almost parallel to the (100) plane in PET crystalline unit cell) into the draw plane, as the chain axis (determined by the ($\bar{1}05$) poles) orients in the stretching direction(s). Random orientation in the plane was obtained in the particular case of equal deformation in both directions (equibiaxial deformation). Independent measurements of refractives indices in equibiaxially deformed PET films also confirmed these conclusions[32]. Both orientation features (chain axis in the draw direction and phenyl rings parallel to the plane) were also observed in the uniaxial deformation of thin films[37]. At small angles, diffraction patterns obtained through the film thickness for a series of deformed specimens ranged from two point- to perfectly circular patterns as the deformation changes from uniaxial to increasingly more equibiaxial. These witnessed the increasing orientation of the crystallites in the plane rather than in a single direction. Simultaneously, with the X-ray beam impinging

through the edge of the film, the typical four point pattern becomes ellipsoidal.

Even the most common semicrystalline polymers have been given very little attention. Early work on LDPE[38] and HDPE[39] blown films has demonstrated the difficulty of preparing truly equibiaxially deformed films with such process. Recently, biaxially drawn polyethylene from bulk and from the gel state have produced perhaps tensile moduli no more than about 10 GPa[40]. The authors found these values a priori deceiving when compared to the extremely high values that can be achieved by uniaxial draw (up to 220 GPa). In any case, this result illustrates how differences in structure, morphology and orientation between uniaxial and biaxial processes can result in major changes in properties.

Only melt-crystallized i-PP has been the subject of a broad comprehensive study of solid state biaxial deformation[29]. R. Saraf characterized by Wide Angle X-ray Diffraction Techniques the resultant crystal texture(s) and proposed the deformation mechanisms of i-PP when subject to a hydrostatic equibiaxial stress field as produced by uniaxial compression. He showed the specimens to possess double crystal texture. The relative amount of each varied as a function of temperature and extent of deformation. These textures correspond to the two possible orientation modes discussed in the prior section for biaxial deformation, namely the Planar and Uniplanar (Fiber) ones. The later was said to represent the ultimate stage in crystal orientation, as opposed to the planar texture, which corresponds to a "frustrated"

orientation state because of the incomplete reorientation of the major slip plane (see next paragraph). In addition, the monoclinic modification was found to partially transform into the semidisordered smectic phase during forging at low temperatures. Its stability was dependant upon the temperature and rate of the forging process. This stress-induced smectic form was found to not only increase the ductility of the material but to also enhance the efficiency of the process by causing an increase of Fiber texture (with respect to the Planar texture) for a given extent of deformation. It thus yield the optimal conditions of equibiaxial deformation of i-PP by forging and provides an explanation in terms of the structural and morphological aspects associated with the deformation in the crystalline phase.

4) Theory of Deformation of Polymers Crystals.

It has been established that most concepts of plastic deformation of crystalline polymers can be derived from the principle of deformation known for metals[41-43]. Namely, plasticity is the result of the stress-induced activation of defined slip mechanisms which provoke molecular shearing along specific slip planes and in specific directions. Superimposition of stress-induced crystalline transitions may occur and further complicate the phenomena. Which process or mechanism preferentially occur may be predicted by the theory of crystallography of slip.

a) General Theory of Crystallography of Slip.

It is not intended to review here all the theory of plasticity, since it has been already quite extensively reviewed by other authors[44,41-43]. We would rather simply point out in this section how the theory can be used to make predictions on the nature of the crystalline orientation (crystal texture) induced by equibiaxial deformation. Or conversely, how the characterization of the crystalline phase (symmetry and texture) in the forged polymers can reveal unique information concerning the prevailing mechanisms during deformation, under different sets of conditions.

At the origin of crystal deformation is the displacement of lattice planes associated with the movement of dislocations. Screw dislocations with Burgers vectors parallel to the chain direction have been experimentally observed[45]. Dislocations may already be present in original crystals or are generated thermally under the action of an applied shear stress[46]. Nevertheless, when the stress surpasses the lattice cohesive forces of a crystal, dislocations propagate and adjacent lattice planes can be displaced by a full lattice period or more. The crystal thus recovers its original state of energy prior to the perturbation. There should be no restoring force from the lattice itself. Strain hardening in metals occurs when further propagation of dislocations is hindered (by other dislocations, for example). Obviously, semicrystalline polymers differ from metals due to their

long chain nature and their intermeshed crystalline and amorphous phases. For example, entropic stresses stored in the amorphous phase may induce molecular scission during the deformation or partial recovery after stress release.

The next question then is: what determines the actual shear movements at the microscopic level? Or in other words, how the dislocations propagate through the crystal? Shearing is restricted to some specific lattice planes (called slip planes) and along some specific crystallographic directions (called slip directions). A slip direction together with a slip plane define a slip system. When a macroscopic stress σ is applied, it is transmitted to each slip system of the crystals as a resolved shear stress $\tau=\sigma\cos\lambda\cos\chi$ in the slip plane along the slip direction. Shearing along this plane in this direction only takes place when the resolved shear stress reaches the critical resolved shear stress (CRSS) characteristic of this slip system. The so called "main slip system" usually refers to the easiest crystal slip process, or in other words the one with the lowest CRSS. This will be the first (and possibly the only one) to be activated on deformation. Other slip systems in the crystals could possibly play a role too, but they require more energy (owing to their higher CRSS) in order to be activated. In summary, any crystal modification possesses a number of slip systems of different critical resolved shear stress. Shear will however be limited to the energetically most favorable processes. For polycrystalline aggregates, a theory stipulates than a minimum of five

slip systems are required for any change of shape[44]. On the other hand, no such limitation applies to semicrystalline polymers, due to the presence of the amorphous phase with large compliance[47].

Simple structural considerations are usually useful to help predict the major slip system(s) in polymer crystals. First, in order to avoid breaking covalent bonds in the chain backbone during deformation, preferred slip planes are most likely to be parallel to the chain direction. Other considerations such as density of packing on nature of secondary interactions (Van der Waals, Hydrogen-bonds or steric hindrance) further discern between various planes. The chain axis commonly represents the major slip direction since it is the strongest direction in polymer crystals. Slip along this direction is often referred to in the literature as the c-slip mechanism. It is also the major contribution to the process of orientation and extension of molecular segments included in the crystals, and thus play a key role in shaping the final structure, orientation and properties of deformed specimens. Transverse slip can also take place but might be limited to fold planes in crystals.

Finally, different stress fields yield different types of orientation (texture) for the deformed crystals[47]. As a result of the geometry of the slip process, a crystal subject to single slip will rotate relative to the principal stress axis. Simple examples are illustrated in Figure 1.4. In the particular case of a single c-slip mechanism, the chain axis in the crystal always rotates towards the

Figure 1.4. Schematic description of slip processes in tension and compression, showing the rotation of the main slip system.

Movement of Slip System on Simple Deformation

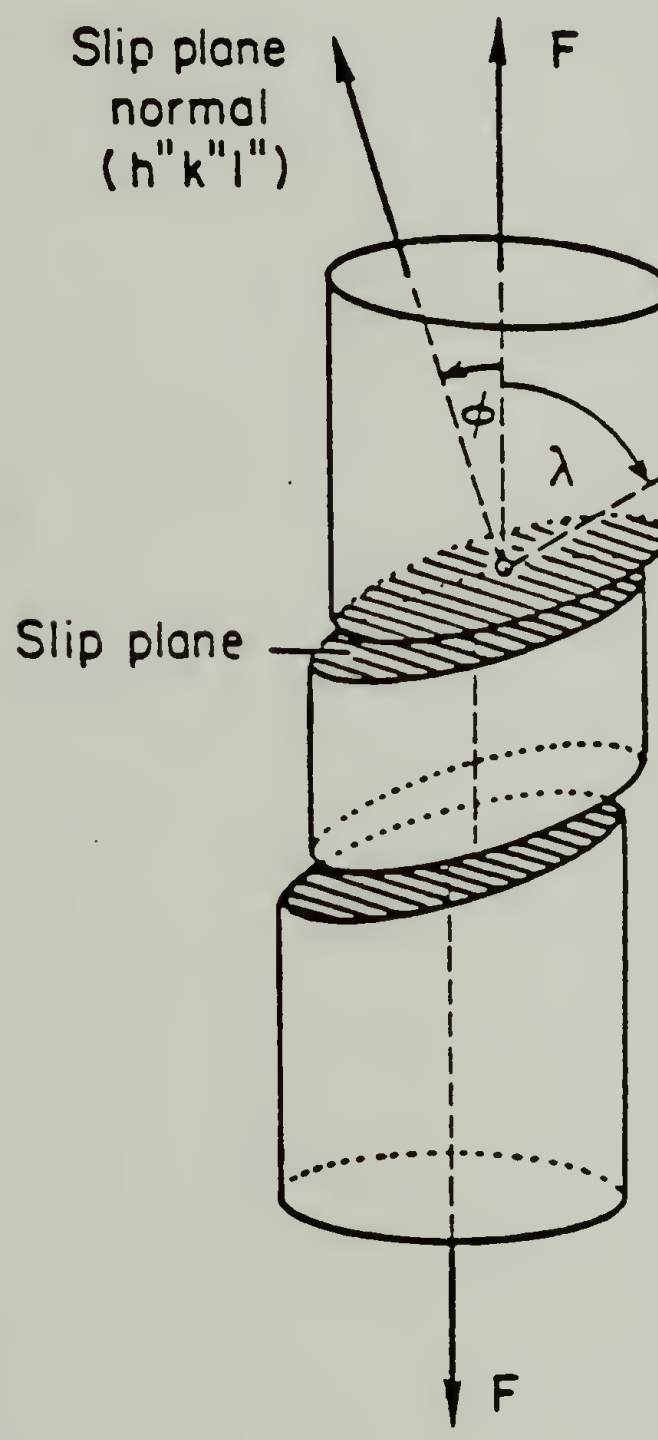

Resolved

Shear Stress

$\tau = \sigma \cos\lambda \cos\phi$

$F > 0$ (Tensile Force) $\lambda \to 0, \phi \to \frac{\pi}{2}$

$F < 0$ (Compressive Force) $\lambda \to \frac{\pi}{2}$ { $\phi \to 0$ Fiber ; $\phi \not\to 0$ Planar

direction of maximum extension. That is towards the tensile direction in a tensile test and away from the compression direction in a compression test. Additionally, for a crystal possessing two major slip directions in the same slip plane (with possibly different CRSS), rotation due to slip in both directions (most likely in the chronological order imposed by the difference in CRSS) will always ultimately align the slip plane to the compression plane (that is perpendicular to the compression direction). Note nontheless that as rotation of the slip plane occurs, the resolved shear stress diminishes and tends towards zero.

Based on these concepts, the behavior of polymers on forging might differ from one polymer to another or with deformation conditions (temperature, rate) because of different crystal deformation mechanisms involved. These differences will reflect in the resultant crystal texture and morphology. A complete characterization of the final crystal orientation will thus allow to help recognize the principal molecular mechanisms and help determine appropriate materials and optimal conditions for equibiaxial deformation. A measure of the minimum stress required for the onset of plasticity in the main slip system is provided by the yield point on the stress-strain curves recorded on line during the process.

b) Twinning and Crystal Transitions.

Finite shearing or molecular displacement in the ordered phase (imposed at the onset of a deformation or during relaxation) can have additional effects on the structure and orientation of crystals besides the ones recalled above. When present, they usually occur at the onset of deformation or during relaxation, in contrast to the slip mechanisms described above which are the only ones able to induce large molecular deformations.

Twinning is usually observed for small strains or on stress relaxation. It simply produces a large rotation of the lattice around the chain axis due to finite transverse displacement of chains in crystals, which nonetheless maintain their original structure. The twinning plane defines the shear direction necessary for twinning. A critical resolved shear stress in the twinning plane defines the onset for twinning.

In contrast, other stress-induced shearing processes can induce a change in crystal symmetry (and also possibly in the chain conformation) prior or simultaneous to the onset of slip. It usually consists in a change in the three-dimensional order (lattice modification) or a partial reduction of order. Many examples of such stress-induced phase transitions (crystal-crystal or order-disorder) exist in the literature and have been collected and classified recently by Saraf[48] (Table 1.3). The stress-induced forms are usually thermodynamically metastable and

Table 1.3 Crystal phase transitions on deformation in semicrystalline polymers. (After Saraf)

Polymer	Crystal Form	Unstretched Structure	L* (°A)	Density (gm/cc)	Crystal Form	Stretched Structure	L* (°A)	Density (gm/cc)	Draw Temperature
Category- (iv)									
i-PP (17)	α	$(TG)_3$ (3/1) Helix	2.17	0.936	Disordered+	Same	2.17	-	< 70°C
PA (133)	I	G_4 (65°) (2/1) Helix	1.94	1.07	III (Disordered)	Same	1.94	-	25°C
PCCB (147)	α	Planar zigzag (1/10)	4.67	1.514	β (Disordered)	Same	4.67	1.448	
Nylon-3 (148)	II α	Planar zigzag	4.80	1.40	I#	Same	4.80	-	
Category- (v) and (vi)									
s-PP (139, 140)	Ortho-rhombic	$(T_2G_2)_2$ (4/1) Helix	1.85	0.93	Disordered	Planar zigzag	2.55	-	25°C
PB-1 (149, 150)	II	(11/3) Helix	1.92	0.92	I	(3/1) Helix $(TG)_3$	2.17	0.95	
t-PI (138)	α	Trans-CTS-Trans-CTS (2/0)	4.38	1.05	β	STS-Trans	4.72	1.05	
PVF_2 (136)	II α	TGTG Glide-type	2.31	1.925	I β	Planar zigzag (deflected)	2.56	1.973	
Nylon-6 (151)	γ	$(T_4STS)_2$ (2/1) Helix	8.44	1.17	α	Planar zigzag (2/1)	8.60	1.23	

Polymer	Crystal Form	Unstretched Structure	L* (°A)	Density (gm/cc)	Crystal Form	Stretched Structure	L* (°A)	Density (gm/cc)	Draw Temp.
Category- (v) and (vi) (continued)									
Nylon-8 (152)	γ	$(T_6STS)_2$ (2/1) Helix	10.85	1.09	α	Planar zigzag (2/1)	11.2	1.14	
PBT (141)	α	See Ref.	11.56	1.40	β	See Ref.	12.95	-	25 °C
PEO (137)	I	(TTG) (7/2) Helix	2.78	1.228	II	Planar zigzag (2/1) Helix	3.56	1.197	25 °C
PEB (153)	α	$(CTSGT)_2$ (2/1) Helix	7.80	1.41	β	Almost Extended	9.53	1.39	120 °C
PCB (154-156)	III	$(T_2G_2)_2$ (2/1) Helix	3.61	1.18	II	T_3GT_3G Glide-type (2/0)	4.21	1.19	25 °C
PD (157)	II	$(G_2TGS)(G_2TGS)$ Glide-type	4.93	1.41	I	(G_2TGS) (5/1) Helix	4.95	1.33	25 °C
PMCB (156)	III	$(T_2G_2)_2$ (2/1) Helix	3.26	0.982	II	T_3GT_3G Glide-type (2/0)	4.18	1.037	20 °C
(PMPL (158)	Ortho-rhombic	$(T_2G_2)_2$ (2/1) Helix	2.98	1.26	Disordered	Planar zigzag	4.7	-	25 °C
Martensitic Transition									
PE (144)	Orthorhombic	Planar zigzag	2.55	1.000	Monoclinic	Same	2.55	0.998	20 °C

L* is the projected monomer length on the fiber axis; +the lateral chain packing is disordered; #b-axis is slightly expanded.

transform back into the parent structure after stress release, as by thermal relaxation.

Crystal transitions in some polymers are likely to modify the overall deformation process by changing the slip systems by which the crystalline phase deforms during the process. In this case, the the final texture course of their deformation, we expect the main slip systems of the deformation-induced species to control the deformation process. If this is right, the nature of the crystalline texture in the deformed specimens is determined by the crystallography of slip for the stress-induced species and by the geometrical relationship between the two forms during the phase transformation. Therefore, unlike twinning, such crystal phase transformations are expected to bear significant effect upon the deformational behavior.

c) Classical Models of Plastic Deformation.

Generally, thermoplastic polymers usually exhibit either one of two typical mechanical behavior during tensile stretching: "Strain hardening" or "Stress softening"[22,23]. Included in the first category are some common polyamides or polyesters. Typically, these polymers exhibit strong secondary interactions between molecules and/or possess large steric groups and have a low initial degree of crystallinity. Deformation-induced crystallization has often been reported. Deformation is usually uniform throughout the sample and the slope of

the stress-strain curve considerably increases as the deformation proceeds. Large deformations are prohibited by failure mechanisms.

On the other hand, the opposite effect, "strain softening", is not only quite generally found in amorphous polymers below T_g but also in many traditional semicrystalline polymers with weak secondary interactions. Typically, at the transition from elastic to plastic behavior, called the yield point, necking occurs that is the sample thins locally reducing the yield stress, and the deformation becomes inhomogeneous. Molecular stretching and crystal shearing essentially takes place inside the neck, which slowly propagates throughout the specimen as the deformation proceeds. The common driving force for the "microneck" initiation found in these materials is generally accepted to come from the local softening at a particular defect-rich locations in the material at the early stages of deformation. Further deformation in the neck then becomes easier due to the local stress increase (reduction of cross section). During neck propagation, the original lamellae break (by lamellar tilt and crystal shear) into smaller crystalline blocks. These become easier to shear due to their smaller size, larger number of defects and high surface to volume ratio. As a result, molecules can more easily be pulled out . Excessively large local strains can be relieved by the pulling out of chains trapped within the crystals which facilitates further deformation at the location where primary deformation had started. The size and perfection of the resultant recrystallized crystals largely depends upon the deformation temperature which defines the degree of undercooling. The closer the deformation

temperature to the melting point, the larger and more perfects the crystals that reform during deformation, the lesser the "strain softening" effect and the more uniform the deformation.

Presumably, if, in addition, the crystalline phase undergoes some phase transformation into a less ordered or less dense modification having looser chain packing, the new form is likely to possess lower critical resolved shear stresses (CRSS's) and as a consequence will exhibit higher ductility. Evidence of such a phenomenon was described for i-PP, which partially transforms into the metastable "smectic" modification during forging below 70°C, promoting ductility to the process[29]. Again, the process temperature is crucial as it controls which crystalline form is stable during the process.

5) Predicting the Optimal Conditions for Equibiaxial Deformation.

In the light of these general concepts on the deformation of semicrystalline polymers, and in view of prior results on forged i-PP[29], conjectures were made on which properties of such polymers would be the most desirable for biaxial deformability. These consider and address two essential aspects associated with the deformation of crystals:

a) Nature of the main slip systems.

b) Deformation-induced structural changes (phase transitions).

a) Ideal Slip Systems.

As mentioned earlier, the fraction of Fiber texture obtained during forging of i-PP (or Uniplanar texture as defined by Heffelfinger and Burton)[24] was said to reflect a state of higher crystalline orientation and was thus considered "the ideal texture". According to the crystal slip theory, this texture is best achieved for crystals possessing one single major slip plane with two directions of relatively easy slip (low CRSS's): Chain direction and Transverse direction. In that case, biaxial deformation induces preferred planar alignement of the major slip plane in the plane of deformation. If slip is mainly restricted to one single slip system (c-slip mechanism in one specific plane, for example), the theory predicts a combination of Fiber and Planar texture for the biaxially deformed crystals. As the deformation proceeds, the chains progressively orient in the plane of deformation (by c-slip mechanism). However, tilting of the slip plane in the plane of deformation may be inhibited by the lack of a second direction of easy slip in the major slip plane. This may leave a fraction of crystals with random orientation of the major slip plane, which thus will have Planar texture.

Finally, the last case corresponds to crystals having several minor slip planes with similar values of critical shear stress (pencil shear). The general mechanism of deformation becomes rapidly confusing as several different slip systems are simultaneously activated in the process of shearing (and orienting) the crystals. This type of

situation is expected to yield the Planar texture. Paradoxally, a large number of slip systems seems therefore unfavorable as it inhibits the obtention of ideal Fiber texture for the crystals in the oriented state.

b) Deformation-induced Phase Transitions.

As stated earlier, structural changes might occur in the crystalline phase during deformation under certain conditions. They may essentially have two effects on the process. They may modify the deformation mechanisms (due to different slip systems) and consequently the final orientation (texture) of the crystals in the deformed specimens. They may also affect the critical shear stress(es) required for the crystals to shear. Lower value(s) for example will promote ductility and favor high deformation.

6) Dissertation Goals.

a) General.

On the basis of the two structural considerations described above, it then seems possible to "a priori" predict which polymers, associated with which deformation conditions, would be expected to yield optimal behavior in equibiaxial deformation by forging. The objective of this work is twofold:

On one hand, it wishes to provide more experimental evidence for the relevance of the two criteria proposed for selecting adequate flexible chain semicrystalline polymers and experimental conditions in biaxial deformation. This requires that some chosen flexible chain semicrystalline polymers be equibiaxially deformed by forging which would have different known structures and deformation behavior under various conditions; And that theoretical predictions of the final crystalline texture and ductility be compared with experimental results. Furthermore, the effect of different mechanisms of deformation on some final specimen properties should also be assessed. Tensile properties will be determined and will provide a measure of process efficiency.

Conversely, if the experiment confirms the predictions, the method could be used as a characterization tool for crystalline properties and phase transitions of semicrystalline polymers by monitoring changes in orientational behavior and mechanical properties.

b) Choice of Polymers for Study.

The dissertation presents results on the structure and equibiaxial deformation studies of selected members of two major families of semicrystalline polymers, namely Polyamides and Polyolefins. Both have been the subject of numerous deformation studies (mainly uniaxial) and attracted great interest for commercial applications. Polyundecanamide (Nylon 11) and High Density Polyethylene (HDPE) were chosen to represent each class.

Table 1.4 Published crystallographic data for nylon 11 α-form (After Dosiere et al)

Unit-cell parameters						Crystalline system	Space group	Monomer by unit cell	Crystal density ($g\ cm^{-3}$)	Reference
a (nm)	b (nm)	c (nm)	α (deg)	β (deg)	γ (deg)					
0.96	0.42	1.50	72	90	64	Triclinic	...	2	1.192	Little
0.49	0.54	1.49	49	77	63	Triclinic	...	1	1.228	Slichter
0.478	0.413	1.49	82	75	66	...	C1-1	1	1.168	Aelion
0.478	0.413	1.31	86	75	66	...	...	1	1.12	Genas
0.95	1.00	1.50	60	90	67	Triclinic	...	8	...	Hasegawa
0.98	0.525	1.49	50.5	90	72	Triclinic	...	2	1.037	Dosiere

Figure 1.5. Polarized optical micrograph showing negatively birefringent spherulites in nylon 11 crystallized from the melt (after Magill).

i) Polyundecanamide: The reason for selecting Nylon 11 is first motivated by its ability to form different crystalline modifications (see the next two chapters). At the origin of these discrepancies is the alternate mode of hydrogen-bonding in crystals, which highly depends upon both temperature and thermal history. One particular form of interest is the α-form with its layer like arrangment of hydrogen-bonds in the (010) plane, which should represent the major slip plane. Spherulites of this crystal form obtained by crystallization from the melt are shown in figure 1.5[50]. Almost no mention has ever been made before about the semi-ordered phase obtained by quenching and which diffraction scan is compared with the α-form in figure 1.6. Previous studies on uniaxial stretching of thin strips of nylon 11 have reported noticeable differences in the final orientation mode as a function of drawing temperature and specimen thermal history[51,52]. It is therefore of particular interest to study and compare if similar differences exist on equibiaxial deformation and to seek correlation between the two processes.

Because of the lack of information or the current confusion in the literature (Table 1.4 shows several the discrepancies for the published crystallographic data for the only α-form!), this work primarily reexamines the structure and stability of the different crystalline modifications of nylon 11. An attempt will be made to correlate thermodynamics and kinetics of crystal formation with the nature of hydrogen bonding which controls the ordered molecular packing.

Figure 1.6. WAXD scans for both quenched and slowly cooled nylon 11 samples.

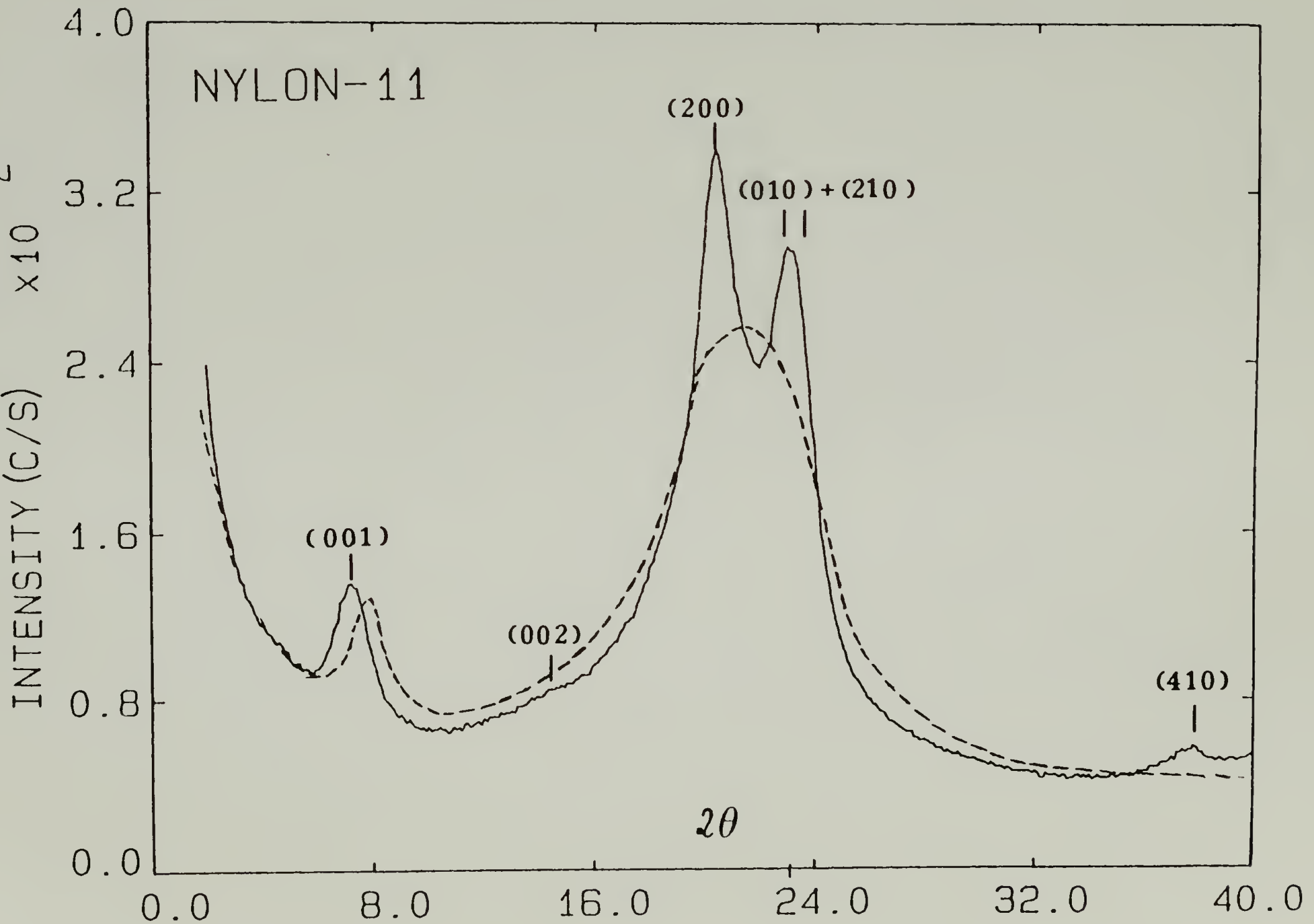
NYLON-11
(200)
(010) + (210)
(001)
(002)
(410)
INTENSITY (C/S) x10 -2
2θ
4.0
3.2
2.4
1.6
0.8
0.0
0.0
8.0
16.0
24.0
32.0
40.0

ii) High Density Polyethylene: As stated earlier, only a few studies have previously considered high density polyethylene for biaxial deformation[38-40]. The in-plane modulus enhancements reported were much lower than in uniaxial deformation studies. No mention has been made of the role of the monoclinic form, which has been shown in the past to partially result from a stress-induced transformation of the orthorhombic form at low temperatures[53,54], on the deformation process. According to the above preliminaries, forging may be able to distinguish between the two forms. We propose to reconsider HDPE for equibiaxial deformation along these lines.

7) Organization of the Dissertation.

Chapters II and III are concerned with a detailed experimental characterization of the different crystalline forms of isotropic Nylon 11 and their transitions. The studies of melting and crystallization described in Chapter II reveal thermodynamic and kinetic aspects of the melting and crystallization for both the "smectic" δ'-form and the crystal α-form and of the transition of the "smectic" into crystal on annealing. The interpretation stresses out the preponderant role played by hydrogen-bonds (between amide groups) in controlling the structure and formation of each of the structure characterized. Chapter III more specifically reconsiders the nature and characteristics of the reversible α-δ crystal-crystal transition previously reported, similar to the Brill transition known for Nylon 6,6. As for this transition, no

definite explanation has thus far been given for nylon 11 which satisfies all experimental observations. Based upon thermal analysis, solid state ^{13}NMR spectroscopy and refractive index measurements, the transition is found to exhibit many aspects of a crystal-condis crystal transition. The breaking of hydrogen-bonds for the layer-like arrangement of the α-form is proposed to be at the origin of conformational isomers in the δ-form. Also, in this chapter, an estimate of the thermodynamic parameters for all the transitions is obtained from the experimental values of both heat of crystal-crystal transition and heat of fusion measured for nylon 11 specimens of various thermal history.

All deformation results on nylon 11 are reported in Chapters IV and V. The first one reveals several aspects of its behavior during uniaxial tensile stretching. It shows how the initial structure and deformation conditions can largely influence the final structure and orientation in the crystalline phase (smectic versus crystal form; uniplanar-axial versus axial texture). The uniplanar-axial orientation is used to derive the parameters of the α-form unit cell, which provides new information on the influence of hydrogen bonds on the mode of molecular packing in nylon 11. Chapter V addresses the results on the equibiaxial deformation of nylon 11 by forging. Two distinct regimes are found which show different structure and orientation for the crystals, depending whether forging is done above or below 100°C (at the forging rate studied). Studies of molecular orientation (by X-rays) and extension (by shrinkage) and tensile properties indicate forging to be

more effective in the high temperatures region above 100°C, where crystals are either of the α- or δ-form (condis crystal) than at lower temperatures where it transforms into the "smectic" form during forging.

In Chapter VI, the behavior of High Density Polyethylene on forging is presented. All results underscore the favorable role played by the stress-induced martensitic transition (Orthorhombic to Martensitic transformation) during deformation at low temperatures (below 100°C) on the mechanics, orientation, deformation extent and mechanical properties of the deformed specimens. In addition, the process brings new insight of the relationship between the two crystalline modifications.

Chapter VII finally summarizes the main results of this investigation and argue about the validity of the criteria to successfully predict the adequate structures and deformation conditions for biaxial deformation. It also recalls some of the structural features found in nylon 11 polymorphs which were attributed to the nature of hydrogen bond interactions in ordered lattices. Suggestions for future work finally close this chapter.

8) Experimental.

a) Description of the Forging Process.

Figure 1.7 shows a schematic description of the forging process. The compression die consists of two 1'' diameter planar plungers axially aligned by guide pins and held by steel plates.

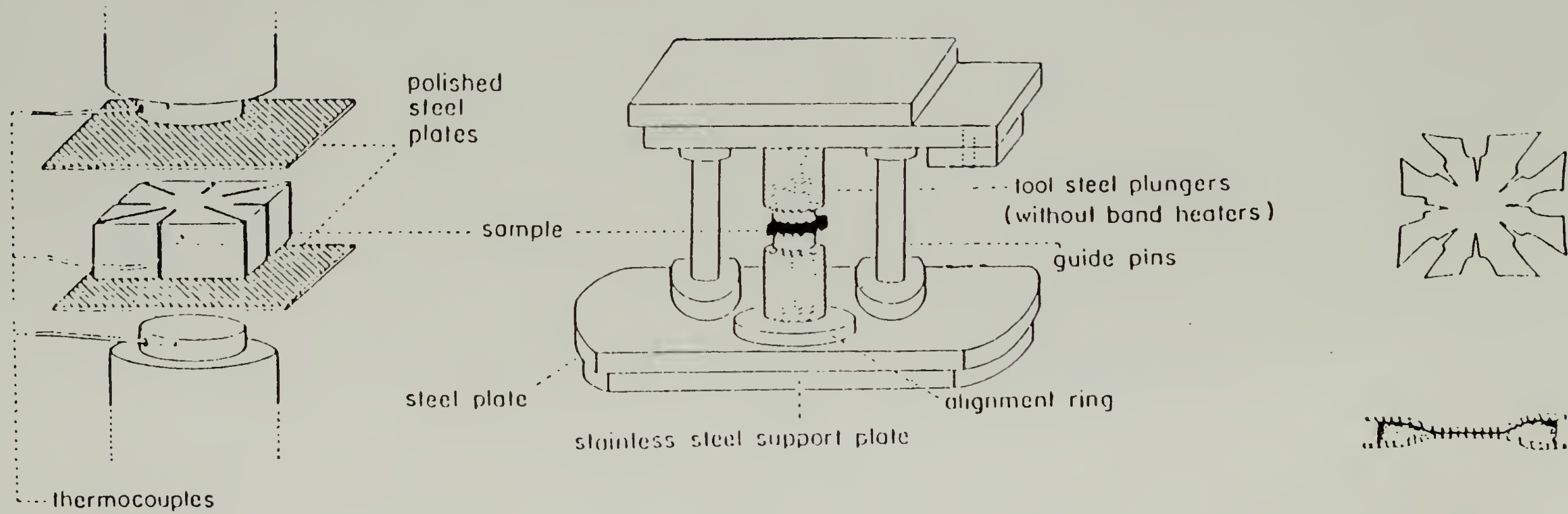

COMPRESSION DIE ASSEMBLY

Figure 1.7. Schematic of the forging process.

Samples under investigation (of approximatively 0.5 cm in thickness) are placed between two flat plungers after having been pre-notched at eight sites to ensure uniform flow and covered on each side by smooth ferrotype plates. The top plunger is allowed to move freely. The compression assembly is then put in an Instron machine set up for compression testing. It can apply loads up to 50000 lbs. The rate of deformation can be set to any desired value. The plungers are heated and thermostated independently to the desired squeezing temperature. The load and displacement are respectively monitored during the deformation by a load cell and a LVDT which are used to investigate the mechanics of the process.

The rheological aspect of this deformation process has already been the subject of a prior study[30]. A rigid-plastic model based on continuum mechanics principles and a yield criteria including hydrostatic pressure dependence has been shown to adequately describe the mechanics of the yield process in the particular case of i-PP. It describes an extensional flow (radially and tangentially) with finite friction at the polymer-metal interface. Evidence of shear flow has been provided for high levels of compression, but is restricted to thin layers at the surfaces of the plates in contact with metal. Although the model permits a quantitative estimate of the yield stress in both tension and compression (from some fitting parameters) in the specific case of i-PP, we will simply deduce the yield stress from the intersection point between the elastic and the plastic regime.

b) Characterization Techniques.

A description of all characterization techniques used will be given when required in the following chapters. These include Wide Angle and Small Angle X-ray Diffraction (Statton camera and diffractometer), thermal analysis by Differential Scanning Calorimetry, on-line stress-strain recording during forging with a Load cell and a LVDT, shrinkage experiments in a silicone oil bath, tensile modulus determination and refractive index measurement with an Abbe refractometer.

C H A P T E R II

EVIDENCE OF POLYMORPHISM IN NYLON 11 BY MELTING AND CRYSTALLIZATION STUDIES

1) Introduction.

Polyundecanamide, commonly known as nylon 11, is a commercial polyamide which can be synthetized by polycondensation of 11-aminoundecanoic acid by simply heating[55]. It thus belongs to the ω-aminoacids homolog series[56]. Members of this series are all unsymmetrical, which means that the atom sequence along the chain depends upon the direction followed along the chain. As a result, the packing of two chain segments alongside each other in an ordered array can be either "parallel" or "antiparallel", depending on whether they are in the same or opposite directions respectively[57,58]. For nylon 11, and other "odd" nylons in general[59], which possess an even number of methylene groups between the regularly spaced amides, simple molecular models indicate that complete hydrogen-bonding between all amide groups in adjacent chains can be achieved for both arrangements in the most extended planar zigzag conformation (2/1 helix), without severe twisting

or distortion of the hydrocarbon segments[60]. This is a major difference from "even" nylons, such as nylon 6 for example, which need to adopt a pleated configuration in order to achieve over 50% hydrogen-bonding between parallel chains (such as in the γ-crystals of nylon 6[61]).

Because hydrogen bonding interactions (between amide groups) are generally at least one order of magnitude larger than dispersion forces (between methylene groups), considerations concerning their formation are particularly relevant, since they they are expected to dictate the structures of the ordered domains. And in fact, many different polymorphs are reported in the literature for nylon 11, which are expected to reflect different modes in hydrogen bonding. Besides solution casting which was found to give different species by simply changing the solvent[62], different structures also appear to form in melt crystallized nylon 11; and these are the ones we wish to focus on.

First of all, all authors agree on the formation of the α-form in isothermal or slow cooling crystallization conditions, although some confusion stands in the literature concerning its exact detailed structure, as was pointed out in table 1.4 of the Introduction. This is essentially because of the limited number of observable reflections in X-ray or e^-- diffraction, which essentially prevent comparison between experimental and calculated intensities based on computed structure factors. In addition, the structural parameters have been found to be quite dependent upon thermal history, temperature and pressure, which

may also explain the discrepancies in the results of former studies. Nevertheless, in this α-form, hydrogen bonds are believed to be arranged at room temperature in parallel layers in the (010) crystallographic plane. Whether hydrogen bonds form between "parallel" or "antiparallel" molecules remains a major question, for the structures first proposed by Slichter[58] ,and later revised by Newman[63], which assume only parallel molecules in crystals seem quite unlikely for statistical reasons and on the viewpoint of chain folding with adjacent reentry (chain folding will reverse the direction of the chain in the lamella)[62]. This question will be addressed in Chapter IV.

Second, the α-form has been reported to adopt a structure of different symmetry at temperatures above 95°C, called the δ-form, according to a change in the thermal expansion coefficients at this temperature as observed by X-ray[63]. Authors interpreted the phenomenon as a consequence of the disruption of the H-bonded layer-like structure of the α-form above this temperature to form an hexagonally packed structure. This transition between the triclinic α-form and the pseudohexagonal δ-form was found to be reversible

Third, mention is made in the literature on the formation of a semidisordered species on quenching nylon 11 from the melt[64,65]. It has been referred to as the δ′-form modification, because of the partial resemblance of its diffraction scan with the high-temperature δ-form of the room temperature α-form. Its WAXD scan exhibits a single broad reflection at d=4.22Å descriptive of the loose packing of the chains. It suggests the existence of a fairly broad distribution in

direction and strength for the hydrogen bonds in these partially ordered species. Despite partial disorder of the molecules in their mode of packing, the observation of a fairly sharp (001) reflection at d=12.9 Å indicates molecular registry in the chain direction. Such an order is reminiscent of the one typically found in smectic phase and thus will be referred to as the smectic form of nylon 11 in the subsequent chapters.

The structural parameters of these three different crystalline forms are collected in Table 2.1. At this point, understanding their relationships and the mechanisms of their transformations would also be of great value. However, additional methods besides X-ray are clearly needed to provide further characterization and distinction between:

i) the crystal α-form or the smectic δ'-form at room temperature.

ii) the α-form and δ-form which were said to reversibly transform into one another at 95°C.

The purpose of this chapter and the next chapter is to address these two points in view of novel data provided by thermal analysis. It will be shown how this characterization method can successfully identify the crystalline modifications listed above and elucidate how thermodynamics and kinetics control their formation and stability. Solid state ^{13}N NMR spectroscopic and refractive index measurements are also implemented.

Most prior thermal analysis studies of nylon 11 have focused on the glass transition[66,67], and only few results are reported concerning

Table 2.1 Structural parameters of all nylon 11 crystalline forms.

Crystal modification	lattice symmetry	d_{001}(Å) (chain axis)	d_{200}(Å) (chain packing)	d_{010}(Å)
smectic	smectic	12.9	≈4.22	≈4.22
low-T α-form	triclinic	13.2	4.37	3.90
high-T δ-form	hexagonal	12.0	4.16	4.16

melting behavior. Northolt[51] first noticed the presence of several endotherms on heating nylon 11, whose characteristics were highly dependent on sample thermal history. Gogolewski confirmed the multimelting behavior but failed to find its origin[68]. Also, in a recent study on the effect of pressure upon melting and crystallization of nylon 11, Chen, Newman and Scheimbein[69] were able to correlate for the first time changes in melting behavior for nylon 11 crystallized at various pressures with possible variations of the crystal forms.

2) Experimental.

Extruded nylon 11 films of 0.5 mm thickness were received from Atochem (France). Their reported weight average molecular weight and polydispersity are Mw=35,000 and 3.5 respectively. The abscence of birefringence indicates no preorientation in the films. They were dried under vacuum at 95°C for 48 hrs before use. Samples of approximately constant weight (about 5 mg) were cut from these films for thermal analysis. Sample size is known to affect thermal analysis results, due to the low thermal conductivity of polymers. Accordingly, comparisons were only carried out between samples of approximately similar weight and shape.

The thermal behavior of nylon 11 at atmospheric pressure was studied using a conventional Perkin-Elmer DSC 4. The specimens were put in aluminum pans and all thermal treatments were done in a dry nitrogen

atmosphere. All thermograms were obtained at heating and cooling rates of 10°C/min unless stated otherwise. An indium standard was used initially for temperature and enthalpy calibration.

In order to ensure that all samples had the same initial thermal history, they were first heated up to 240°C at 40°C/min and kept in the melt for 15 min before being subject to any particular thermal treatment. All thermal preparations of the samples were performed in the DSC cell, except for quenching which was performed in a mixture of dry ice and methanol after samples had been melted in a vacuum oven. Detailed descriptions of the specific thermal treatments for each set of experiments are given separately in each following section.

Finally, 2θ X-ray scans were obtained on a Siemens D-500 four circle diffractometer in symmetrical geometry with the CuKα radiation selected by a Ni filter.

3) Results and Discussion.

a) Conditions of Crystallization for the Different Species.

The drastic effect of cooling rate on the crystallization of nylon 11 is first displayed in Figure 2.1. Quenched nylon 11 (in a mixture of dry ice and acetone) exhibits a single asymmetric endotherm on remelting with a peak maximum at 187°C, when heated at at rate of 10°C/min. The small exothermic peak, whose onset starts just above the reported $T_g \approx 50^{\circ}C$ also suggests that a fraction of the material cold-

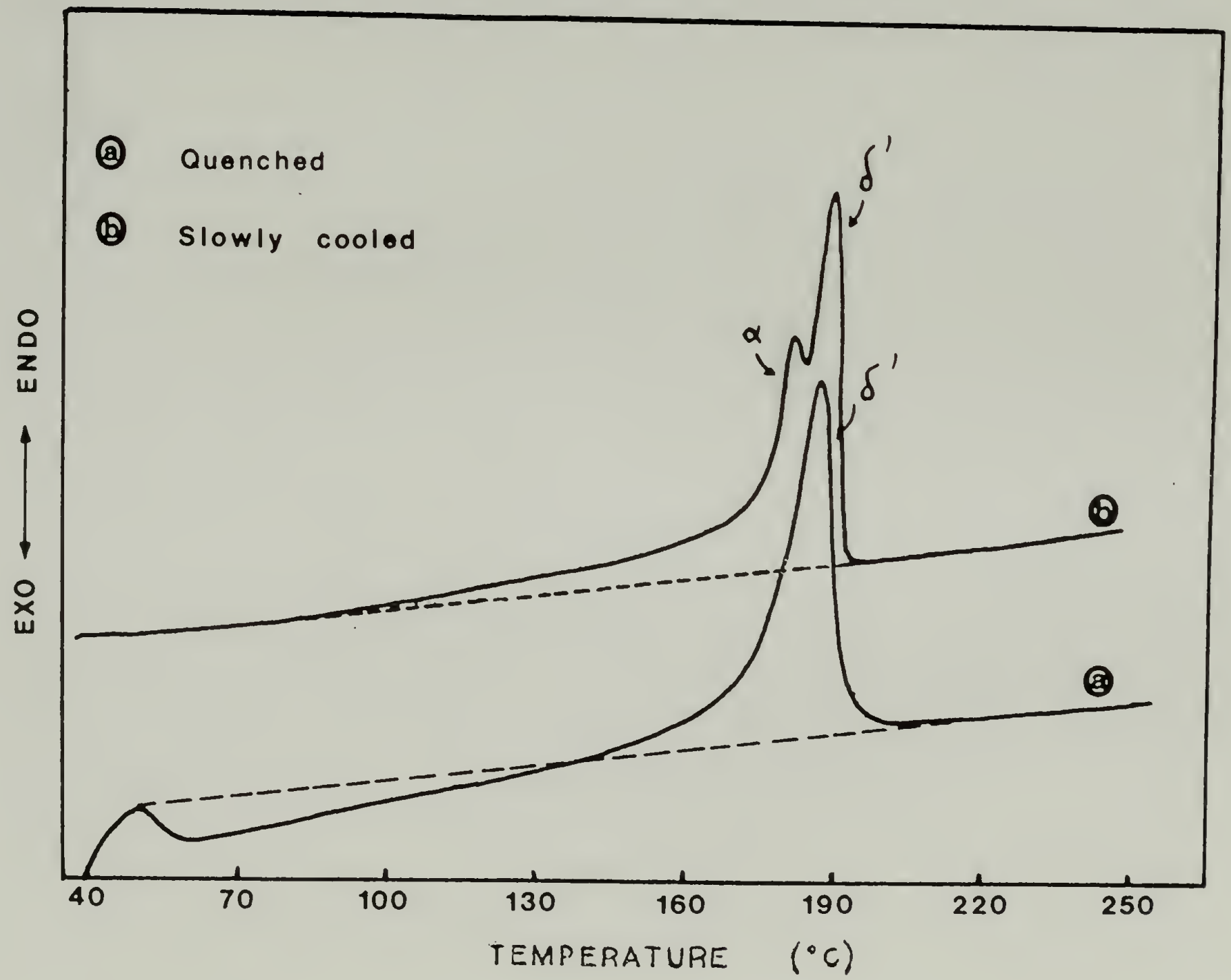

Figure 2.1. DSC heating curves (10°C/min) for quenched (-250°C/min) and slowly cooled (-100°C/min) nylon 11 from the melt (240C).

crystallizes on heating. Its relatively small size compared to the size of the melting peak however indicates that a dominant fraction (≈4/5) of crystallization has already taken place during cooling. In contrast, nylon 11 crystallized in the DSC cell at a lower cooling rate (-100°C/min) exhibits an additional endothermic peak on the low temperature side of the former melting endotherm (with a peak at about 180°C) (Figure 2.1b). Cold crystallization is not observed.

Fast crystallization kinetics for nylon 11 and other "odd" nylons, in contrast with "even" nylons, have already noted in the past by Lord[60], who studied the heating behavior of several quenched polyamides of the ω-aminoacid series. On the heating curves following quenching, he observed that large cold-crystallization exotherms of a size comparable to their melting peaks characterize the "even" nylons, whereas no significant cold crystallization exotherm could be seen for quenched "odd" nylons, which nontheless exhibited a melting endotherm. In other words, "even" nylons can be obtained in a completely amorphous state on quenching whereas crystallization would always take place in odd nylons. This was a clear indication of the large difference in crystallization rate for the two sets of nylons. On a general point of view, crystallization in polyamides is largely dictated by the polar amide groups and their coupling through hydrogen bonding in the solid state. And indeed, as stated in introduction, a major difference exists between the two families. Maximum molecular coupling can be achieved through hydrogen-bonding in both "parallel" and "antiparallel" configurations for nylon 11, as for other "odd" nylons, in the most

energetically favored extended conformation. No structural constraints limits the stabilizing effect of achieving maximum hydrogen bonding in a kind of ordered array. Since hydrogen bonding is believed to even persist in the melt[70] resulting in microregions of mixed "parallel" and "antiparallel" configurations, these regions may well be maintained during quenching and form some partially ordered domains in the solid state. This argument underlines the correlation between the fast kinetics of crystallization of "odd' nylons and their ability to easily achieve total hydrogen bonding in the pseudo-array of extended molecules indifferentiably of the molecular arrangement (parallel versus antiparallel). X-ray characterization of quenched nylon 11 confirms the formation of the smectic δ'-form during quenching (figure 1.5 or lower diffraction scan in figure 2.2). At the origin of partial chain packing disorder might be the spatially random arrangement of "parallel" and "antiparallel" molecules. In conclusion, DSC melting scans indicate that the high temperature melting peak observed on figure 2.1a can be undoubtedly attributed to the melting of the smectic form.

It was already said earlier how crystallization at slower cooling rates induced the appearance of a second endotherm (figure 2.1b) at the low-temperature side of the melting of the smectic. Annealing of a quenched specimen at temperatures below the melting of the smectic phase also induces a second endothermic peak at a lower temperature which is highy dependent upon the annealing temperature (Figure 2.7A). This is indicative of some morphological phenomenon associated with slow

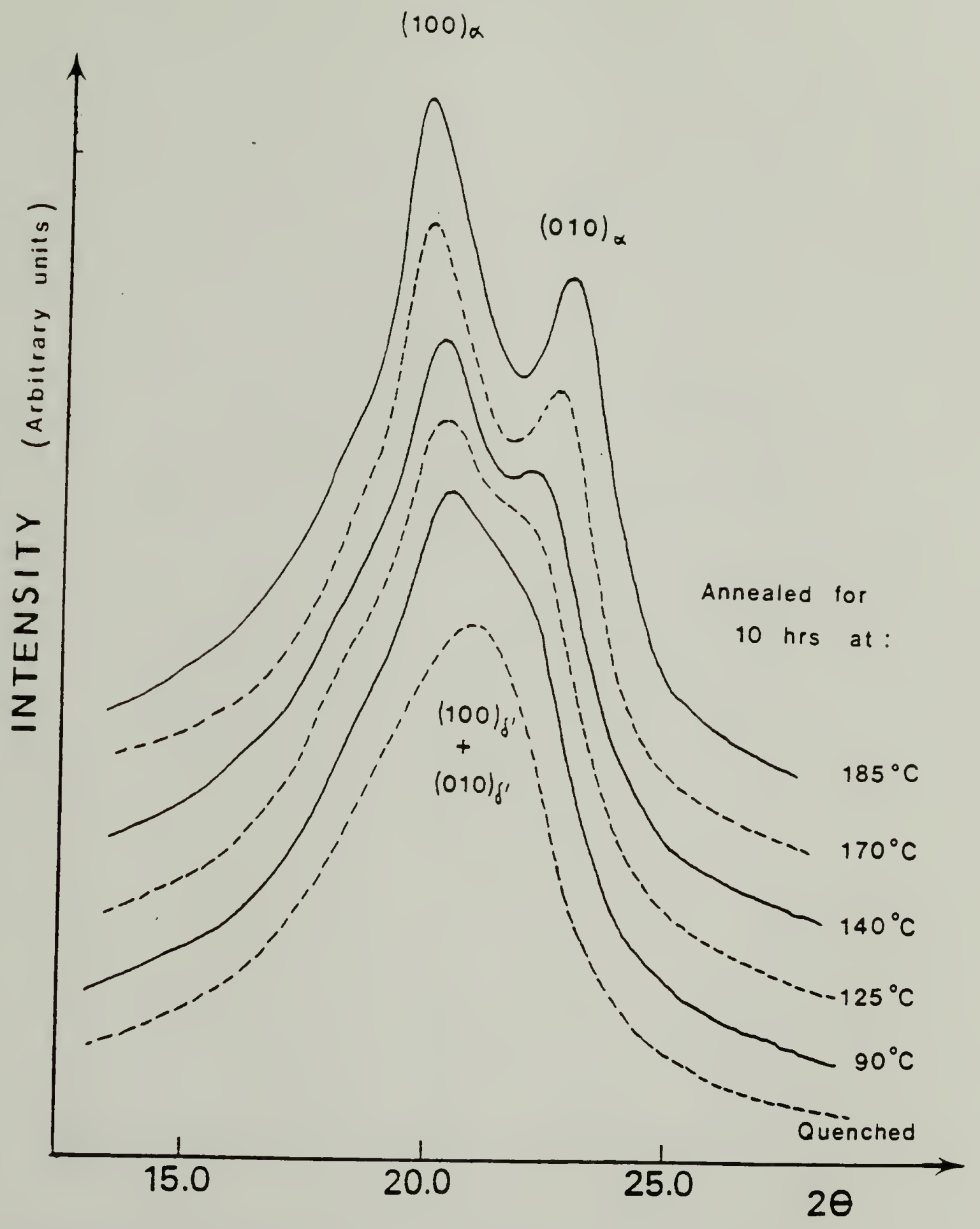

Figure 2.2. WAXD (θ-2θ) scans of quenched nylon 11 subsequently held at indicated temperatures (for 10 hrs). The range of d-spacings shown indicates changes in the lateral chain packing in the ordered lattice.

crystallization or with thermal annealing of the smectic form. Similar observations have been also reported for nylon 66[71] without definite explanation. Again, X-ray diffraction was used to investigate any change in the crystal structure. Figure 2.2 shows X-ray scans of nylon 11 samples quenched from the melt and subsequently annealed at several temperatures below T_m for 10 hours. Clearly, the broad peak characteristic of the smectic form (at $2\theta=21.0^{\circ}$) progressively splits into distinct peaks as the annealing temperature was increased which indicates an increase in the content of the crystals (α-form) at the expense of the smectic (δ'-form). Similarly, an increase in the amount of the α-form was found by decreasing the cooling rate. Therefore, the results of these combined studies suggest that two species of crystals are involved in the melting of nylon 11 for samples either slowly crystallized or quenched and annealed from the melt: The smectic modification (δ'-form) which is the high melting species and the crystal modification (α-form) which appears as the low melting species. The study by Chen and al.[69] revealed that, under hydrostatic pressures, the high melting species undergoes a phase transition into the low melting species before melting. Also the amount of material involved in the transition depends on the pressure. Our results indicate that the irreversible transition from smectic to crystal also partially takes place by simple thermal aging at atmospheric pressure even at temperatures below the melting peak of the smectic phase (figure 2.2). Figure 2.3 represents schematics for each ordered form of nylon 11 which describe the differences in molecular packing and in the mode of

hydrogen bonding. The higher melting temperature of the smectic compared to the crystal can be attributed to its lower entropy of melting as compared to the crystal (because of partial packing disorder). This of course supposes a larger difference in their respective entropies of fusion than in their enthalpies of fusion. Estimations of the thermodynamic parameters for each modification will be determined in the following chapter.

b) Effect of Time and Temperature of Crystallization on Melting.

Given the fact that crystallization of nylon 11 at intermediates conditions, that is between fast quenching and isothermal crystallization at low undercooling, induces formation of both smectic and crystal forms in various proportions , it is of interest to examine the relative changes on the heating scans for specimens crystallized under various conditions. A series of nylon 11 samples were crystallized from the melt at various degrees of supercooling. They were cooled rapidly (-150^{o}C/min) in the DSC cell down to five different temperatures, kept at constant temperature T_c for 5 min before being cooled rapidly to ambient. The consequent heating thermograms are plotted in Figure 2.4. Also shown for comparison is the melting endotherm of a quenched specimen. Several observations can be made from the variations in melting behavior as a function of crystallization temperature.

Figure 2.3. Schematic drawings (side-view and top-view) of nylon 11 crystallites in the smectic and crystals forms. The broken lines represent hydrogen bonding between adjacent chains (continuous lines). It describes the ordering process during the annealing of the smectic into the crystal form.

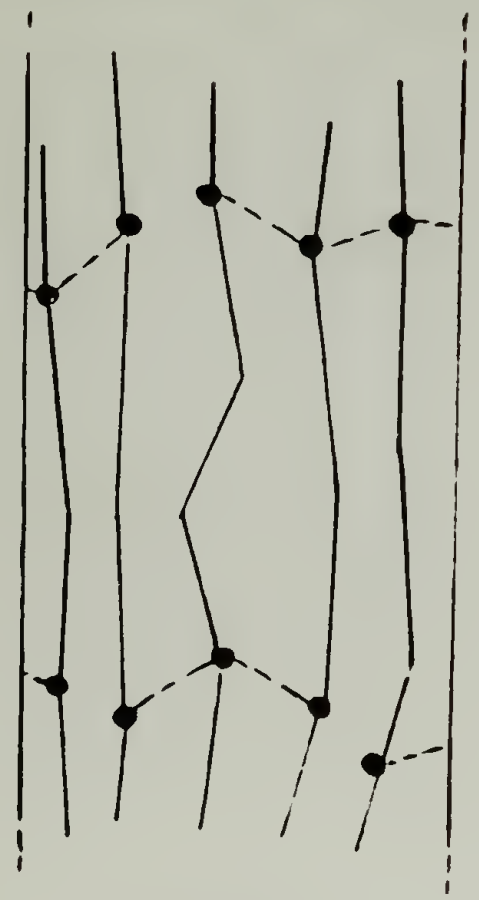

Smectic

δ'-form

thermal

annealing

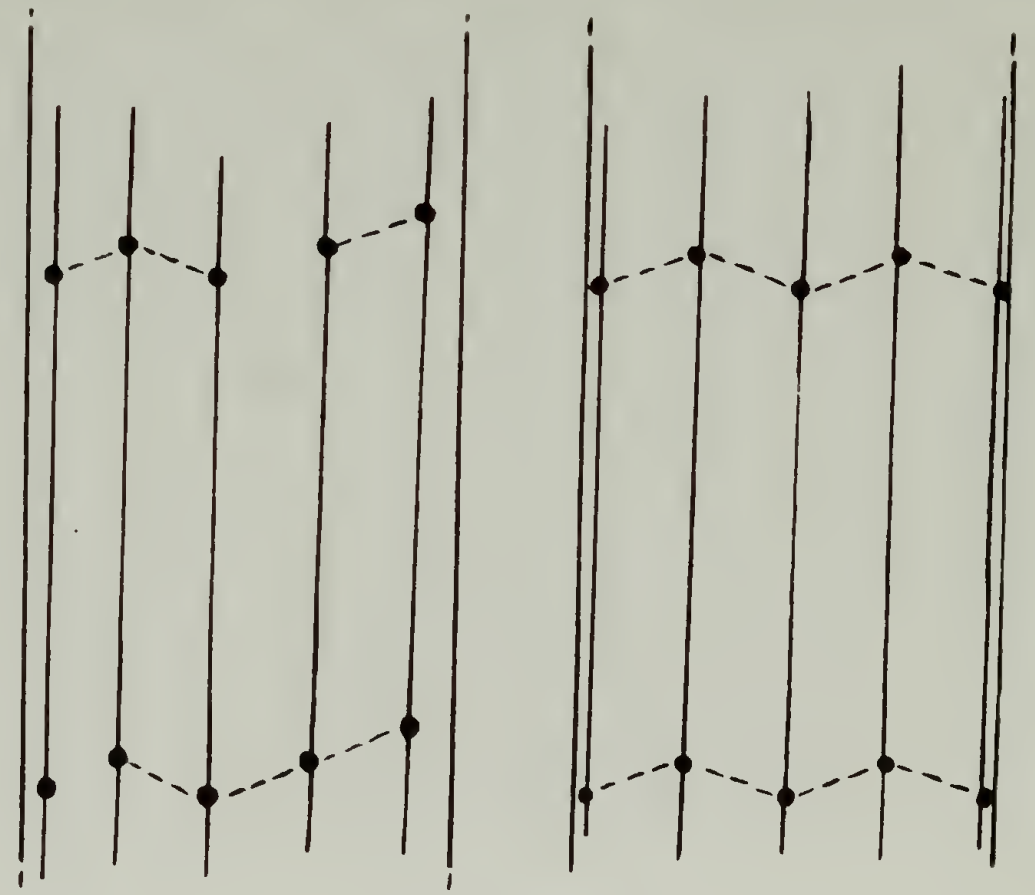

Crystals

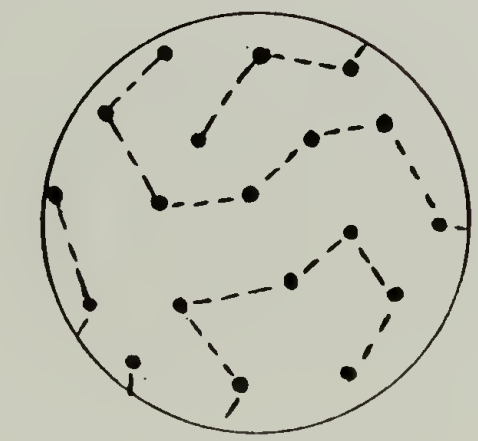

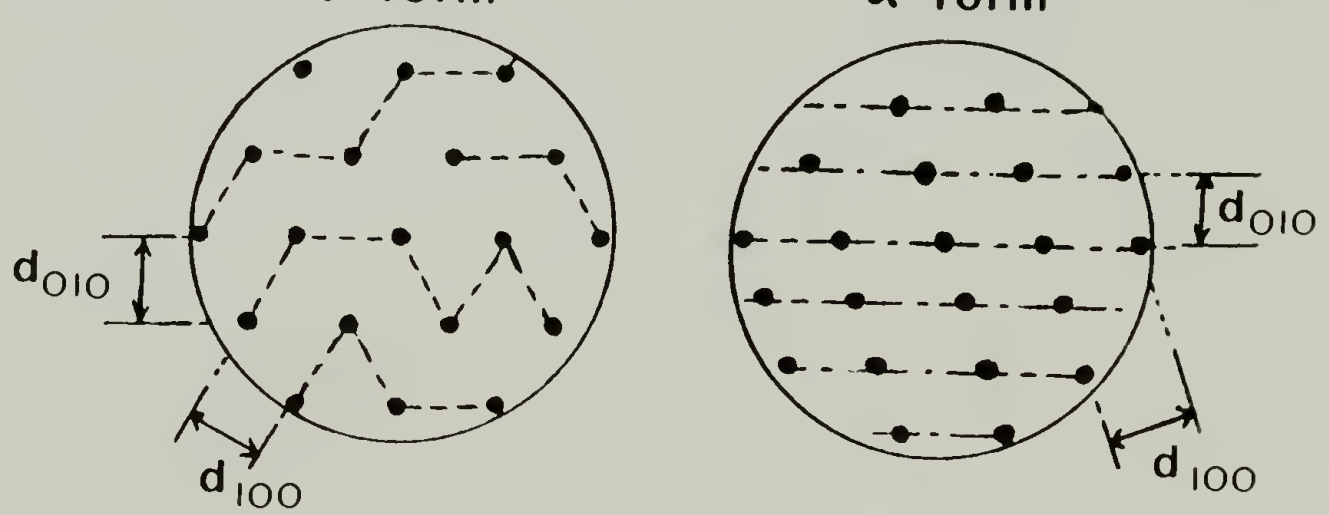

First, as expected, two superimposed melting endotherms are seen in the temperature range around 180°C, each representing the melting of fraction of both crystal and smectic present in the specimens. The high temperature peak characteristic of the smectic remains at an approximately constant temperature, but decreases in size as T_c was increased. At the same time, the low temp. melting peak increases in size and its maximum moved to higher temperatures. The double endotherm is again indicative of the competitive formation of both species in the crystallization process. Variations in the relative peak size indicate that a high degree of supercooling favors the formation of the smectic form, whereas a low degree of supercooling induces preferentially formation of crystals with the α-form.

Besides the two high melting endotherms discussed above, another small endotherm is also discerned at lower temperatures which shows the following characteristics: its onset is systematically located a few degrees above the chosen crystallization temperature and its size increases significantly with T_c. Since the formation of the α-form crystals is more directly dependent upon conditions of crystallization, it is reasonable to associate this thermal event to the fraction of α-form crystals present. Therefore, unlike the smectic form which exhibits a constant melting point, the α-crystals display important variations in their thermal behavior as a function of thermal history; And this reveals large possible morphological differences. The experimental scans in figure 2.4 illustrate that the higher the temperature of crystallization (the lower the supercooling), the higher

Figure 2.4. DSC heating curves at 10°C/min for nylon 11 crystallized from the melt (240°C) at various degrees of supercooling for 5 min and subsequently cooled to ambient. The heating curve for quenched nylon 11 is shown for comparison.

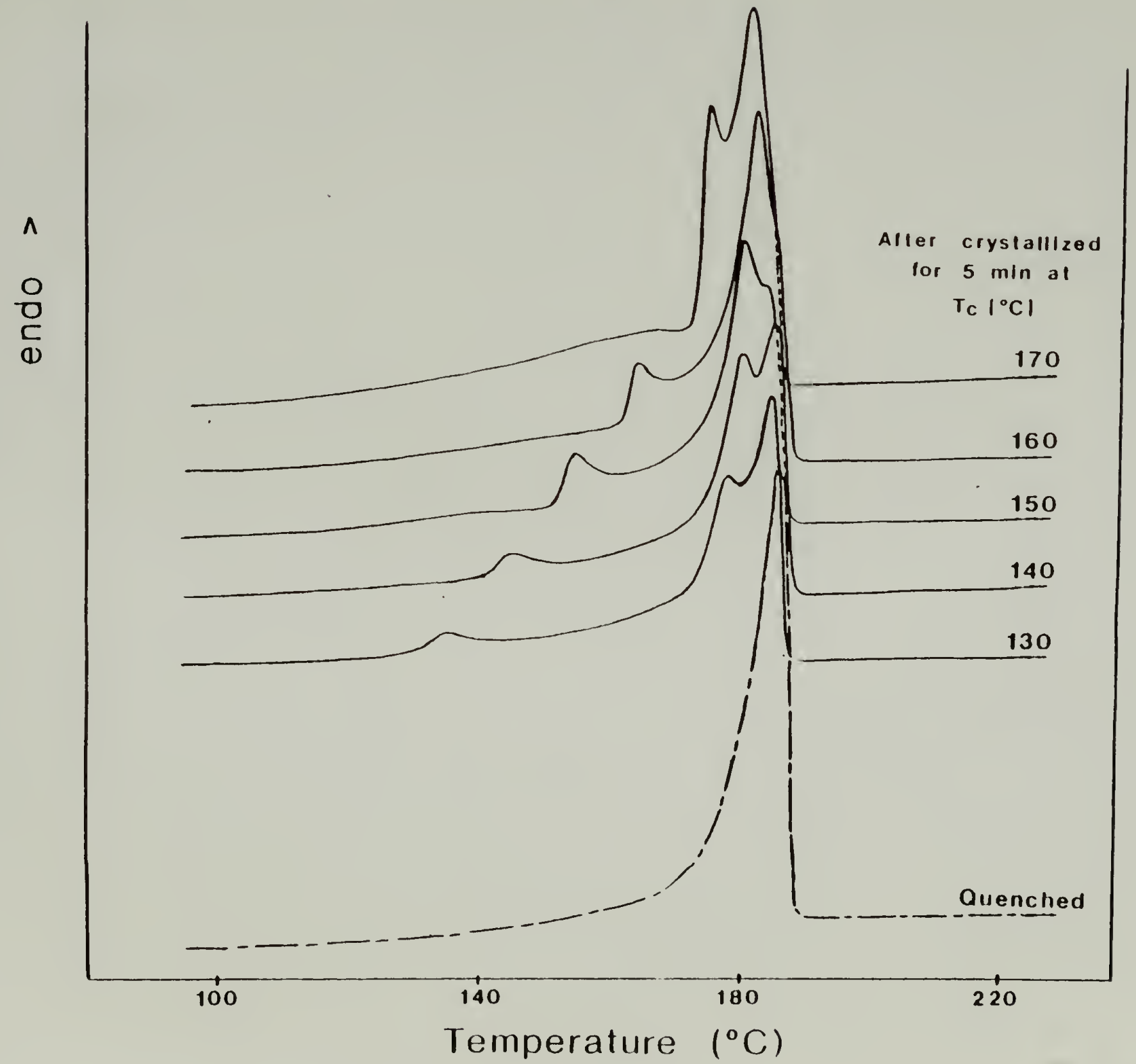
endo >
After crystallized
for 5 min at
Tc (°C)
170
160
150
140
130
Quenched
100
140
180
220
Temperature (°C)

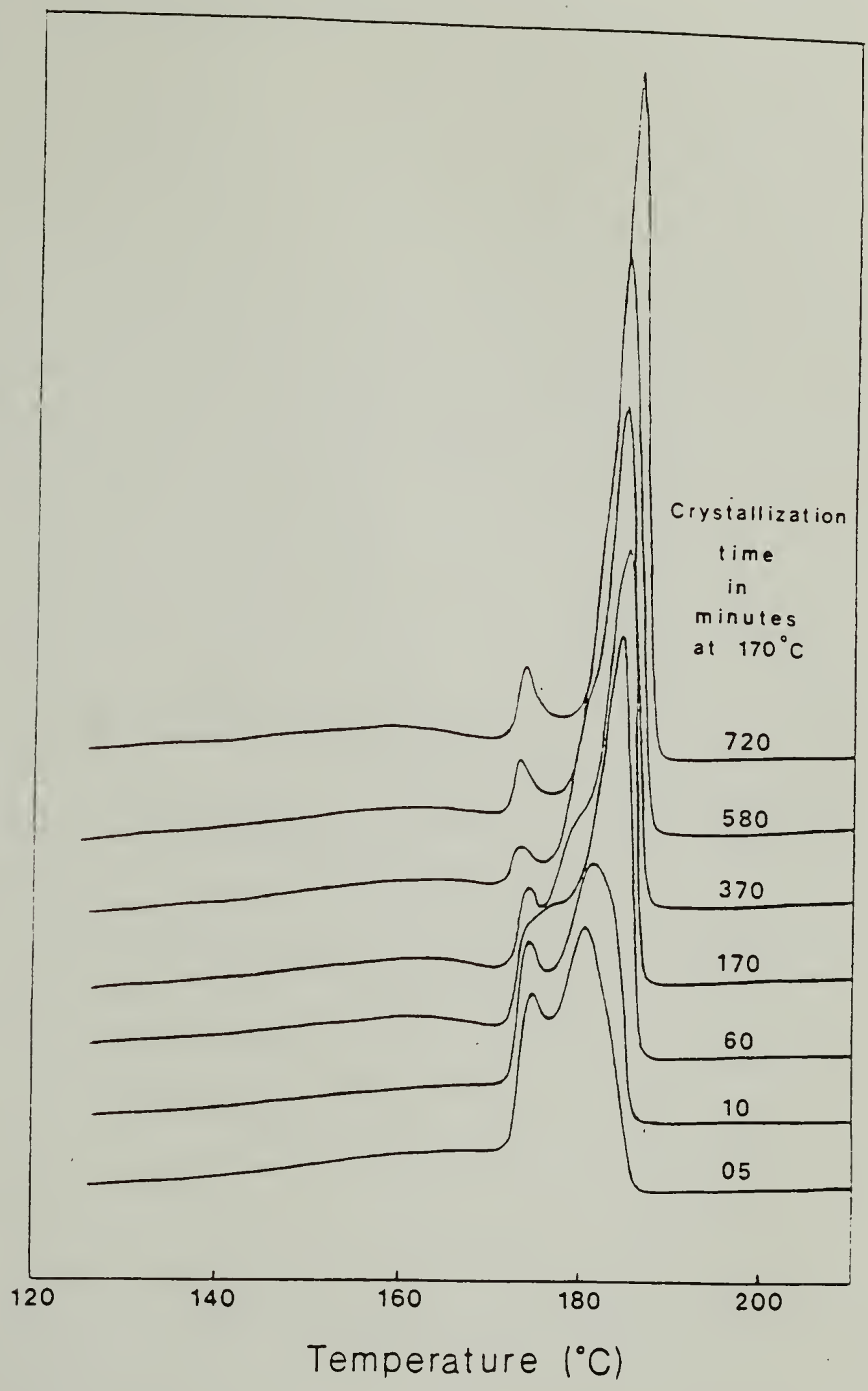

Figure 2.5. DSC heating traces at 10°C/min for nylon 11 isothermally crystallized at 170°C from the melt for various indicated amounts of time.

the temperatures for the two melting endotherms. And this can be interpreted as as an increase in size and perfection of the 3-dimensionally ordered crystals. The same effect is also seen in figure 2.5 for the low temperature melting peak characteristic of the α-crystals crystallized at 170°C for various amounts of time (before being cooled to room temperature). The peak temperature increases progressively with crystallization time up to values which can eventually exceed the melting point found for the smectic (≈187°C). Naturally, no smectic remains in such a specimen for it has totally transformed into crystal.

Returning to the heating curves of figure 2.4, two endotherms have been attributed to the fraction of crystals of the α-form present in each specimen. Comparable observations have been made in prior investigations by various authors for other polyamides[72,73], polyesters[74,75], isotactic polystyrene[76], PEEK[77] and poly(ε-caprolactone)[78], which have not systematically been understood. One interpretation given suggested double melting behavior on heating[77,78]. Namely, the low temperature endotherm corresponds to the melting of crystals that exist prior to heating (which is therefore highly dependent upon conditions of crystallization), whereas the high temperature melting peak is the crystals formed by simultaneous recrystallization during the heating scan[78]. On the other hand, Bassett and coworkers[79] recently offered a new interpretation based on the comparison of thermal analysis and electron microscopy for crystallized PEEK. They stated that the two melting peaks normally present in

crystalline PEEK represent different components of the morphology initially present prior to the heating scan. The dominant and other primary lamellae forming the architecture of the spherulite melt in the upper peak, whereas crystallites, which have been reorganized at the annealing temperature and thus melt just above this temperature, are located between them. The next set of experiments is designed to further investigate this conjecture.

c) Double Melting Behavior of α-crystals.

Rim and Runt[78] stated from their model that, if their conjecture was valid, scanning identical samples at various heating rates should induce a superheating effect on the melting of the original crystals (due to their low thermal conductivity). This would induce an increase of the low-T melting peak with heating rate. Also, a concommittant decrease of the melting point of the recrystallized material should result since shorter recrystallization times will affect the size and perfection of the recrystallized crystals and consequently lower their melting temperature. Data shown in figure 2.6 for the variations of the two endotherms of nylon 11 α-crystals crystallized from the melt at 166^{o}C for 60 min with heating rate are in accordance with expectations for the double melting model.

According to this model, recrystallization takes place on heating above the first endotherm. Nontheless, the shape of the

Figure 2.6. Effect of heating rate on the positions of the two endothermic peaks of nylon 11 α-crystals crystallized from the melt at 166°C for 60 min.

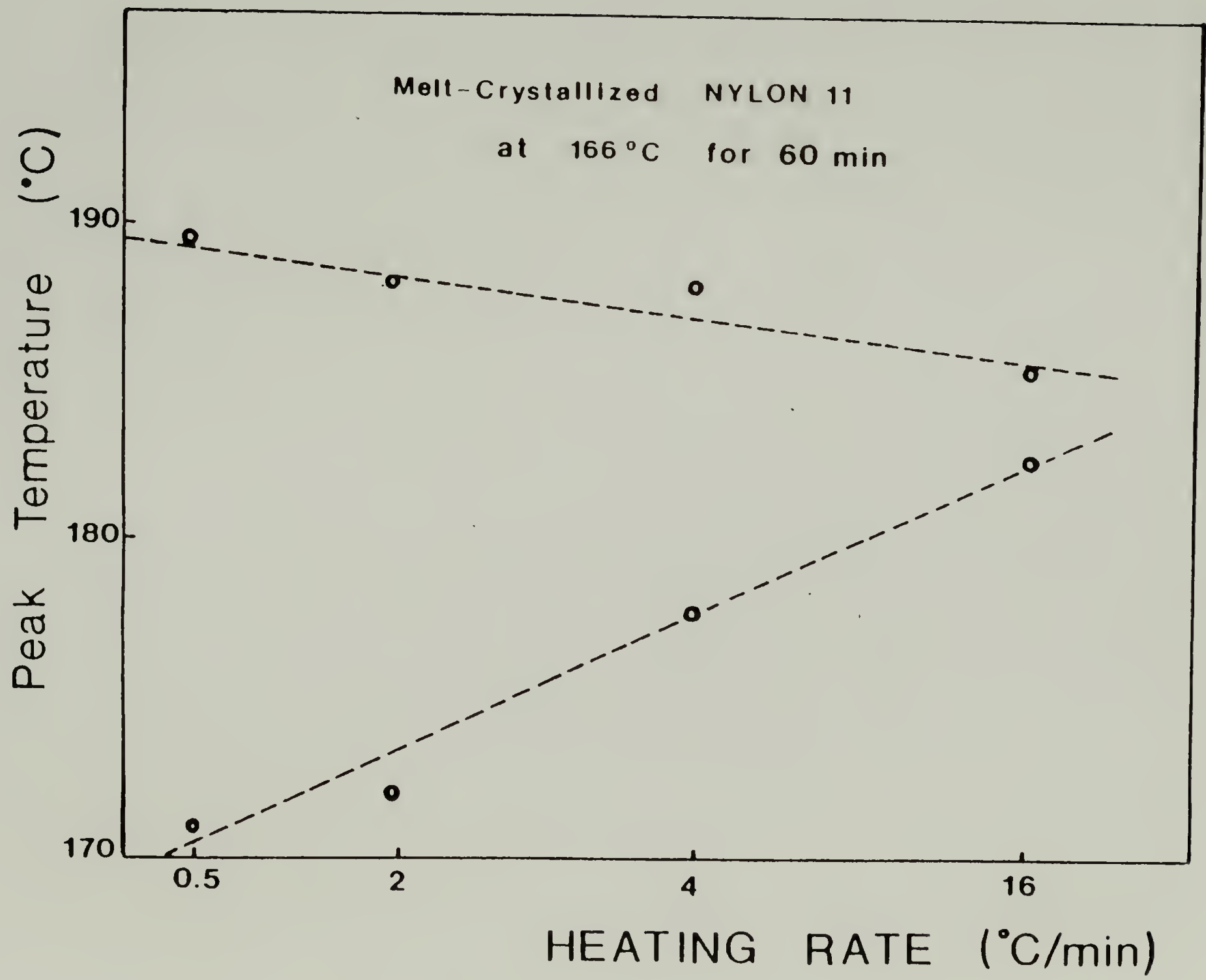
Melt-Crystallized NYLON 11
at 166 °C for 60 min
Peak Temperature (°C)
190
180
170
0.5
2
4
16
HEATING RATE (°C/min)

recrystallization exotherm cannot be measured directly by DSC, since only the net sum of two opposing contributions is detected. However, the following experiment can give an idea of the shape of the recrystallization exotherm. Four identical samples of nylon 11 were quenched from the melt and annealed at T_a=158°C for 10 hrs. Figure 2.7A shows their characteristic heating scan. According to our conjecture, the low melting endotherm corresponds to the melting of the fraction of α-crystals partially formed during annealing of the smectic at this temperature. For the three other samples, heating scans were stopped at the peak temperatures of the low- and high-temperature endotherms (2.7B and 2.7D, respectively) and in the middle of the two melting peaks (2.7C), whereafter all the samples were immediately cooled (-150°C/min) and rescanned. The three second scans are plotted together in Figure 2.7 and compared to the first scan. For all, the second scan shows a new melting endotherm at a temperature greater than the stopping temperature (T_s), due to the melting of material recrystallized up to T_s. This provides evidence that recrystallization occurs in conjunction with the partial melting of the crystals during heating (Figure 7B and 7C). In addition, thermogram 7D shows that crystals still form at T_{m2}, since a new sharp endotherm appears having a maximum just above T_{m2}. This suggests not only recrystallization of the original α-crystals during the heating run, but also a progressive ordering process in the smectic yielding the α-form. The two mechanisms might be at the origin of the broad endotherm corresponding to the melting of both transformed smectic and recrystallized crystals. In conclusion, the double melting

Figure 2.7. DSC heating curves at $10^{\circ}C$/min for quenched nylon 11 annealed at $158^{\circ}C$ for 10 hrs. Original trace is shown in **A**. Heating was stopped at the low-temperature melting peak for $\mathbf{B}_L$ at the high-temperature melting peak for **D** and between the two peaks for **C** ($175^{\circ}C$). When heating stopped, each sample was immediately cooled and the following scans were recorded.

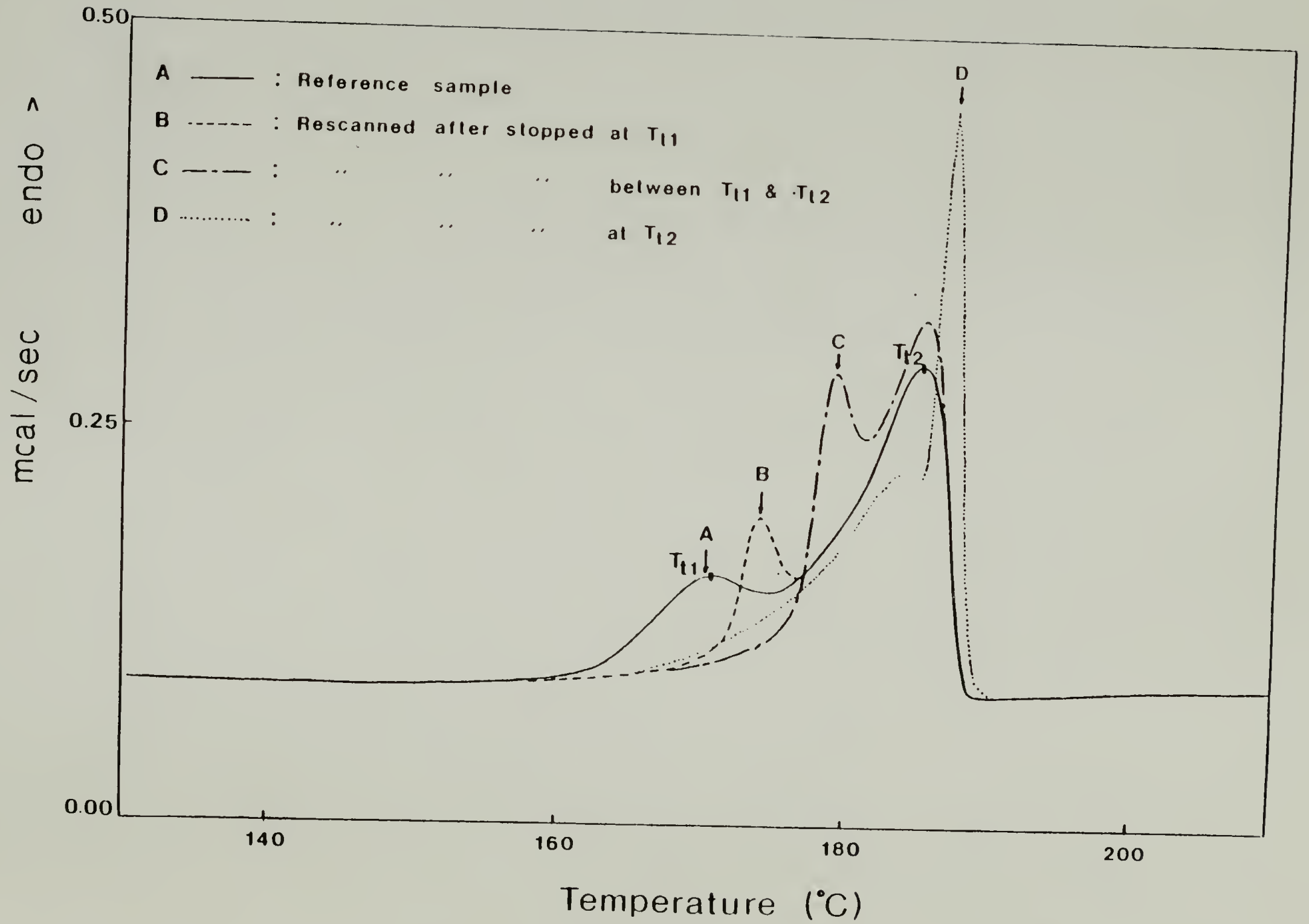
A ——— : Reference sample
B ------ : Rescanned after stopped at T_{t1}
C —·— : " " " between T_{t1} & T_{t2}
D ..... : " " " at T_{t2}
mcal / sec endo ^
0.50
0.25
0.00
A
B
C
D
T_{t1}
T_{t2}
140
160
180
200
Temperature (°C)

behavior model of Rim and Runt applies to the fraction of α-crystals in nylon 11 during heating, but is superimposed with the progressive transformation of the smectic also into the α-form. However, there is a difference in the heating curves for nylon 11 quenched and annealed (cold-crystallized) at T_a, and nylon 11 isothermally crystallized at T_c from the melt. The high melting peak has only one maximum in the first case (figure 2.7A,B,C), whereas it splits into two maxima in the second one (Figure 2.4). It could reflect morphological difference for a fraction of α-crystals prepared by each method. Therefore, Bassett's interpretation in the case of PEEK cannot be ruled out for nylon 11.

d) Effect of the α→δ Transition on Melting.

Next, the same nylon 11 samples were scanned at various heating rates and the traces are shown in figure 2.8. As the scanning rate is lowered, the first melting endotherm moves to lower temperatures and decreases in size until it disappears (eg $1^{o}C$/min). At this rate, the two opposing contributions of melting and recrystallization occur over the same temperature range and therefore cancel out. At high scanning rates, the low temperature endotherm moves up and, at $20^{o}C$/min, it appears beyond the melting endotherm of the smectic phase present. Such a significant superheating indicates a large kinetic effect for the melting of the α-crystals, which cannot be solely justified by a poor thermal conductivity.

Figure 2.8. DSC heating curves for quenched nylon 11 annealed at 158°C for 10 hrs, showing the effect of heating rate on the relative peak positions of the smectic and crystal endotherms.

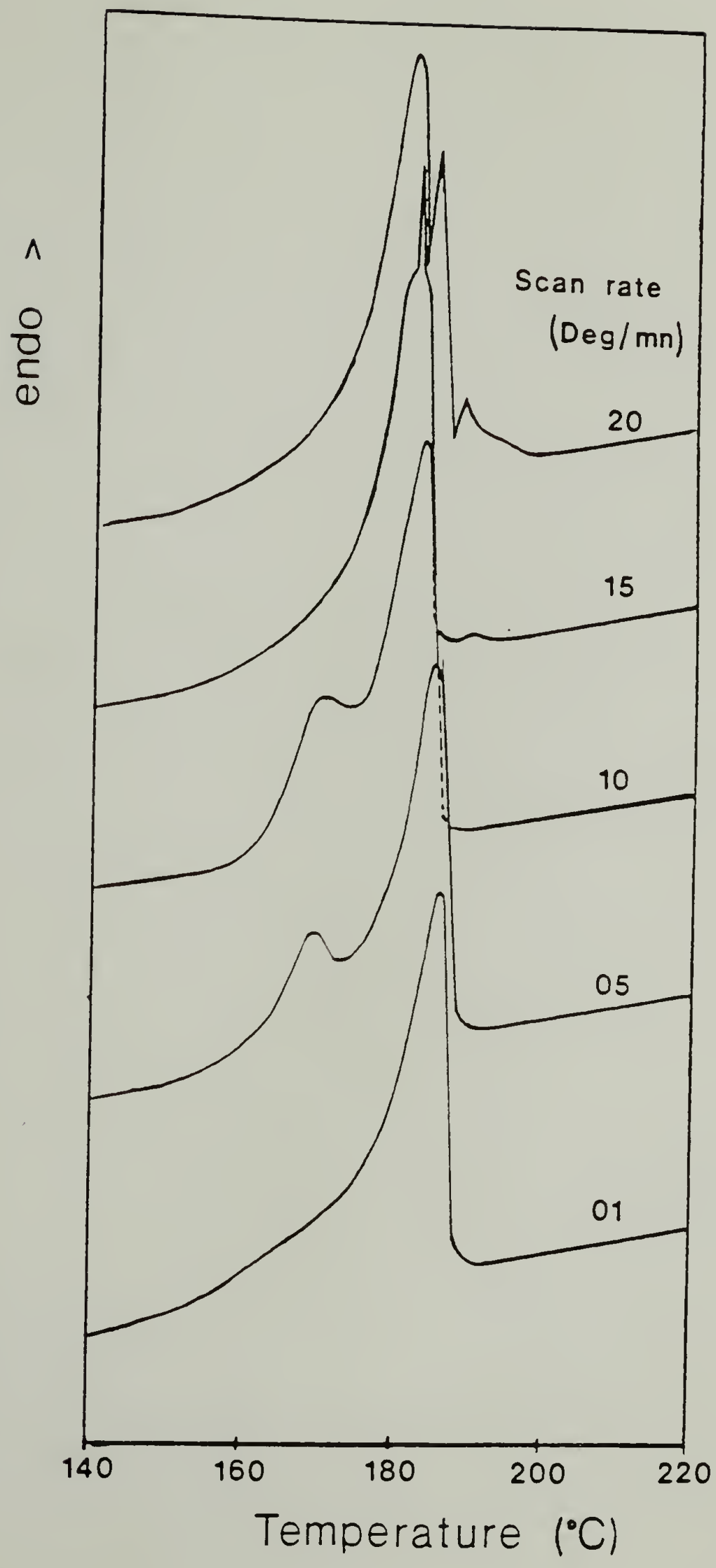
endo >
Scan rate
(Deg/mn)
20
15
10
05
01
140
160
180
200
220
Temperature (°C)

We recalled in the introduction that the crystalline phase was reported to undergo a reversible transition from the α-form to the δ-form at 95°C upon heating. To check whether this transition contributes to the superheating effect observed in figure 2.8, two identical samples were crystallized from the melt at T_c=158°C for 9 hrs to ensure maximum crystallization. The first one (Figure 2.9a) was then reheated directly from T_c (at 10°C/min), whereas the second (figure 2.9b) was first cooled to ambient at -150°C/min before rescanning (at the same rate). No apparent change is observed for the high temperature endotherm. However, the low temperature endotherm moves up by 5°C for the sample rescanned from the ambient and which thus has undergone α→δ crystal-crystal transition on heating. Therefore, this indicates a partial contribution of the crystalline transition on the observed effect of kinetics on melting. A detailed thermal study of the transition is presented in Chapter 3.

e) Crystallization Kinetics of Smectic and Crystal.

The first part of this study has provided experimental evidence of the formation of two distinct crystalline species and has defined the kinetic and thermodynamic conditions which control their crystallization and melting behavior. The melting behavior shown in figure 2.5 for nylon 11 crystallized at 170°C for various amounts of time before cooling to room temperature indicated the presence of both smectic and crystal present in the specimens for short crystallization

Figure 2.9. DSC heating traces at 10°C/min for nylon 11 melt crystallized at 158°C for 10 hrs, showing the effect of starting temperature of the scan on the α-crystals peak position. In **A**, scan was started from T_c; In **B**, scan was started from 50°C.

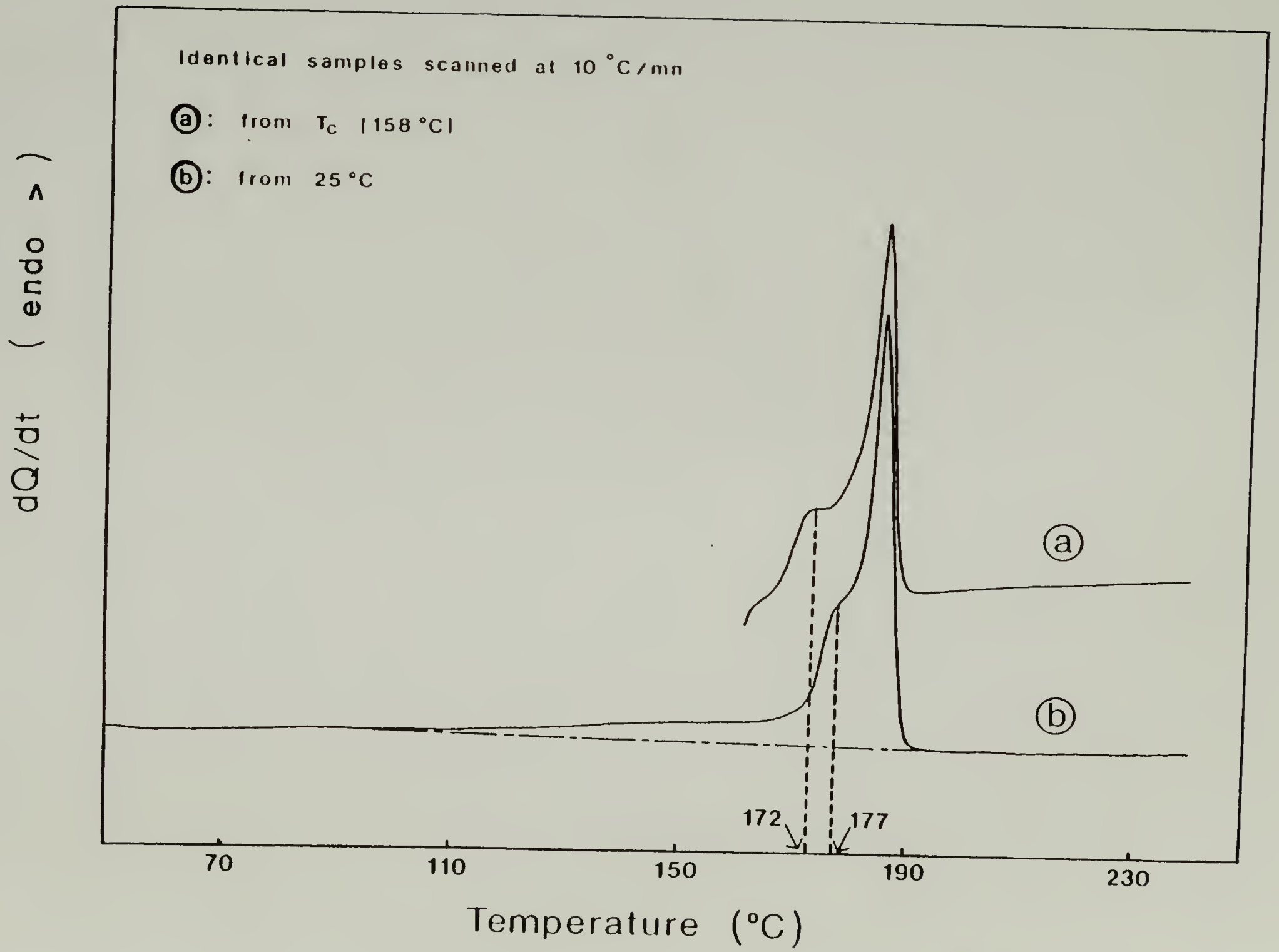
Identical samples scanned at 10 °C/mn
ⓐ: from T_c (158 °C)
ⓑ: from 25 °C
dQ/dt (endo >)
ⓐ
ⓑ
172
177
70
110
150
190
230
Temperature (°C)

times but as crystallization proceeds, the α-form content increases as its peak moves up and its size increases. Our objective here is to examine whether a kinetic study can distinguish between the kinetics of formation for the two crystallizing species.

Some data on the crystallization of nylon 11 have been previously reported by Inoue[80]. He found the crystallization exotherm peak at 160°C for a cooling rate of 6°C/min. He also reported the heat of crystallization to be equal to 9.6 cal/g corresponding to a degree of crystallinity of 17.7%. Figure 2.10 represents an isothermal crystallization trace for nylon 11 at T_c=170°C. Nylon 11 was cooled from the melt at -150°C/min in the DSC cell down to T_c and kept at this temperature while the crystallization was followed as a function of time. The T_c of 170°C was chosen since it corresponds to the highest possible supercooling for which crystallization did not start during cooling. The crystallization process shown in figure 2.10 maximizes after about three minutes and is mostly completed after 15 min. The broad shoulder just beyond the maximum signifies a possible exothermic molecular rearrangement within the crystalline entities while growth still proceeds.

To get a better insight of the crystallization under these conditions, nylon 11 was subjected to isothermal crystallization from the melt at 170°C for discrete amounts of time and subsequently heated directly from T_c. The position of the higher peak and the enthalpy of melting are plotted in Figure 2.11 as a function of log crystallization

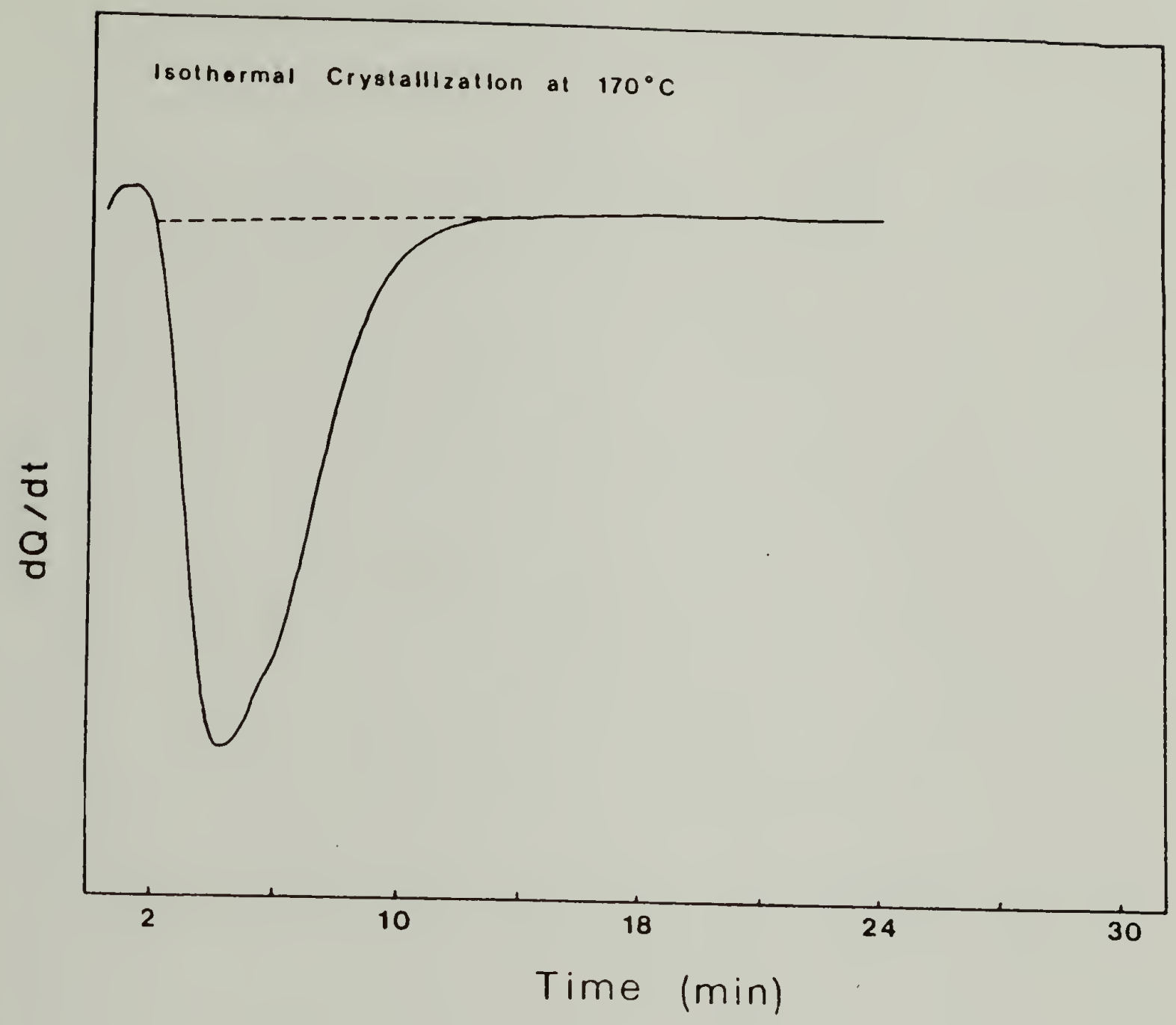

Figure 2.10. DSC isothermal crystallization exotherm for nylon 11 cooled to 170°C from the melt (240°C).

time. First, the variations in the enthalpy of melting indicate that crystallization essentially starts after 4 minutes and is for the most part completed after 15 minutes. Second, the melting temperature exhibits a sudden discete change of over 1°C after about 10 min that is when the crystallization rate reaches its maximum. It is not clear from these data whether the smectic δ'-form is a precursor of the α-form, or if the α-form forms directly from the melt at this crystallization temperature. Application of the Avrami theory[81] to the crystallization behavior of the α-form may indicate the nature of the process (homogeneous versus inhomogeneous) from the determination of the Avrami coefficient. However, for lower crystallization temperatures, an increasing fraction of smectic is formed which can convert into α-crystals on thermal annealing. For prolonged crystallization times, the simultaneous increase in both heat of fusion and melting peak clearly reflects additional crystallization from the amorphous phase as well as an increase in size and perfection of the crystals.

Gogolewski[68] previously reported results on the effect of annealing on the melting temperature, heat of melting and density of nylon 11 samples isothermally crystallized at 175°C for 20 hours and subsequently annealed at 180°C for various amounts of time. His results are shown in figure 2.12. Our results represents an extension of his study for short crystallization times and a good agreement found in the overlapping regions of the two studies. His additional characterization by optical microscopy and small-angle X-ray scattering allowed him to conclude that nylon 11 had formed lamellar spherulites of the α-crystalline

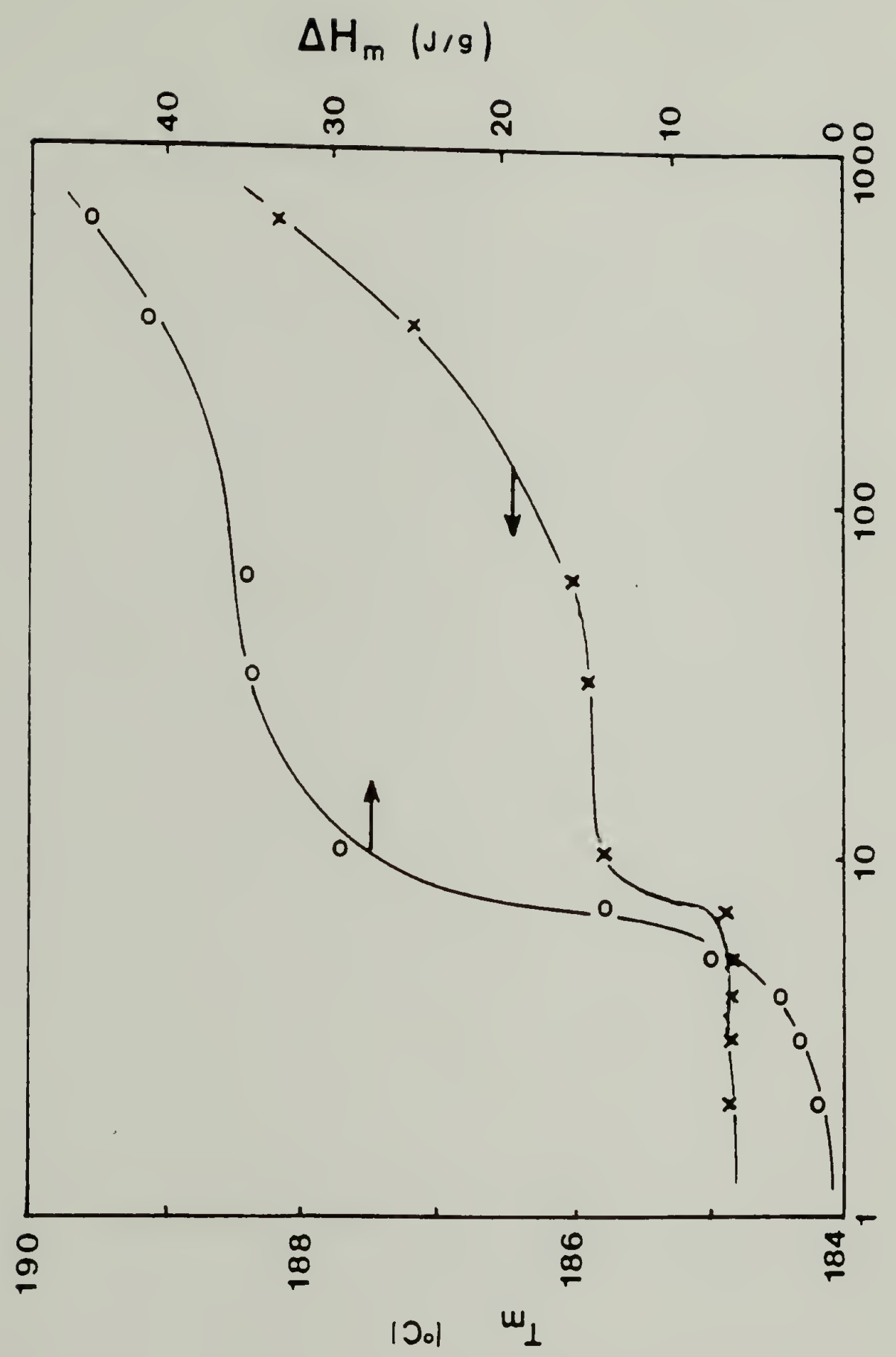

Figure 2.11. Melting peak temperature and heat of fusion versus crystallization time for nylon 11 crystallized at 170°C from the melt (240°C).

modification and that the thickness of the lamellae had increased with time of annealing from 50 to 165Å (for 20 and 2000 hours respectively). He reports an extrapolated heat of melting of the crystalline phase of nylon 11 to be 47 cal/g.

4) Conclusions.

This study first clearly reveals how Differential Scanning Calorimetry can successfully resolve the different crystalline polymorphs in melt crystallized nylon 11 from the melting behavior. Indeed, polymorphism is found to be partly at the origin of the dual melting behavior. Thermal history is found to drastically influence the structure and morphology of the crystalline phase of nylon 11 and its melting. Results concerning each phase can be summarized as follows.

The semiordered smectic δ'-form is kinetically favored and forms rapidly on quenching. The rationale for its formation comes from the ability of molecules to easily maximize hydrogen bonding without severe geometrical constraints. The gain in energy must compensate for partial disorder in the packing of the hydrocarbon segments along the chain. Its melting point is found at 187°C.

The formation of the three-dimensional crystal form (α-form) is thermodynamically driven and can be obtained either by slow crystallization from the melt or from an ordering of the metastable smectic modification by thermal annealing. Double melting behavior has been observed for this crystalline form and was found to depend largely

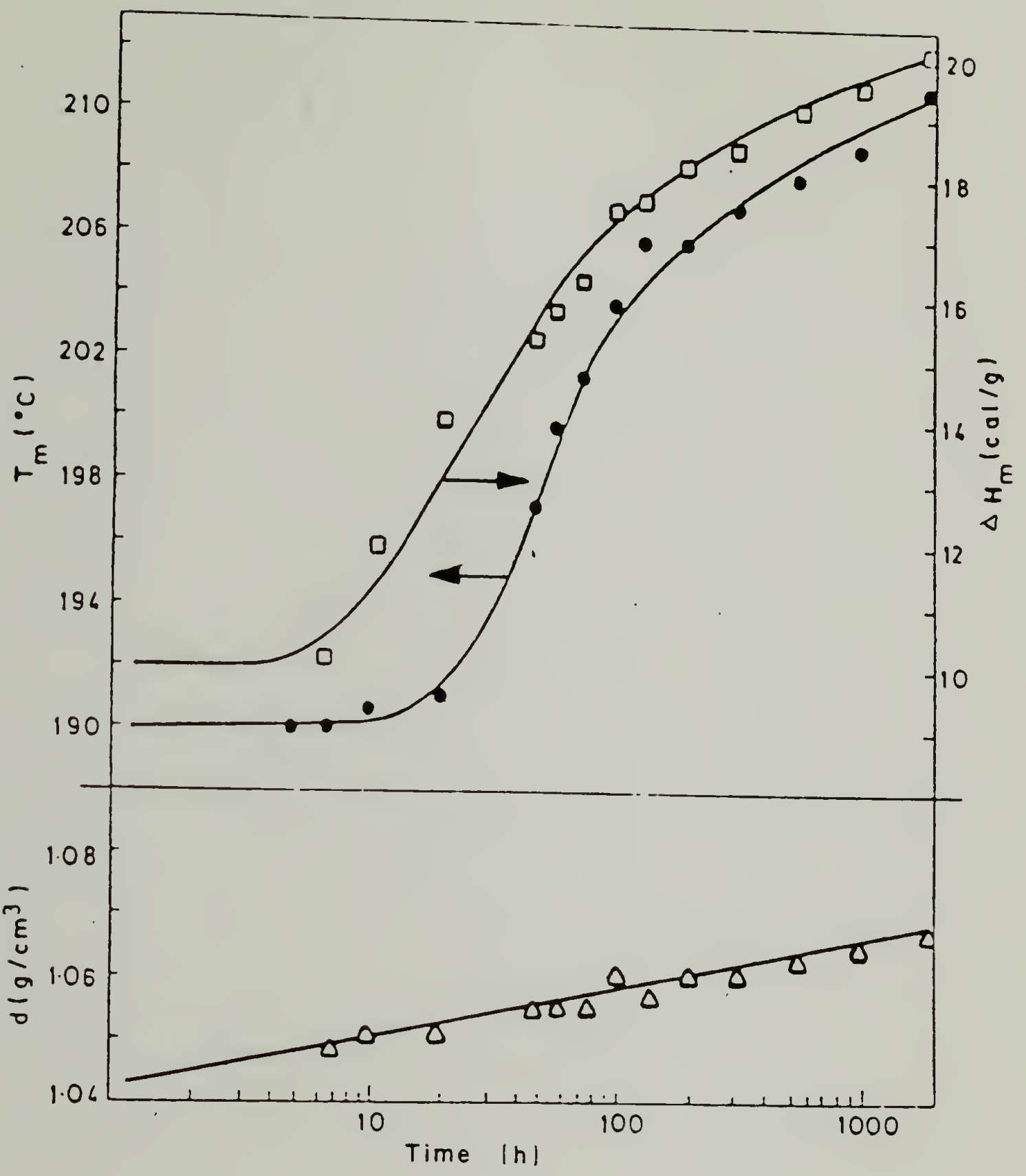

Figure 2.12. Effect of annealing time on peak maxima, heat of fusion and density of nylon 11 crystallized at 175°C and annealed at 180°C. (After Gogolewski)

on crystallization conditions. The model by Rim and Runt can be used to explain the origin of it in terms of the superimposition of melting, recrystallization and remelting processes. However, differences in morphology cannot be ruled out. Note the the melting points are lower than for the smectic when the two form coexist.

The crystal-crystal transition reported at 95^{o}C and investigated in the next chapter has been shown to significantly affect the kinetics of melting of the α-crystals. Superheating of over 20^{o}C has been observed.

Our kinetic study of crystallization at 170^{o}C does not clearly indicate whether the transient formation of crystalline species with smectic order also takes place in the case of slow crystallization.

C H A P T E R III

THERMAL ANALYSIS INVESTIGATION OF THE α↔δ TRANSITION AND DETERMINATION OF THERMODYNAMIC PROPERTIES OF NYLON 11

1) Introduction.

The existence of two distinct crystalline structures in nylon 11 crystallized from the melt has been reexamined by means of DSC in the previous chapter. Thermal analysis appeared to be a sensitive method to evaluate the melting and crystallization behavior for both metastable smectic δ'- and stable crystal α-forms. It clearly showed qualitatively how various proportions of the two forms are obtained for different crystallization conditions and thermal history. Finally, an attempt was made to justify the characteristics of each form in terms of the thermodynamics and kinetics of hydrogen bonding in an ordered lattice.

In this chapter, Differential Scanning Calorimetry is used to reconsider the nature of the reversible transition in the crystals between the low-temperature α-form and the high-temperature δ-form. The existence of this transition was first revealed in the case of nylon 11

by Newman and co-workers[63,82] and later confirmed by Katz & Gelfandbein[83,84]. At this temperature, the low temperature triclinic α-form is believed to reversibly transform into the high temperature pseudohexagonal form (denoted the δ-form) on heating. The latter cell was described as being also triclinic with the $\underset{\sim}{c}$-axis of the polymer chains remaining tilted with respect to the ($\underset{\sim}{a}$,$\underset{\sim}{b}$) plane, but with an hexagonal projection of the unit cell on the plane normal to the $\underset{\sim}{c}$-axis. This was deduced from X-rays observations of the variations of the d-spacings with temperature for the two reflections (200) and (010) which describe crystallographic directions perpendicular to the chain axis. Figure 3.1 shows the results as reported by Katz & Gelfandbein[83] which also include the temperature dependence of the $\underset{\sim}{c}^{*}$-axis. The anisotropic thermal expansion of the initial crystals in the α-form at low temperatures between 20°C and 95°C, causing the two X-ray reflections to approach each other and finally merge at 95°C, becomes isotropic at 95°C and remains such on a further increase of temperature. It led the authors to conclude on the formation of a laterally isotropic structure stable up to the melting point which they called the δ-form.

This transition is undoubtetly reminiscent of the Brill transition, as it came to be known for the α-form of a particular even-even nylon, namely nylon 66, since its discovery by Brill in 1942[85]. Considering the striking similarity in the diffraction patterns fo the "odd" nylons (nylon 7, 9 or 11) and even-even nylons (nylon 66, 610), as noted by Kinoshita, this may not be fortuituous. This transition in nylon 66 has

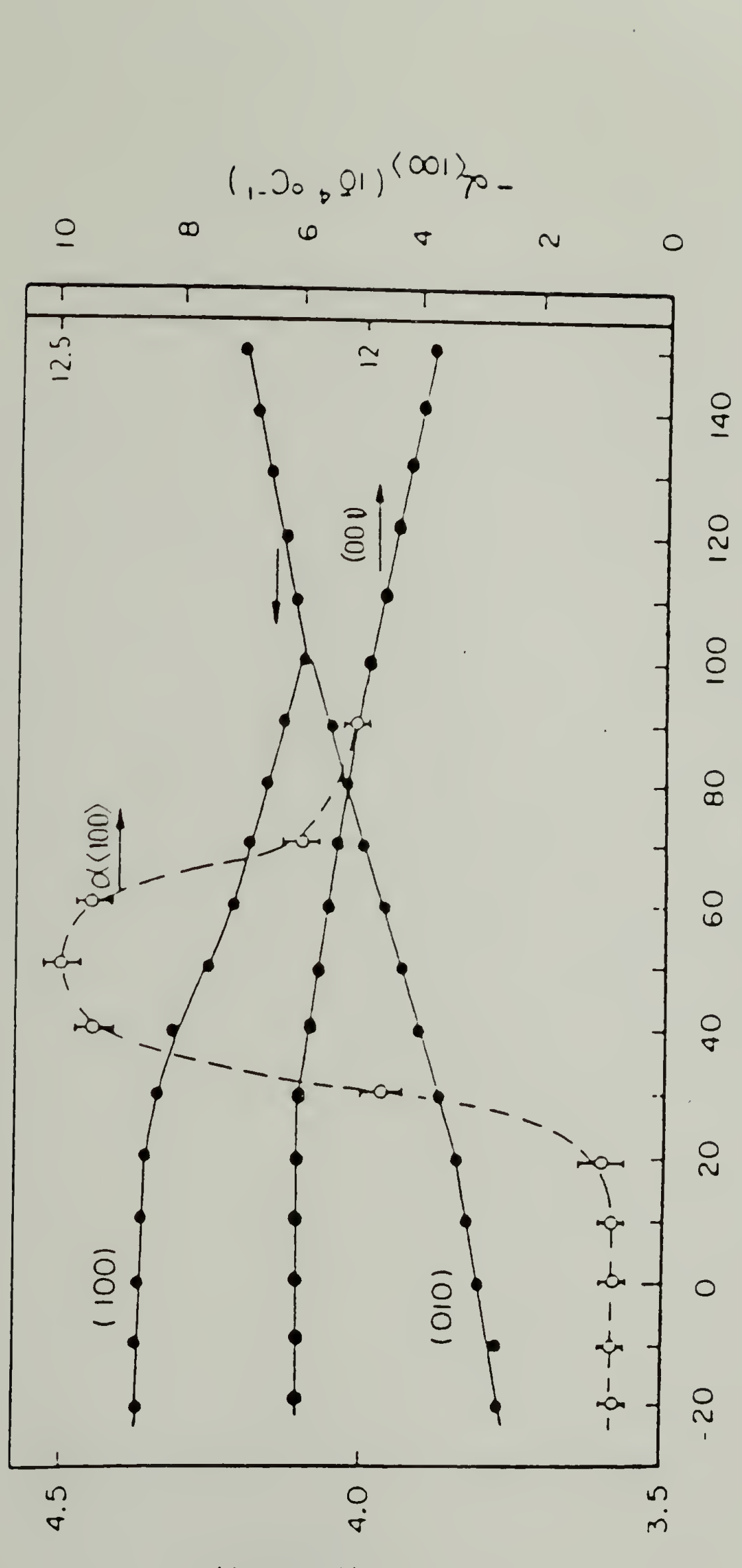

Figure 3.1. Variations in d-spacings (for (100), (010) and (001) reflections) and thermal expansion coefficient (in the (001) direction) for nylon 11 in the α-form. (after Gelfandbein and Katz)

since its first discovery received the attention of many researchers who tried to understand the mechanism and the origin of this transition. This however led to a great deal of contention, as the temperature of the transition was reported variably from 100°C to 240°C, and appeared to be sensitive ot the crystallization, annealing and deformation history of the sample. Also, the original interpretation of the phenomenon proposed by Brill[85] and later confirmed by Schmidt[64], who had postulated the formation of a "temporal (dynamic) three-dimensional network of hydrogen bonds in the high-temperature symmetrical structure" (as opposed to the layered structure of hydrogen bonds in the α- form at low temperatures), was later on reconsidered by other authors. Despite the variety of characterization techniques used such as X-ray diffraction[86], spectroscopic techniques such as solid state NMR[87-89] or IR[86], or birefringence[90], the mechanism of this transition still remains very controversed.

The resembling phenomenon observed in nylon 11 is also contentious. Because of its polar structure, the α-form was expected to display significant piezo- or pyroelectric properties. The rearrangement in the mode of hydrogen-bonding at the "Brill transition", however, should make it a Curie point for this material. Failure to observe such a change by Scheimbein[91,92] raises questions about the validity of the phenomenon. Also, Newman and his co-workers earlier denied such a transition for nylon 11 α-crystals cast from a 15% solution in m-cresol[82]. This throws some doubt concerning the actual nature of such a crystal-crystal transition.

No study has yet reported on thermal effects in the temperature region of this transition in the case of nylon 11. In the case of nylon 66, there has been some early reports of a small latent heat associated with the Brill transition[94,95], but no study of its thermodynamic properties. Recently, Starkweather et al.[95] measured a latent heat of about 4.5 cal/g at the Brill transition near 200°C for nylon 66 powders crystallized from solution. However, they were unable to expain the disappearance of the endotherm in the second heating run after the sample was heated at temperatures above 245°C. The focus of this study is to report some thermal observations of this transition in the case of melt-crystallized nylon 11 which bring new insight about its nature.

Finally, the experimental values measured for the enthalpy of transition are used to quantitatively derive the thermodynamic properties of transition between the two crystalline polymorphs. Also, a method is proposed to quantitatively evaluate the difference in enthalpy of melting between the smectic and the crystal forms from the experimental values of heat of fusion measured for two series of nylon 11 specimens prepared with different thermal history.

2) Experimental

The nylon 11 specimens and thermal analysis technique used in this chapter are exactly identical as in the first part of the study introduced in the experimental section of the previous chapter. Again,

the specific thermal treatments applied are described when needed in the course of the next paragraph. The refractive index of the hot-rolled film of nylon 11 were measured in the three principal directions with an Abbe refractometer with the temperature controlled by a thermostated fluid. ^{15}N CP/MAS NMR measurements mentioned later were made at the University of Southern Mississipi in collaboration with Prof. Mathias[89].

3) Results and Discussion

Transitions between phases of different symmetry are usually first order transitions. More specifically, a transition between two different crystal modifications is usually effected by means of a sudden rearrangement of the crystal lattice and therefore induces a discontinuous change in the state of the body. The change from one phase to another is accompanied by the evolution or the absorption of the heat of transition which should be proportional to the amount of crystals undergoing the transition. This heat is detected and reproduced as exo- or endothermic peaks in a DSC thermogram.

Figure 3.2 shows the typical thermogram of nylon 11 when it is cooled down from the melt (at $-10^{\circ}C$/min). Besides the large crystallization exotherm which exhibits a minimum at $153^{\circ}C$, a small exotherm can also be depicted in the temperature range around $95^{\circ}C$, which matches the temperature range previously reported for the $\delta \rightarrow \alpha$ transition. Our goal is examine this exotherm in more details. We want to know:

Figure 3.2. DSC cooling curve at -10°C/min for nylon 11 crystallizing from the melt. Note the low-temperature exothermic peak at 95°C in addition to the crystallization exotherm at 153°C.

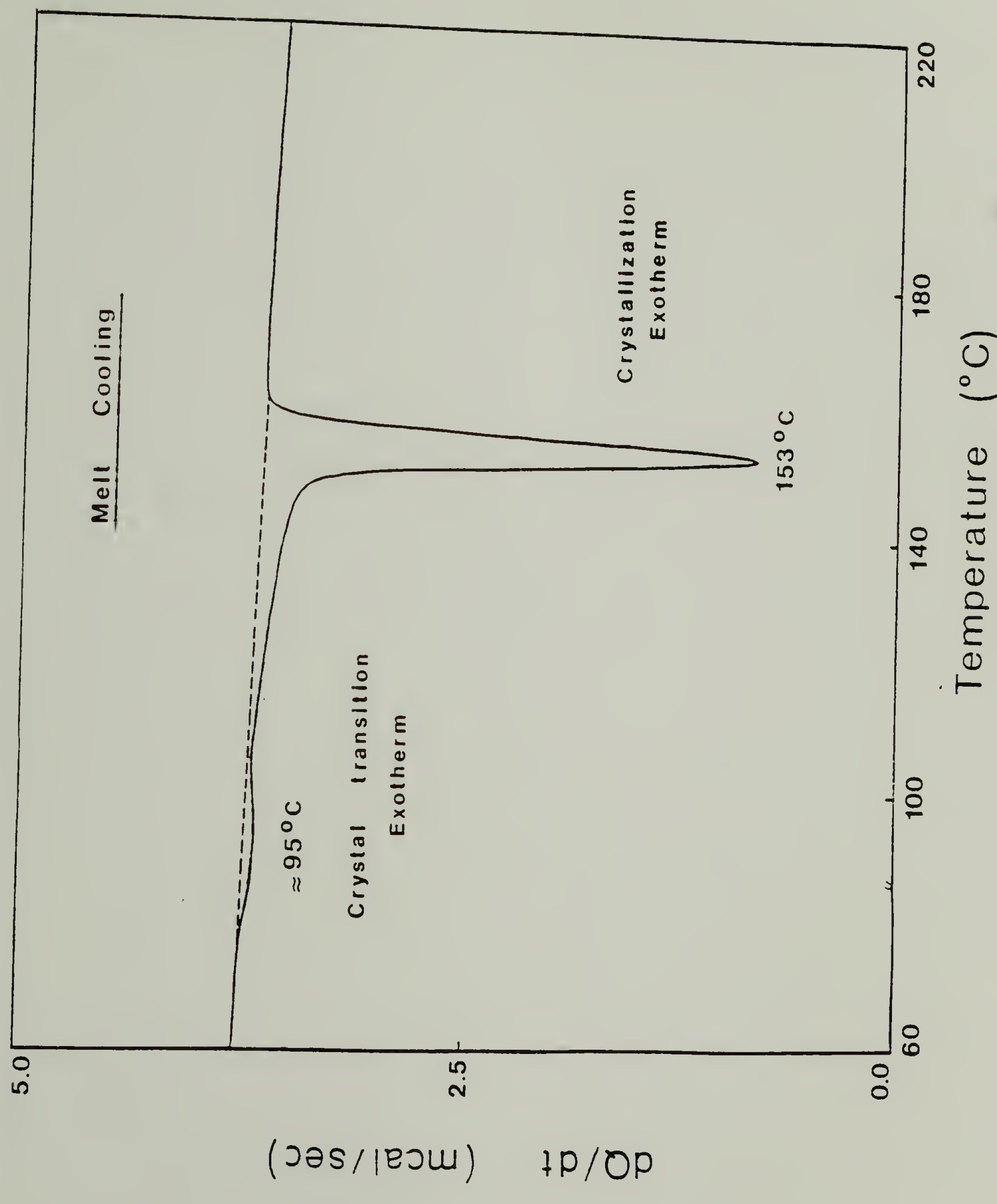
Melt Cooling
Crystallization Exotherm
153°C
≈95°C
Crystal transition Exotherm
5.0
2.5
0.0
dQ/dt (mcal/sec)
60
100
140
180
220
Temperature (°C)

i) whether the exotherm truly represents heat evolved during the crystal-crystal transition.

ii) get some insight concerning the nature of the transition by varying samples and scanning conditions.

a) Nature of the Transition Exotherm.

The temperature region of the crystal-crystal transition was first investigated for nylon 11 fast quenched from the melt in a mixture of dry ice and acetone. This process was shown to yield the smectic form of nylon 11 in the previous chapter. Following quenching, the sample was slowly heated up to 170°C (at the onset of melting of the smectic) and finally scanned on cooling down to 50°C. The same sample was also subsequently heated up successively to several increasing temperatures from 170°C to 184°C and each time rescanned on cooling in the same conditions. The procedure induces melting of an increasing fraction of smectic and recrystallization in the α-form because of the slow cooling rate of the scan. The experimental cooling curves are reproduced in figure 3.3. Also shown on the same scale is the melting endotherm for the smectic. First, figure 3.3 shows an increase of the crystallization exotherm obtained after heating to progressively higher temperatures and confirms the increasing amount of melted smectic on heating. Also, the recrystallization seems to be faster, the larger the fraction of the smectic remaining in the specimen (which can help

Figure 3.3. DSC cooling curves at -10°C/min for quenched nylon 11 from increasing temperatures over the melting region of the smectic form. Also shown on the same scale is the melting endotherm of quenched nylon 11 smectic form.

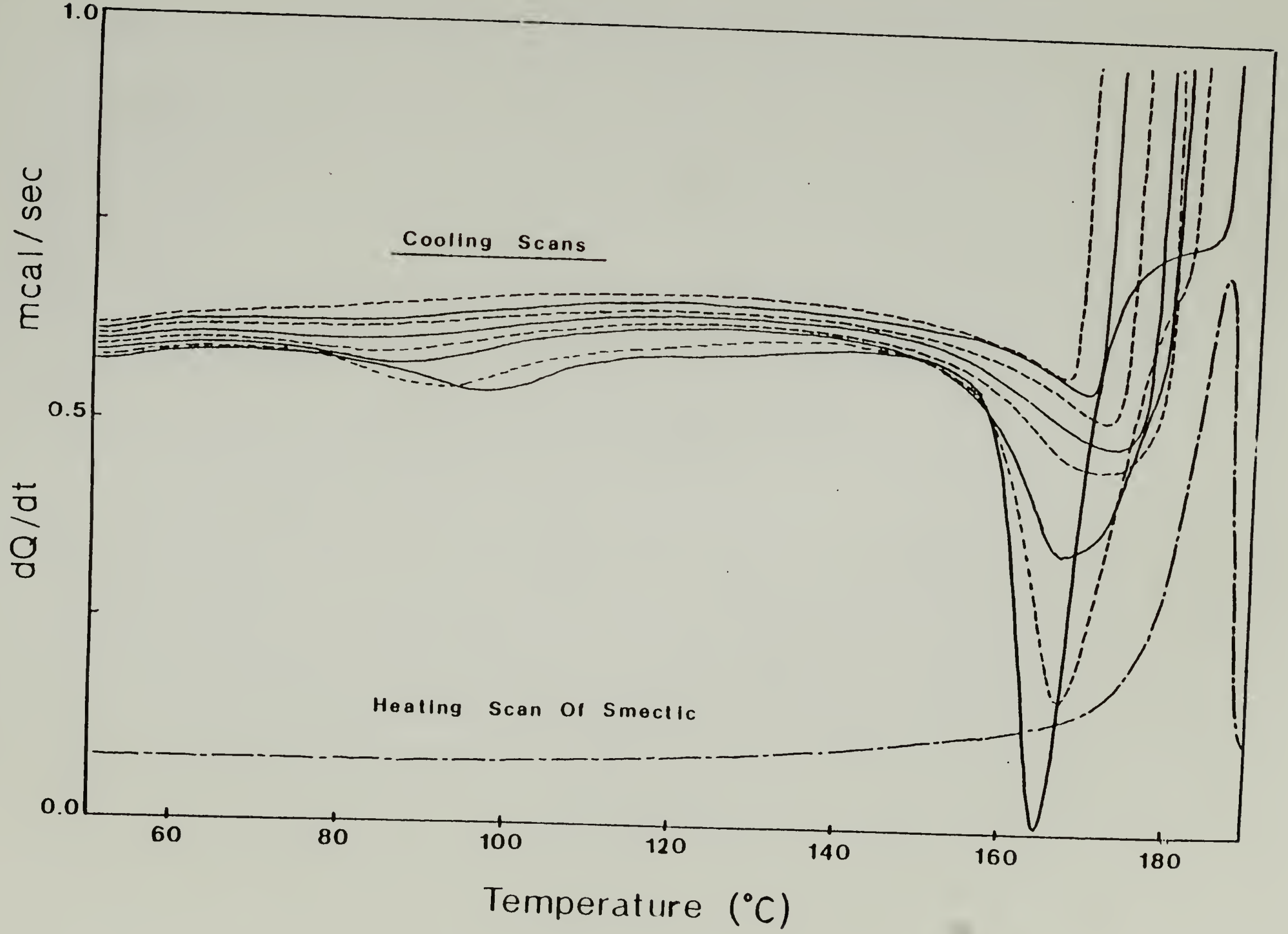
1.0
0.5
0.0
dQ/dt mcal/sec
Cooling Scans
Heating Scan Of Smectic
60
80
100
120
140
160
180
Temperature (°C)

nucleate the new crystals), as indicated by the higher temperature of the crystallization peak.

Second, the region of the crystal transition around 95°C is shown in magnification on figure 3.4. No transition exotherm appears during the cooling of the smectic (from 170°C). However, the larger the conversion from smectic to crystal before scanning over the transition domain, the larger the size of the transition exotherm. Therefore, these observations not only provide another experimental evidence of the formation of two distinct ordered species (smectic δ'-form and crystal α-form) in various proportions depending on cooling conditions; But they also provide evidence that the transition observed at 95°C is exclusively associated with the crystals present in the specimen, for the smectic form undergoes no change at this temperature. Consequently, the α→δ transition may provide an absolute method to evaluate the fraction of crystals present in the crystalline phase of nylon 11.

b) Thermal Characterization of the Transition.

For this purpose, a nylon 11 sample was prepared in the following way: it was first isothermally crystallized from the melt for 20 hours at 170°C and slowly cooled down to 50°C, prior to any temperature scan. Such a preparation favors the selective crystallization of crystals in the α-form. Also ,no crystallization exotherm is expected to superimpose to the transition exotherm on cooling, if no melting takes place. Typical heating and cooling runs

Figure 3.4. Magnification of the crystal transition exotherm in the cooling thermograms of figure 3.3. Indicated are the increasing temperatures to which quenched nylon 11 was successively heated prior to each cooling run.

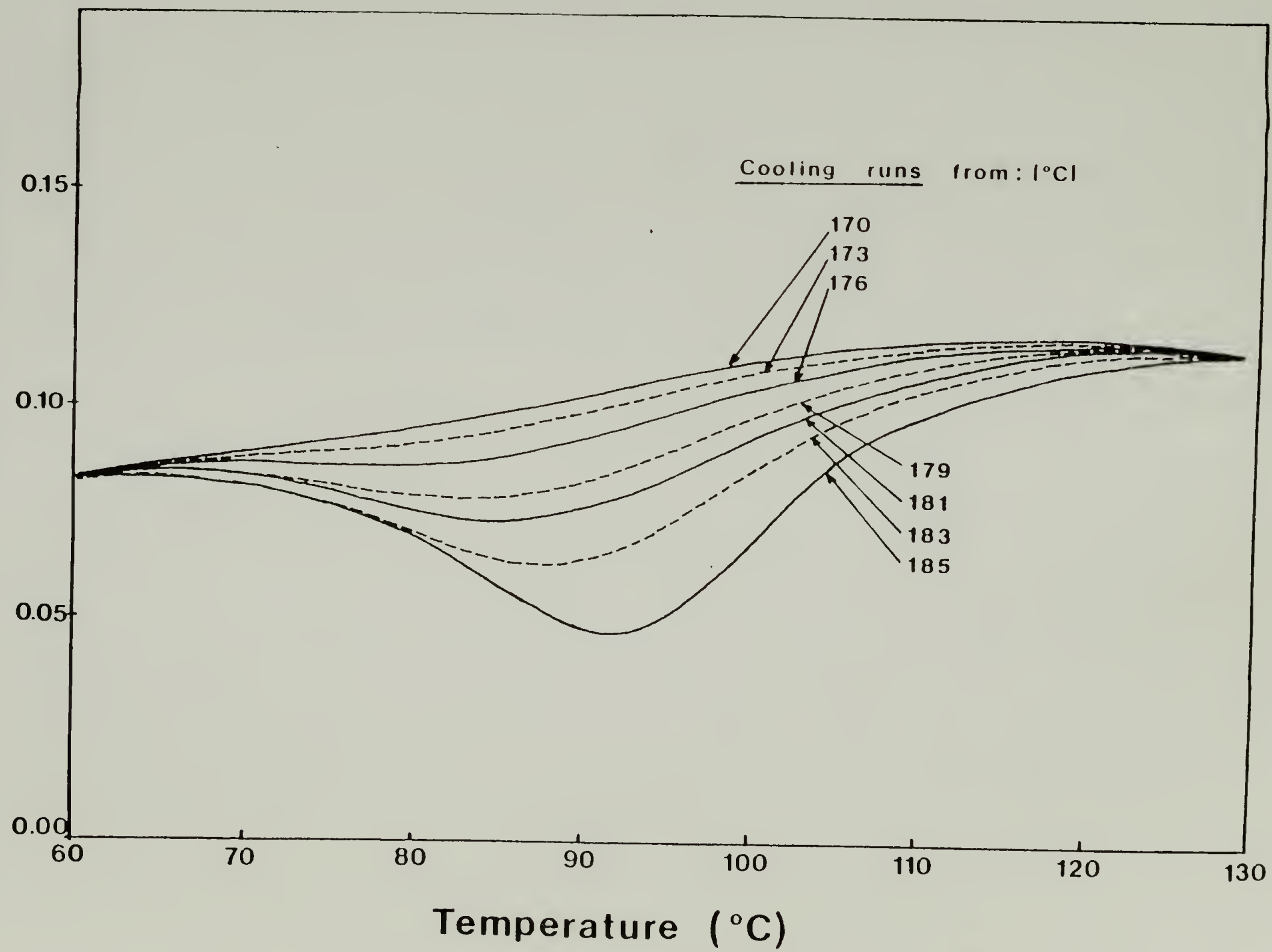
dQ/dt (mcal/sec)
0.15
0.10
0.05
0.00
Cooling runs from: I°C
170
173
176
179
181
183
185
60
70
80
90
100
110
120
130
Temperature (°C)

between 50°C and 170°C (at 10°C/min) were recorded and are presented in figure 3.5 (full curves). The most stricking feature is the absence of any discernable endotherm on heating corresponding to the range of temperature where the exotherm of the $\delta \rightarrow \alpha$ transition is observed on cooling. Instead, the heating run suggests a continuous increase of the specific heat stretching from 100°C to the onset of the first melting peak of the crystals (172°C in this case).

In order to get more insight about the phenomenon associated with the $\alpha \rightarrow \delta$ transition on heating, the following experiment was performed. The sample was heated from 50°C up to several temperatures in the interval between 100°C and T_{m1} (172°C for this sample isothermally crystallized at 170°C) and subsequently cooled back to 50°C at the same rate of -10°C/min. Figure 3.5 shows three cooling runs (broken curves) and compares them with the one cooled from 170°C. It appears that the lower the temperature to which the sample was heated above 95°C before being recooled, the smaller the size of the exotherm observed in the cooling scan and the lower its peak temperature; and consequently, it suggests that fewer crystals underwent transition from the low temperature α-form to the high temperature δ-form during heating. The difference of temperature and range for the transition in heating and cooling is underscored. The transition exotherm is relatively sharp and remains between 80°C and 95°C, while the endotherm is widely spred out between about 95°C up to the first onset of melting, which makes it hardly detectable. To check that dynamic effect are not at the origin of the wide spreading of the transition on heating, the same sample was

Figure 3.5. Characteristic cooling and heating thermograms at $\pm$ 10°C/min for nylon 11 crystallized at 170°C for 20 hrs when cycled between 50°C and 170°C over the reversible crystal transition region (solid curves). Broken curves show variation of the exotherm on cooling for sample heated up to various intermediate temperatures, 125°C, 140°C and 155°C.

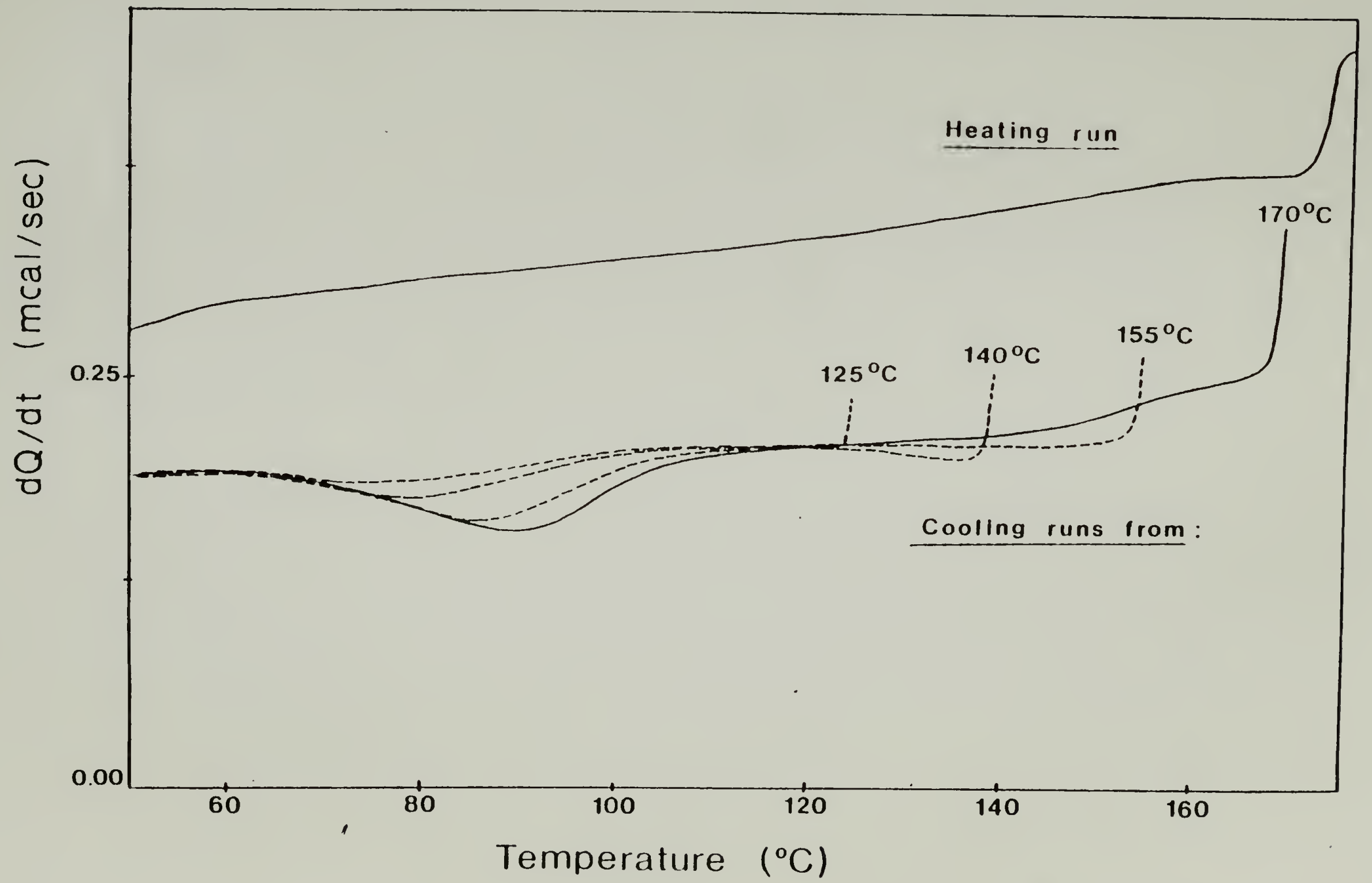
dQ/dt (mcal/sec)
0.25
0.00
60
80
100
120
140
160
Temperature (°C)
Heating run
170°C
155°C
140°C
125°C
Cooling runs from :

heated four times between 50°C and 140°C but kept for different amount of time at 140°C (between 1 min. and 2 hours) in order to reach thermodynamic equilibrium before cooling runs were recorded again. The resulting exotherms show no significant change with time and indicate no significant kinetic effect on the extent of the transition. Figure 3.6 shows the hysteretic dependence of the extent of crystal transition with temperature, as deduced from the above results.

c) Refractive Index Measurements.

Figure 3.7 shows the temperature dependence of the refractive indices obtained for both an isotropic as well as for a hot-rolled plate of nylon 11 between 20°C and 100°C. This measurements were made with an Abbe refractometer designed to determine refractive indices along three orthogonal directions[96]. For the isotropic film, the refractive index is identical in all three principal directions. On the other hand, anisotropy is clearly depicted in the rolled specimen as indicated by the differences in the values shown in figure 3.7 for the three principal refractive indices. Solid state rolling of nylon 11 has proven in former studies to orient crystals with their chain axis in the rolling direction and with hydrogen-bonded planes parallel to the compression plane[97,98]. Therefore, the positive birefringence Δ_{xy} perpendicular to the chain axis reflects the anisotropic state of hydrogen bonding in the molecular packing of the crystals of the α-form. As indicated by the data, the birefringence and hence the anisotropic

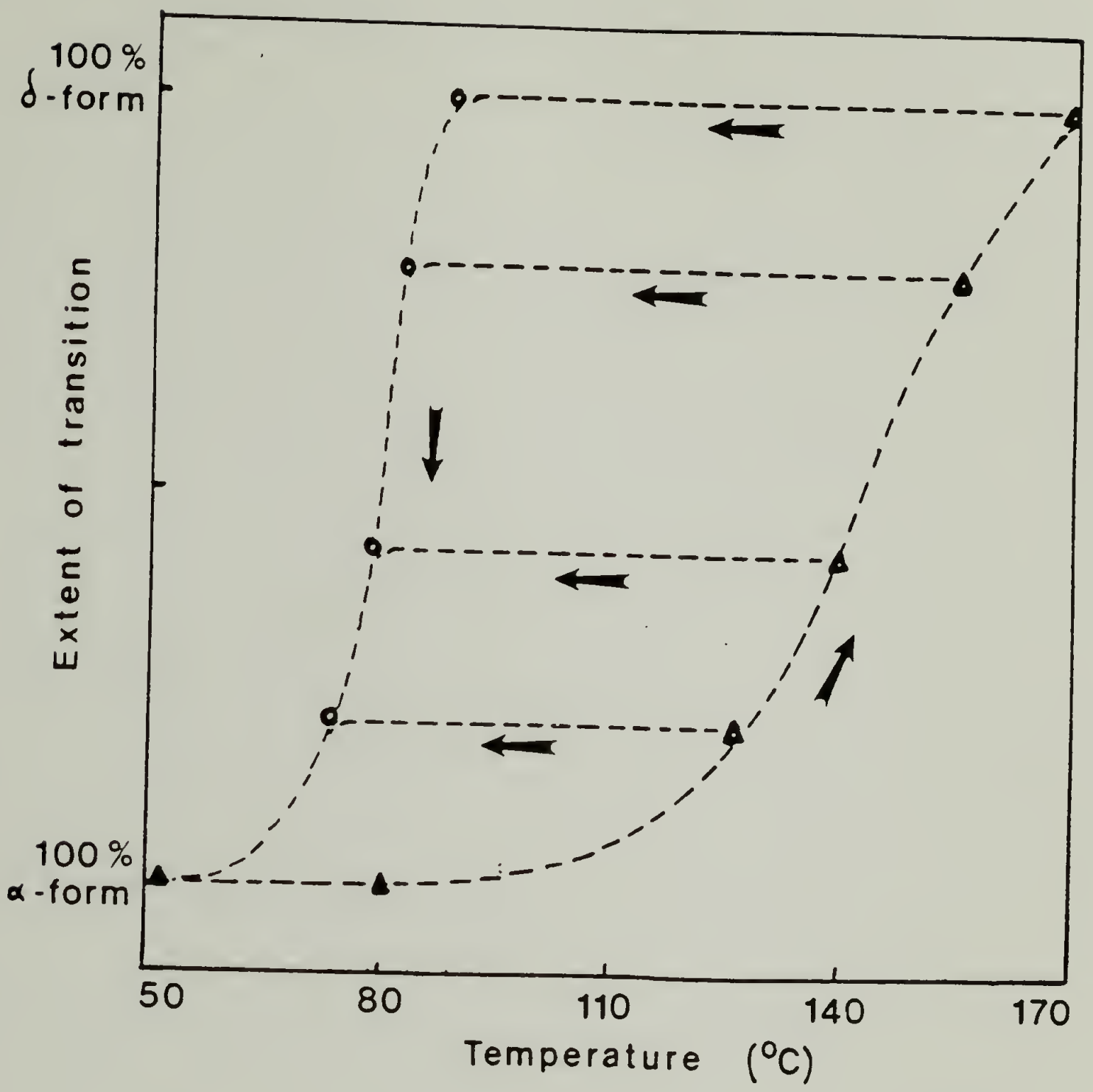

Figure 3.6. Hysteretic dependence of the extent of crystal transition in nylon 11 (between the α- and the δ-form) versus temperature during heating and cooling runs between 50°C and 170°C (same sample as in figure 5), as measured from the transition exotherm. Note the progressive transition on heating (hardly detectable by thermal analysis) as opposed to the rapid transformation on cooling.

Figure 3.7 . Principal refractive indices for isotropic (o) and rolled and annealed (●) nylon 11 plate at 160°C (α-form) to DR=4.3 versus temperature. n_C, n_H and $n_\perp$ represent respectively the refractive index in the rolling direction (C-axis), in the transverse direction (direction of H-bonding in the crystal α-form) and in the normal direction, respectively.
Note that the difference $(n_H - n_\perp)$ remains approximatively constant up to 95°C, and only seems to progressively decrease above this temperature. It denies complete randomization of H-bonds at 95°C for the α→δ transition as previously suggested by Newman.

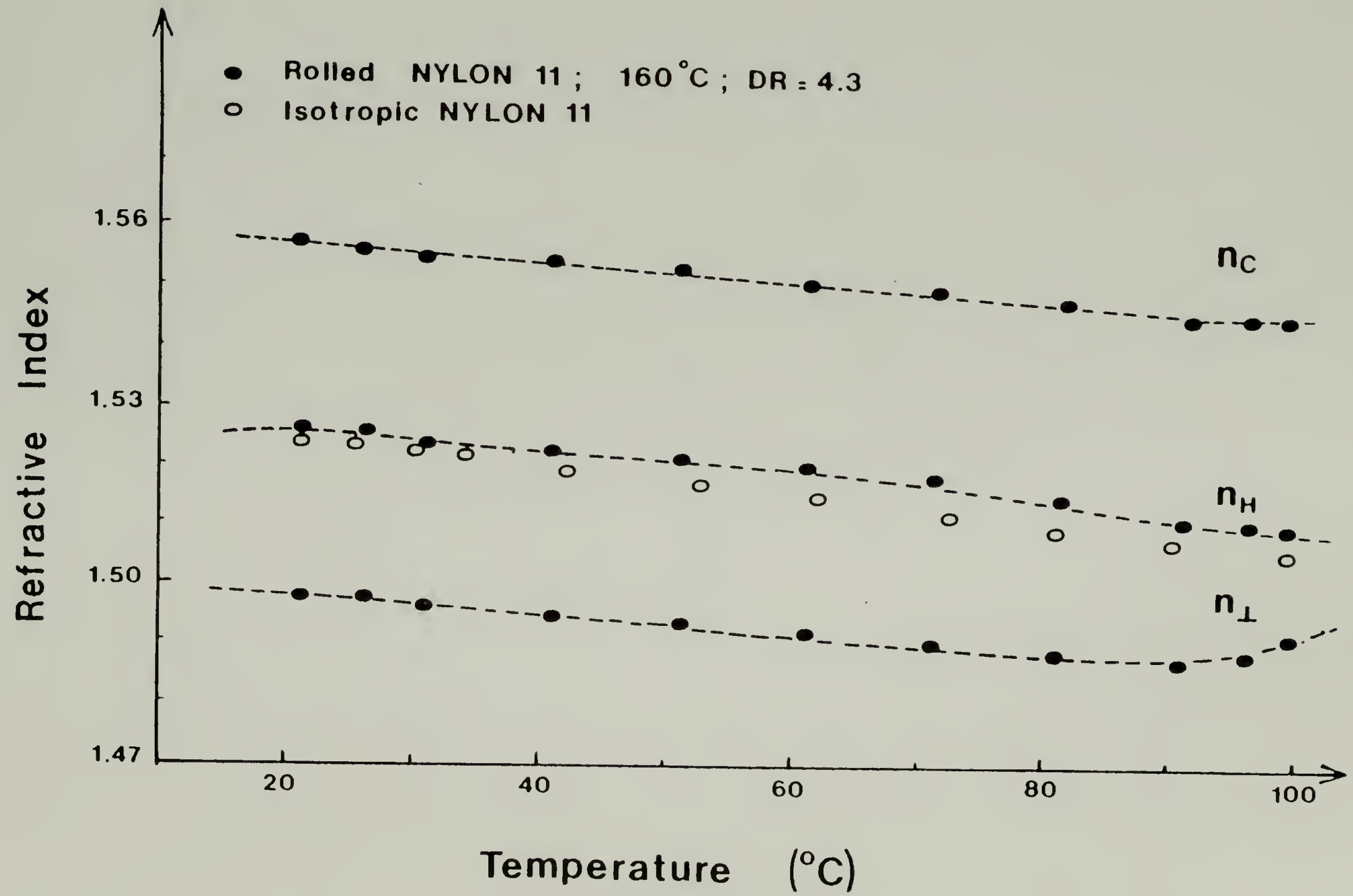
Rolled NYLON 11 ; 160°C ; DR = 4.3
Isotropic NYLON 11
Refractive Index
1.56
1.53
1.50
1.47
n_C
n_H
$n_\perp$
20
40
60
80
100
Temperature (°C)

state of orientation of the hydrogen bonds remains constant during heating up to 95°C. Also, no discrete change is seen at this particular temperature although it had been reported to be the transition temperature for the α→δ transition. Only raising further the temperature seems to progressively decrease the birefringence and induce partial randomization of the direction of hydrogen bonds. Birefringence measurements are therefore in accordance with thermal analysis data in assessing the progressive character of the α→δ crystal transformation on heating from 95°C up to the first melting point.

d) Comparison with Spectroscopic Results.

It should be of interest to confront the above results with other experimental techniques sensitive to chain conformation and molecular interaction at the atomic scale. Spectroscopic techniques are usually the most appropriate to provide information at this level. Previous results published by Strovanek et al.[99] describe the changes of the amide I region from 1600 cm^{-1} to 1700 cm^{-1} with temperature for a thin film of nylon 11 cast from solution. The crystal form present in the film was reported to be of the α-form. They showed this region of the spectrum to be highly sensitive to conformation changes through dipole-dipole interactions. Accordingly, infrared bands attributed to ordered and disordered hydrogen-bonded amide groups as well as "free" amide groups could be discerned and deconvoluted. The respective area

for each band after deconvolution is shown in figure 3.8. The authors explained the decrease of the ordered band with temperature to reflect a reduction of the overall degree of crystallinity of the sample and a corresponding increase of the amount of the amorphous material. Since the decrease of the ordered band is actually significant only above 100°C, it is likely that the change of the mode of hydrogen bonding as described above during the progressive crystal transition is in fact responsible for the observed decay.

Solid state ^{15}N NMR measurements were also performed in collaboration with prof. Mathias on melt-crystallized nylon 11 films identical to the one used for thermal analysis. ^{15}N CP/MAS NMR is already known to be a sensitive technique for examining the crystal structure of solid polyamides[100] and determining the specific conformations about the amide group. Isotropic ^{15}N enrichment is required to be able to observe both crystalline and non-crystalline resonances, and to determine T_1 relaxation times. Experimental spectra clearly showed that the different crystal forms could be differentiated by chemical shift. ^{15}N spin lattice (T_1) relaxation experiments were used to observe the relative mobility of the phases and gave the expected order: $\delta' \leq \delta \leq \alpha$. From changes of chemical shift with temperature, the crystal-related phenomenon was confirmed at temperatures around 95°C. Nontheless, the ^{15}N CSA data argue againt a drastic reorganization of hydrogen bonds in the crystal at this temperature[101]. Deuterium NMR studies of nylon 66 by English and his

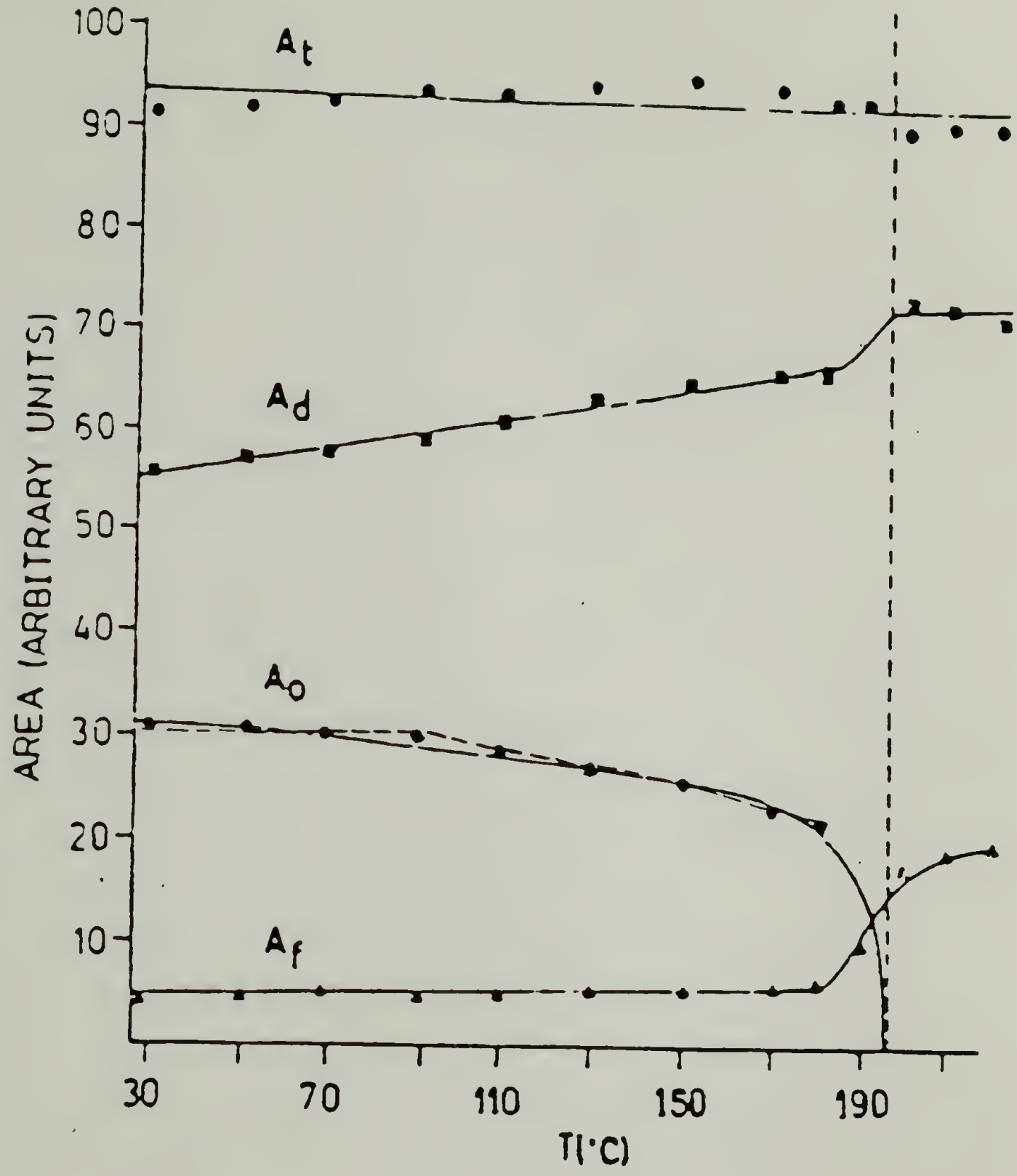

Figure 3.8. Plots of areas for "free" (A_f), ordered (A_o) and disordered (A_d) hydrogen-bonded and total (A_t) carbonyl groups obtained from the IR amide I region versus temperature for nylon 11 (after Skrovanek and al.) . The decrease in ordered hydrogen bonded carbonyl groups becomes significant only above 95°C, which is the onset temperature for the $\alpha \rightarrow \delta$ transition.

coworkers[88] also supports the stability of the nearly "rigid lattice" for the amide N-D bond even above the Brill transition. Their results also indicate considerable rotational freedom of the methylene groups well below the melting point. A model of motion based on large amplitude librations about "odd" bonds was found to fit well with the experimental spectra. Moreover, they noted that the bimodal character of the distribution of librational amplitudes $P(\Delta\theta)$ could well imply the presence of two co-existing crystal phases in the region of the Brill transition.

e) A Model for the $\alpha \rightarrow \delta$ Transition: The "Crystal-Condis Crystal" Transition.

In this paragraph, a new model is advanced for this transition to account for the hysteretic nature found by thermal analysis and the diffuse and progressive character of the transition observed by all experimental means. This study, as well as prior studies, described the high-temperature δ-form as an ordered hexagonal dynamic hydrogen-bonded network. Unlike in the α-form, H-bonds are not confined in adjacent layers but can rather form and disrupt in all six hexagonal directions perpendicular to the chain axis. Figure 3.9 compares both crystal symmetries from their c-axis projections. Such a mesophase is best described by a condis crystal, according to the definition given by Wunderlich and coauthors[102], as it exhibits dynamic conformational disorder and long-range positional order. The $\alpha \rightarrow \delta$ transition might

then be well described by a crystal-condis crystal transition. The existence of such transitions have been recently reviewed by the authors mentioned above. They developed models assuming the existence of conformational isomers (of different energy) in thermodynamic equilibrium and applied the principal of statistical mechanics. The theory predicts the variations of heat capacity with temperature over the transition domain as a function of system variables.

Here are summarized the major implications of the model:
in internal equilibrium, short range intramolecular forces cannot solely induce drastic conformational change of system consisting of molecules which can form several conformational isomers. However, if intermolecular interactions take place and induce a tendency to aggregation, a crystal-condis crystal transition may appear either as a diffuse but clear defined transition or as a discontinuous, first order transition, depending upon the tendency of molecules with same conformation to cluster.

in the case of the $\alpha \rightarrow \delta$ transition in nylon 11, any change in conformation for crystalline molecules are undoubtedly affected by intermolecular interactions since it is likely to modify the state of hydrogen bonding. Therefore the interaction energy between molecules significantly increases when they adopt a high energy conformation. Also, a certain degree of cooperativity in the process of disrupting and reforming hydrogen-bonds may legitimely be expected and may then favor the formation of aggregates. Both considerations are expected to influence the final shape of the transition, which is the case of nylon

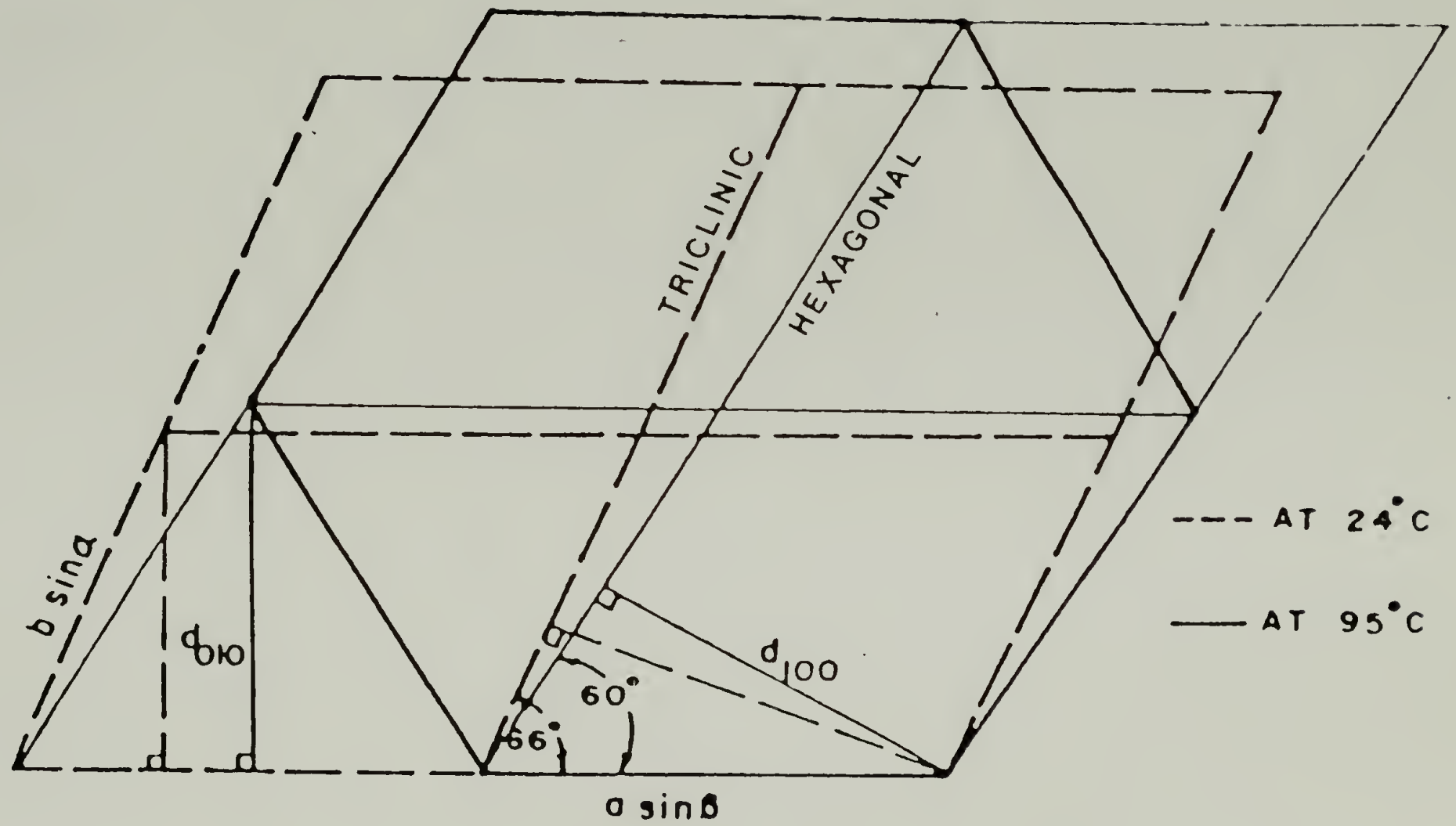

Figure 3.9. ζ-axis projection of the triclinic unit cell at 24°C (α-form) and 95°C (pseudo-hexagonal δ-form) (after Scheinbeim).

11 crystals was found to be more diffuse on heating than on cooling. This implies the larger cooperativity of the process of aligning hydrogen bonds into layers on cooling than of the process of dirupting these layers on heating. Finally, all data are consistent with this description of the transition: the progressive decrease in the value of the (001) d-spacing along the chain axis over the transition domain as temperature increases reflects the progressive deviation of molecules from their low energy planar zigzag conformation. No sharp transition also are found by spectroscopy. Finally, a similar approach may very well explain the Brill transition in nylon 66, and its bimodal distribution of hydrogen bonds over the transition range.

f) Thermodynamic Properties of Nylon 11 Crystal Forms.

All the results on the phase behavior of nylon 11 derived in the last two chapters are included in figure 3.10. The domain of stability for each form is given as a function of annealing temperature for an initially quenched nylon 11 specimen on a Hoffman-weeks plot. In the domain where both smectic and crystal coexist, the relative amount of smectic progressively decreases as it transforms into crystal by heat treatment. In this paragraph, we propose to introduce a method which can be used to separate the contribution of smectic and crystal in the total heat of melting of any specimen of nylon 11 and to quantitatively evaluate their enthalpies of transition based on experimental data. The method is based on the fact that the exotherm measured for the

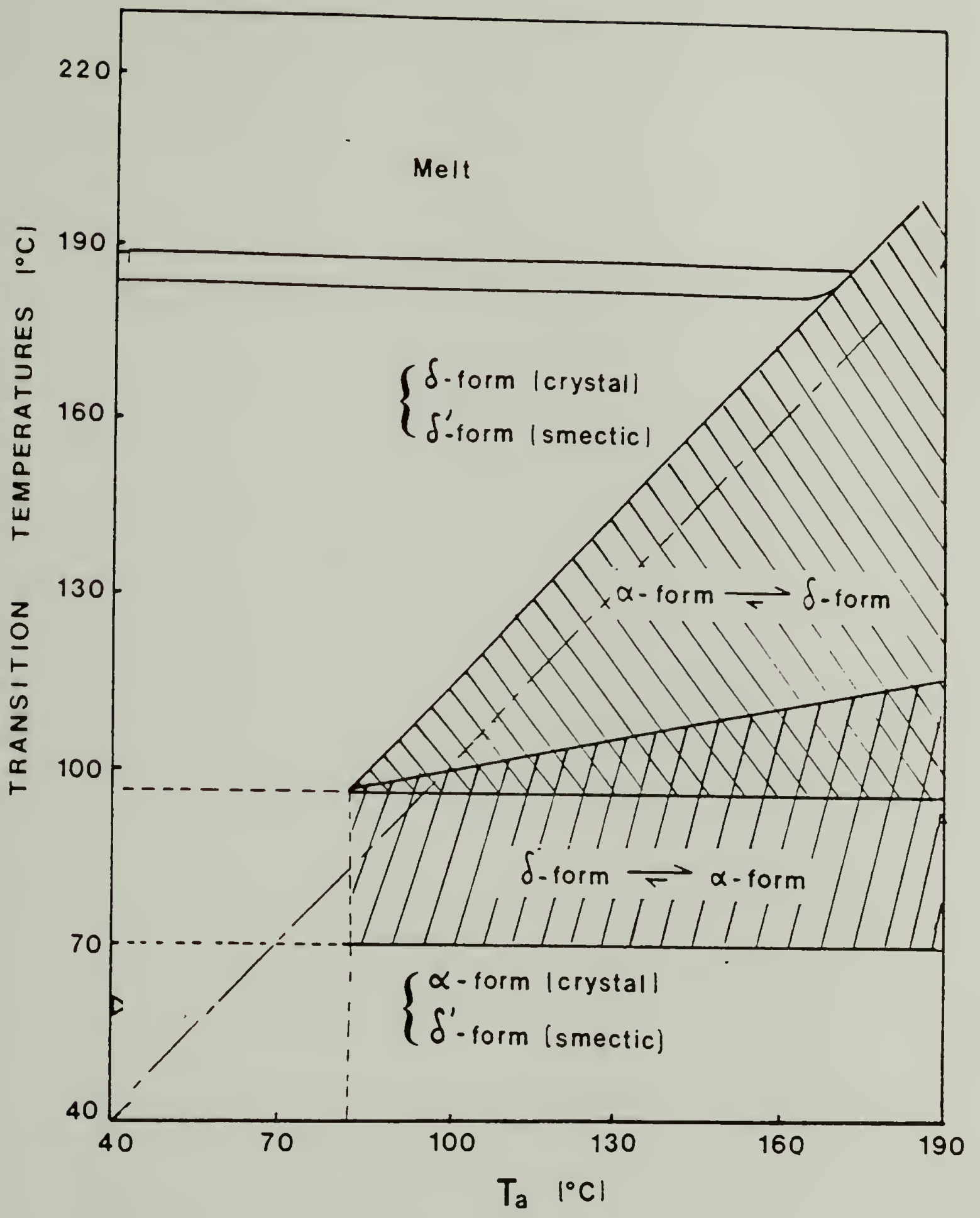

Figure 3.10. Hoffman-Weeks plot for cold-crystallized nylon 11. The domains of stability for all crystals forms are shown versus cold-crystallization (or annealing) temperature.

crystal-condis crystal transition on cooling exclusively reflects the fraction of crystals present, on not the smectic. The heat evolved on cooling between 60°C and 120°C is thus proportional to the concentration of crystals in the specimen.

model:

Consider x_α to be the fraction of the 3D-crystals (in the α-form). These adopt the α-form at low temperatures and the δ-form at high temperatures, when the transformation is complete. Hence, this fraction can be also called x_δ.

Consider x_δ, to be the fraction of the smectic. Then, $1-x_\delta-x_\delta$, represents the fraction of the amorphous phase in the material. We denote $\Delta H^\circ_{\delta',\to m}$ and $\Delta H^\circ_{\delta\to m}$ the latent heats of fusion of the smectic and the crystal respectively, and $\Delta H^\circ_{\alpha\to\delta}$ the heat of the $\alpha\to\delta$ thansition and take these values to be positive.

Consider first the case of a cooling scan: For a specimen already crystallized, the heat of the exotherm measured between 60°C and 120°C corresponds exclusively to the $\delta\to\alpha$ crystal transition. Therefore:

$$\Delta H_{cooling} = -x_\alpha \Delta H^\circ_{\alpha\to\delta} = -x_\delta \Delta H^\circ_{\alpha\to\delta} \,, \qquad (3.1)$$

The heat of transition is a linear function of the content of 3D-crystals in the specimens. In figure 3.11, experimental values for the measured heat of transition of several nylon 11 samples are reported and plotted linearly to yield the crystal content for each sample. These include: nylon 11 isothermally crystallized at 164°C for different amounts of time: nylon 11 crystallized for various undercoolings for 5 min: and quenched nylon 11. Results confirm that lower undercoolings and longer crystallization times favor the formation of the crystal forms (at the expense of the smectic form)

Additionally, heating scans of the same specimens were recorded and the aera of the endotherm computed between 100°C and 230°C. This include three contributions: The heat absorbed during the crystal-crystal transition on heating, the heat of melting of the fraction of smectic present and the heat of melting of the fraction of crystal present;

$$\Delta H_{heating} = x_{\alpha} \Delta H^{\circ}_{\alpha \to \delta} + x_{\delta} \Delta H^{\circ}_{\delta \to m} + x_{\delta'} \Delta H^{\circ}_{\delta' \to m} .$$

As a first approximation, the first contribution can be eliminated by simply subtracting the heat of the transition as measured during cooling,

$$\Delta H_{heating} - \Delta H_{cooling} = x_{\delta} \Delta H^{\circ}_{\delta \to m} + x_{\delta'} \Delta H^{\circ}_{\delta' \to m} . \quad (3.2)$$

These values are reported in figure 3.12 for the same specimens shown in figure 3.11 and as a function of the crystal content which had been determined on figure 3.11. Values of about 13.5 cal/gram are obtained for crystallization times where essentially no smectic is left. When compared with the reported value of 47 cal/gram for the latent heat of fusion[68], it gives a crystal content of about 28%. Implementing the degree of crystallinity in equation 3.1 gives the latent heat of crystal transition equal to about 4.0 cal/gram. In the case of quenched nylon 11 where the crystalline phase is essentially composed of the smectic modification, the heat of melting decreases down to about 10.5 cal/gram. There can be two reasons at the origin of this: A lower degree of crystallinity and/or a lower latent heat of fusion for the smectic. For the intermediate cases, however, where both crystal and smectic coexist in comparable amounts, it is reascnable to assume that the total amount of crystallinity does not change significantly. The enthalpy term in equation 3.2 should then show linear dependence of x_δ. Figure 3.13 provides such an agreement. The extrapolated value for the heat of melting of the smectic form gives 10.5 cal/gram, which corresponds to a latent heat of melting of 36.5 cal/gram.

Entropies of melting can be calculated for the value of melting points reported earlier with the equation $\Delta S_m=\Delta H_m/T_m$. It follows:

$$\Delta S_{\delta,\rightarrow m}=0.055 \text{ cal/(g.}^{\circ}\text{C)}; \quad \Delta S_{\delta\rightarrow m}=0.071 \text{ cal/(g.}^{\circ}\text{C)} \ .$$

Figure 3.11. Linear plot for the enthalpy of crystal transition (as measured from the exotherm on cooling) versus fraction of α-form crystals for several nylon 11 samples.

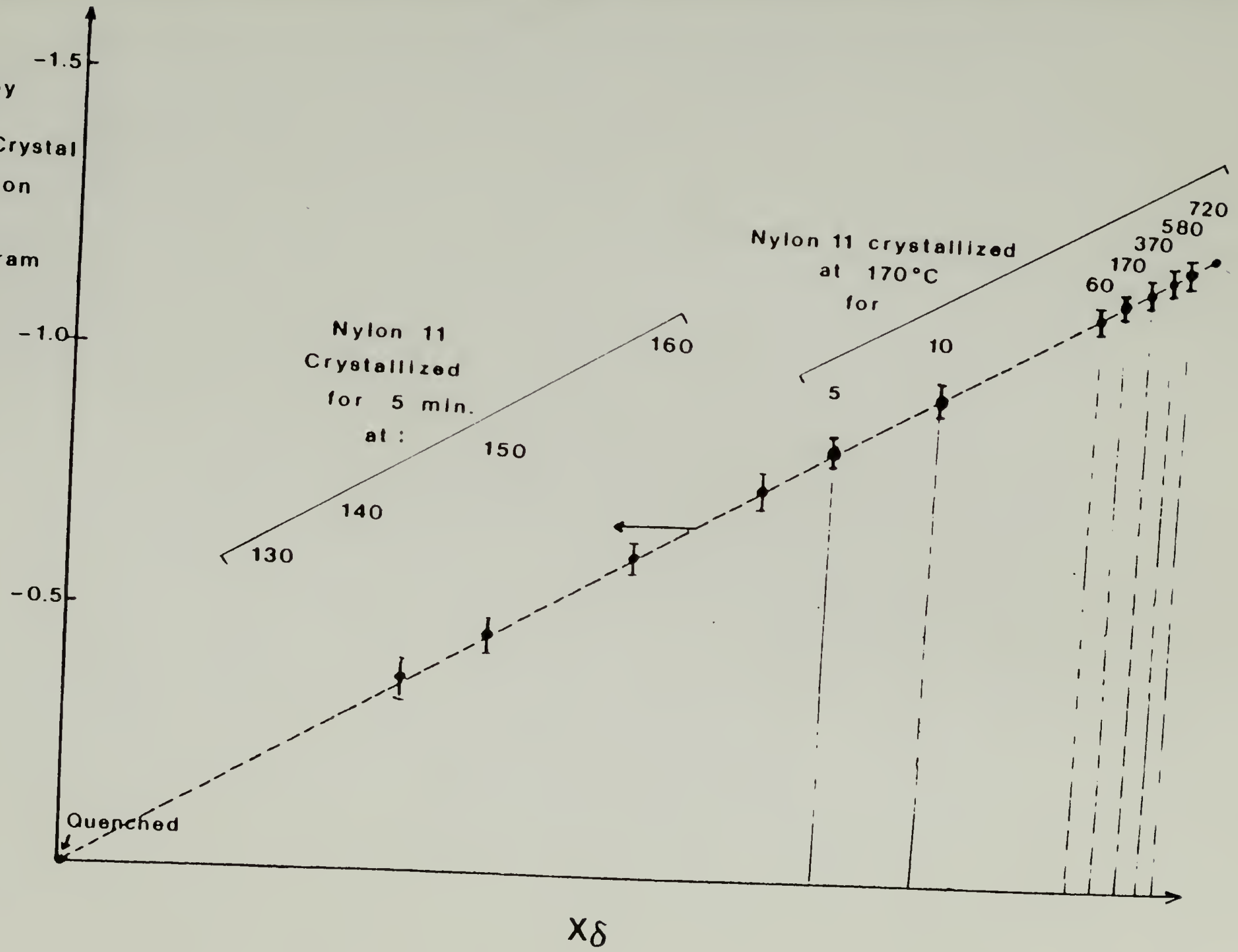
-1.5
Enthalpy
of
Crystal-Crystal
Transition
Cal/Gram
-1.0
-0.5
Nylon 11
Crystallized
for 5 min.
at :
160
150
140
130
Nylon 11 crystallized
at 170°C
for
720
580
370
170
60
10
5
Quenched
Xδ

Figure 3.12. Given the crystal fractions determined in figure 3.11, the heat of fusion for the same nylon 11 specimens (as measured by the total endotherm on heating) are reported. Note that the linear portion of the curve gives the crystallinity range where the total amount of smectic and crystal remains approximatively constant. The enthalpies of melting of the smectic and crystal forms can be derived as well as the heat of crystal transition.

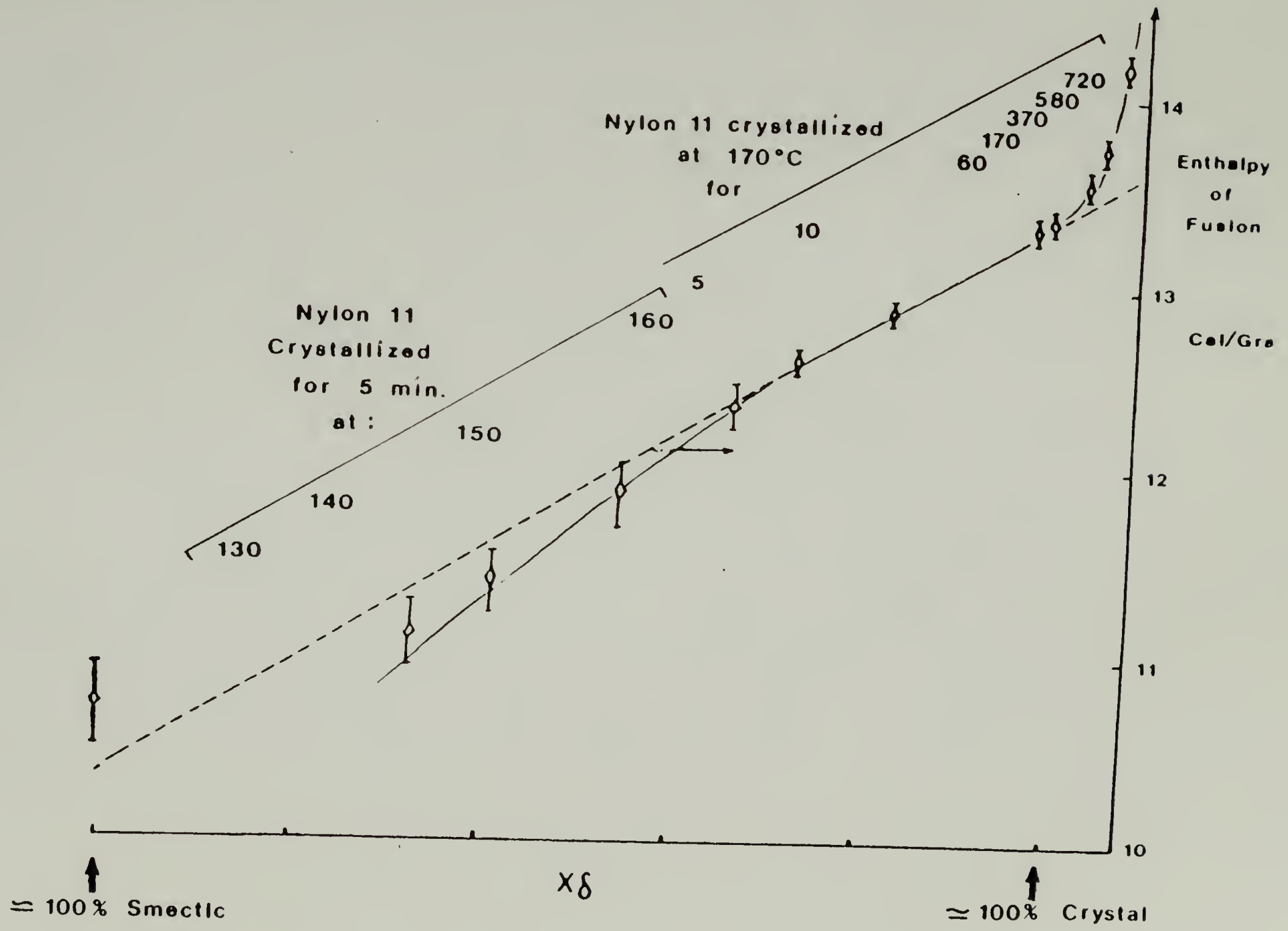
Nylon 11 crystallized at 170°C for
720
580
370
170
60
10
5
Nylon 11 Crystallized for 5 min. at :
160
150
140
130
14
13
12
11
10
Enthalpy of Fusion
Cal/Gra
Xδ
≃ 100% Smectic
≃ 100% Crystal

4) Conclusions.

The reversible $\alpha \rightarrow \delta$ transition in nylon 11, previously suggested from X-ray data and similar to the Brill transition reported for even-even nylons, has been identified by thermal analysis. It appears as a relatively sharp transition on cooling, but is spread over a wide temperature range on heating, thus exhibiting an hysteresis over temperature cycles. The crystal-condis crystal model by Wunderlich et al. is found to successfully describe the characteristics of the transformation. It does not induce any drastic structural modification of the crystal, but rather a continuous transformation, as indicated by X-ray diffraction, spectroscopic studies and refractive ndex measurements. Strong intermolecular interactions and tendency of aggregation can explain the shape of the heat capacity curves. The higher cooperativity of the cooling process is at the origin of the sharper transformation. The progressive change in the mode of hydrogen bonding from the layerlike arrangement of the α-form to the dynamic hexagonal network on heating is proposed.

A graphical method has been successfully applied to determine the crystal content and the thermodynamic properties of the transitions in nylon 11 from the experimental enthalpy of the $\alpha \rightarrow \delta$ transition on one hand, and from the enthalpy of melting on the other. Thermodynamic quantities such as latent heats of fusion of both smectic and crystal modifications, latent heat of the crystal-crystal transition and entropies of melting and crystal transition were derived, assuming the

latent heat of fusion of a 100% α-crystalline sample to be equal to the value reported by Gogolewski[68].

C H A P T E R IV

SOLID STATE UNIAXIAL DEFORMATION STUDIES OF NYLON 11

1) Introduction.

In this chapter, the results of our study of nylon 11 subject to uniaxial deformation by free tensile drawing are reported. Of a particular interest for our comparative study with biaxial deformation, are all the phenomena associated with the ordered phase. These are considered essential as they largely influence the final structure, morphology and final properties of the drawn specimens. Particular attention will be given to the role played on the deformation mechanism by the different structures which have been found to exist in melt crystallized nylon 11. Finally, structural analysis by WAXD on uniaxially stretched specimens should provide more information on the exact structure of each crystal species; And on the role of hydrogen bonds for each of them.

2) Results and Discussion.

a) Crystal Behavior at the Early Stages of Deformation.

In order to investigate the initial plastic deformation modes in the crystal lattice of nylon 11 subjected to tensile drawing, a thin istropic film of nylon 11 was crystallized at 175°C for 60 minutes and slowly cooled down to room temperature. It had about 25% crystallinity and contained spherulites of crystals in the α-form. It was then stretched 15% and held under tension while a X-ray diffraction pattern was taken with the X-ray beam perpendicular to the stretching axis and to the plane of the sample. It is shown on figure 4.1, in addition to the two load-displacement curves of two specimens cut out of the same initial film but having different size. It is clear from the diffraction pattern that although there is no detectable c-axis orientation for such a low draw ratio, the specimen under tension exhibits a fairly textured (hk0) pattern. Such a crystallographic effect had been first seen for semicrystalline spherulitic nylon 66[104] and had been explained by a twinning mechanism. For the fraction of crystals oriented with the chains axis and the hydrogen bonds perpendicular to the tensile direction, the (210) twinning process can explain the drastic orientation changes for the strongest (hk0) reflections. The transverse displacement of chains associated with this twinning process exhibits the following characteristics:

Figure 4.1. Load-Displacement curves for nylon 11 cold-crystallized at 170°C during tensile drawing at room temperature. The two curves correspond to two different specimens size. The WAXD pattern illustrates the partial twinning process which takes place in the α-form crystals at 15% stretching.

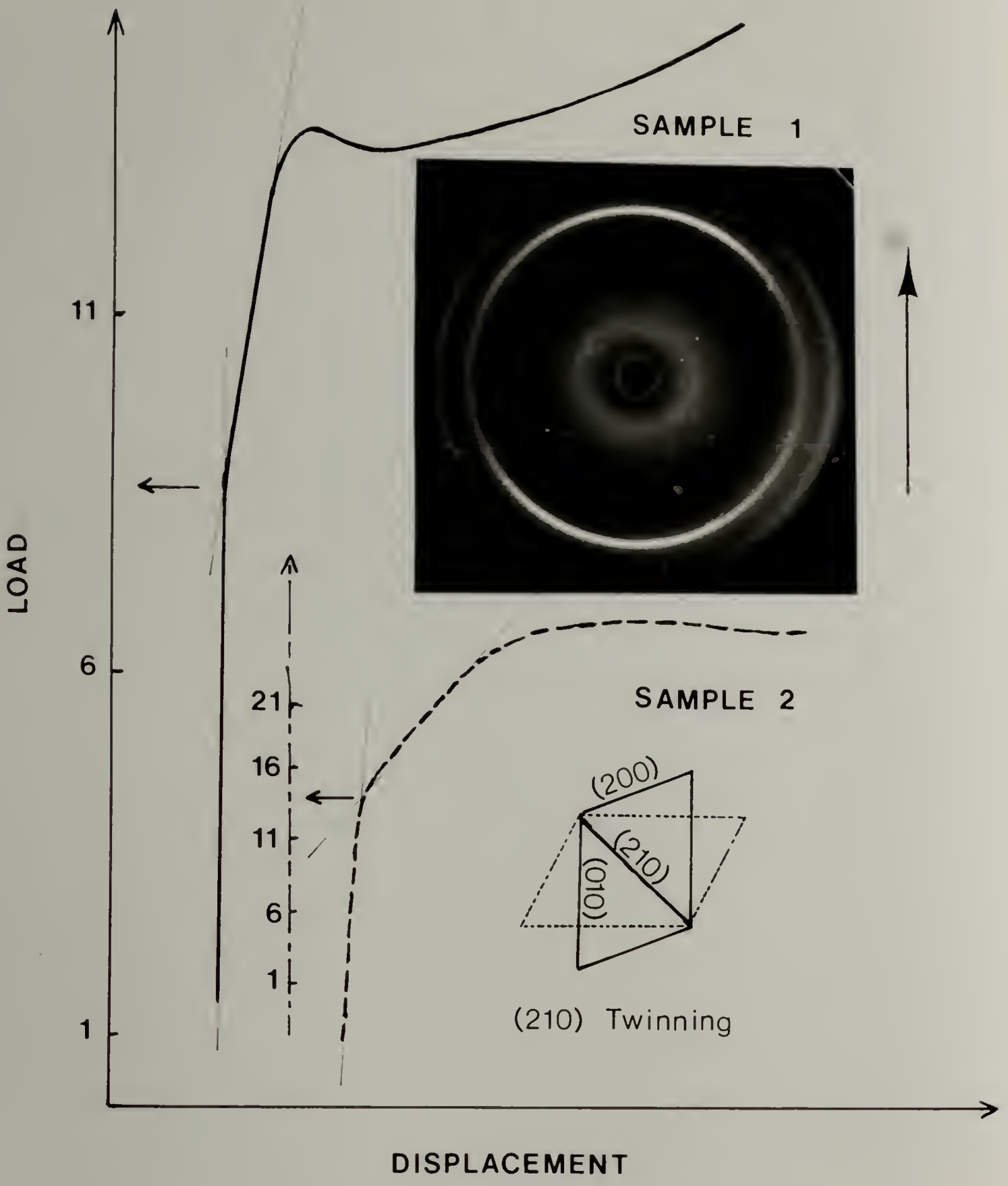
SAMPLE 1
11
6
1
LOAD
21
16
11
6
1
SAMPLE 2
(200)
(210)
(010)
(210) Twinning
DISPLACEMENT

i) it is a reversible process as the chains in the crystals return to their original position on stress release.

ii) it indicates the underlying switching of hydrogen bonding between neighbor molecules in the α-form at room temperature under stress.

iii) this switching process induces, when it occurs, the rotation of the hydrogen bonds in the direction of stretching.

The load-displacement curves indicate the existence of two linear elastic regimes with two different moduli at the early stages of the deformation at room temperature before necking occurs and marks the onset of plastic deformation. The diffraction pattern discussed above was obtained for a 15% stretching which lies in the second elastic regime. This correlation suggests that the second elastic behavior may originate from the finite and well defined transverse displacement of the chains in the crystals undergoing the twinning process (lower modulus). For higher stresses, the elastic regime of the deformation ends which corresponds to the further lateral displacement of the chains in both crystalline and amorphous phases in the neck region.

b) Crystal Texture Development at Large Deformations:

Northolt and coworkers first investigated in 1972 the tensile behavior of quenched nylon 11 thin films at relatively low temperatures to their maximum draw ratio of about 4[51]. They reported two different

modes of orientation for the crystalline phase found in the deformed and annealed samples, depending on whether the deformation took place below or above T_g at about 45°C. They quite normally attributed these differences to the alternate behavior of the amorphous phase upon deformation above and below T_g. However, further experimental observations by the same authors indicated that when annealed at a temperature T_a above T_g, these films would exhibit the same difference in orientation when deformed above and below the annealing temperature instead of above and below T_g[52]. Considering again the phenomenon to be associated with the amorphous phase, the authors proposed that the state of the amorphous hydrogen-bonded network had been strenghten by thermal treatment, due to partial molecular molecular reorganization for enhanced hydrogen-bonding. This of course implied that the general concept of glass transition would have to be revised in the case of nylons to account for the more significant dependence of the glassy state upon thermal history[66,105].

According to the published data[52], the two types of orientation for the crystals (after annealing) are either uniplanar-axial or simply axial whether deformation takes place below or above T_a, respectively. Description of these two modes of orientation were given in introduction (Table 1.2). Briefly, one particular crystallographic plane, namely the hydrogen-bonded planes ((010) planes) of the crystal α-form tend to align parallel to the film plane (in addition of the c-axis alignment in the tensile direction) when deformation takes place below T_a. Also the deformation is inhomogeneous and takes place by necking below T_a while

it becomes homogeneous above T_a. Therefore, below T_a crystals do not show cylindrical symmetry around the fiber axis. The fact that uniaxially oriented thin strips dont necessarily have cylindrical symmetry in their final crystal texture is not so surprising, since the decrease in thickness during stretching may be much more important than the width reduction[106]. Other similar observations have been reported for other polymers like for example other nylons, PET and lightly crosslinked polyethylene[107a,b,c]. Nontheless, the particularity of nylon 11 rests upon its alternate behavior depending upon thermal treatment and temperature of deformation. Figure 4.2 exhibits the difference by WAXD between the two orientation modes (as they were reproduced in our laboratory) with the incident X-ray beam parallel to the tensile direction.

Northolt's interpretation was based on the assumption that quenched nylon 11 films were "non crystalline". However, it was demonstrated in Chapter 1 how nylon 11 does in fact crystallize even on quenching to yield ordered domains of smectic (about 20% smectic) with a melting point at 187°C. Also, it was shown how thermal annealing gradually transforms the smectic into a three dimensionally ordered crystal (in the α- or δ-form) by molecular reorganization in the solid state. This process was described as a lateral ordering process. Both the time and temperature of annealing were found to strongly affect the structure and stability of the crystals formed, by controlling the extent of structural rearrangement. For instance, thermograms of specimens of nylon 11 on heating after annealing at a particular temperature T_a

Figure 4.2. Distinction by WAXD of the two alternate crystal textures (uniplanar-axial on the left; uniaxial on the right) found in tensile stretched nylon 11 over different temperature ranges. The incident beam is parallel to the tensile direction (c-axis).

$T_{def} < T_{an}$

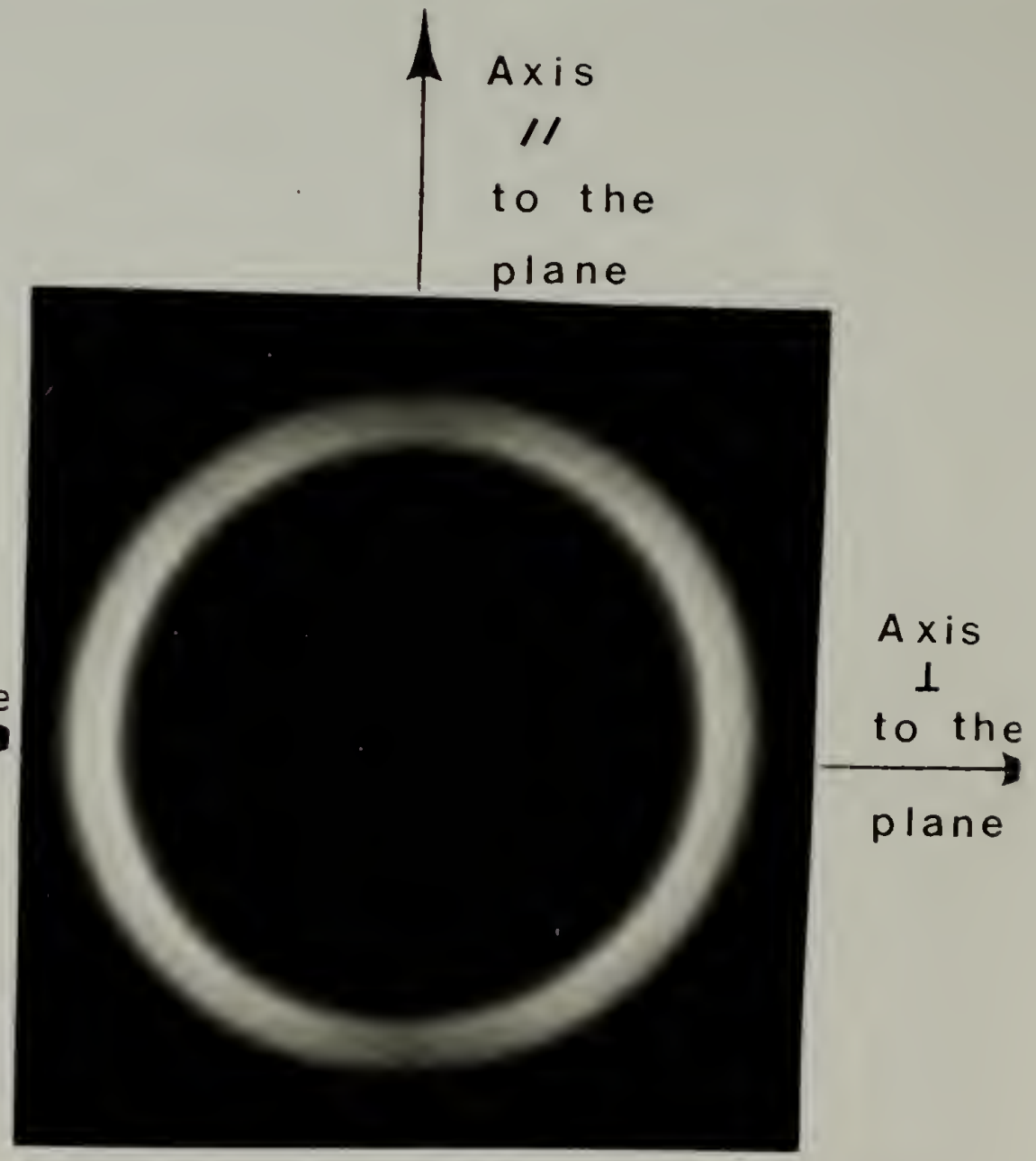

$T_{def} > T_{an}$

systematically exhibit an endothermic peak just above the annealing temperature (figure 2.7), indicative of the thermal instability of the crystals formed above T_a.

Our conjecture is that the alternate orientability of the crystals is closely related to the state of hydrogen-bonding in the crystalline phase, which as we now know depends upon thermal history. Deformation at temperatures below T_a involves mechanisms associated with the α-form induced from the original smectic form during the annealing treatment. Its layer-like anosotropic structure combines with the assymetric sample geometry to yield the uniplanar-axial texture. And the expected major slip plane, i.e. the hydrogen-bonded plane of the α-form aligns parallel to the film plane. At temperatures above T_a however, the deformation becomes homogeneous during the course of the deformation (no necking) and the final crystal texture exhibits cylindrical symmetry. Crystals in that temperature range have been proven to be of the hexagonal δ-form and undergo melting and recrystallization processes. Thus, gest that at these temperatures, the anisotropic α-form becomes thermally too unstable (or simply disrupts) to control the crystallography of the deformation (by slip). In summary, the tensile behavior of nylon 11 films in free drawing is sensitive to the type of crystals initially present, and indirectly to their state of hydrogen-bonding. Typical WAXD and SAXD patterns of the uniplanar-axial texture developed in nylon 11 during free drawing at room temperature (after subsequent annealing under no tension) are given in Figure 4.3 for two different orientations of the X-ray beam with respect to the stretched specimen. Note that the

Figure 4.3. WAXD (**A** and **C**) and SAXD (**B** and **D**) patterns (for two orientations of the incident beam) of the uniplanar-axial texture formed in cold-crystallized nylon 11 tensile stretched below the annealing temperature.

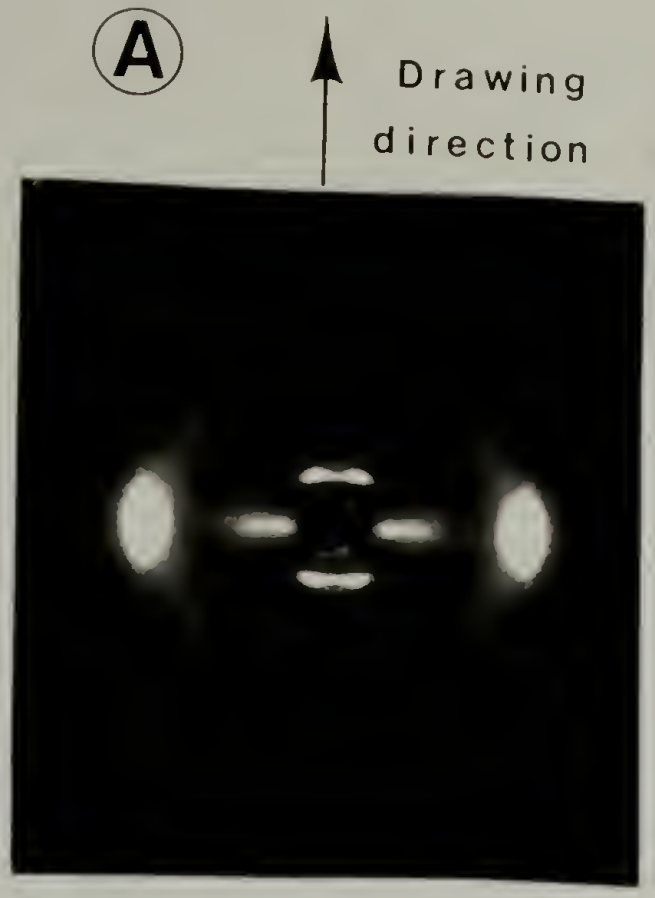
A
Drawing
direction
Axis
⊥
to the
plane
B

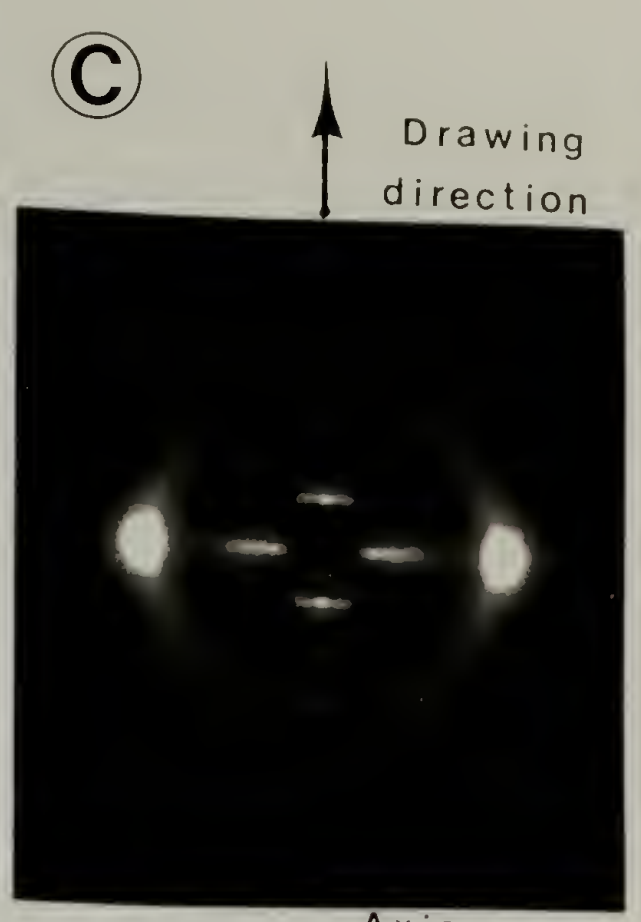
C
Drawing
direction
Axis
//
to the
plane
D

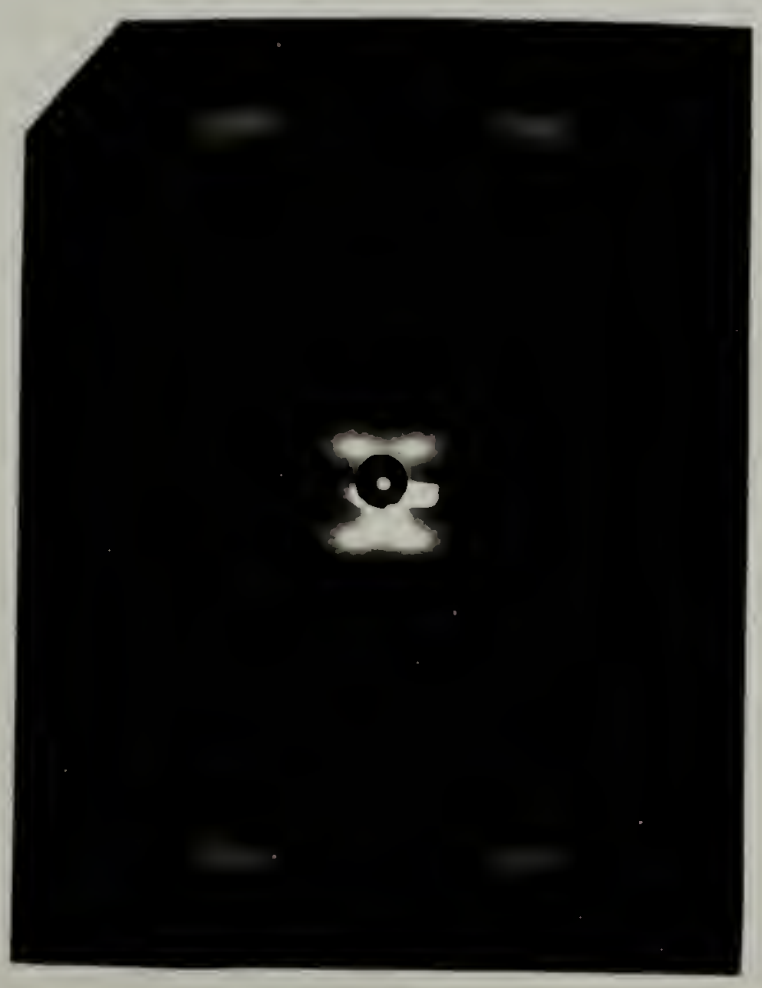

25 °C

same anisotropy in the structure is found at both Wide and Small angle X-ray diffraction geometries. The "single crystal-like" texture in these doubly oriented stretched ribbon offers the possibility of reinvestigating the crystalline structure from the observed wide-angle X-ray reflections and to comment on the supermolecular morphology from the small-angle X-ray reflections. This is presented in the next paragraph.

c) Stress-induced Order-Disorder Transition.

Structural investigation by X-ray of specimens deformed at relatively large draw ratios and low temperatures indicate the broadening and overlapping of the two X-ray reflections ((200) and (010) reflections) descriptive of the chain packing perpendicular to the chain axis. More precisely, this fingerprint of the deformation-induced form resembles the smectic form found in quenched nylon 11 films (see Chapter 2). This suggests partial transformation of the crystals from their original α-form into the smectic form. To further investigate this order-disorder transition, thermograms of nylon 11 specimens drawn to several different draw ratios at room temperatures were recorded and are shown in Figure 4.4. The major difference depicted between these heating scans is located in the temperature region prior to the melting endotherm. A broad and diffuse exotherm increases in size in that region as the draw ratio increases. If the exotherm results from the smectic-to-crystal conversion induced during the heating scan, this

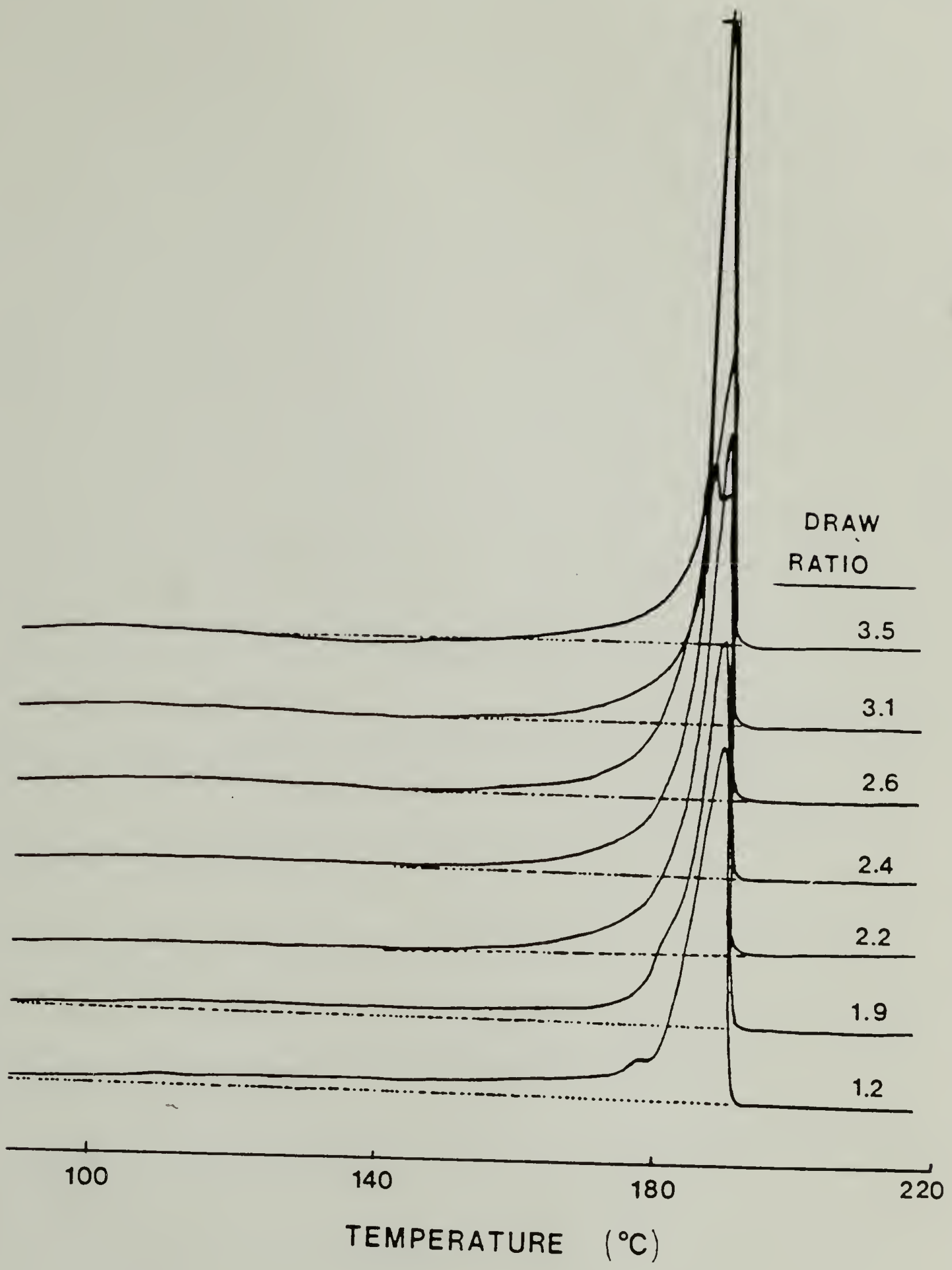

Figure 4.4. DSC heating curves at 10°C/min for tensile drawn nylon 11 up to different draw ratios (at room temperature).

result is consistent with an increase of the crystal-smectic conversion on cold drawing with draw ratio. Upon annealing, this stress-induced smectic form transforms back into the parent crystal it originated from (and with a preferred orientation of the main shear plane, the (010) crystallographic plane, parallel to the film plane). These yields the diffractions patterns depicted in Figures 4.2 and 4.3. A measure of the kinetics of the smectic to crystal conversion is shown in figure 4.5, where heating scans of stretched nylon 11 (at room temperature) were compared at various heating rates. The larger the scanning rate, the lesser the extent of conversion during heating (and the smaller the exotherm). At high temperatures (above $\approx 100^{\circ}C$), no smectic is produced and crystals of the α-form remain after deformation.

It is not clear yet what mechanism causes the formation of the disordered smectic on deformation at low temperatures in nylon 11. Several generic models exist in the literature and helped explain the same feature in other polymers which are reviewed here:

i) Occurrence of lateral chain packing disorder can result from the application of large shear stress on small lamellar fragments with high surface to volume ratio. Such a process should be particularly well suited for polymers with small crystal size and low crystallinity when deformed to relatively low draw ratio at low temperature.

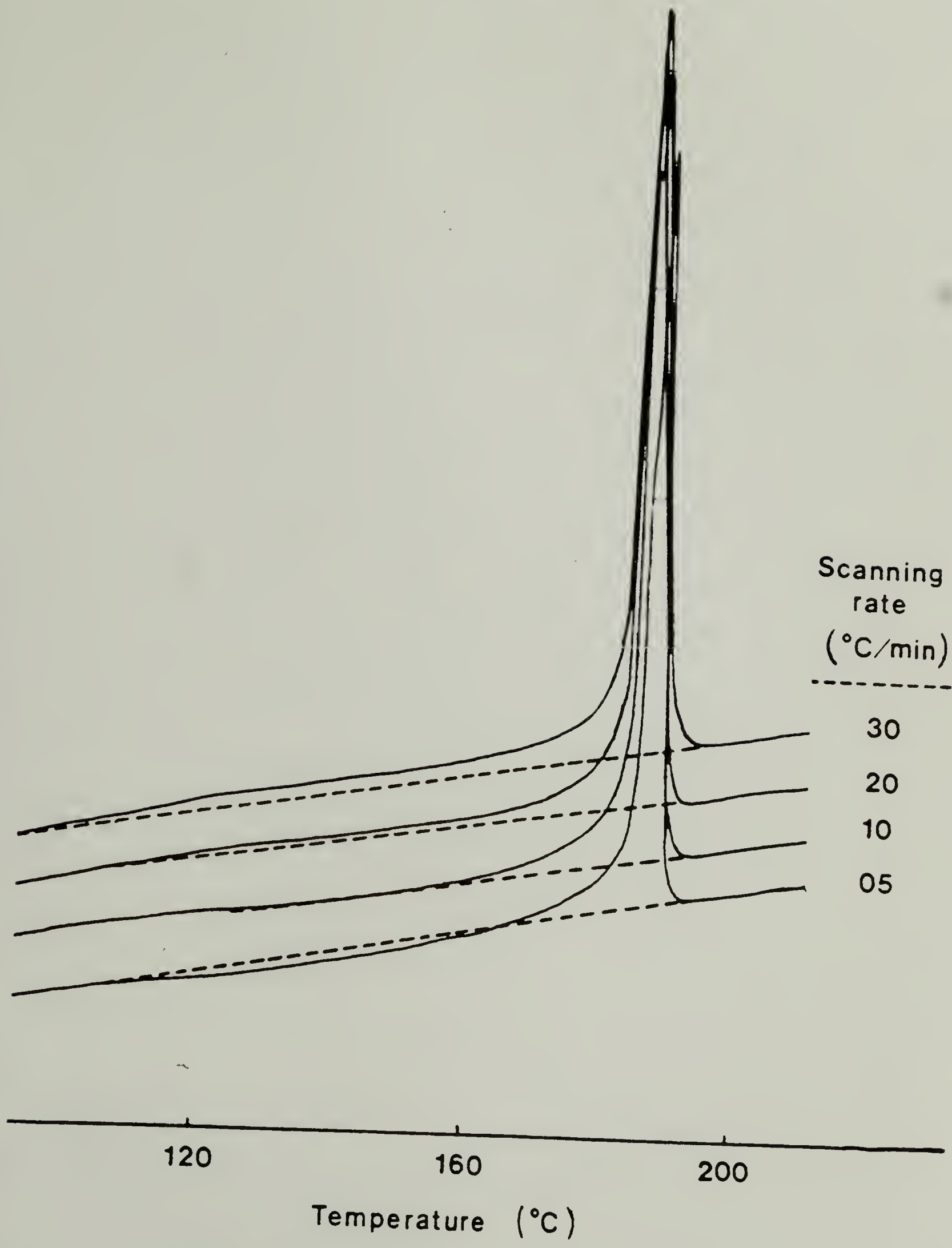

Figure 4.5. DSC heating curves at 4 different heating rates for tensile drawn nylon 11 to DR=3.55 at room temperature and at 1cm/min.

ii) At high draw and low temperature, it might also simply come from recrystallization of unravelled and pulled out molecules into the smectic form due to the large undercooling.

This process is a priori quite unlikely in the case of nylon 11 for two reasons: The draw ratio attained without sample mechanical failure are too low to justify complete molecular unravelling of the chains from the lamellar crystals. Also, such a process require the simultaneous breaking of all hydrogen bonds for the pulled out molecular segment and thus has a very high activation energy. In fact, the easiest and only molecular movement that can be reasonably considered for nylons in general in crystals is molecular shearing parallel to a plane containing the largest number of hydrogen bonds. In that case, the smallest possible number of hydrogen bonds needs be disrupted during the shear process.

Therefore, the first mechanism mentionned above is believed to be responsible for the formation of the smectic during deformation at low temperature. Annealing transforms the stress-induced smectic back into the parent crystal.

d) Characterization of Crystal Forms in Nylon 11.

i) General Considerations.

Evidence of polymorphism in melt-crystallized nylon 11 has been cited. The existence of the various ordered forms depends upon the

thermodynamic and kinetic conditions of crystallization (see Chapters 2 & 3) and deformation (see this chapter). From the geometrical viewpoint of molecular structure, the symmetry of the lattice is function of the chain mode of packing (parallel versus antiparallel), the side-by-side mode of packing of the hydrogen bonded sheets (progressive shift versus staggered shift) and the molecular conformation in the hydrocarbon segments which maximizes hydrogen bonding between amide groups as well as Van der Waals interactions (extended planar zigzag versus pleated conformation). The general nomenclature in nylons is based on these factors.

Odd nylons ,such as nylon 11, represent a particular category since maximum hydrogen bonding is geometrically possible between both parallel and antiparallel molecules in the planar extended conformation without molecular distortion. As a first approximation, both situations can therefore be a priori equally expected for the molecular packing within nylon 11 crystals. We propose to review the different forms and assess the nature of chain packing and the mode of hydrogen bonding from the structural parameters of the different forms.

ii) The Smectic δ'-form.

This form exhibits a "smectic-like" order. It crystallizes in nylon 11 at high undercoolings (Chapter 2), but also partially forms during deformation at low temperatures (Figure 4.4). Partial disorder is found in the chains packing perpendicular to the chain axis. It is

likely the result of a statistically random distribution of parallel and antiparallel chains connected by hydrogen bonds of various strength and directions. There is however molecular registry along the chain axis with an identity period significantly shorter than the expected extended conformation (12.9 Å instead of 14.9 Å). This indicates the major role of amide groups (and hydrogen-bonds) in controlling the lateral placement of adjacent chains despite important distortions between recurring amide groups along the chain axis. A shematic description was displayed on figure 2.3. The average distance between the chains is equal to 4.22 Å at room temperature:

The rationale for the formation of this phase can be justified as follows. Different types of molecular packing have been found geometrically possible and are likely to have comparable energies. Therefore, during quenching, it is likely that the system does not separate out the most energetically favorable packing, leading to a mixture of different types of interactions. On deformation also, crystal shearing to different extent induces partial disorder in the mode of hydrogen bonding, as was already mentionned in the mechanism proposed in the former paragraph. Annealing however allows the molecular segment to rearrange into the most thermodynamically stable three-dimensionally ordered crystalline α-form.

Table 4.1 Comparison of calculated and observed d-spacings for the new unit cell proposed for nylon 11.

Miller's indices hkl	Observed d-spacings d_{hkl} (Å)	Calculated d-spacings d_{hkl} (Å)
001	13.19	13.16
002	6.53	6.58
003	4.41	4.38
010	3.90	3.88
200	4.37	4.38
400	2.21	2.19
210	3.87	3.89
410	3.38	2.42
$\bar{2}01$	4.28	4.40
$\bar{2}02$	3.97	3.98
$\bar{2}03$	3.44	3.41
006	2.21	2.19
$(001)_c$	14.45	----
$(002)_c$	7.25	7.32
$(003)_c$	4.87	4.88
$(004)_c$	3.69	3.67
$(005)_c$	2.94	----
$(006)_c$	2.47	2.44

Figure 4.6. Indexation of the observed WAXD reflections for tensile stretched nylon 11 α-form at room temperature.

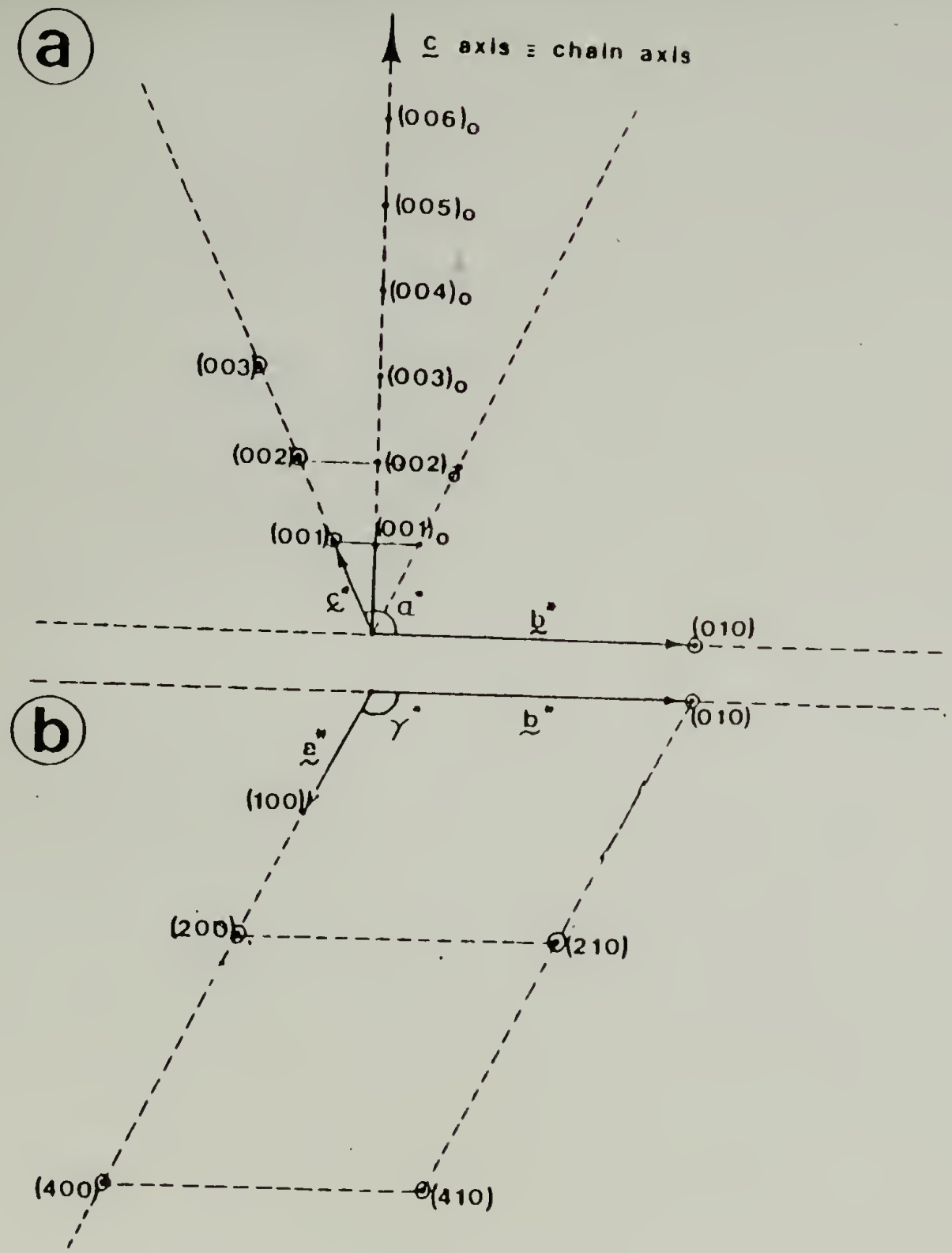
a
c axis ≡ chain axis
(006)o
(005)o
(004)o
(003)o
(003)
(002)o
(002)
(001)o
(001)
ε*
a*
b*
(010)
b
γ*
b*
ε*
(010)
(100)
(200)
(210)
(400)
(410)

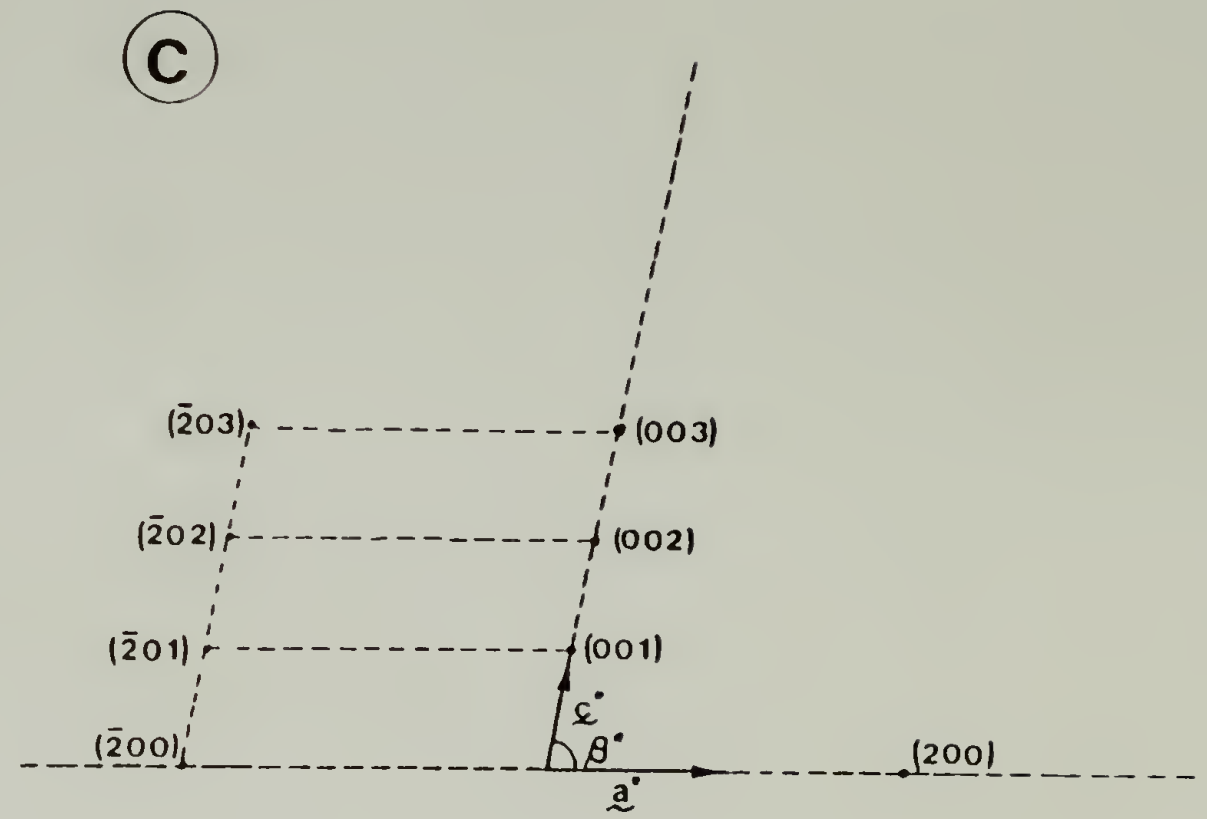
c
(2̄03)
(003)
(2̄02)
(002)
(2̄01)
(001)
ε*
(2̄00)
β*
(200)
a*

Figure 4.7. The triclinic unit cell of nylon 11 α-form at room temperature in tensile stretched specimens in real and reciprocal spaces.

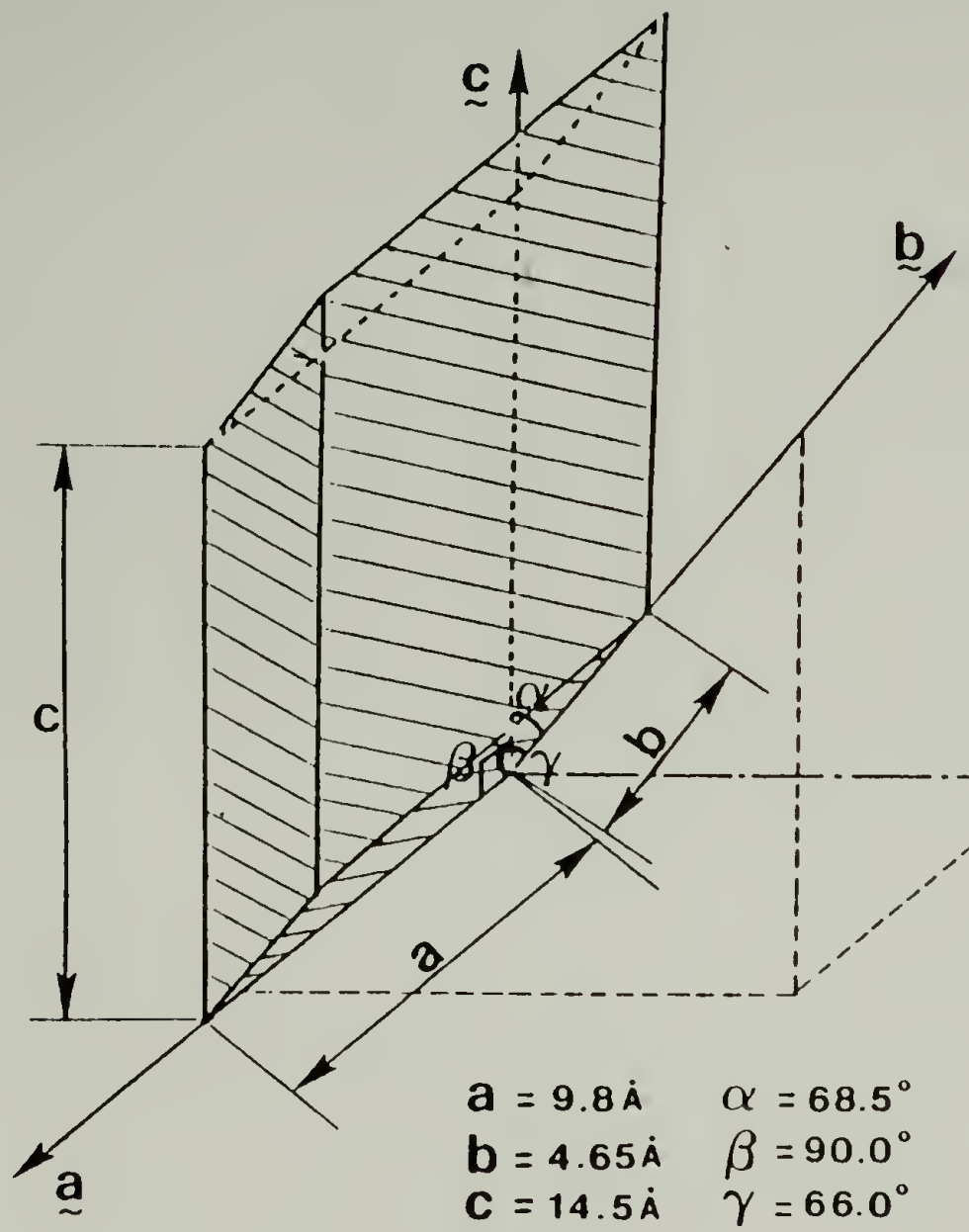

$a = 9.8\text{Å}$ $\alpha = 68.5°$
$b = 4.65\text{Å}$ $\beta = 90.0°$
$c = 14.5\text{Å}$ $\gamma = 66.0°$

Unit Cell of Nylon 11 α-FORM
IN Real Space

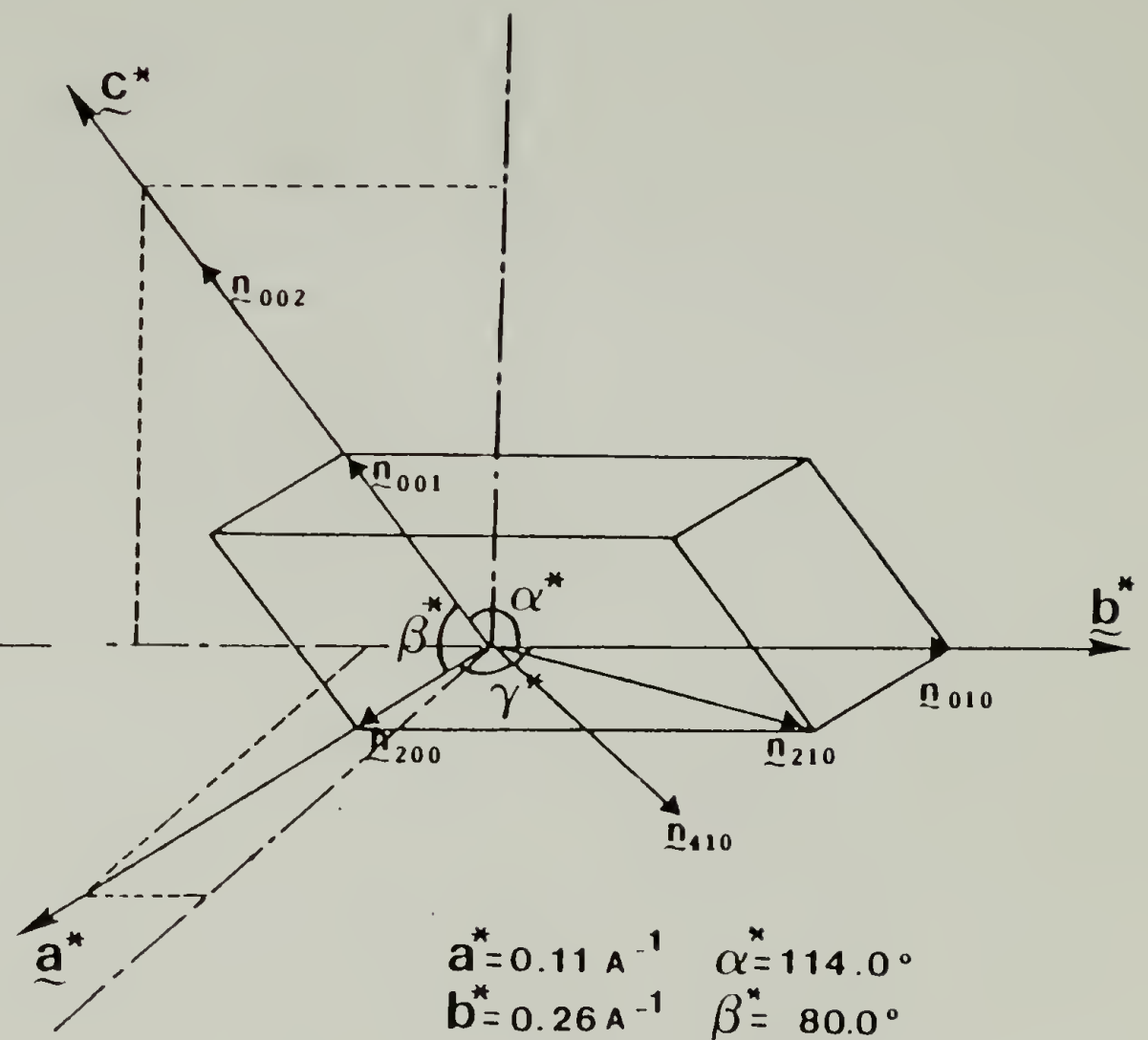

$a^* = 0.11\ \text{Å}^{-1}$ $\alpha^* = 114.0°$
$b^* = 0.26\ \text{Å}^{-1}$ $\beta^* = 80.0°$
$c^* = 0.08\ \text{Å}^{-1}$ $\gamma^* = 116.5°$

Unit Cell of Nylon 11 α-FORM
IN Reciprocal Space

iii) the Crystalline α-form.

Former investigations showed some disagreement for the crystal structure of the a-form (table 1.4) and suggest reconsideration. Figure 4.6 shows our indexation of all the observed X-ray reflections obtained for different orientations of the incident X-ray beam with respect to the tensile stretched specimen in the reciprocal space for the tensile drawn and annealed specimens with "single-crystal-like" texture. The unit cell parameters of nylon 11 in this form can be deduced at room temperature in both real and reciprocal spaces and are given in Figure 4.7:

$$a=9.8\ \mathring{A};\ b=4.65\ \mathring{A};\ c=14.45\ \mathring{A};$$

$$\alpha=68.5^{\circ};\ \beta=90.0^{\circ}\ ;\ \gamma=66.0^{\circ};$$

Each unit cell contains two monomers. The hydrocarbon segments are close to their most extended 2/1 helix configuration. Table 4.1 compares the experimental and theoretical values obtained for all d-spacings with our proposed unit cell. Details of the calculations of the d-spacings and diffraction angles are given in Appendix B. Some important implications are subjacent to the geometry of the unit cell.

Since $\beta = 90^{\circ}$, a and c are normal vectors, which indicates that hydrogen bonding preferentially takes place between antiparallel molecules. Also, hydrogen bonded sheets are parallel to the (a,c) plane. Because $\alpha \neq 90^{\circ}$, they are progressively shifted by a constant value (1.7 $\mathring{A}$) along the c-axis direction. Again, these layers are

oriented parallel to the plane of the deformed sample and the chains are parallel to the tensile axis. Figure 4.8 describes the molecular configuration of the unit cell. Among the unit cells previously reported, the one proposed by Dosiere and Point for rolled and annealed Nylon 11 samples[107] agrees best, but has different parameters. It contradicts the original structure proposed by Slichter[58] and depicted in figure 4.9, which assumes hydrogen bonding between parallel chains to be preferred over antiparallel ones. Our result thus indicates that the most stable configuration is given by the antiparallel arrangement of molecules in the hydrogen bonded planes. Moreover, we might expect this feature to be quite general since, for nylon 11 and other "odd" nylons, maximum hydrogen bonding can be achieved for similar conformation of the hydrocarbon segments, which therefore should not affect the final result.

It is of interest to recall the known structures adopted by "even" nylons and compare them from the viewpoint addressed above. "Even" nylons with short CH_2 sequence (nylons 4 or 6) usually contain the α-form with antiparallel arrangement[59,108], whereas the ones with long CH_2 sequence (nylons 8, 10 or 12) appear preferentially in the γ-form with parallel conformation[109,110]. This difference corresponds to a radical modification of the molecular conformation since molecules adopt a pleated structure which permits maximum hydrogen bonding. However, recent studies showed that crystallization (or annealing) at high pressure or solution casting of these polyamides[111-113] can also induce

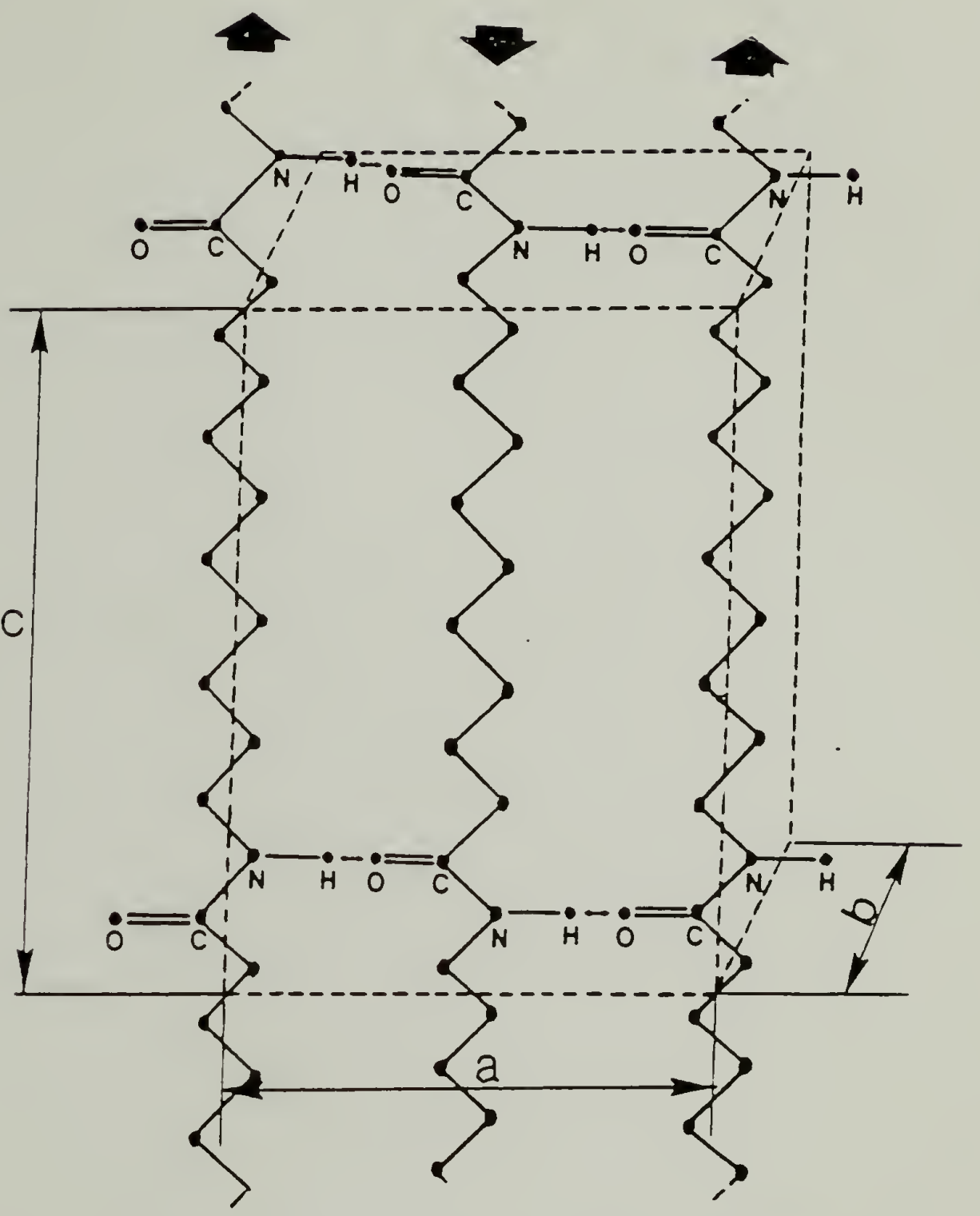

Figure 4.8. Suggested molecular structure in nylon 11 α-form. It assumes hydrogen bonding between antiparallel segments and shifted sheets packing. Hydrocarbon segments are also slightly distorted from the perfectly extended planar zigzag conformation.

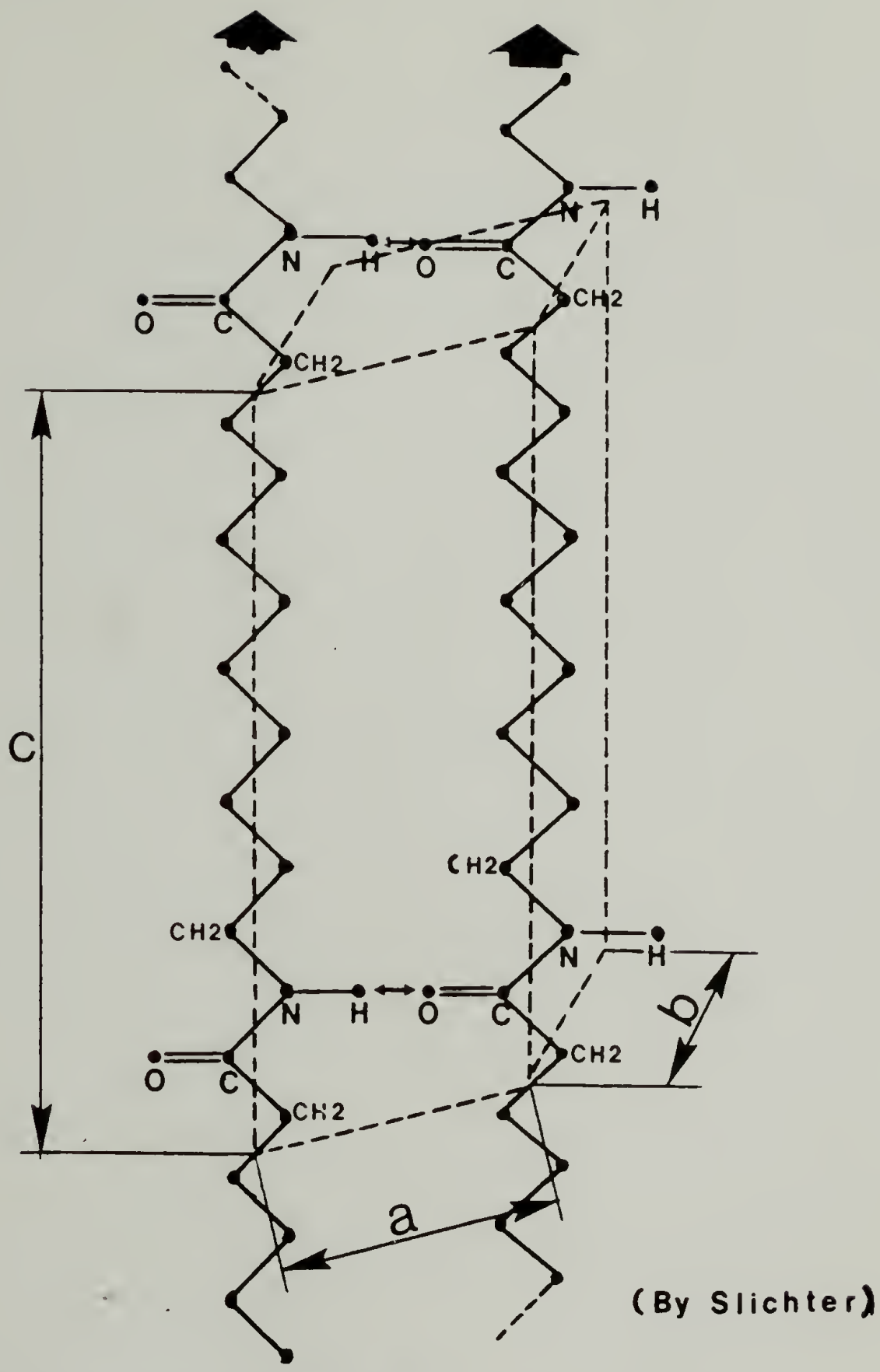

Figure 4.9 Triclinic Unit Cell assuming Parallel Chains and Shifted Sheets Packing

the apparition of the α-form for these nylons. These observations lead to the following conclusions:

For chort CH_2 sequence, the fraction of amide groups is high and hydrogen bonding between antiparallel molecules is preferred.

Inversely, as the length of the CH_2 sequence between amide groups increases, the relative amount of Van der Waals interactions between hydrocarbon segments of adjacent chains also increases in proportion to hydrogen bonding interactions. Their input contributes largely in defining the structure of lowest energy. And, hydrogen bonding between parallel segments is experimentally found to be preferred. Nontheless, by allowing these systems to crystallize under conditions which favor maximum coupling by hydrogen bonds between amide groups, antiparallel arrangement is again favored.

Therefore our result for odd nylons may be generalized to all ω-amino-carboxylic acid polyamides, in that the thermodynamically preferred arrangement dictated by hydrogen bonding is the antiparallel one.

Another aspect of the diffraction patterns also deserves particular attention. The prominent reflections situated diagonally on either side of the meridian were indexed according to the triclinic unit cell and were attributed to the progressive shifting in the packing of the hydrogen-bonded layers. In addition to these, streaks can be seen along several of the observed layer lines (mainly first and second). Similar observations have been made earlier, although they were considered as

meridional reflections by the authors, rather than continuous streaks[114].

The first assumption that these reflections could originate from an additional crystalline modification seems quite unlikely for two reasons: They are the only ones which cannot be indexed according to the triclinic unit cell; Also, the quantitative determination of the intensity of the reflection along the layer line (after correction) shows no intensity maximum on the meridian. Therefore, other explanations need to be provided to explain this spreading of the diagonal reflections along the layer line.

Our next conjecture is that the structural disorder created by the essentially random positioning of the hydrogen-bonded sheets parallel to the chain backbone in the crystals is at the origin of this particular feature. Figure 4.10 shows theta-two theta scans recorded along the meridian and along the diagonal defined by the $\underset{\sim}{c}^*$-axis. The following remarks can be made in view of these results:

i) Reflections can only be seen on the first and the second layer lines along the $\underset{\sim}{c}^*$-axis, which are indexed as (001) and (002). The small additional broad reflection at about $2\theta=20.0^{\circ}$ originates from the amorphous halo, and the broad reflection at $2\theta=40.0^{\circ}$ is in a different range.

ii) Six orders of reflections, on the other hand, are observed along the meridian and are labeled by the subscript c to indicate that they were recorded in the direction of the chain axis. the d-spacing of the first order reflection equals 14.45 $\mathring{A}$ and is equal to the one

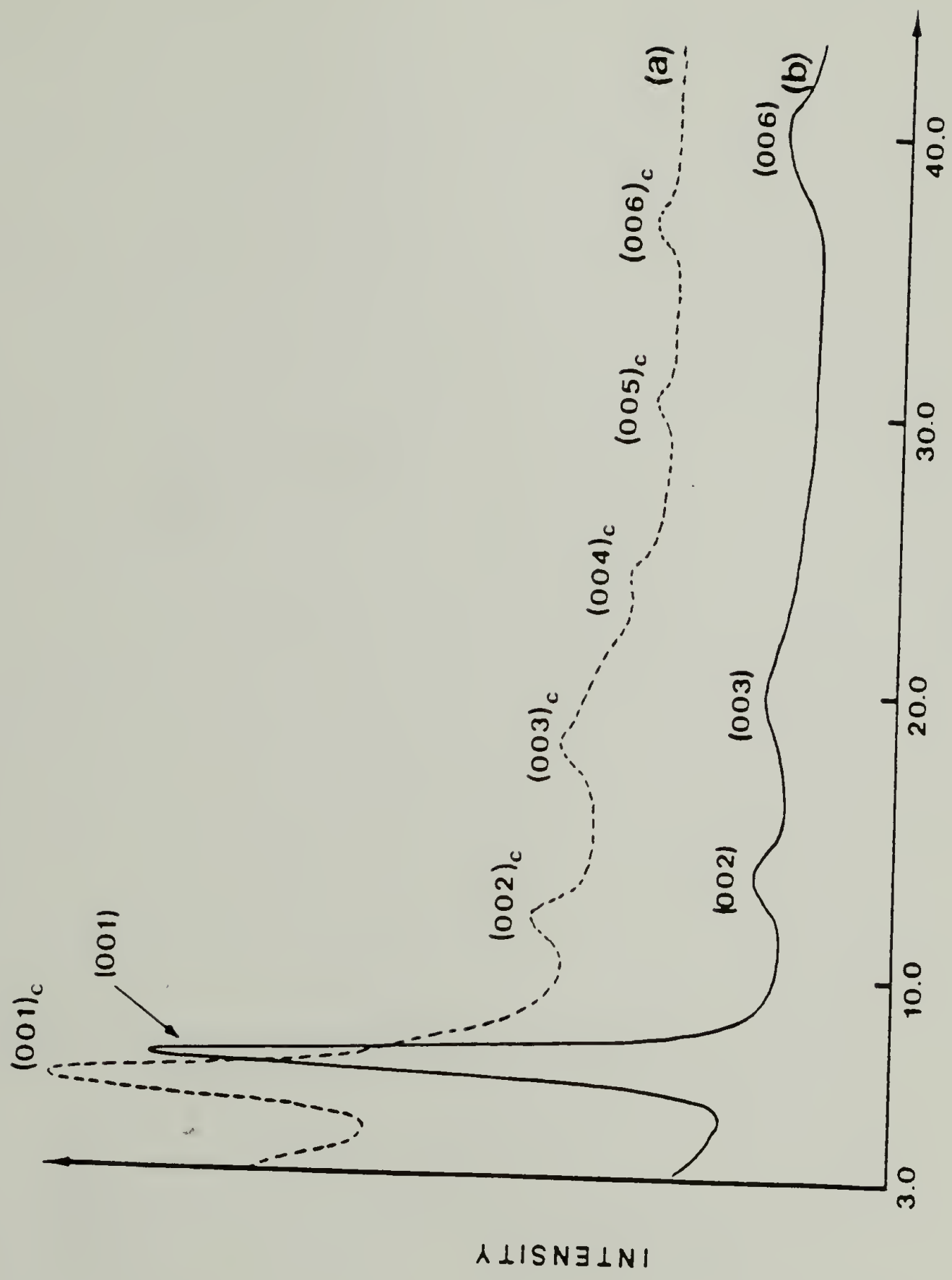

Figure 4.10. WAXD (θ-2θ) scans at room temperature for tensile drawn nylon 11 α-form:
a) along the chain axis (ç-axis);
b) along the ç -axis.

derived from the (001) reflection. It thus indicates the same conformational disposition of chains. All higher orders of reflections are found to correlate quite well with the expected d-spacings of the subcells made up varying numbers of methylene groups along the chain axis (see Appendix B).

Two conclusions can clearly be drawn from these structural data:

First, the spreading of the (001) and (002) reflections on the first two layer lines is an indication of the monodimensional disorder in the hydrogen-bonded sheet packing. In our structure, hydrogen bonds layers are progressively shifted which results in the triclinic symmetry. Interactions between neighboring sheets are strictly limited to Van der Waals type. There might be more than one possible translational vector for the mutual displacement of sheets with the same packing energy. In particular, a translation of the same amount in two opposite directions would yielding a staggered sheet packing and the presence of two distinct "triclinicities" in the sheet packing. A similar structural model have been recently proposed for nylon 10's α-form to account for anomalies in the X-ray diffraction spectrum.[112]

Second, the higher orders of reflections characteristic of the hydrocarbon subcells are observed along the chain axis and therefore indicates monoclinic symmetry in the sublattice.

iv) The High-Temperature Condis Crystal δ-form.

Chapter III demonstrated how this form could be assimilated to the high-temperature condis crystal of the low-temperature α-form. A possible description of the transition mechanism was advanced. When complete, the transition transforms the layerlike structure of the α-form into a dynamic hexagonal hydrogen-bonded network owing to the high thermal mobility of the hydrocarbon segments. The dimensions of the δ-form unit cell at 95°C would be:

$a=b=4.1\mathring{A}$; $c=12.0\mathring{A}$;

$\alpha=\beta=90^{\circ}$; $\gamma=120^{\circ}$;

It indicates a slight contraction of the chain conformation along the chain axis, whereas the projection of the $\underset{\sim}{a}$- and $\underset{\sim}{b}$-axis in the plane perpendicular to the chain axis becomes equal.

e) Macrostructure.

Figure 4.3 exhibits typical SAXS patterns of nylon 11 uniplanar-axial crystalline texture (with the α-form). Meridional reflections are obtained with the incident beam normal to the film plane, whereas a four-point diagram is seen with the beam parallel to it. Similar morphological observations are commonly reported for other cold drawn and/or rolled doubly-oriented semicrystaline polymers. And although a

truly unequivocal explanation of the origin of four point diagrams cannot universally apply to all systems, it is quite well admitted for nylons that it is usually the result of the quasiperiodic arrangement of crystalline and amorphous domains with an average inclination with respect to the chain axis to the right and left. The angle of inclination is directly determined from the direction of the SAXS maxima in the diffraction pattern. In the simplest case of meridional reflections, this angle is zero and the scattering elements are perpendicular to the chain axis. Our SAXS patterns clearly indicate that the spatial arrangement of the crystalline entities in the deformed specimen possess the same triclinic symmetry as the molecular packing in the crystals themselves. However, with the traditional interpretation of the SAXS maxima based on the two phase model and which assumes the fold surfaces to be normal to the direction of the SAS maxima, there is no simple indexation of the fold plane in terms of crystal planes. An estimate of the average Bragg spacing of the scattering elements was found equal to 82 Å. Before annealing (which converts the smectic structure into the triclinic one), only weak and broad meridional reflections could be observed which had a shorter long spacing.

3) Conclusions.

The results of the uniaxial deformation study of nylon 11 can be summarized as follows:

A reversible twinning process occur in the crystals of the α-form in the initial elastic part of the deformation, which affects the modulus of nylon 11.

At large deformations, the initial structure of the crystalline phase as well the deformation temperature are found to influence the crystal texture formed in the deformed films. Our observations are found to correlate well with the stability domains and the slip mechanisms of the crystalline forms.

Deformation at low temperatures induces the partial formation of the smectic, as shown by both X-ray and DSC, similar to the smectic form prepared during crystallization at high undercoolings.

The structures of the ordered species have been revised by WAXD. Our study underscores the differences in molecular arrangement and draws conclusions about the role of hydrogen-bonds for each of them. Hydrogen bonding between antiparallel molecules is found for the triclinic α-form and thus seems preferred over the parallel arrangement. This concept can be generalized to other ω-aminocarboxylic acid nylons and can help explain also the structures found in even nylons. The hydrogen bonded planes are progressively shifed in the α-form, although inclusions of staggered planes induces some disorder. In the high-temperature condis crystals (δ-form), the chain mobility is large enough to form a dynamic H-bonded network. The smectic exhibits a higher degree of configurational, smectic-like disorder.

C H A P T E R V

EQUIBIAXIAL DEFORMATION STUDY OF NYLON 11 BY FORGING.

1) Introduction.

After having established the phase behavior of nylon 11 and reconsidered some aspects of its behavior on tensile deformation, the study focuses on the equibiaxial deformation of nylon 11 by forging. The scope of this part of the work is to determine the behavior of this polymer during forging. This consists in characterizing the changes in structure, orientation and properties with deformation. Various conditions of forging (temperature, rate and initial structure) are examined and compared in an attempt to find the ones yielding highest orientation and optimal properties. Also, an effort is made to correlate the state of structure and orientation in forged specimens with the experimentally measured properties. Finally, the validity of the criteria mentioned in introduction to predict the optimal structure and deformation conditions on the basis of theory of crystal deformation is discussed.

2) Experimental.

The specimens used for this study are thick molded plates of nearly 5.5 mm thickness, whick showed no detectable initial orientation of the crystals as indicated by X-rays. They were again kindly provided by Atochem Corp. (France) and had same molecular weight $\overline{M}_w$ = 35,000. Initial plates contain a large fraction of smectic, which could be converted to the most part into crystal form by annealing at 180°C prior to the deformation. In fact, two sets of experiments were performed with specimens having initial smectic and crystal form respectively. Since the rate of forging was found to only have little effect on the deformation over the range studied, only results for the compression rate of 0.054 cm/min are reported. Forging temperatures investigated varied from room temperature up to 180°C with 10° increment. For each temperature, forging was carried out up to the highest compression achievable before mechanical failure of the specimens. For all specimens, the extent of deformation is described by the compression ratio as measured from the change in thickness. Only at temperatures above 160°C did the capacity of the Instron limit the deformation below its maximum possible compression ratio. Thus, for these temperatures, the experimental compression ratios are lower than the maximum that could possibly be achieved. The values of the Maximum Compression Ratios obtained versus forging temperature are reported in Table 5.1. These are denoted as MCR in the subsequent paragraphs.

Table 5.1 Values of maximum compression ratios (MCR) achieved versus forging temperature for original and heat treated nylon 11

Compression Temperature (^{o}C)	Maximum Compression Ratio	
	with initial smectic	with initial crystal
30	5.6	5.1
60	5.8	6.1
90	6.8	8.4
110	7.1	10.0
150	8.2	12.1
180	11.1	14.7

Load-displacement curves of the compression process were recorded on line during the deformation. After forging, the structure and properties of the deformed specimens were characterized. An examination of the structure and orientation of the crystals present in the deformed specimens was performed by WAXD. Thermal analysis was also conducted to determine changes in crystallinity, melting point or crystal phases with deformation. Thermograms were obtained on a Perkin-Elmer DSC 4 calibrated with an indium standart. A shrinkage test was also used to measure the amount of elastic recovery in the deformed specimens and evaluate the degree of chain extension. This was simply achieved by submersing the thin specimens in a silicone oil bath maintained at a constant temperature and measuring the change in dimension after relaxation. Finally, mechanical properties were determined by measuring the in-plane tensile moduli in the forged specimens.

3) Results and Discussion

a) Structure and Orientation of the Crystalline Phase BY WAXD and SAXD.

Rectangular samples cut along the radial direction of the forged specimens were exposed to X-rays in a Statton camera. Their diffraction patterns were recorded for two distinct orientations of the incident beam with respect to the coordinates in the sample. Examples of such patterns are shown in figure 5.1 for nylon 11 deformed at room

Figure 5.1. WAXD patterns for nylon 11 cold-crystallized at 180°C and forged at 25°C to CR=5.0:
a) The incident X-ray beam is parallel to the compression axis.
b) The incident beam is perpendicular to the compression axis.
c) After annealing of the forged specimen at 180°C.

WAXD PATTERNS OF FORGED NYLON 11

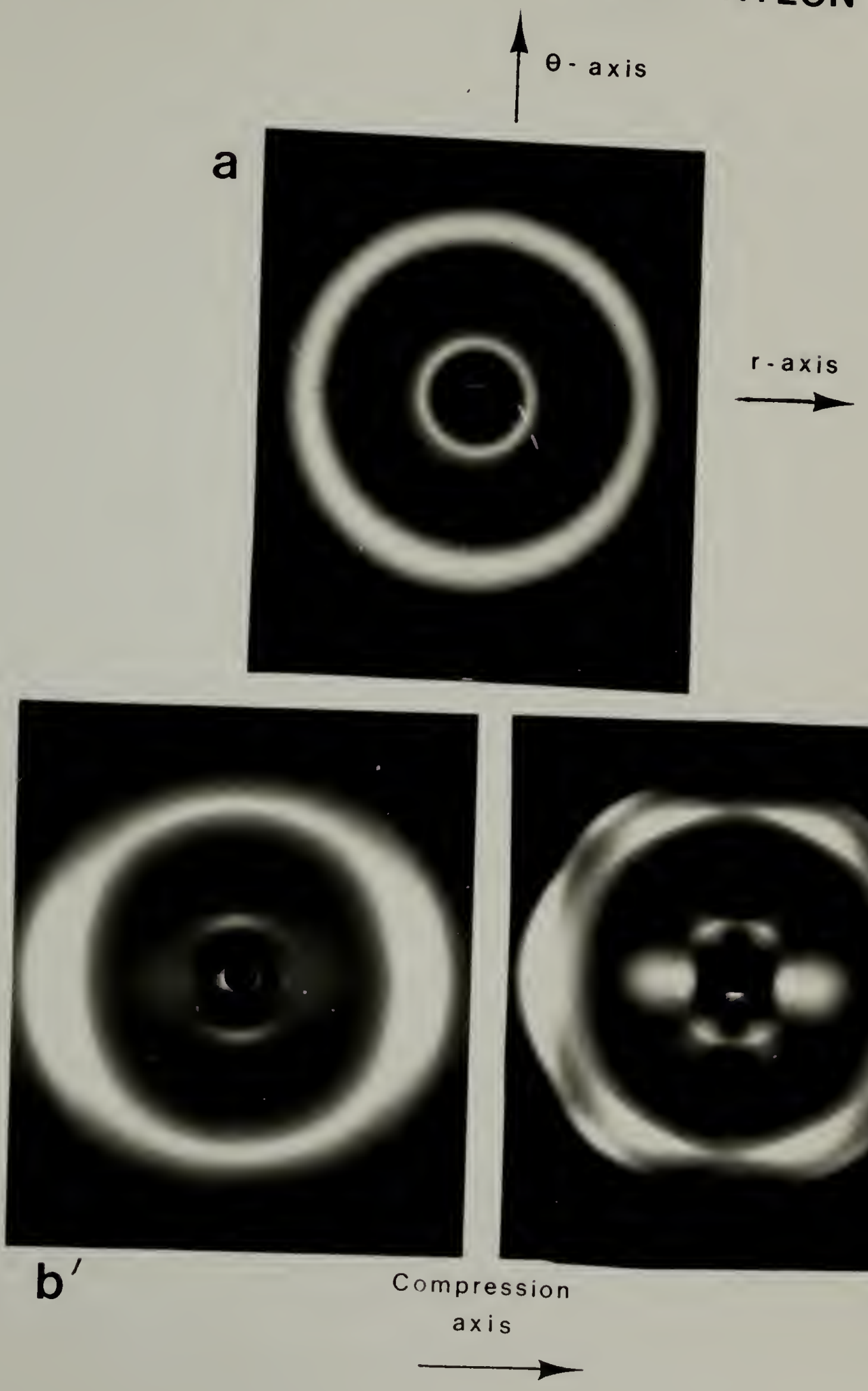

temperature. With the incident beam parallel to the compression axis (photo 5.1a), the isointensity rings in the patterns signify random orientation around the compression axis. This is in agreement with the equibiaxial nature of the process already noted for i-PP[29]. Because of equibiaxiality, one single pattern with the X-ray beam perpendicular to the compression axis is sufficient to fully describe the texture of the specimens, since all directions in the plane are equivalent. Figures 5.1b' and 5.1b'' reflect the high orientation of the crystalline phase towards the plane of deformation, prior and after annealing, respectively. In conclusion, figure 5.1 describes the random planar orientation of the molecules in the plane of compression.

Figure 5.2 compares the WAXD patterns obtained for initial nylon 11 specimens (smectic) when forged to the highest achievable compression ratios at 25, 100 and 180°C. Patterns were taken with the incident beam perpendicular to the compression axis. Concerning the crystal structure first, the broad reflection along the compression axis observed for deformation below 100°C reflects the presence of smectic independently of the initial structure prior to forging. A remaining fraction of α-form is suggested by the broad shoulder at higher diffraction angles, in the case where the α-form is initially present before deformation (figure 5.1b'). For deformation above 100°C however, the α-form content in forged nylon 11 becomes significant and increases with forging temperature. This is indicated by the progressive splitting of the (200) and (010) reflections. Again, the initial structure does not seem to affect the final structure in forged nylon 11 which is mainly

Figure 5.2. WAXD patterns for quenched nylon 11 forged to the largest achievable compression ratios at 25°C, 100°C and 180°C. Notice the smectic form at low temperatures in contrast to the α-form at high temperatures.

25 °C

Compression axis

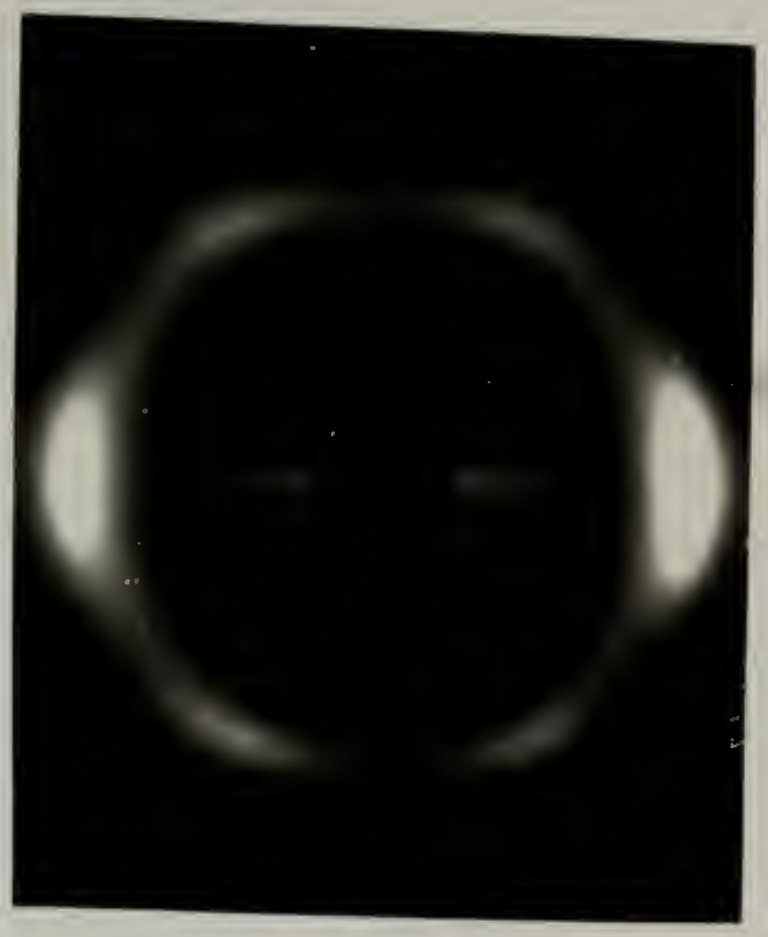

100°C

Nylon 11

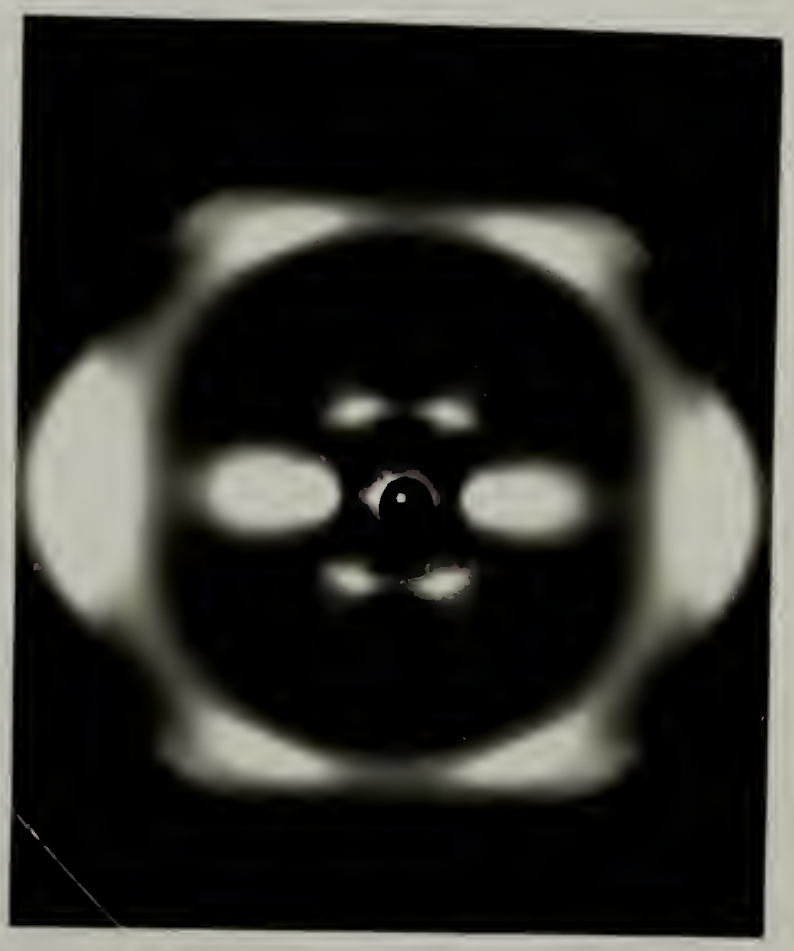

WAXD Patterns

180 °C

controlled by the forging temperature. However, Table 5.1 indicates that it affects the value of the maximum achievable compression ratio, as the difference in behavior between the smectic and crystal increases with temperature. In conclusion, this X-ray characterization provides evidence of the change of crystal structure in nylon 11 when forged below and above 100°C. This transition temperature is roughly in agreement with the one reported for uniaxial deformation.

Turning on to the orientation of the crystals, referred to as the crystal texture, the following conclusion emerge. Recalling the the symmetry argument exposed in introduction, crystals can only adopt two types of texture: The Planar texture and the Uniplanar texture, also referred to as Fiber texture. Each type of texture leads to significantly different azimuthal distributions functions of the diffracting planes in the reciprocal space. They can therefore easily be distinguished qualitatively on the diffraction pattern.

Due to its "smectic-like" order, the smectic form can only orient with the Planar texture, because all directions perpendicular to the chain axis are equivalent.

For the α-form obtained in nylon 11 forged above 100°C, table 5.2 compares azimuthal angles for each visible reflection of the Statton pattern with the ones that would correspond to the two only possible textures defined above. Clearly, the Fiber texture with the reciprocal vector $\underset{\sim}{b}^*$ parallel to the compression axis best fits the data, and is schematically shown in figure 5.3. As predicted, this texture describes the preferred alignement of the hydrogen bonded planes parallel

Table 5.2 Comparison between experimental azimuthal angles and calculated ones for the α-form in forged nylon 11 assuming both Fiber and Planar textures .

TRICLINIC α-FORM

Reflection hkl	d_{hkl} (Å)	ϕ observed	ϕ_f expected Fiber texture ($\underset{\sim}{b}^*$ // ND)	ϕ_p expected Planar texture ($\underset{\sim}{c}$ // XOY)
010	3.88	≈0°	0°	0.0°
200	4.38	≈65°	63.5°	0.0°
210	3.89	≈55°	51.0°	0.0°
001	13.16	≈65°	65.5°	24.0°

to the compression plane (in the α-form). Also, annealing of the smectic phase gives rise to its conversion into the a-form which mainly adopt Fiber texture (figure 5.1b''). Our conjecture for this phenomenon is that a small fraction of the a-form present with fiber texture in the deformed specimens is enough to induce preferred alignement of the hydrogen bonded planes of the transformed crystals parallel to the compression plane.

Finally, WAXS and SAXS patterns of a nylon 11 specimen forged and annealed at 180°C are displayed in figure 5.4 in order to compare the micro- and macrostructure of the crystalline phase. It is well established that reflections at small angles originate from difference in electron density between the regularly spaced crystalline lamellae and their amorphous surroundings. In addition, for lamellar crystalline entities, prior studies[97,98,115] have often considered the direction of the reflection to represent the normal to the fold planes. Our four-point pattern therefore indicates double texture in the orientation of the lamellae. Normals to their surfaces are found to make an angle Φ_n = 36° with the deformation plane on each side of it. Given the orientation of the unit cell from our WAXS pattern as a comparison, it turns out that there is no simple possible indexation of the fold planes in terms of crystallographic planes. This is in agreement with previous observations by others[115] and with the results depicted in Chapter IV for the case of uniaxial deformation. It suggests the presence of probable stacking faults in the lamellar crystals which affect the lamellar surface.

Crystal Texture in Forged Nylon 11

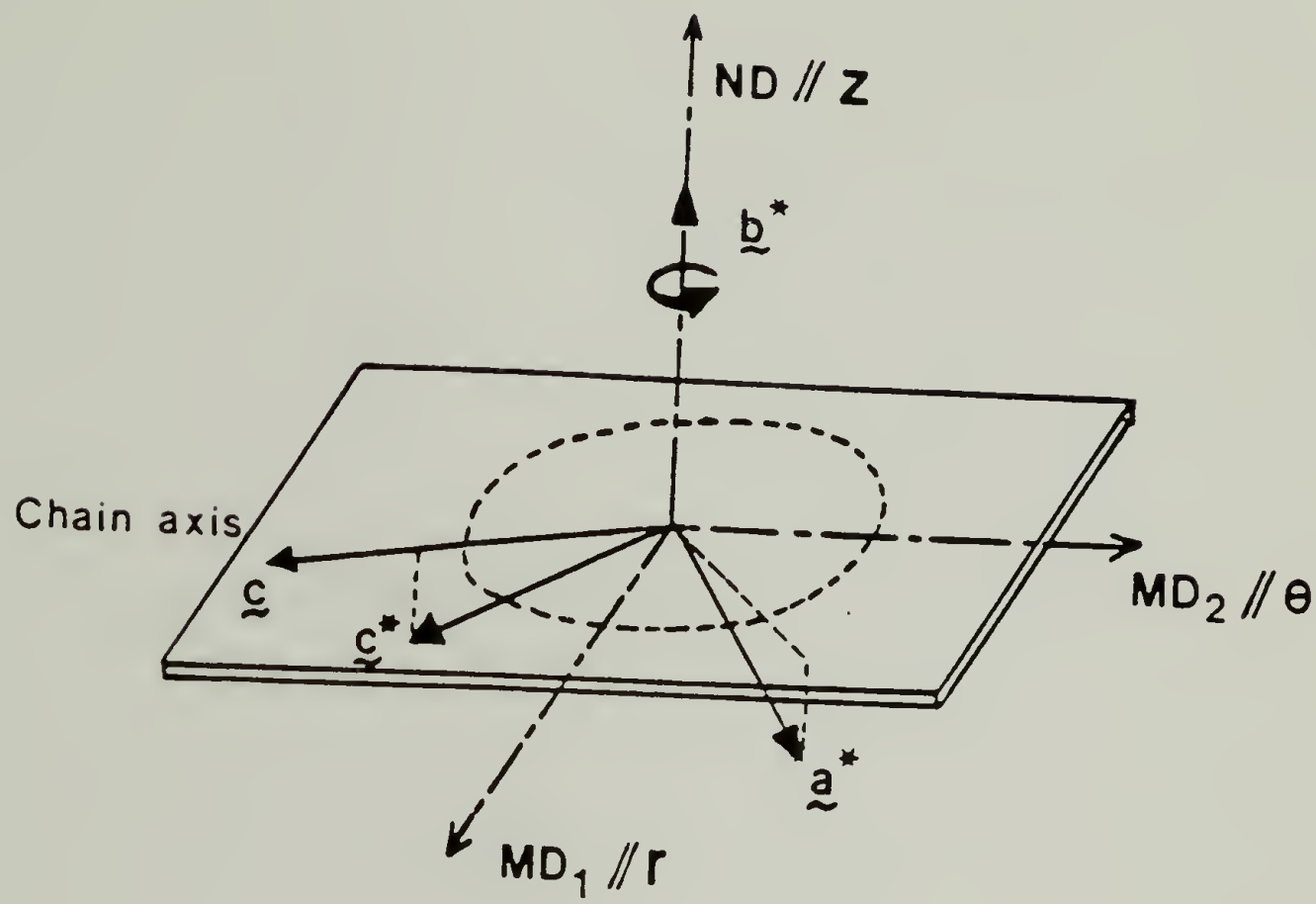

Crystal α-Form in Fiber texture :

- $\underset{\sim}{b}^*$ along Compression axis
- $\underset{\sim}{a}^*$ and $\underset{\sim}{c}^*$ random

Figure 5.3. Texture of the α-form crystals in forged nylon 11 at temperatures above 100°C; Crystals are randomly distributed around the $\underset{\sim}{b}^*$ -axis parallel to the compression axis.

Figure 5.4. WAXD and SAXD patterns of nylon 11 forged and annealed at 180°C with the incident beam perpendicular to the compression axis.

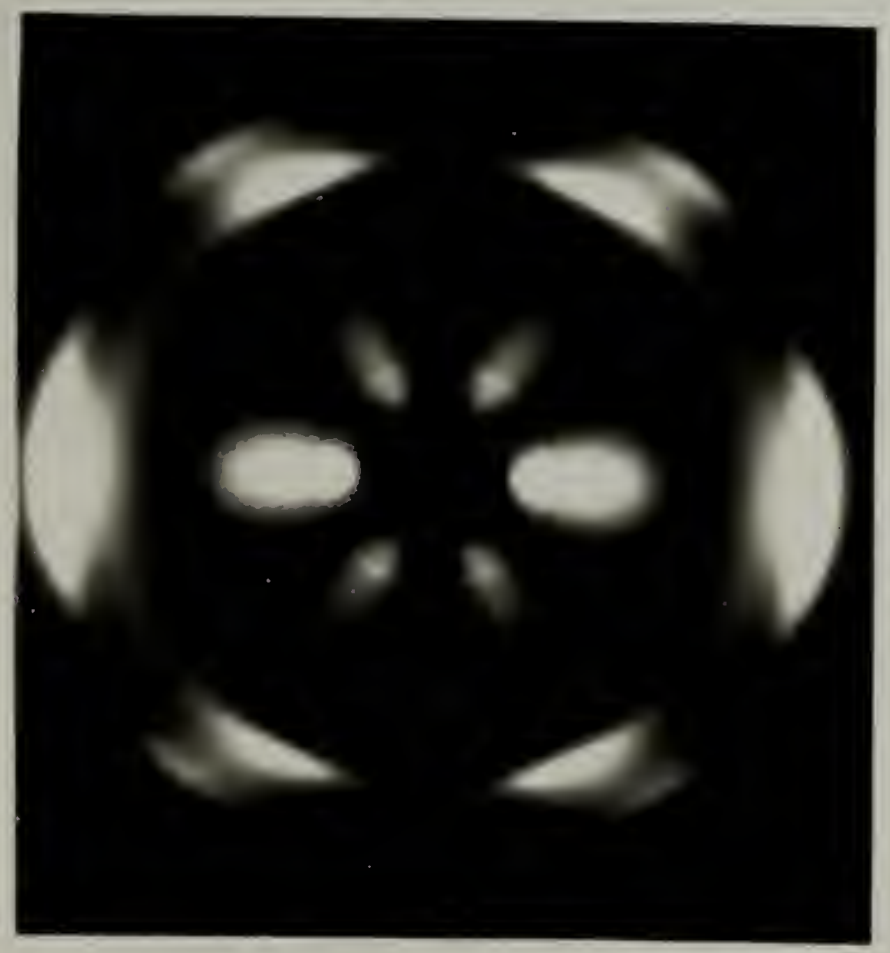

WAXS

Compression axis

SAXS

b) Thermal Analysis of Forged Specimens.

An alternate way to obtain information about the crystalline phase may be from the occurrence of its characteristic thermal transitions which can be depicted by thermal analysis. DSC heating scans were run at a constant heating rate of 10°C/min between 50°C and 230°C for specimens selected from the two series of forging experiments performed on original and preannealed nylon 11. Figure 5.5 shows thermograms recorded for the preannealed samples forged at the indicated temperatures. The recorded scans are systematically compared with their baseline extrapolated from the heat capacity of the specimen in the melt. Clearly, for deformation up to 90°C, the plot reveals the presence of a small and broad exotherm before the onset of the melting endotherm. Two processes can be thought of which could take place and give rise to an exotherm on reheating, namely crystallization or smectic to crystal transition. In order to differentiate between the two possibilities, the total heat of transition (defined as the sum of the exotherm, if present, and the melting endotherm) was measured for both original (smectic) and preannealed (α-form crystals) specimens forged at several temperatures. Figure 5.6 represents a plot of ΔH versus deformation temperature for both sample types. Also indicated for comparison is the difference in their enthalpies of fusion in the initial undeformed state. It was demonstrated earlier in chapter III how these values mainly reflect different compositions of the two ordered structures (smectic and α-form) in the crystalline phase rather

Figure 5.5. DSC heating thermograms at 10°C/min for nylon 11 specimens cold-crystallized at 180°C and forged to their largest compression ratio for each indicated temperature.

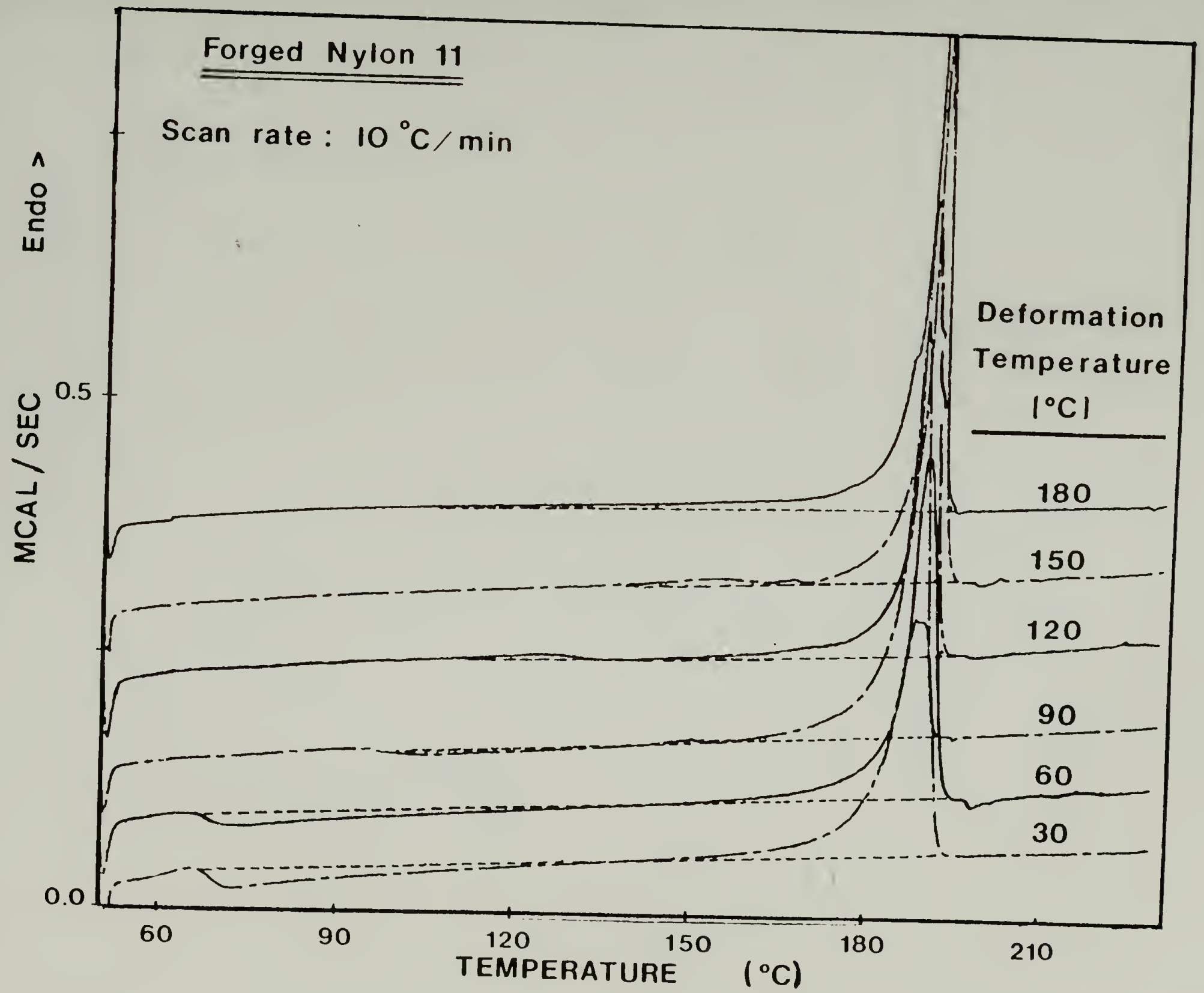
Forged Nylon 11
Scan rate : 10 °C/min
Endo >
MCAL / SEC
0.5
0.0
Deformation Temperature (°C)
180
150
120
90
60
30
60
90
120
150
180
210
TEMPERATURE (°C)

Figure 5.6. Total enthalpy of transition (including crystal transition and melting) versus forging temperature for nylon 11 either quenched (smectic) and cold-crystallized at 180°C (α-form) prior to deformation. Also shown are the initial heats of melting for both forms.

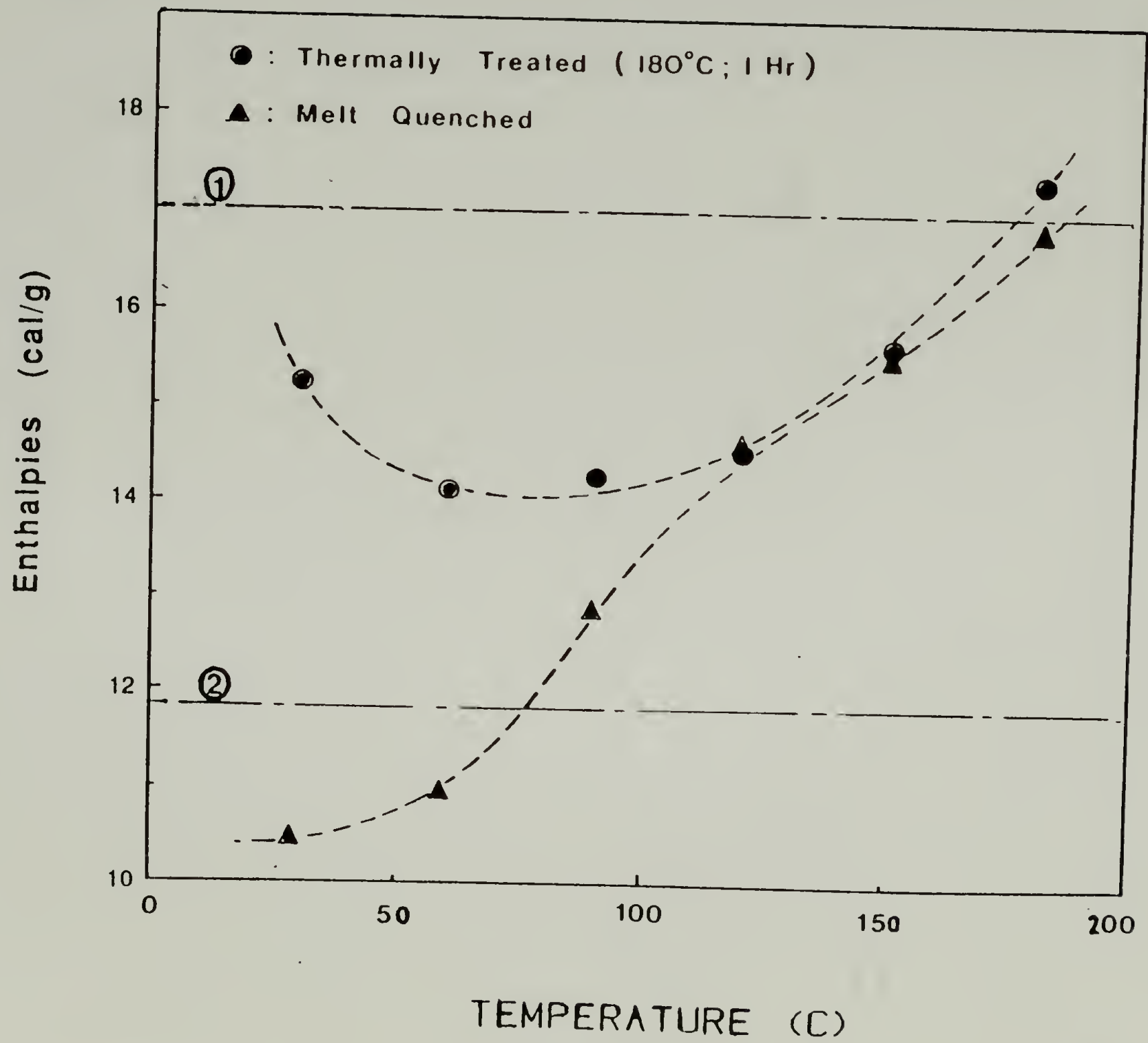
● : Thermally Treated (180°C ; 1 Hr)
▲ : Melt Quenched
①
②
18
16
14
12
10
0
50
100
150
200
Enthalpies (cal/g)
TEMPERATURE (C)

than a change in crystallinity. In fact, an approximate constant value of 25% was given for the crystallinity. The changes in enthalpy versus forging temperature depicted in figure 5.6 indicate two distinct regimes:

i) Up to forging temperatures of approximately 90°C, forging does not affect the degree of crystallinity of initially smectic nylon 11 as the heat of fusion remains approximatively constant. The enthalpy of melting of preannealed specimens (α-form) is however noticeably reduced which confirms the partial transformation of the initial crystalline α-form into the smectic δ'-form.

ii) As the temperature of deformation is chosen above 90°C, data indicate that the formation of the α-form is now favored by the forging process. This is observed on the set of data of the originally smectic specimens where the enthalpy rises significantly above this temperature. Also, for the preannealed specimens, the initial decrease due to conversion into the smectic at low temperatures is now reversed, and the α-form content increases.

Therefore, thermal analysis results are in accordance with X-ray data and confirm that forging at low temperatures favors the formation of the smectic below 90°C, and of the α-form above. At high temperatures, forged specimens have comparable enthalpies irrespective of the initial difference (in enthalpy) between the two sets of specimens. This also confirms our prior result that the initial difference in the enthalpy accounts essentially for the difference in composition of the crystalline phase, but not for a significant change

in the overall degree of crystallinity. All measured enthalpies are in between the initial values for the smectic and crystal and reflect various compositions of smectic and crystal. Therefore, the exotherm in figure 5.5 is consistent with the smectic to crystal conversion which takes place during heating.

c) Changes in Yield Behavior with Forging Temperature.

The load-displacement curves recorded on line during the forging process of nylon 11 provide a good description of the mechanics of the deformation. Examples of such curves are given in figure 5.7 for two different deformation temperatures. They can be used to determine some specific parameters characteristic of the mechanics of the deformation. One parameter of special interest for our study of deformation of nylon 11 by forging is the compressive yield stress, which marks the onset of plasticity during the compression process[116]. It indicates the stress necessary for the crystals to start deforming plastically, or in other words to undergo shearing via slip processes. In compression tests, the yield point is commonly defined as the point of intersection of two linear regions associated with the elastic and plastic behavior respectively. This method was applied to determine the yield stress in all the load-displacement curves obtained during forging of the two series of nylon 11 specimens. First of all, qualitative differences are depicted in the load-displacement curves for the initial and preannealed specimens;

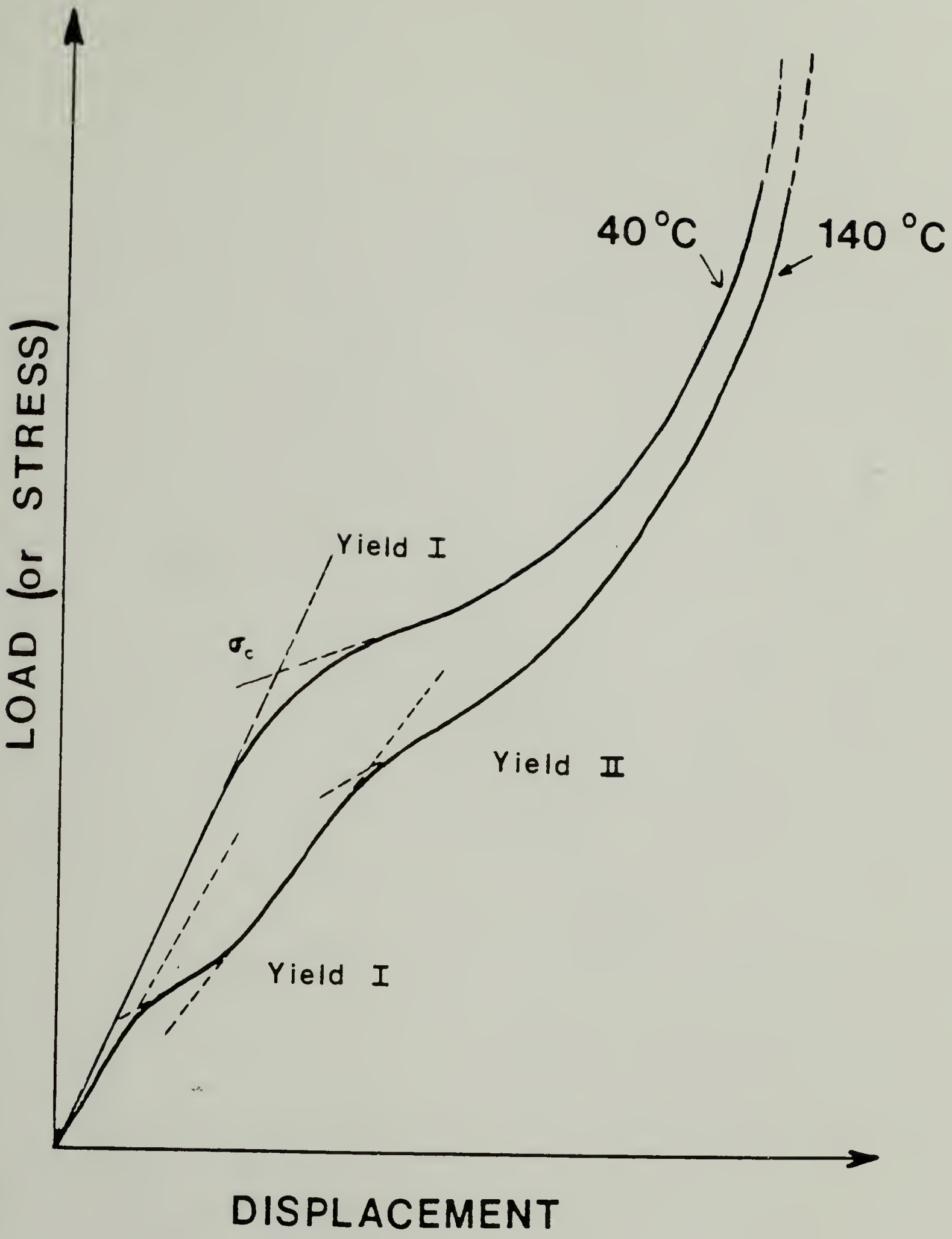

Figure 5.7. Load-Displacement curves for quenched nylon 11 in uniaxial compression at a rate of 0.054 cm/min at 40°C and 140°C. Notice the single yield behavior at low temperatures versus the double yield at high temperatures.

i) The initial smectic specimens display one single yield point when forged below 100°C but show double yield behavior for higher deformation temperatures. Examples of these two regimes are shown on figure 5.7 (for deformation at 40°C and 140°C, respectively).

ii) The preannealed nylon 11 specimens on the other hand show one single yield at all temperatures.

All the experimentally determined yield stress values are plotted versus the deformation temperature on a single graph shown in figure 5.8. The data are shown on an Arrhenius plot which thus provides the activation energy of the yield process. The data reveal several aspects of the deformation that can be summarized as follows:

i) At low temperatures, both original and preannealed specimens exhibit a linear dependence of $Ln(\sigma_c)$ as a function of the inverse of the temperature, with same activation energy. The yield stress values are simply larger for nylon 11 containing the α-form than for the ones largely made of the smectic phase.

ii) At temperatures above 100°C, the first yield process of the original samples apparently corresponds to the yielding of the smectic form as it maintains the same activation energy as at low temperatures. On the other hand, the second yield observed exhibits similar compressive stresses as for the preannealed specimens and must therefore reflect the same process as for the α-form.

The following interpretation for these observations is proposed in accordance with our WAXD and thermal analysis results. At low

Figure 5.8. Arrhenius plot of compressive yield stress versus forging temperature for quenched (●) and annealed (★) nylon 11. Both yield stresses are plotted in the case of double yield behavior. Compression rate: 0.054 cm/min.

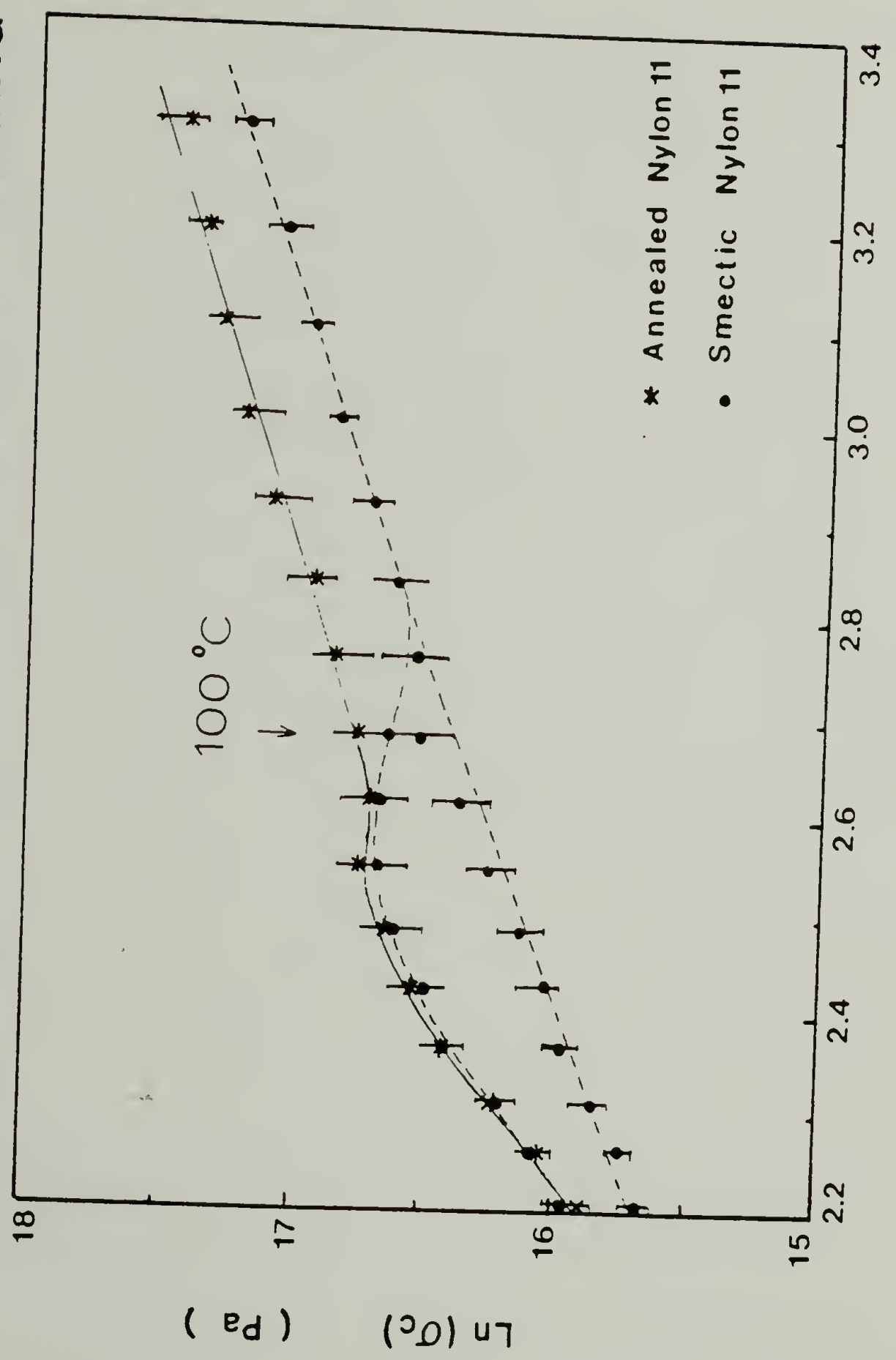
COMPRESSIVE YIELD STRESS IN FORGING
★ Annealed Nylon 11
• Smectic Nylon 11
100 °C
Ln (σc) (Pa)
18
17
16
15
2.2
2.4
2.6
2.8
3.0
3.2
3.4
10³/ Tdef (1/K)

temperatures below 90°C, the difference in the measured yield stresses simply reflects differences between the two crystals forms. As expected, because of its higher energy of packing, the α-form requires a higher stress to plastically deform than the semidisordered smectic form. Nontheless, the two moieties are found to have approximately the same activation energy. At high temperatures, on the other hand, deformation favors the formation of the α-form in the crystalline phase as indicated by WAXD. Thus, if initially present, the smectic has to transform during the course of the process. Our conjecture is that the second yielding process which occurs after the onset of plastic deformation of the smectic corresponds to the plastic deformation of α-crystals which form during the process from the smectic under stress. This is consistent with the smectic-crystal transformation already characterized during forging above 100°C.

Hydrostatic pressure is generally known to affect the yield behavior of amorphous and semicrystalline polymers. And a measure of the hydrostatic component of stress can be estimated from the difference between the tensile and compressive yield stress. The original yield criteria have been modified to include a hydrostatic component of stress. These include the Tresca yield criterion[117], which states a critical value for the shear stress, and the von Mises criterion[118], which considers a critical value for the total energy defined by the second stress invariant. These are known as the modified Tresca or modified von Mises criteria. Both yield a linear

dependence of the yield stress with hydrostatic pressure and were previously found to fit experimental data satisfactorily.

$$\tau_m = \tau_o + \gamma_o P_h \; ; \qquad (5.1)$$

$$\tau_{oct} = \tau'_o + \gamma'_o P_h ; \qquad (5.2)$$

These two criteria have been shown to be equivalent and define identical critical stress conditions for yielding. The associated parameters can be easily determined for the experimental values of the yield stress measured in both tension and compression[29]. They are given by the following expressions:

$$\tau_o = \frac{\sigma_t \sigma_c}{\sigma_t + \sigma_c}; \qquad \gamma_o = \frac{3}{2} \frac{\sigma_t - \sigma_c}{\sigma_t + \sigma_c}; \qquad (5.3)$$

In order to determine the tensile yield stress of nylon 11 for various temperatures of deformation, preannealed films were tensile stretched in an Instron under controlled conditions at a typical rate of 1 cm/min (chapter IV) and the load-displacement curves were recorded on line. The yield stress was taken as the stress at the maximum observed load and the results are shown in figure 5.9 on an Arrhenius plot. Also reported in table 5.3 are all the experimental values of the tensile and compressive yield stress at all temperatures along with the calculated parameters for the modified Tresca yield criterion. Most particularly, the variations with temperature of the hydrostatic pressure coefficient

Figure 5.9. Arrhenius plot of tensile yield stress versus drawing temperature for quenched (●) and annealed (★) nylon 11. Drawing rate: 1cm/min.

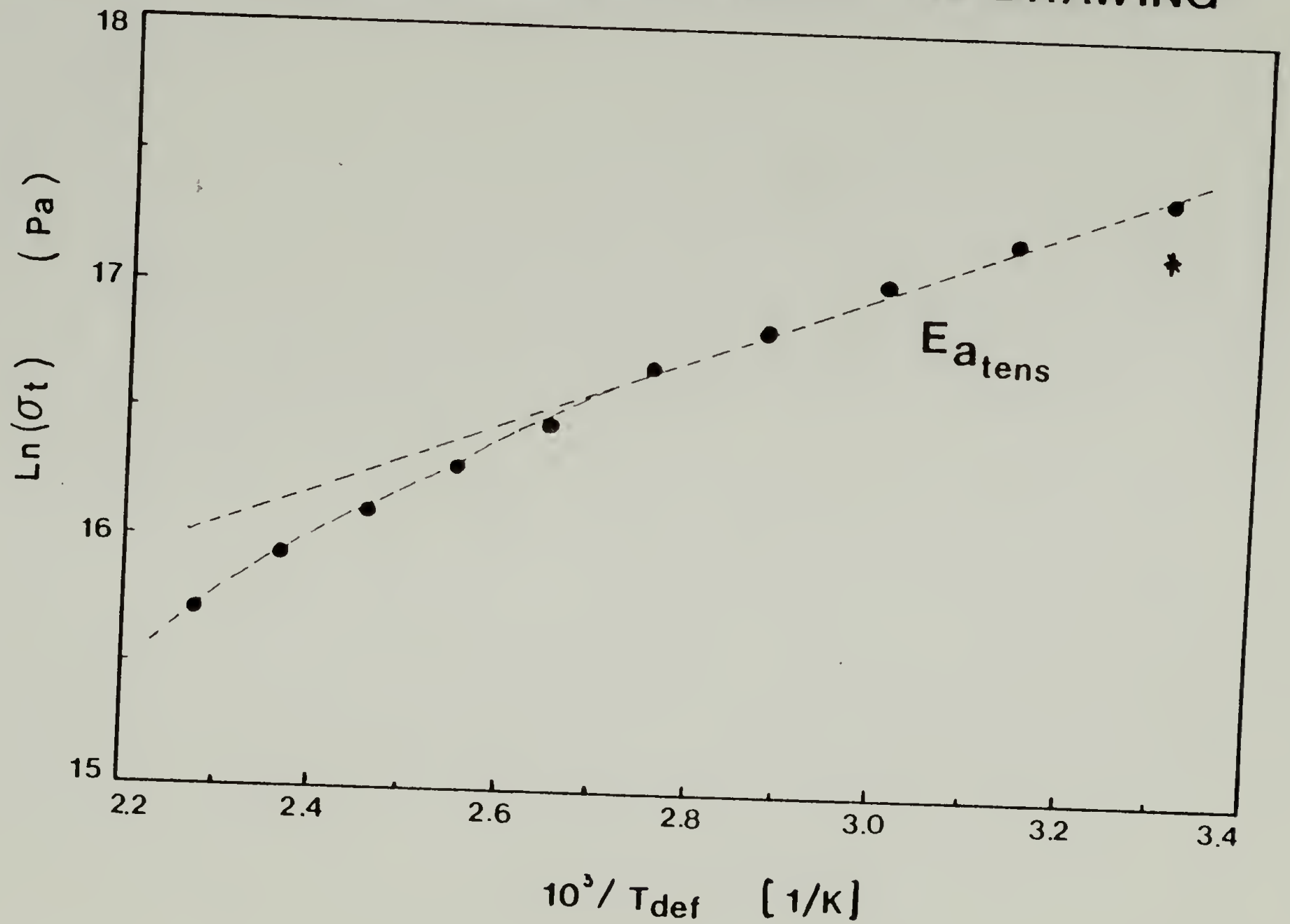
TENSILE YIELD STRESS IN DRAWING
Ln(σt) (Pa)
18
17
16
15
2.2
2.4
2.6
2.8
3.0
3.2
3.4
Ea tens
10³/ Tdef [1/K]

in the yield stress expression, υ_o, are represented in figure 5.10. This coefficient has been referred to in the past as the Bauschinger coefficient. Our data indicate two increasing jumps for its value: one at about 50°C, which corresponds to the glass transition region of nylon 11, and the other even more pronounced around 110°C, which was found to correspond to the onset of the stress-induced formation of the α-form in the crystalline phase. In both cases, hydrostatic pressure causes "stiffening" of the material since the yield surface is inflated by an amount proportional to the Bauschinger coefficient. This result clearly provides another indication of the major role played by the hydrostatic pressure on the occurrence of the stress-induced crystal transformation at high temperatures in nylon 11. Our absolute values of the Bauschinger coefficient range from 0.06 to above 0.3 depending upon the temperature, which are relatively high in comparison to other polymers. A reported value for crystalline PET has been for example 0.075[119].

d) Shrinkage Measurements.

The efficiency of the forging process, that is its ability to stretch and orient chain molecules in the draw plane can be further assessed by measuring the entropic shape recovery induced thermally by raising the temperature up to the melting point. The rationale beyond the schrinkage method is the tendency for the chains to return to the their original most probable unperturbed conformation, when given enough mobility. Heating above T_g and T_m is necessary to allow relaxation in

Table 5.3 Variations of tensile and compressive yield stresses with deformation temperature for nylon 11. Calculated parameters of the modified Von Mises Yield Criterion .

Deformation Temperature T_{draw} (^{o}C)	Compressive Yield stress $\sigma_c x10^{-7}$ (Pa)	Tensile Yield stress $\sigma_t x10^{-7}$ (Pa)	atm. pres. Yield stress $\tau_o x10^{-7}$ (Pa)	Bauschinger coefficient μ_o
30	3.71	3.57	1.82	0.029
40	3.53	3.26	1.69	0.060
50	3.26	2.83	1.51	0.106
60	2.98	2.46	1.35	0.143
70	2.70	2.18	1.21	0.160
80	2.30	2.00	1.07	0.105
90	2.12	1.79	0.97	0.127
100	1.94	1.60	0.88	0.144
110	1.83	1.37	0.78	0.216
120	1.88	1.18	0.72	0.343
130	1.70	1.09	0.66	0.328
140	1.52	0.96	0.59	0.339
150	1.32	0.85	0.52	0.325
160	1.10	0.76	0.45	0.274
170	0.93	0.69	0.40	0.315
180	0.87	0.57	0.34	0.261

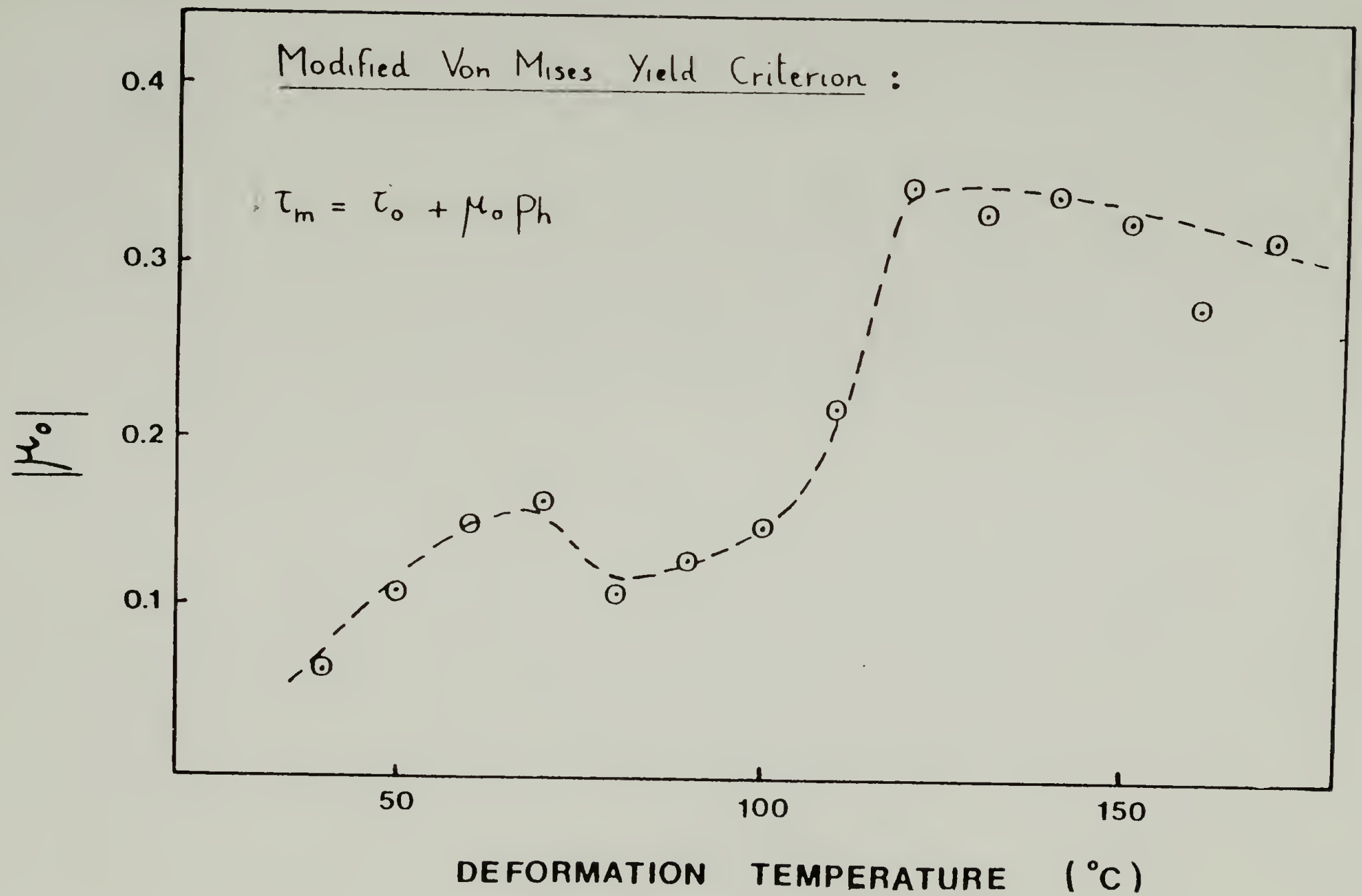

Figure 5.10. Hydrostatic pressure coefficient (in the modified Von Mises Yield criterion) versus deformation temperature for nylon 11 quenched and annealed at 180°C prior to deformation. The data were obtained from the comparison of the experimental yield stress found during drawing and forging.

the amorphous and crystalline phase, respectively. The difference in size prior and after the shrinkage test gives a measure of the molecular recovery at any given temperature. This is assumed to reflect the actual molecular draw of the chains if the shrinkage is perfectly all elastic with no visous dissipation through network slip. For our case of equibiaxial deformation by forging, the elastic recovery ratio, R, can be defined as:

$$R=\frac{H_c - H_s}{H_c - H_o}; \qquad (5.4)$$

where H_c, H_o and H_s are sample thickness after forging, before forging and after shrinkage, respectively. This parameter measures the efficiency of the process at any forging temperature and for any given compression ratio by comparing the relative molecular draw of the chains as given by the shrinkage test with the draw expected from the change in dimensions of the specimens during the process.

Data for forged nylon 11 are shown on figure 5.11. They correspond to nylon 11 plates "as received" which were forged at the indicated temperatures up to the MCR prior to specimen failure. From our recovery data in the melt at 200°C, the efficiency of the process appears to be the largest for high forging temperatures, the maximum been at 110°C. As mentioned earlier, forging nylon 11 above 160°C had to be aborted before the limit of deformation of the material could be reached due to equipment limitation. Thus, the recovery ratio measured for these specimens may underestimate the maximum value achievable. In any case, results indicate the high efficiency of the forging process over the

Figure 5.11. Elastic recovery ratio ($R=\frac{H_c - H_s}{H_c - H_o}$) versus temperature of recovery for nylon 11 specimens forged to the highest possible compression ratio at a constant rate of 0.054 cm/min and at the following temperatures: 40, 70, 110, 140 and 180°C.

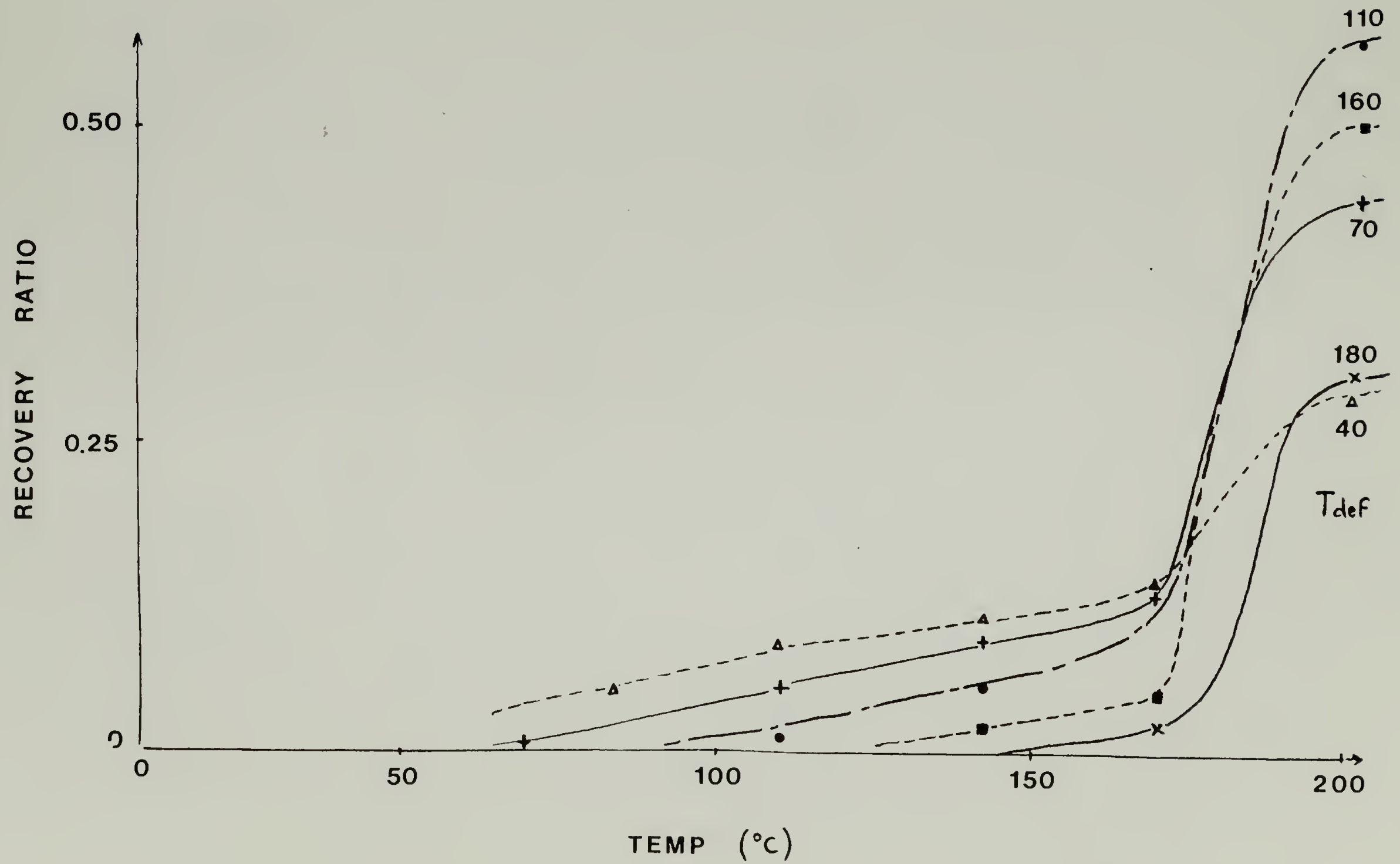
RECOVERY RATIO
0.50
0.25
0
0
50
100
150
200
TEMP (°C)
110
160
70
180
40
Tdef

high temperature regime of the deformation, where the process involves deformation of the α-form. Relatively low value of the elastic recovery ratio (R=0.58 in the best case) indicates significant departure from affine deformation. For specimens forged at lower temperatures, relaxation phenomena are found to be already quite significant even below the melting point and can repesent up to 1/3 of the total recovery ratio after melting. Forging at higher temperatures, however, induces greater dimensional stability of specimens at all temperatures in the solid state even above T_g and provides evidence of a "pseudo-continuous" crystalline phase throughout the forged nylon 11 specimens.

e) **Mechanical Properties: Tensile Modulus.**

Among the mechanical properties of polymers in the oriented state, the modulus is known to be a sensitive measure of the degree of molecular orientation and extension as well as the morphology of specimens. Tensile moduli were measured in the plane of forged specimens of nylon 11 at room temperature with the use of an Instron. Dogbone-shaped samples were cut out along the radial direction (all directions are equivalent) and their length, width and thickness were accurately measured prior to the tensile test. Specimens tested belong to the two series which had been forged at various temperatures, at a rate of 0.054 cm/min, having either the smectic δ'-form or the crystal α-form as the initial crystal form. They also did not receive any thermal treatment prior to the tensile test. All specimens (except for

temperatures above 160°C) were forged to the highest compression ratio which could be possibly achieved without sample failure at each chosen set of deformation conditions. Therefore, the moduli measured for each set of forging conditions can be expected to indicate the largest modulus which can possibly prepared under this set of conditions. Values of such moduli are presented in figure 5.12 as a function of compression ratio for the two series of measurements.

There is little or no improvement of the tensile modulus in the plane for nylon 11 forged below 90°C as compared with the isotropic state. Therefore, the modulus remains in the range of 1 GPa. However, at temperatures above 100°C, higher moduli are obtained which increase with compression ratio. It has to be noted also that higher draw ratios and larger moduli were systematically obtained with nylon 11 initially in the α-form (instead of the smectic form). In any case, the optimal modulus achieved is lower than 3 GPa.

Interestingly, the temperature range where forging has no effect on the tensile modulus corresponds to the range of formation and/or stability of the smectic form. In contrast, high-temperatures, which favors stability of the α-crystals, set the most favorable conditions of equibiaxial deformation in terms of tensile modulus improvement.

It might be of interest to compare the experimental moduli with theoretical predictions. In reference to the Introduction chapter, an estimation of the average tensile modulus in the deformation plane can be calculated if the forged specimens are considered to be equivalent to planar composites made of randomly oriented fibers. The analytical

Figure 5.12. Experimental in-plane tensile modulus versus compression ratio for nylon 11 specimens forged to the highest possible compression ratio at 30, 60, 90, 110, 150 and 180°C.
(o) Original quenched nylon 11 (smectic);
(*) annealed at 180°C (essentially α-form).
For comparison, tensile modulus for uniaxially drawn nylon 11 versus draw ratio are also indicated:
(▲) coextruded at 194°C.
(⧫) drawn at 120°C.

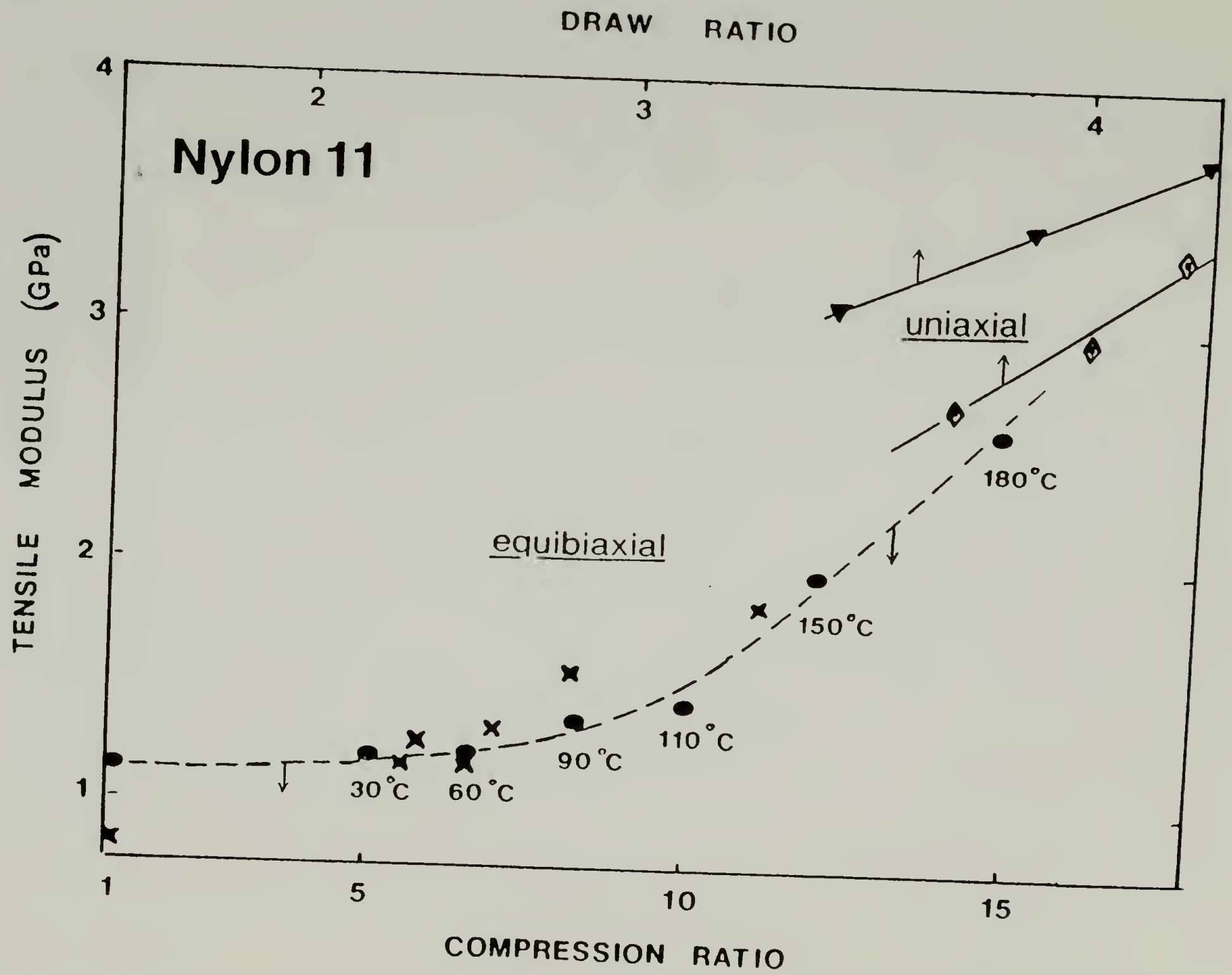
DRAW RATIO
Nylon 11
MODULUS (GPa)
TENSILE
uniaxial
equibiaxial
180°C
150°C
110°C
90°C
60°C
30°C
COMPRESSION RATIO

expression for the compliance (which is simply the inverse of the modulus) was shown in introduction to be:

$$J = \langle J^{\theta} \rangle = \frac{2}{\pi} \int_0^{\pi/2} J^{\theta} d\theta \qquad (5.5)$$

where J^{θ} is given by the equation:

$$J^{\theta} = \cos^4\theta \; J^u + \sin^4\theta \; J^t + L \sin^2\theta \cos^2\theta \; ; \qquad (5.6)$$

$J^t = \frac{1}{E^t}$ is the tensile compliance along the draw direction and $J^u = \frac{1}{E^u}$ is the transverse compliance for the fibers which make up the composite. The modulus of the fictive fibers should clearly be a function of the extent of draw in the plane (as produced by forging). In the simplest case where the density would remain constant during the process, mass conservation dictates that a compression ratio CR would yield a maximum draw ratio $DR=\sqrt{CR}$ in all directions of the plane. This equivalence can be used as a basis for comparison of modulus enhancement in uniaxial and equibiaxial processes. If the dependence of the tensile modulus of the fiber is known as a function of draw ratio for the polymer studied, it can be used to evaluate the modulus of the fictious fibers which make up the composite. Given the tensile and transverse moduli for these fibers, the modulus of the random distribution of these fibers in a plane by equation 5.5. In any case, the tensile modulus for the composite should always be intermediate between the modulus for the isotropic polymer and the modulus in uniaxial for a draw ratio $DR=\sqrt{CR}$.

Two sets of data for the tensile modulus of nylon 11 as a function of draw ratio are plotted in figure 5.12 and compared with the moduli of the forged specimens. The high moduli obtained by forging at high temperatures are close to the ones obtained uniaxially for the corresponding draw ratio, which confirms the high efficiency of the forging process under these conditions of deformation.

4) Conclusions.

All characterization methods used for the study of equibiaxial deformation of nylon 11 by forging have indicated the occurrence of two distinct mechanisms in the deformation process for temperatures above and below 90°-100°C. Forging at high temperatures thermodynamically favors the α-form crystals which orient with the Fiber texture, in contrast to the metastable δ'-smectic form which prevails during forging at low temperatures (and has Planar texture). Optimal deformation conditions are found over the high-temperature range, as evidenced by the larger compression ratios which can be achieved (CR=14.8 at 180°C), the higher draw efficiency (R≥ 50%) and the large tensile moduli obtained. On the other hand, no modulus enhancement is found for nylon 11 deformed below 90°C. An explanation is proposed based on the theory of crystallography of slip by comparing the slip mechanisms and ductility of each crystal form. Smaller compression ratios were systematically obtained when deforming the smectic, despite it looser structure and expected highest ductility. No preferred slip mechanism

controls the shearing of this form. On the other hand, the existence of a major slip plane (the hydrogen bonded plane) with two possible slip directions (c-slip and transverse slip) makes the α-form a priori a better candidate for biaxial deformation. Therefore, in the case of nylon 11, our criteria to select the ideal conditions for biaxial for biaxial deformation on the basis of slip systems and shear mechanisms in the crystalline phase can apply.

C H A P T E R VI

EQUIBIAXIAL DEFORMATION STUDY OF HDPE BY FORGING

1) Introduction.

Among all the slip mechanisms which participates to the plastic deformation of polyethylene crystals in semicrystalline high density polyethylene, such as crystal shearing, twinning or martensitic transformations, shear processes are the only one capable of producing large plastic strains. For this reason, they are often simply called slip processes. They have received considerable attention, especially in the field of fibers, where solid state deformation and extension techniques are been developed to prepare highly drawn filaments exhibiting extreme mechanical properties.

Prior investigations have focused on trying to elucidate the active slip systems in polyethylene crystals. Despite the confusion arising from the superimposition of several phenomena associated with the deformation, the following events have been generally recognized. Uniaxial deformation naturally induces rotation of the crystal chain axis towards the draw direction which confirms that chain slip mechanisms, also called c-slip, are dominant in HDPE (as in most

semicrystalline polymers). The use of deformation processes of lower symmetry, such as rolling, rolltrusion or simply unidirectional compression of uniaxially drawn specimens was however necessary to acquire additional information about the active slip systems. Such processes are useful in predicting the major slip system(s) since they normally promote the rotation of the major slip plane perpendicularly to the compression direction as the deformation proceeds (in addition to chain orientation in the Machine Direction). Early work by Frank et al.[120] reported four different modes of plastic deformation for the OR form, namely (100) and (110) slips and (110) and (310) twinnings. At high temperatures and for the early stages of the deformation, the (100) orientation in the sheet plane has been reported[54,121]; However, on further deformation, the (100) orientation is not stable but rather shifts towards the (110) plane alignment[54,122]. First, Hay and Keller[122] interpreted this orientation change as the result of (310) and (110) twinning processes in the crystalline phase. These were said to be activated by the elastic restoring forces generated during the stress relaxation of the amorphous phase on pressure removal after rolling. An alternate interpretation was given later by Seto and coworkers[54], who simply assumed "rotation of lattices accompanied with slips" on the (110) plane during the later stages of the deformation. In addition, from the examination of slip traces of the surface of PE single crystals deformed upon a Cu single crystal substrate, Gleiter and Argon[123] suggested that chain-slip could actually take place on any (hk0) plane. Young[124] evaluated the critical resolved shear stress of the (100)[001]

slip to be of the order of 10 MPa, compared to a value of at least 15 MPa for other chain slips (all at 25°C). Transverse slips have also been considered; and the (100)[010] mechanism was said to be the easiest one[125]. This would justify the rapid orientation of the (100) plane perpendicular to the direction of compression at early stages of a deformation mentionned above. Nontheless, (110)[1$\bar{1}$0] slip has also been shown to be possible . Shortly, all these experiments have not yet converged towards a unique and satisfying description of the mechanisms involved in the deformation process in HDPE crystals.

In addition, a martensitic transition has also been reported for HDPE, which transforms the crystal symmetry from orthorhombic to monoclinic under the effect of relatively high compressive forces[53,54]. The transformation occurs by means of a finite shear deformation of the orthorhombic cell. It thus takes place when the [100] axis of the OR form is inclined such that the resolved shear stress is maximum. The monoclinic form was said to be only metastable and to transform back into its parent structure during annealing. Its stability seems to depend on the conditions of its formation; and Kanamoto recently was able to detect some remaining fraction of this form in highly drawn fibers at 100°C[126]. The lattice correspondence between the two forms has been first established by Seto[54] and recently confirmed by Takahashi et al.[127]. The (110), (100) and (1$\bar{1}$0) crystallographic planes of the orthorhombic form transform into the (100), (2$\bar{1}$0) and (010) of the monoclinic form, respectively. Figure 6.1 compares the projections

along the chain axis (defined as the $\underset{\sim}{c}$-axis in both forms) of the two lattices. Finally, according to Tanaka[128], the predominant modes of deformation for the monoclinic form are the (010) slip and (010) and $(4\bar{1}0)$ twinnings.

In the light of these results, this study proposes to investigate the behavior of HDPE when subjected to the forging process. The study will first concentrate on characterizing the changes in structure and orientation induced by the process over a range of different forging conditions. Also, the effect of equibiaxial deformation on the resultant mechanical properties will be determined by measuring tensile moduli in the draw plane of the forging process. An attempt will be made to correlate the crystal structure and orientation with the measured tensile properties. Finally, in view of the results, the optimal forging conditions for HDPE will be stated and compared with predictions, as presented in Introduction.

2) Experimental.

Sample preparation: High density polyethylene pellets of molecular weight $\bar{M}_w$=59,000 were molded in a heated press into 5.5 mm thick sheets. The sheets was opaque and had a degree of crystallinity of 73% as determined by DSC. Crystals are shown by WAXD to be orthorhombic form and to have random orientation. Square samples 1.2

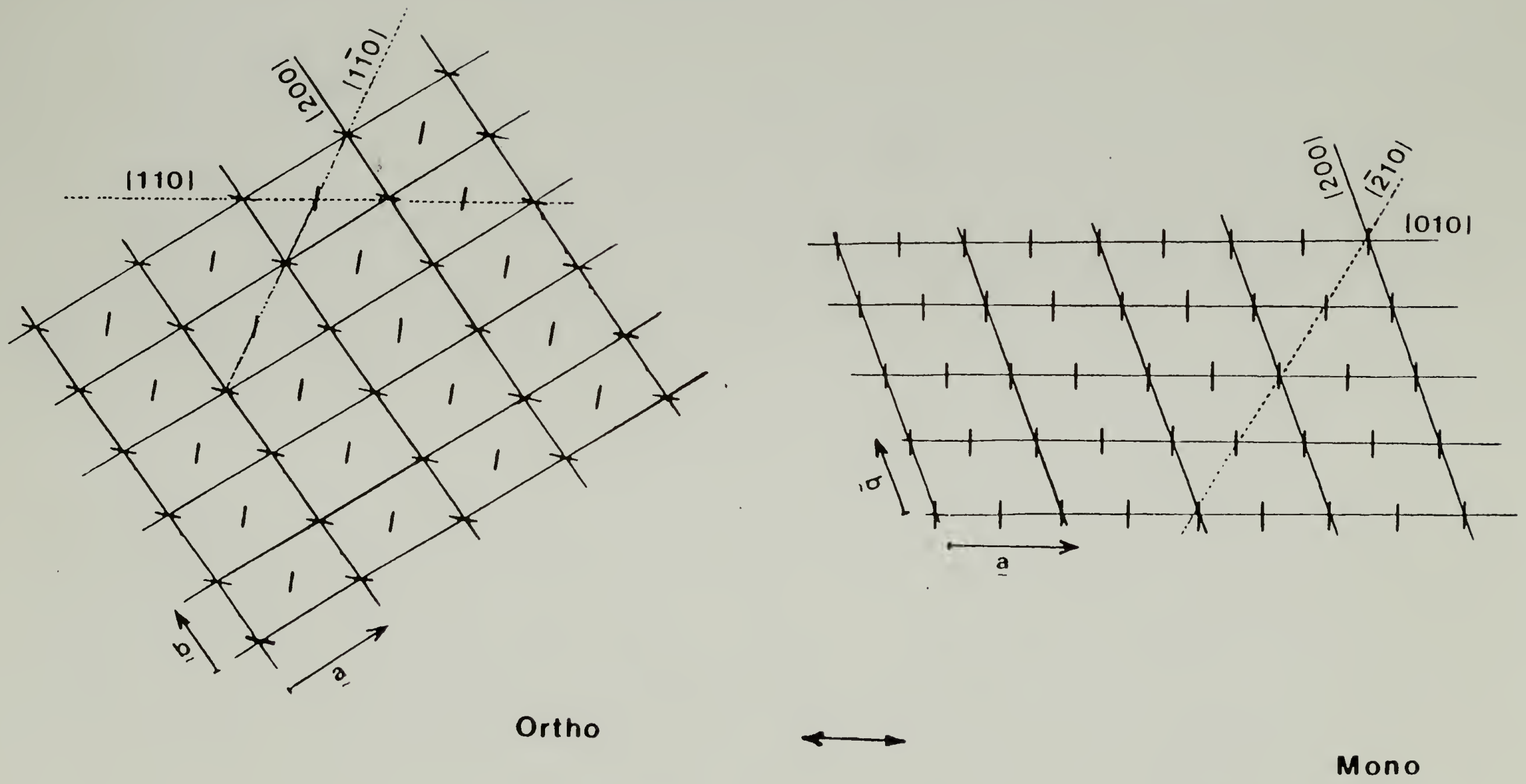

Figure 6.1. Projections along the c-axis of the Orthorhombic and Monoclinic unit cells in HDPE. Chains are in the planar zigzag conformation.

inch wide were cut out of the sheet and prenotched radially at eight sites (to ensure uniform flow on deformation).

The uniaxial compression process used is described in introduction. It allows to carry out the deformation up to 50,000 pounds load in various conditions of rate and temperature. Forging was performed at two different rates, 0.023 and 0.25 cm/min, and for various temperatures from room temperature to 130^{o}C. For each set of conditions, the specimens were forged all the way to the limit where the onset of mechanical failure could be detected. Thus, the compression ratios obtained represent the largest that can be achieved by forging for each set of conditions chosen and are referred to as Maximum Compression ratio (MCR). These values are listed in Table 6.1 and are for the lower rate of deformation.

Load-dislacement curves recorded on line provide information of the process mechanics. Specifically, the yield stress in compression, which describes the onset of plastic deformation (beyond the elastic regime), is measured.

Qualitative WAXD patterns of the highly compressed specimens were first obtained in a flat film Statton camera with Ni-filtered CuKα radiation (40 kV, 30 mA) at room temperature. A rectangular sample was cut along the radial direction of the uniaxially-compressed specimens. As already stated, complete characterization of the crystal texture only requires two different positions/orientations of the sample with respect to the X-ray beam (because of equibiaxial symmetry). Two sets of

Table 6.1 Variations of deformation extent, thermodynamic properties and density for HDPE forged at various temperatures.

Temperature of Deformation (^{o}C)	Maximum Compression Ratio	Enthalpy of Fusion (cal/gram)	Melting Point T_{max} (^{o}C)	Density (gram/cm^3)
24	13.5	45.7	135.7	0.9435
40	17.1	46.9	136.6	0.9428
50	20.2	48.0	137.4	0.9416
60	24.1	50.0	138.8	0.9433
70	29.2	50.6	138.3	0.9525
80	39.6	51.2	139.0	0.9590
90	48.3	52.1	139.3	0.9618
100	58.4	53.2	139.1	0.9632
110	67.3	54.4	138.8	0.9654
120	76.5	55.1	142.6	0.9685
130	85.4	56.1	148.1	0.9732
undeformed		50.9	133.1	0.9575

pictures were therefore taken of specimens deformed at different temperatures with the X-ray beam either parallel or perpendicular to the compression direction.

Quantitative determination of the pole density distribution for each crystalline reflection requires the use of a four circle diffractometer with a one dimensional scintillation counter detector. X-ray diffraction profiles of the forged were acquired between 0^{o} and 90^{o} with 5^{o} increment. This is done in reflection from α=0 to 45^{o}C and in transmission from α= 30^{o} up to 90^{o}. The ovelapping region is used to normalize the intensities measured in reflection and transmission geometry after these had been corrected for background, absorption and incident area. Details of such a general procedure have been described by Alexander[129] and reviewed by Saraf[29]. In addition, a deconvolution procedure is necessary in order to resolve the overlapping peaks of both crystal forms in the experimental X-ray profiles. This is performed by fitting experimental profiles with the sum of Gaussian-Cauchy functions by means of a least-squares minimization procedure.

Thermal analysis was carried out on a Perkin-Elmer DSC 4 in order to investigate the heating behavior of forged PE samples and evaluate changes in crystallinity and melting point with deformation conditions. Annealing of deformed specimens was performed in a silicone oil bath for 1 hour without constraints.

Finally, in-plane tensile moduli for measured with an Instron for samples which had been cut out along the radial direction of forged specimens.

3) Results and Discussion.

a) Textural Analysis of Forged HDPE by WAXD.

Figure 6.2 shows WAXD photographs taken of a specimen forged at 100°C for two different incidences of the X-ray beam with respect to the sample. They simply confirm the equibiaxial symmetry of the process. The isointensity rings observed with the beam parallel to the compression axis indicate random orientation of the crystals around the compression axis. This result was found to be independent of the temperature, rate and extent of deformation as well as the location between the dies (center versus edge). On the other hand, the highly textured X-ray pattern recorded with the beam perpendicular to the compression axis (and along any direction) indicates the significant anisotropy in the crystal orientation due to molecular orientation in the plane of compression.

The next step consists in using such X-ray diffraction patterns to determine the crystal textures adopted by the crystalline phase in our series of forged HDPE specimens. Once again, given the equibiaxial symmetry of the process and according to our arguments developed in chapter I, crystals can only adopt two different types of orientation: Fiber and/or Planar textures. Our objective is then to describe the crystalline orientation for every different forging conditions as a combination of Fiber and Planar textures for both crystal forms present.

Figure 6.2. WAXD patterns at room temperature for forged HDPE at 100°C to its Maximum Compression Ratio (MCR) of 58.4 prior failure.
a) Incident beam is parallel to the compression axis.
b) " " perpendicular " " " .

WAXD PATTERNS OF HDPE COMPRESSED AT $100^{0}C$:

beam parallel to the compression axis.

beam perpendicular to the compression axis.

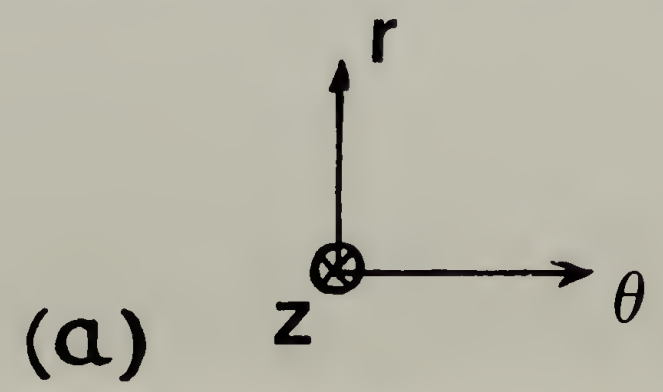

(a)

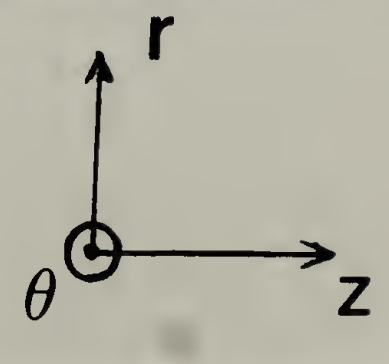

(b)

In this regard, the azimuthal angles theoretically expected for all the observed reflections are calculated according to the procedure described in Appendix 1 for several possible Fiber and planar textures. Results are shown in tables 6.2 and 6.3 for the monoclinic and orthorhombic forms respectively. These are compared with experimental diffraction patterns obtained for different forging temperatures.

WAXD patterns of PE samples compressed at some discrete temperatures chosen in the range studied are shown in figure 6.3. The incident X-ray beam was again parallel to the compression plane and the compression axis is vertical on these photographs. The major differences depicted in these patterns can be described as such:

i) At the lowest temperature ($24^{o}C$), a significant fraction of monoclinic (MC) coexists with the initial orthorhombic (OR) form. It is highly oriented as indicated by its sharp and intense (010) reflection on the meridien and of its weaker (200) reflections at a defined angle on each side of the compression axis. Its texture corresponds to the (010) Fiber texture. For the orthorhombic form, both (110) and (200) reflections are relatively weak and exhibit 6 spots patterns with two on the meridian and four at fixed angles to it. To possibly explain all the reflections, the total population of OR crystals need to be split into two fractions, according to Table 6.3: The major one which exhibits (110) Fiber texture, and the smaller one which may be undistinguishly described by a (100) fiber texture or simply the Planar texture. Note that since (110) and $(1\bar{1}0)$ are crystallographically equivalent in the orthorhombic form of polyethylene, (110) and $(1\bar{1}0)$

Table 6.2 Comparison between experimental azimuthal angles and calculated ones for the stress-induced monoclinic form of HDPE produced by forging at low temperatures assuming different Fiber and Planar textures. .

MONOCLINIC FORM

$a=8.09$ Å

$b=4.79$ Å

$c=2.534$ Å

$\alpha=\beta=90^{o}$

$\gamma=107.9^{o}$

$a^{*}=0.130$ Å $^{-1}$

$b^{*}=0.219$ Å $^{-1}$

$c^{*}=ab\sin\gamma/V=0.395$ Å $^{-1}$

$\alpha^{*}=\beta^{*}=90^{o}$

$\gamma^{*}=72.1^{o}$

Experimental and calculated azimuthal angles for (hkl) reflections for Planar and Fiber Textures:

Reflection	d_{hkl} Å	ϕ observed	ϕ_f expected Fiber texture ($\underset{\sim}{b}^{*}$ // ND)	ϕ_p expected Planar texture ($\underset{\sim}{c}$ // XOY)
(010)	4.55	0^{o}	0.0^{o}	0.0^{o}
(200)	3.85	$\simeq 70^{o}$	72.1^{o}	0.0^{o}
($\bar{2}$10)	3.52	$\simeq 65^{o}$	65.8^{o}	0.0^{o}

Table 6.3 Comparison between experimental azimuthal angles and calculated ones for the orthorhombic form in HDPE forged at high temperatures for several Fiber and Planar textures

ORTHORHOMBIC FORM:

$a=7.40$ Å

$b=4.94$ Å

$c=2.354$ Å

$\alpha=\beta=\gamma=90^{o}$

$a^{*}=0.135$ Å^{-1}

$b^{*}=0.202$ Å^{-1}

$c^{*}=0.395$ Å^{-1}

$\alpha^{*}=\beta^{*}=\gamma^{*}=90^{o}$

Experimental and calculated azimuthal angles for (hkl) reflections for several Fiber Textures and Planar textures

Reflection	d_{hkl} (Å)	ϕ observed at 24°C	ϕ observed at 100°C	ϕ_f expected Fiber tex. ($\underset{\sim}{a}^{*}+\underset{\sim}{b}^{*}$ // ND)	ϕ_f expected Fiber tex. ($\underset{\sim}{a}^{*}$ // ND)	ϕ_p expected Planar tex. ($\underset{\sim}{c}$ //XOY)
(110) (or (1$\bar{1}$0))	4.11	≈10° ≈70°	0°	0.0° 67.4°	56.3°	0.0°
(200)	3.70	≈62°	0°	56.3°	0.0°	0.0°

Figure 6.3. WAXD patterns for forged HDPE up to MCR at 24, 70, 100 and 120°C. The incident beam is perpendicular to the compression axis. The patterns at 24 and 70°C are shown for two different exposures.

WAXD PATTERNS OF HDPE FOR VARIOUS DEFORMATION TEMPERATURES

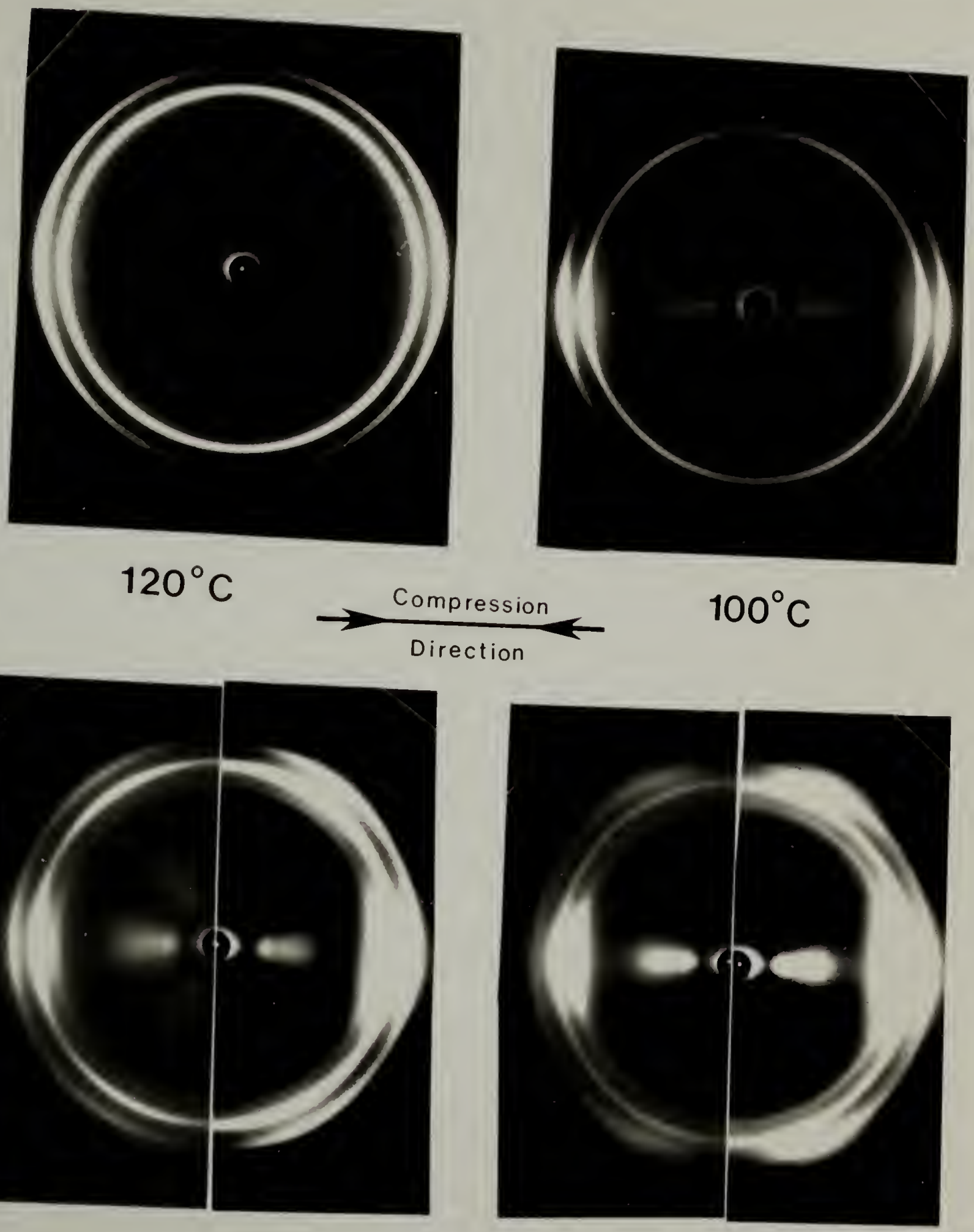

Figure 6.4. Crystal textures in HDPE forged at 24°C to the MCR for both MC and OR forms.

SCHEMATIC REPRESENTATION OF CRYSTAL TEXTURE IN EQUIBIAXIALLY DEFORMED POLYETHYLENE AT 24^0C

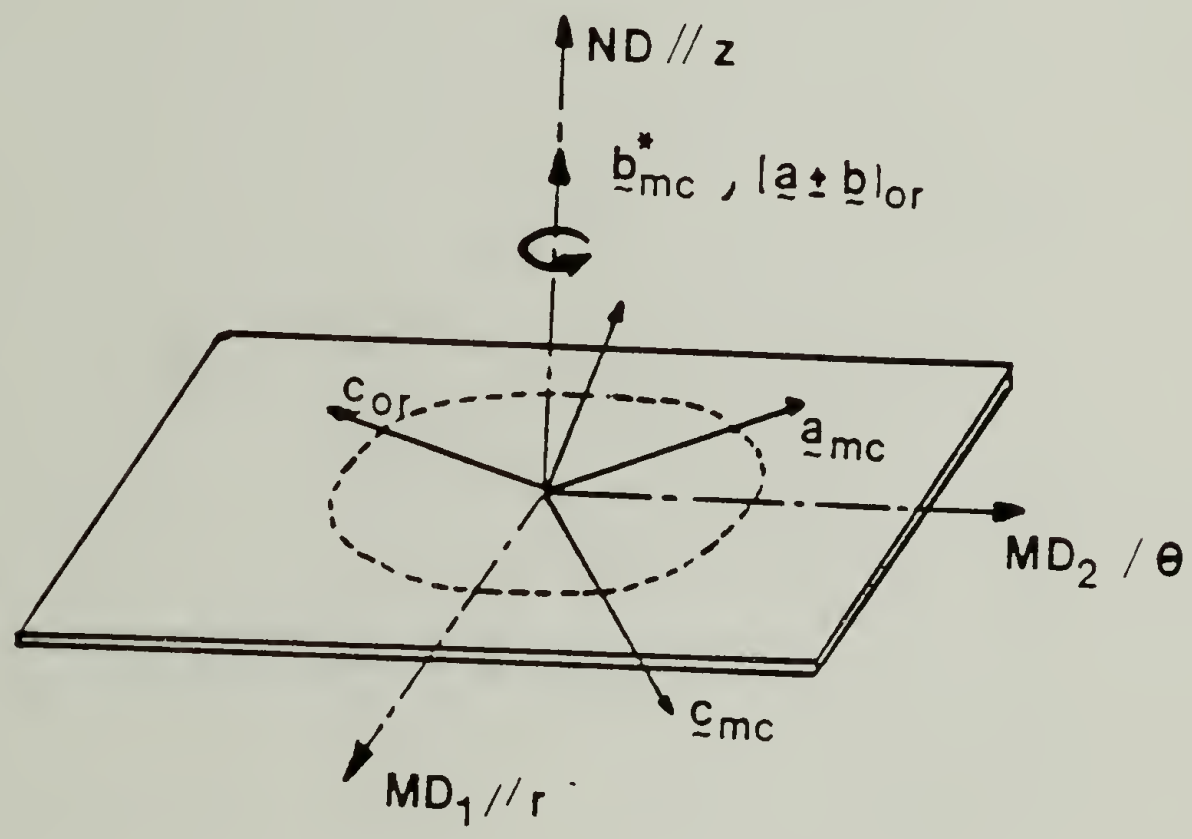

- MC form : essentially with Fiber Texture
  ($\underset{\sim}{b}^*_{mc}$ along ND)
- OR form : mainly with Fiber Texture
  ($(\underset{\sim}{a}+\underset{\sim}{b})_{or}$ or $(\underset{\sim}{a}-\underset{\sim}{b})_{or}$ along ND)
  : also, fraction of another Texture
  - $\underset{\sim}{a}$ along ND

  or
  - planar texture

Figure 6.5. Normalized Pole Density Distribution Function versus azimuthal angle for both monoclinic and orthorhombic main reflections in HDPE forged at 24°C.

(Cont. to page 226).

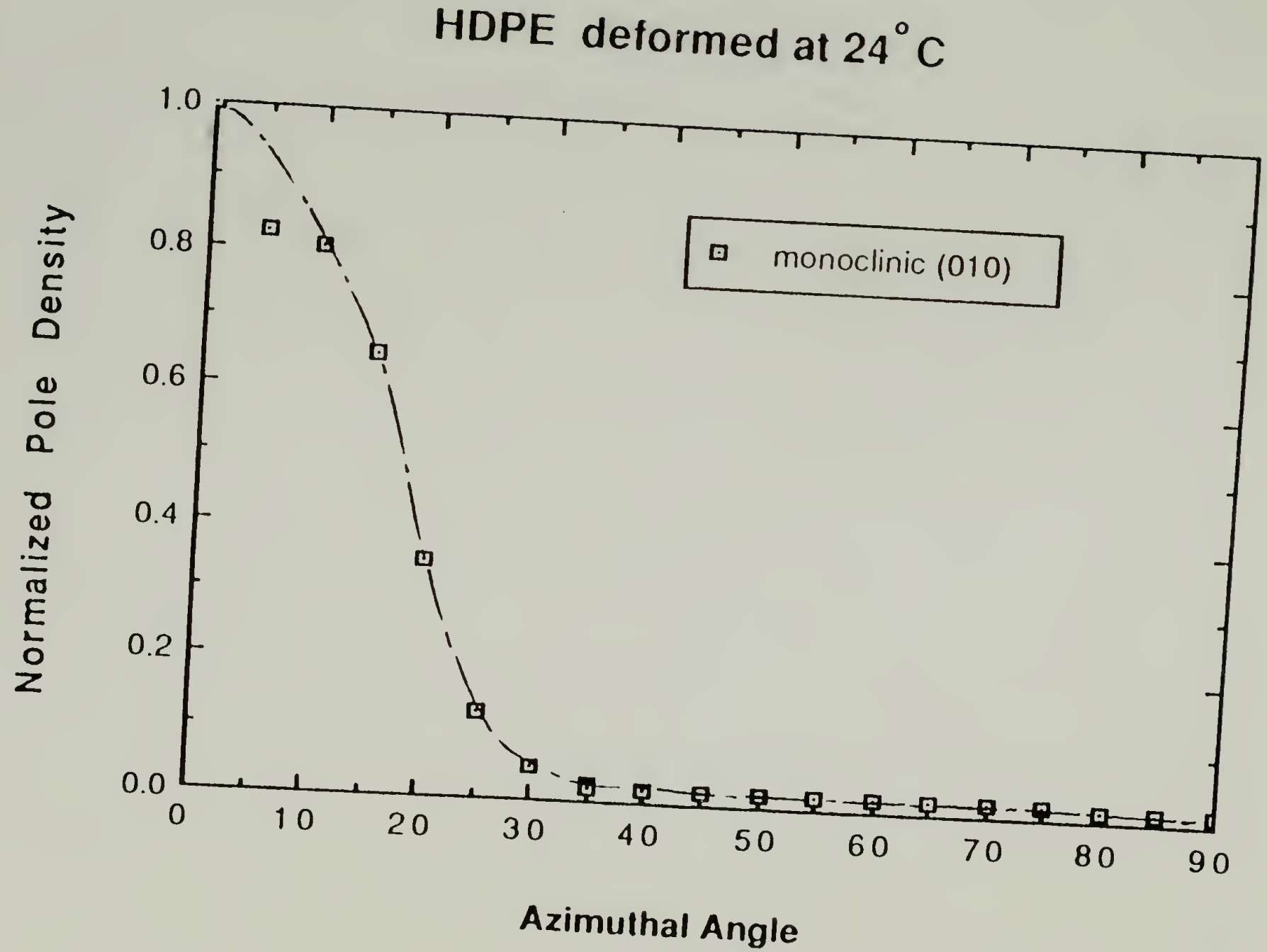
HDPE deformed at 24°C
Normalized Pole Density
1.0
0.8
0.6
0.4
0.2
0.0
0
10
20
30
40
50
60
70
80
90
monoclinic (010)
Azimuthal Angle

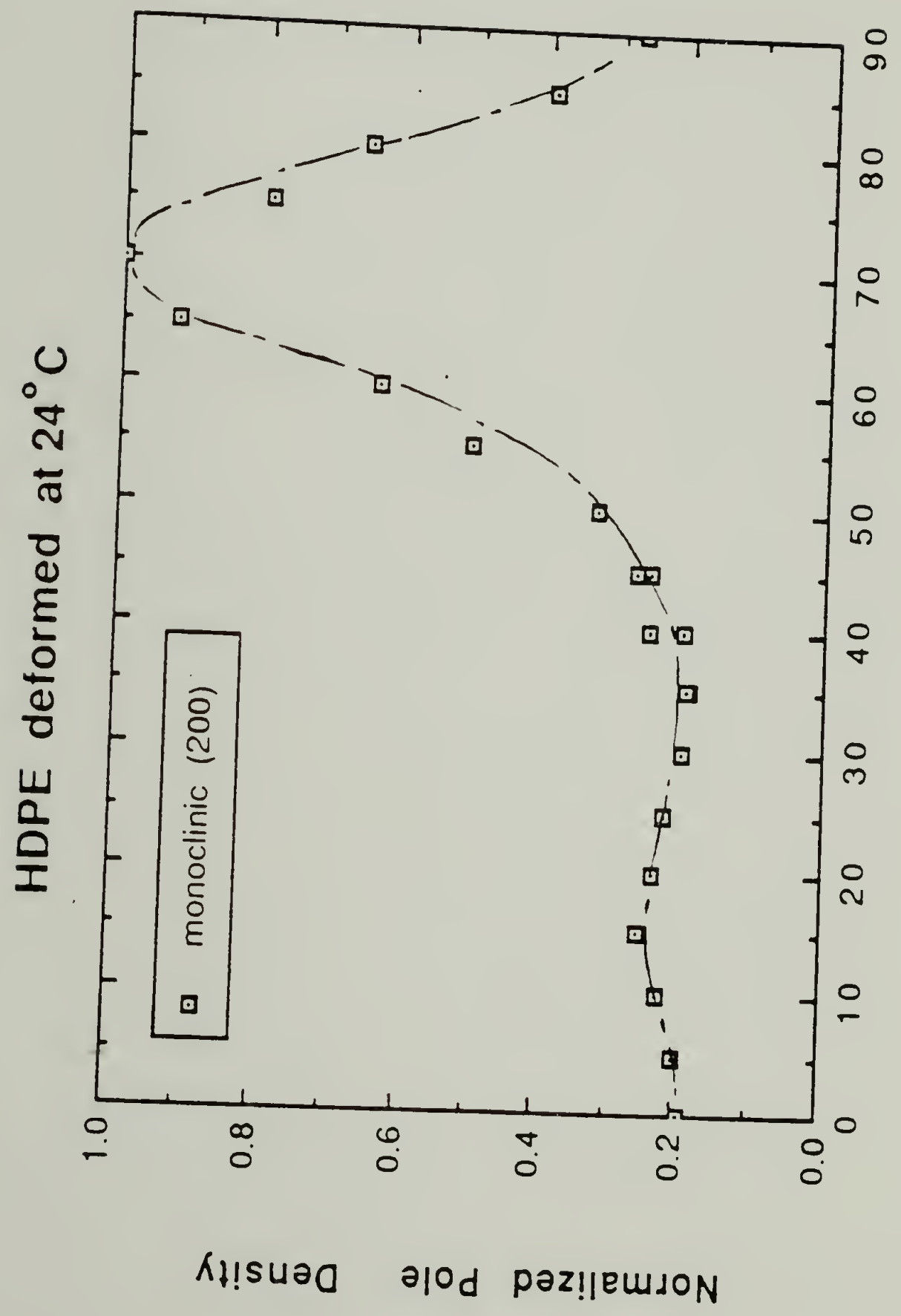
HDPE deformed at 24°C
monoclinic (200)
Normalized Pole Density
Azimuthal Angle
0.0
0.2
0.4
0.6
0.8
1.0
0
10
20
30
40
50
60
70
80
90

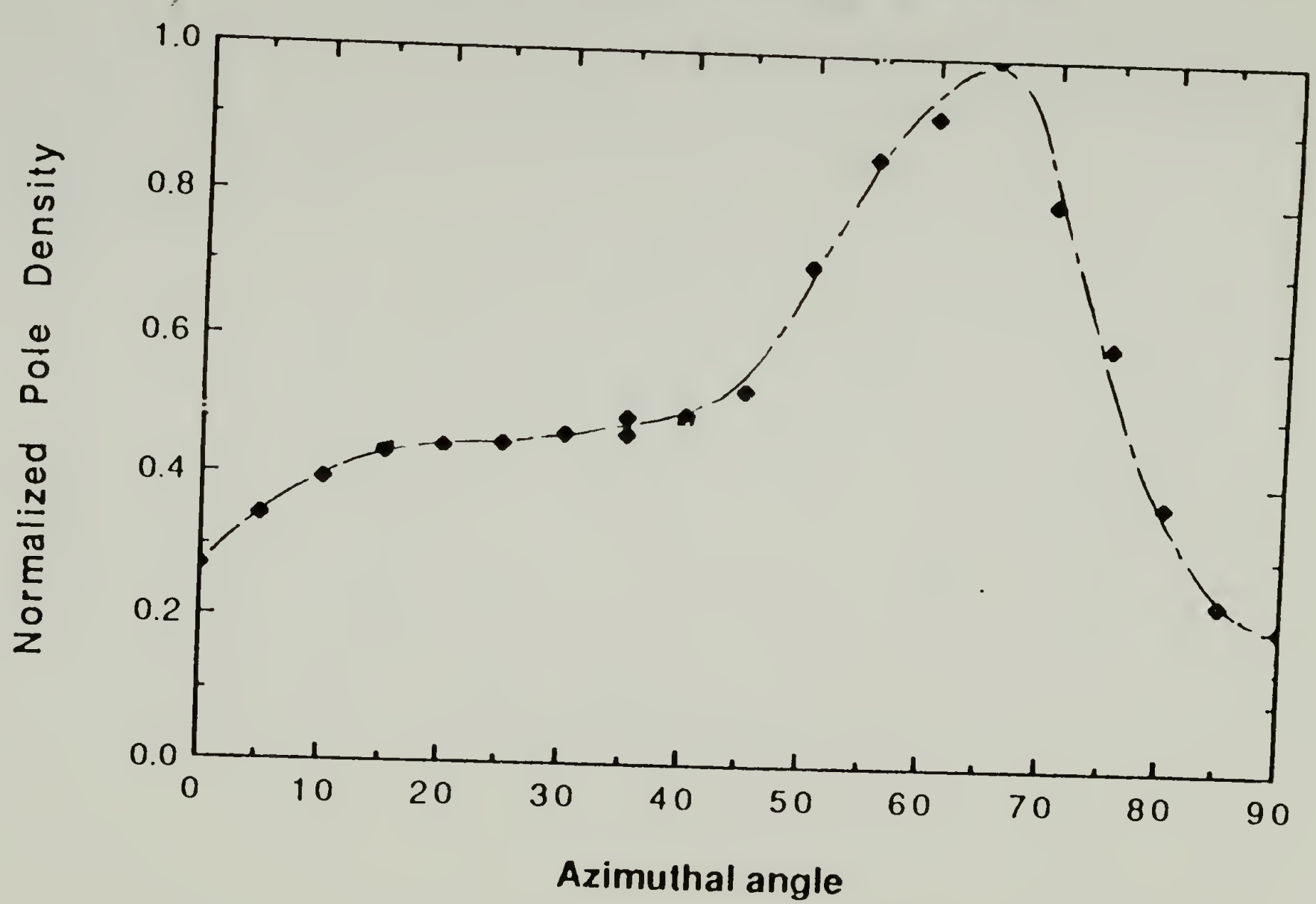
OR (200) in PE deformed at 24 C
Normalized Pole Density
1.0
0.8
0.6
0.4
0.2
0.0
0
10
20
30
40
50
60
70
80
90
Azimuthal angle

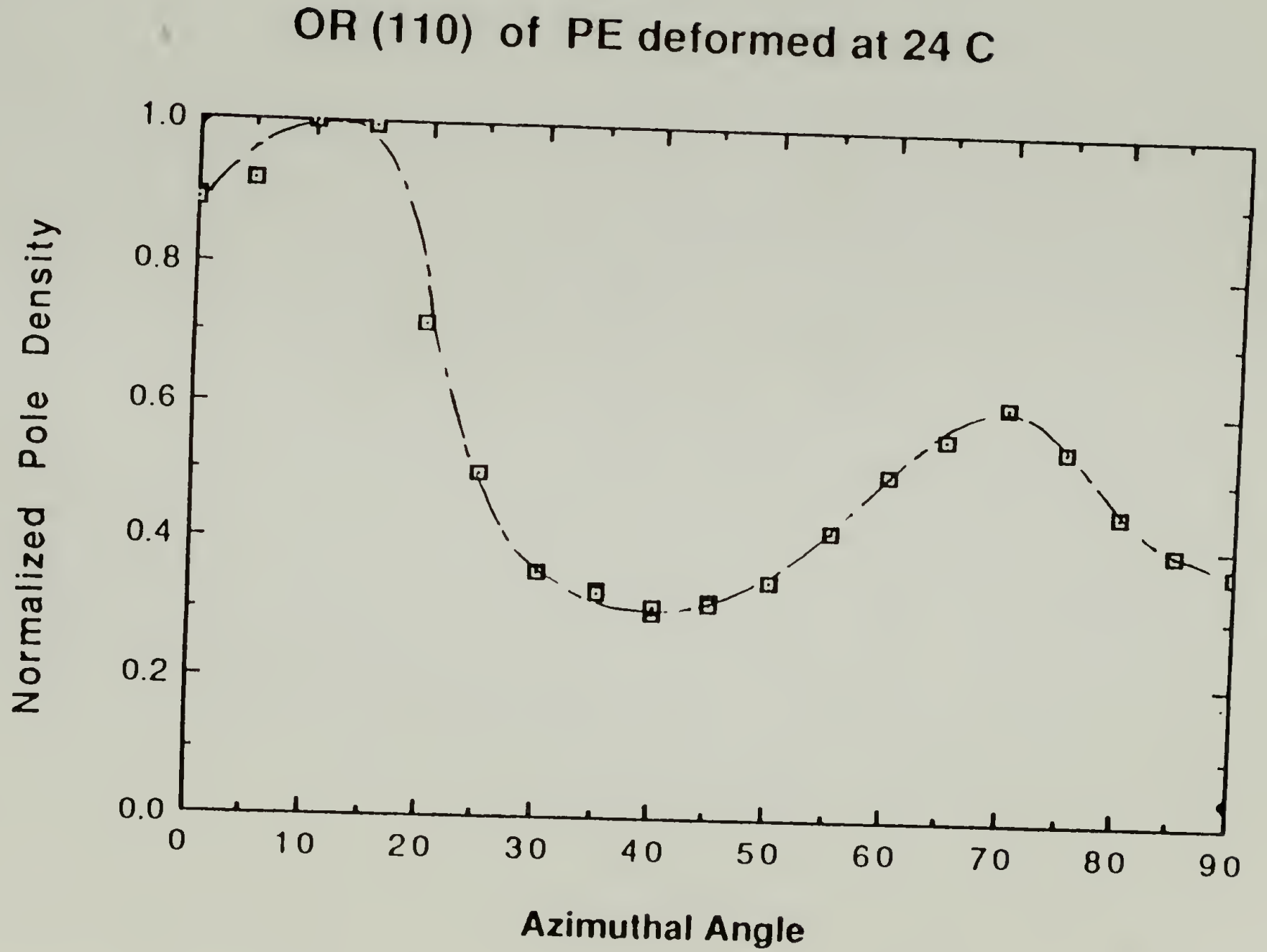
OR (110) of PE deformed at 24 C
Normalized Pole Density
1.0
0.8
0.6
0.4
0.2
0.0
0
10
20
30
40
50
60
70
80
90
Azimuthal Angle

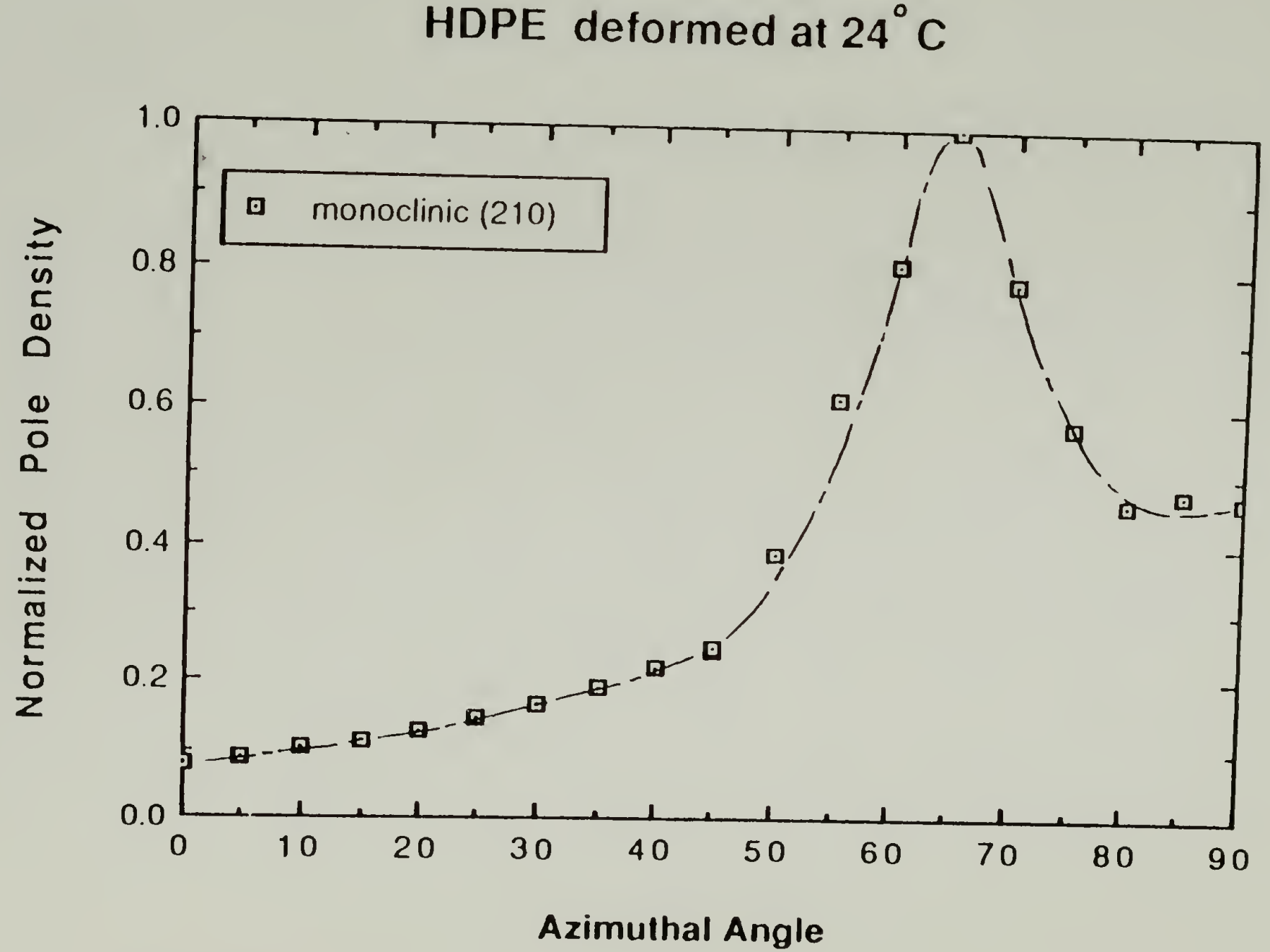
HDPE deformed at 24° C
monoclinic (210)
Normalized Pole Density
1.0
0.8
0.6
0.4
0.2
0.0
0
10
20
30
40
50
60
70
80
90
Azimuthal Angle

Fiber textures represent the same orientation. Figure 6.4 schematically describes all the textures found in forged HDPE at 24°C. In figure 6.5 are reported the normalized pole density distributions for the main reflections of the monoclinic and orthorhombic as a function of azimuthal angle.

ii) As the deformation temperature was increased between 24°C and 100°C, the intensity of both (010) and (200) monoclinic reflections decreased continuously until it essentially disappears at 100°C. This clearly confirmed that the stability of the deformation-induced monoclinic form decreased as the deformation temperature was raised. The same (010) Fiber texture as the one found at 24°C is maintained for the remaining fraction of monoclinic. To the contrary, continuous changes are depicted in the azimuthal distribution of the (110) and (200) poles of the OR form, as the amount of monoclinic decreases. As the chosen deformation temperature is set closer to 100°C, intensity of the reflections on the meridian progressively increases at the expense of the others; and at 100°C, these are essentially the only ones remaining. This is evidenced of the progressive increase of the Planar texture with increasing temperature at the expense of the (110) (or $(1\bar{1}0)$) Fiber texture.

iii) After deformation at 100°C, the monoclinic is no longer stable and only the orthorhombic form remains. The normalized pole density distributions for the (110) and (200) reflections as a function of azimuthal angle are given in figure 6.6. They indicate the orthorhombic form to be in Planar texture exclusively (figure 6.7).

Figure 6.6. Normalized Pole Density Distribution Function versus azimuthal angle for the orthorhombic reflections in HDPE forged at 100°C.

(Cont. to page 230).

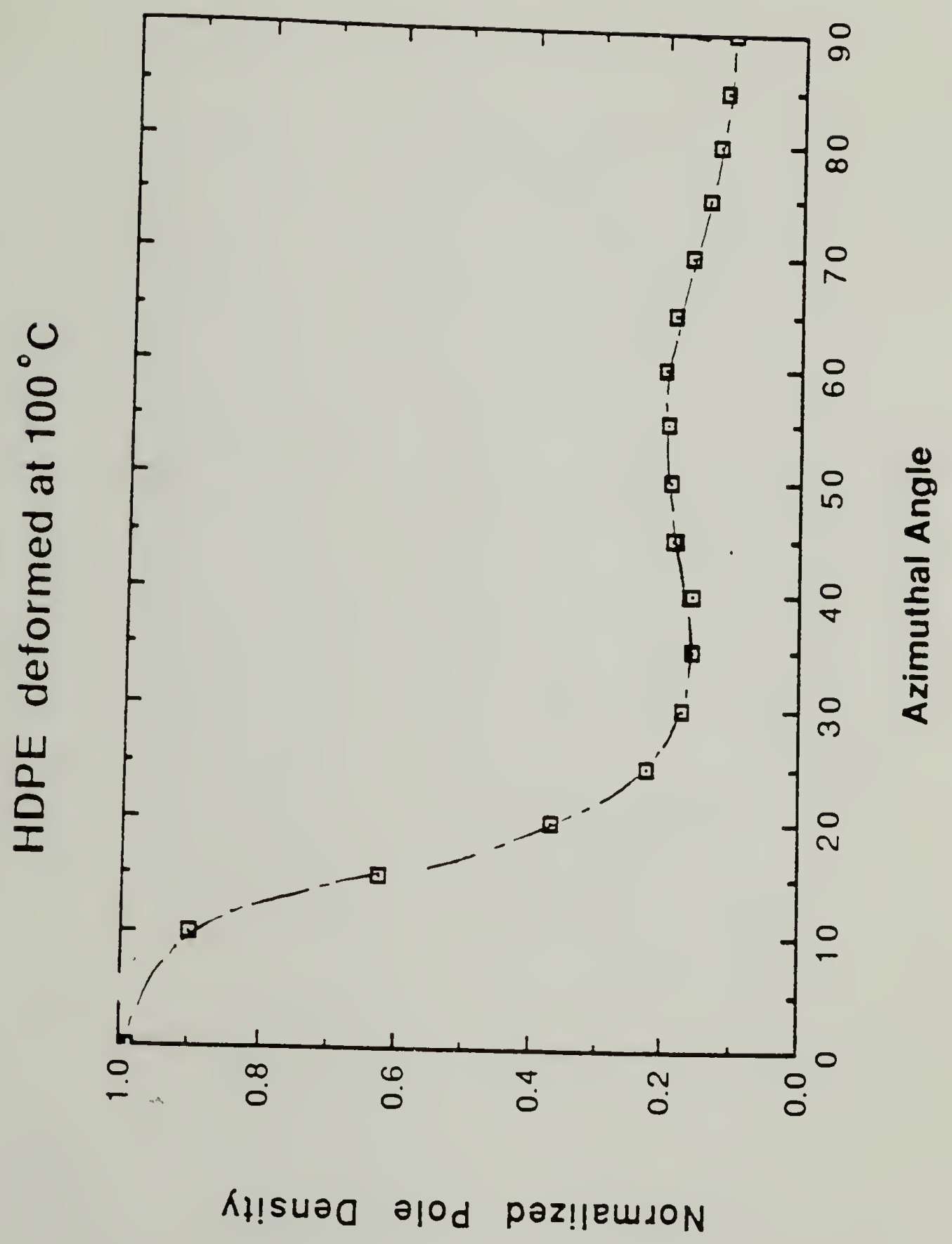
HDPE deformed at 100°C
Normalized Pole Density
1.0
0.8
0.6
0.4
0.2
0.0
0
10
20
30
40
50
60
70
80
90
Azimuthal Angle

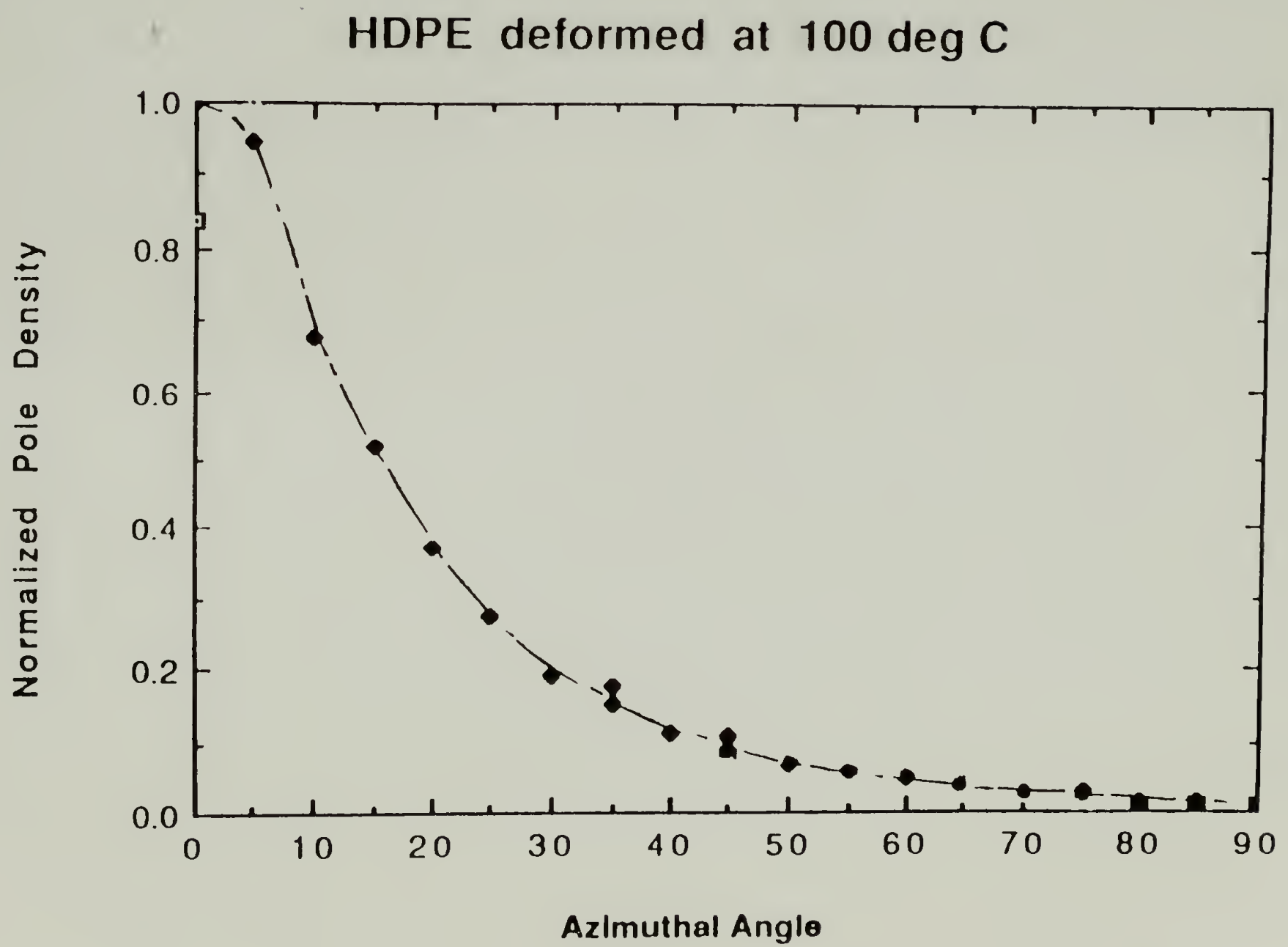
HDPE deformed at 100 deg C
Normalized Pole Density
1.0
0.8
0.6
0.4
0.2
0.0
0
10
20
30
40
50
60
70
80
90
Azimuthal Angle

SCHEMATIC REPRESENTATION OF CRYSTAL TEXTURE IN EQUIBIAXIALLY DEFORMED POLYETHYLENE AT $100^{0}C$

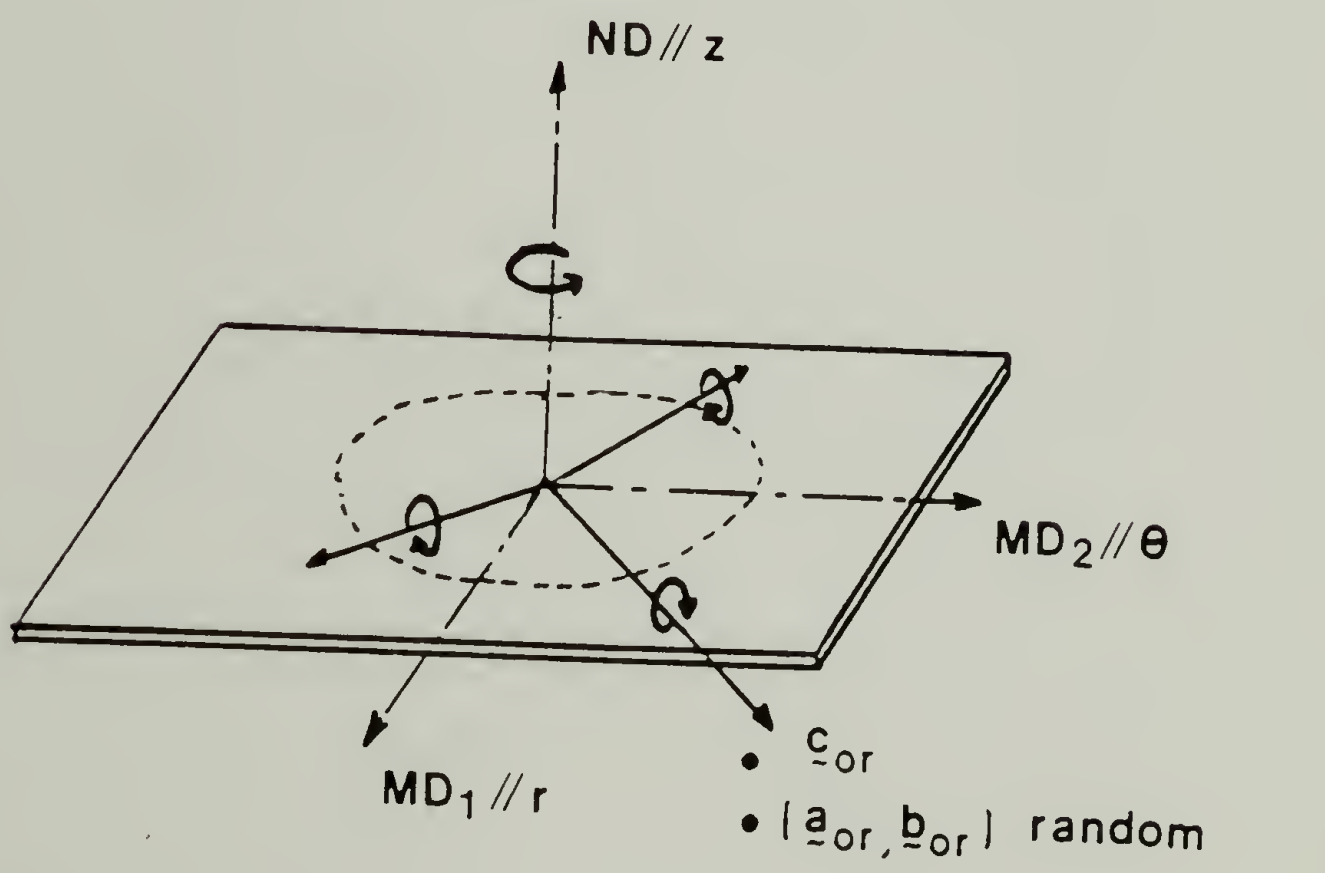

Figure 6.7. Crystal texture in HDPE forged at $100^{0}C$ to the MCR for the OR form.

iv) Finally, at 120°C, the spreading of the reflections becomes more prominent and apparently indicates significant molecular relaxation during or after forging.

b) Effect of Annealing on the Crystal Texture.

In order to better compare the textures which develop in HDPE forged at 24°C and 100°C and get more insight about the difference in the deformation mechanism at these two temperatures, the specimen forged at 24°C was subsequently annealed at 100°C. By this treatment, the deformation-induced monoclinic form anneals back into the orthorhombic form and reduces the comparison to a single crystal form. Our objective is twofold:

we want to clarify the geometrical relationship between the two crystal forms during their transition.

We want to be able to directly compare the final textures of the orthorhombic crystals prepared by the two methods.

Figure 6.8 compares the WAXD patterns for HDPE forged at 24°C and 100°C after both are annealed at 100°C without constraints. Also, in figure 6.9 are represented the azimuthal density distributions for the two orthorhombic reflections in both cases. Clearly, a large fraction of orthorhombic crystals with (110) Fiber texture is present in HDPE forged at 24°C after annealing at 100°C. It has replaced the large monoclinic fraction initially induced in HDPE during forging at 24°C and which was found to possess (010) Fiber texture. Not only does this

Figure 6.8. Comparison of WAXD patterns for HDPE specimens:
(**A**) Forged and annealed at 100°C to the MCR, where the crystals remained in the OR form during the deformation.
(**B**) Forged at 24°C and annealed at 100°C, in which crystals underwent partial transformation into the MC form, before annealing back into the OR form.

WAXD PATTERNS OF EQUIBIAXIALLY DEFORMED HDPE:

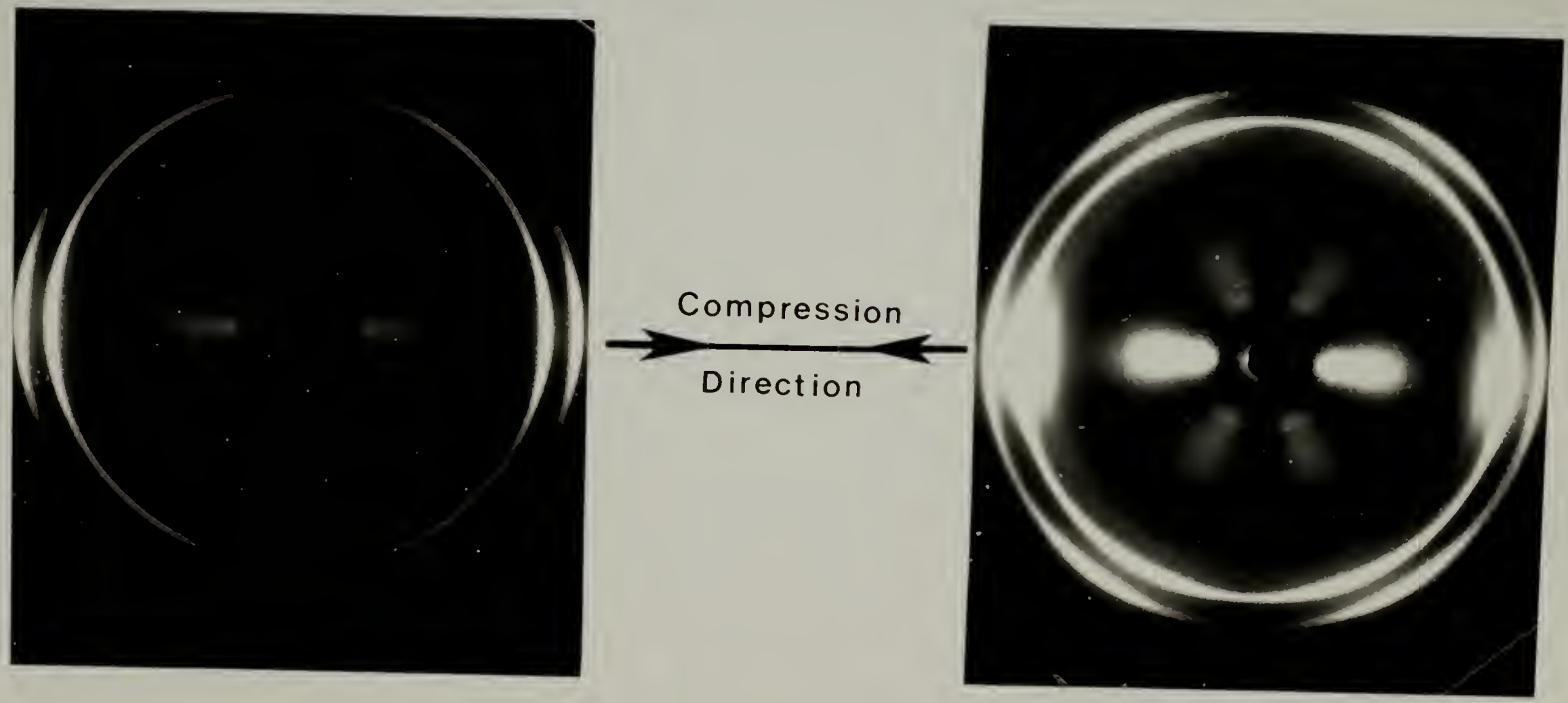

(A) Deformed at 100°C

Annealed at 100°C

(B) Deformed at 24°C

Annealed at 100°C

Figure 6.9. Comparison of normalized Pole Density Distribution Function versus azimuthal angle for:
(A) HDPE forged at 24°C and annealed at 100°C.
(B) HDPE forged at 100°C (and annealed also at 100°C).

(Cont. to Page 237).

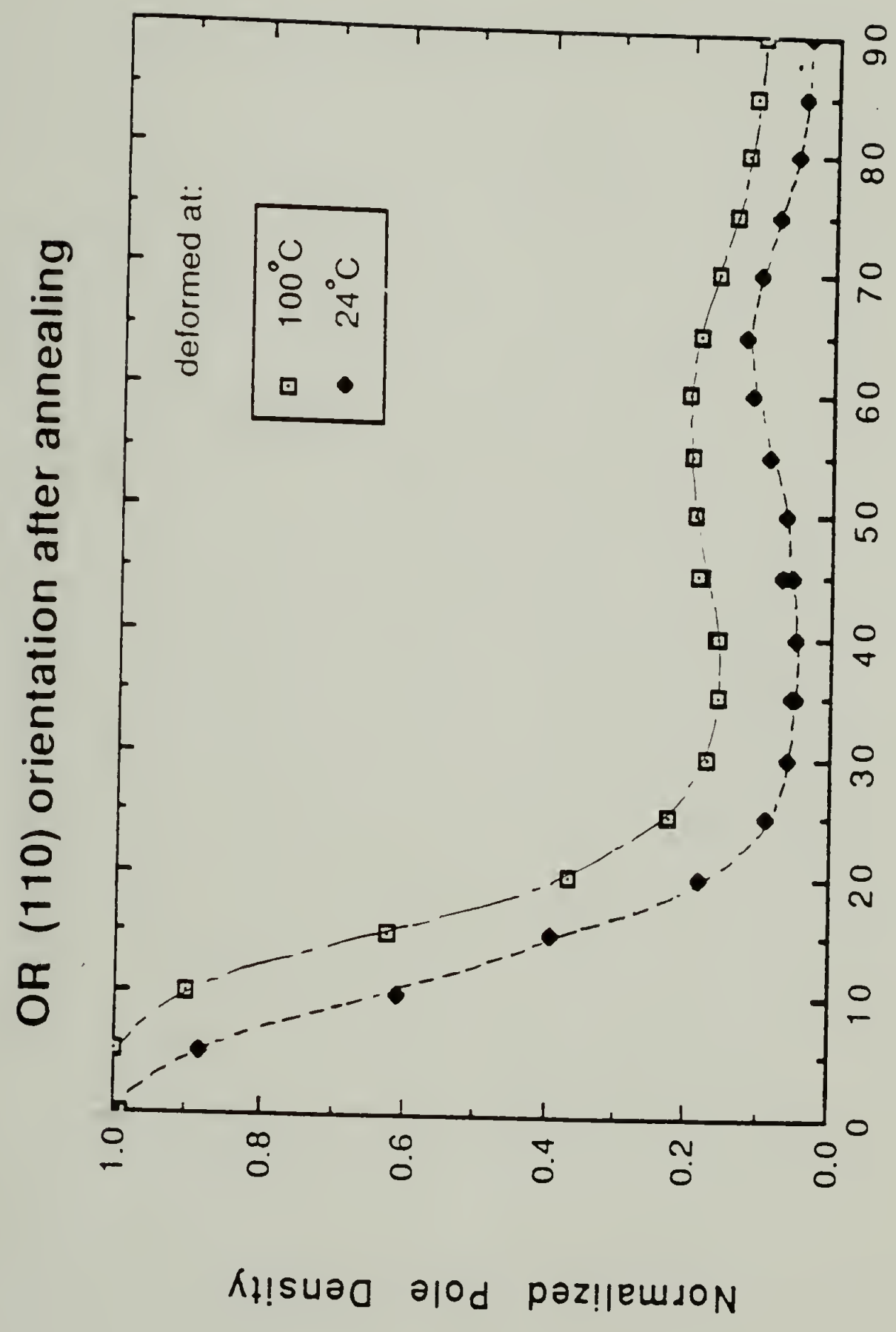
OR (110) orientation after annealing
deformed at:
100°C
24°C
Normalized Pole Density
1.0
0.8
0.6
0.4
0.2
0.0
0
10
20
30
40
50
60
70
80
90
Azimuthal Angle

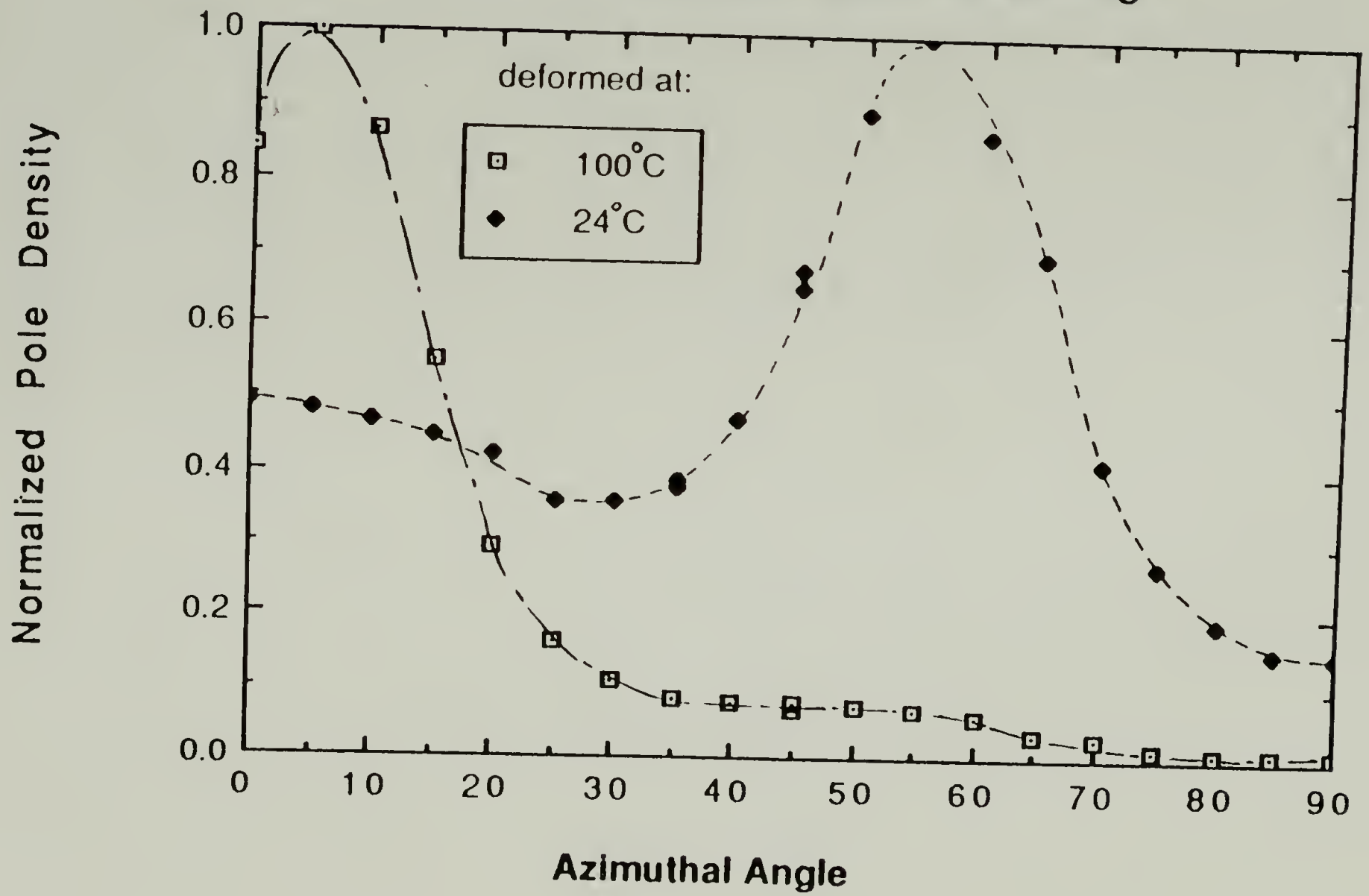
OR (200) orientation after annealing
deformed at:
100°C
24°C
Normalized Pole Density
1.0
0.8
0.6
0.4
0.2
0.0
0
10
20
30
40
50
60
70
80
90
Azimuthal Angle

indicate that the transformation from monoclinic to orthorhombic takes place in a well defined geometrical relationship; But it also confirms the latest correlation proposed by Takahashi[127] between the (010) plane of the monoclinic and the (110) plane of the orthorhombic in this transformation.

By comparing this texture for the orthorhombic with the one obtained by forging at 100°C (and annealed at the same temperature), the drastic difference can be seen in the final crystal orientation in forged HDPE prepared by the two methods. It strongly suggests major discrepancies in the deformation mechanisms of the monoclinic and orthorhombic forms. According to our diffraction analysis, the following aspects of the forging deformation emerge:

i) At low temperatures up to 100°C, the stress-induced phase transformation from orthorhombic to monoclinic partially takes place as the deformation proceeds. The monoclinic form is found to possess a (010) Fiber texture, which according the the crystallography of slip, indicates the (010) plane to be the major slip plane (with at least two directions of easy shear). As the deformation temperature was increased, the fraction of stable monoclinic decreases at the expense of the orthorhombic form. The orthorhombic possesses double texture. Its (110) Fiber texture may well result from annealing a fraction of monoclinic in (010) Fiber texture. Its other texture is Planar.

ii) For deformation above 100°C, practically no trace of monoclinic are present in the forged specimens after deformation. Concurrently, the orthorhombic form is now found to be essentially

oriented with the Planar texture. Several possibilities can lead to the formation of Planar texture as it has been conjectured in the Introduction Chapter. The most probable one in the case of HDPE orthorhombic form is likely to be because of the number of competing slip mechanisms. Due to its orthorhombic symmetry, the (110) and $(1\bar{1}0)$ crystallographic planes are totally equivalent and therefore offers alternate slip systems. According to the predictions discussed in the Introduction chapter, such a Planar texture describes a state of incomplete orientation and might reflect non-ideal mechanisms of deformation.

c) Changes in Compressive Yield Stress with Deformation Temperature.

It has been already established that deformation of semicrystalline polymers (above the glass transition temperature) generally changes from elastic to plastic when the applied stress reaches the yield stress. This particular stress defines the onset of the molecular processes responsible for plastic flow within the lamellar crystals. It corresponds to the minimum value of the critical resolved shear required for shearing. Any change in structure, morphology or orientation of a specimen prior to or during its deformation is expected to modify the value of the yield stress. X-rays data recognized the crystal-crystal transition from orthorhombic to monoclinic under compressive stress during the equibiaxial deformation of Polyethylene

below 100°C and revealed a drastic change in the deformation mechanism acompanying the transition.

Our objective is to investigate whether the compressive yield stress as determined from the plateau in our stress-strain curves recorded during the deformation reflects the change of crystal structure (and deformation mechanism) with temperature. Results are shown in figure 6.10 which represents an Arrhenius plot of $Ln(\sigma_c^*)$ versus $1/T_D$, where σ_c^* is the compressive yield stress and T_D the deformation temperature (between 25°C and 130°C). Two sets of data are plotted for two different compression speeds, one being approximately 10 fold larger than the other. It is found that both sets of data break up into two linear domains and that the transition point is approximately located between 100°C and 110°C in both cases. The change in slope provides evidence of a change in activation energy for the process above and below 100°C. Interestingly, the lower value, as found at temperatures below 100°C, correlates with the stability domain of the smectic as determined by WAXD. This implies that this generated MC form promotes ductility in the solid state deformation of PE. It may be argued that the higher ductility of the latter is a thermodynamic driving force for the OR-MC transition during deformation. It is therefore likely that crystal shearing along its main slip plane (the (010) slip plane according to its (010) Fiber texture) has a lower critical resolved shear stress than any slip systems of the OR form. This may well be justified by the fact that the monoclinic has same chain conformation but a slightly lower density than the orthorhombic form and thus has a

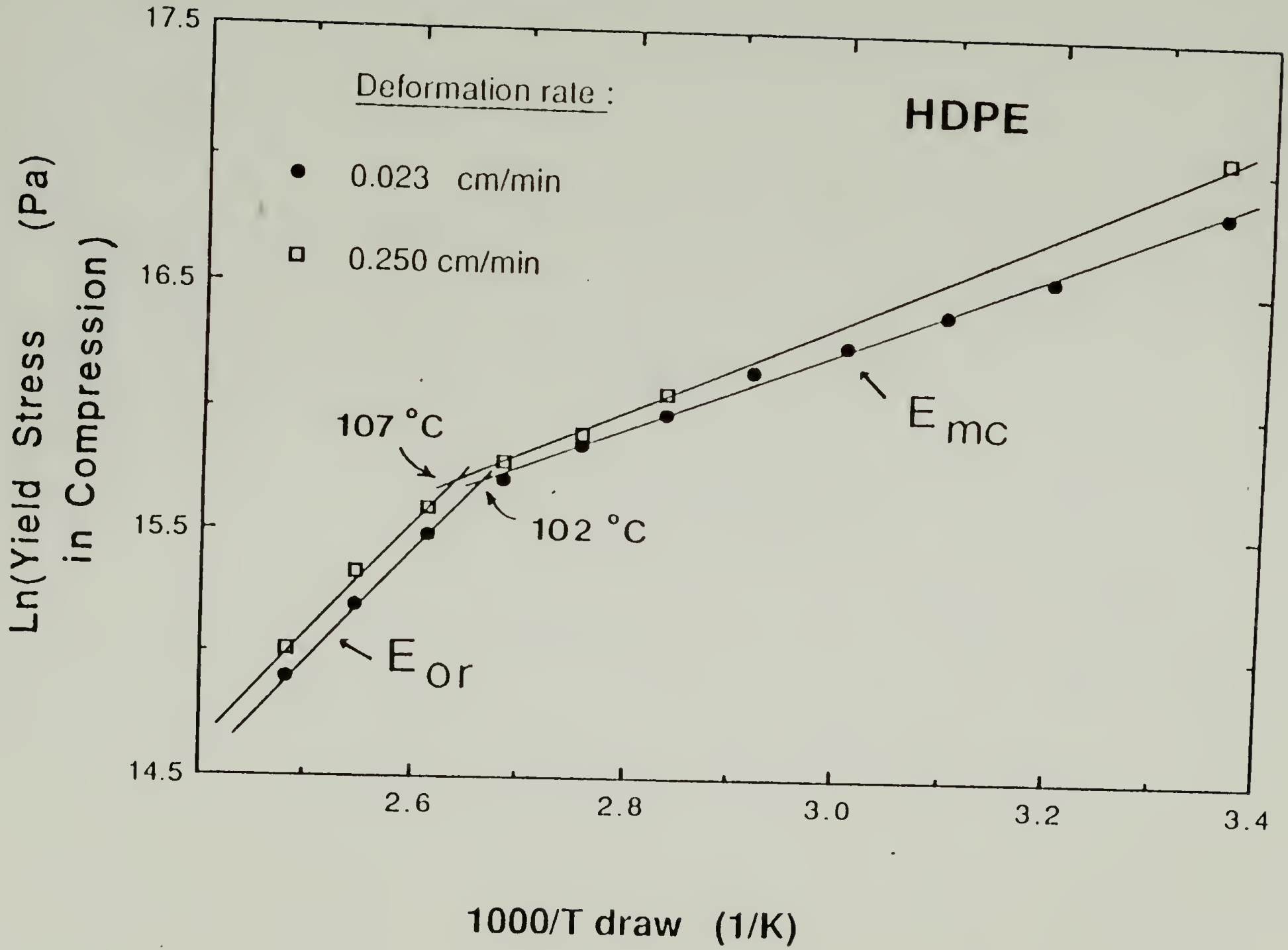

Figure 6.10. Arrhenius plot of the compressive yield stress versus forging temperature for HDPE uniaxially compressed at two compression speeds: 0.023 and 0.250 cm/min.

looser chain packing. The experimental activation energies are 26 and 29 kcal/mole above and below 100°C, respectively.. Takayanagi[129] has reported the activation energy for uniaxial drawing in the temperature range below 60°C to be 28 kcal/mole.

d) Thermal Properties of Forged HDPE.

Enthalpic changes during heating of PE compressed at various temperatures were determined by DSC between 40°C and 200°C at 20°C/min. Thermograms were conducted to such a high temperature (50°C above the melting point) to better establish the baseline obtained from extrapolating the specific heat of the molten state over the condensed state. This is based on the result that the specific heat of the crystal close to melting is less than 1% different from that of the melt[130]. Experimental values for the melting point (as obtained by the peak maxima) and enthalpies of fusion for the series of forged HDPE are listed in Table 6.1 and compared to the values in the isotropic state prior to deformation. Also reported in the same table are the changes in density as measured by means of a gradient column.

First, our results indicate a higher melting point for all deformed specimens as compared with the initial polyethylene. It continuously increases with increasing compression temperature, and especially above 110°C, where superheating as high as 15°C are observed. Similar observations have been observed and reported for HDPE in uniaxial deformation studies[131] and attributed to the apparition of chain

extended crystals. Also increasing similarly with temperature of deformation are the heat of fusion as well as the density of forged HDPE. Nontheless, for deformation below 80°C, both enthalpy of fusion and density of HDPE are lower after forging than before, as previously reported in uniaxial deformation. However, differences observed in the case of forging are noticeably larger than for drawn polyethylene[131].

Figure 6.11a shows a heating thermogram for HDPE forged at 25°C. Because of the reduction of the ordinate scale, the melting peak is troncated. On the other hand, it permits to better visualize the more subtile phenomena occurring below the melting point. Clearly, an exotherm can easily be seen to have a minimum at around 70°C. It was shown to have the following characteristics: It is seen only for PE compressed below 70°C; its location is independent of the temperature of deformation below 70°C; it is also independent of the heating rate (between 10°C/min and 70°C/min). A second heating of the same sample after slow cooling shows no exotherm (fig 6.11e). Also, curves 6.11b,11c,11d show thermograms after annealing specimens at 90°C for 3sec, 3 min and 3 hrs. Identically, the small exotherm has disappeared and replaced by an small endotherm, whose size and temperature increases with time. To investigate which phenomena are associated with the exotherm, the changes in enthalpy for each phase present in HDPE forged at 24°C are considered. Figure 6.12 summarizes all the transitions which can possibly expected. There are only two possible exothermic processes: crystallization (or recrystallization) from the amorphous phase and reverse martensitic transition (which transforms the

Figure 6.11. DSC heating curves at 20°C/min of HDPE forged at 24°C at a speed of 0.25 cm/min up to the MCR=13.5;
a) First heating.
b) After annealed at 93°C for 3 sec.
c) " " " 3 min.
d) " " " 3 hrs.
e) Second heating run after melting.

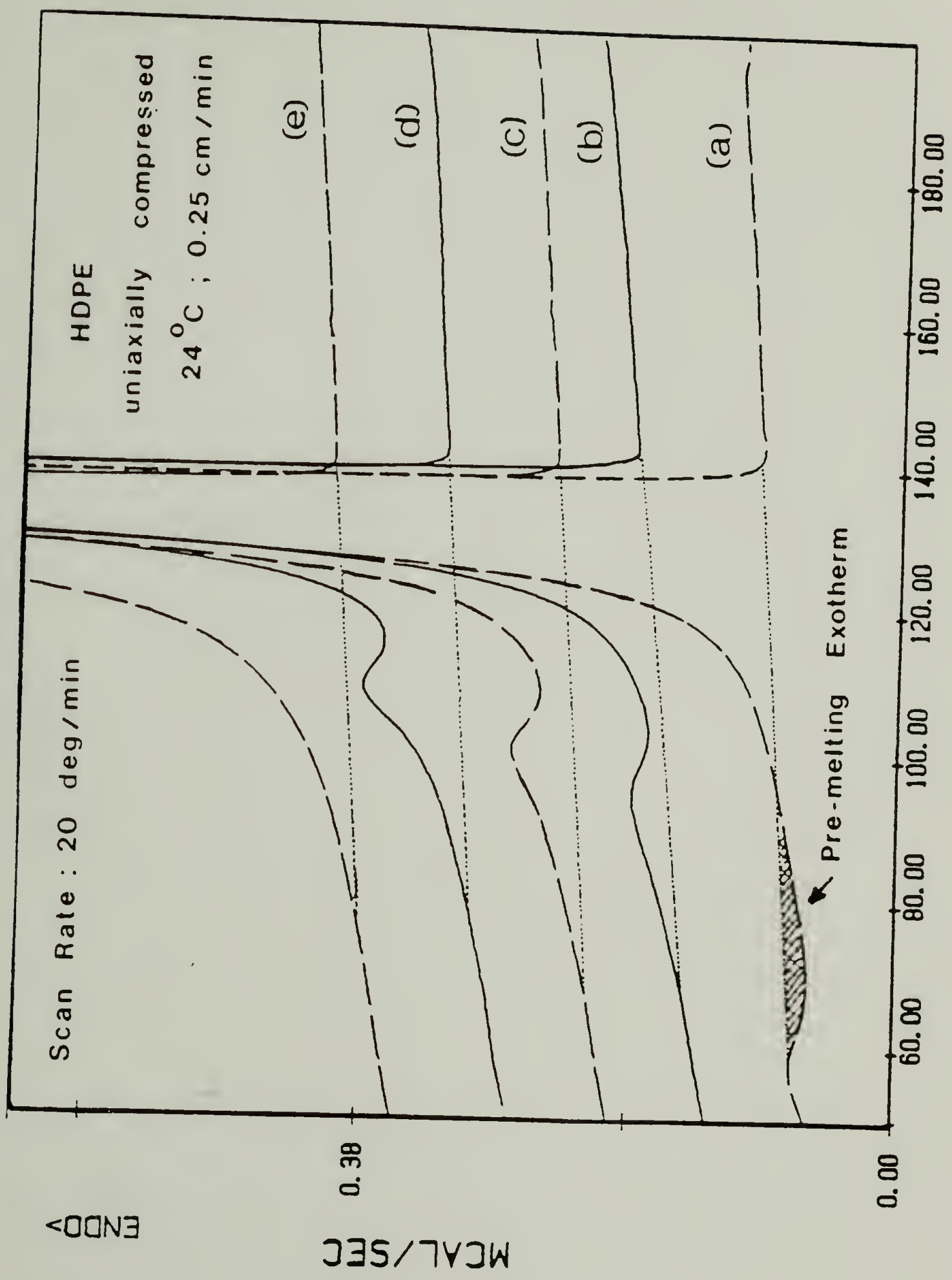
HDPE
uniaxially compressed
24 °C ; 0.25 cm/min
(e)
(d)
(c)
(b)
(a)
Scan Rate : 20 deg/min
Pre-melting Exotherm
ENDO
0.38
0.00
MCAL/SEC
120.00
140.00
160.00
180.00
60.00
80.00
100.00
TEMPERATURE (C)

Figure 6.12. Qualitative changes predicted for the enthalpy of phases in forged HDPE at $24^{o}C$ during heating up to the melt.

POSSIBLE TRANSITIONS IN HDPE COMPRESSED AT 24^{0}C ON HEATING

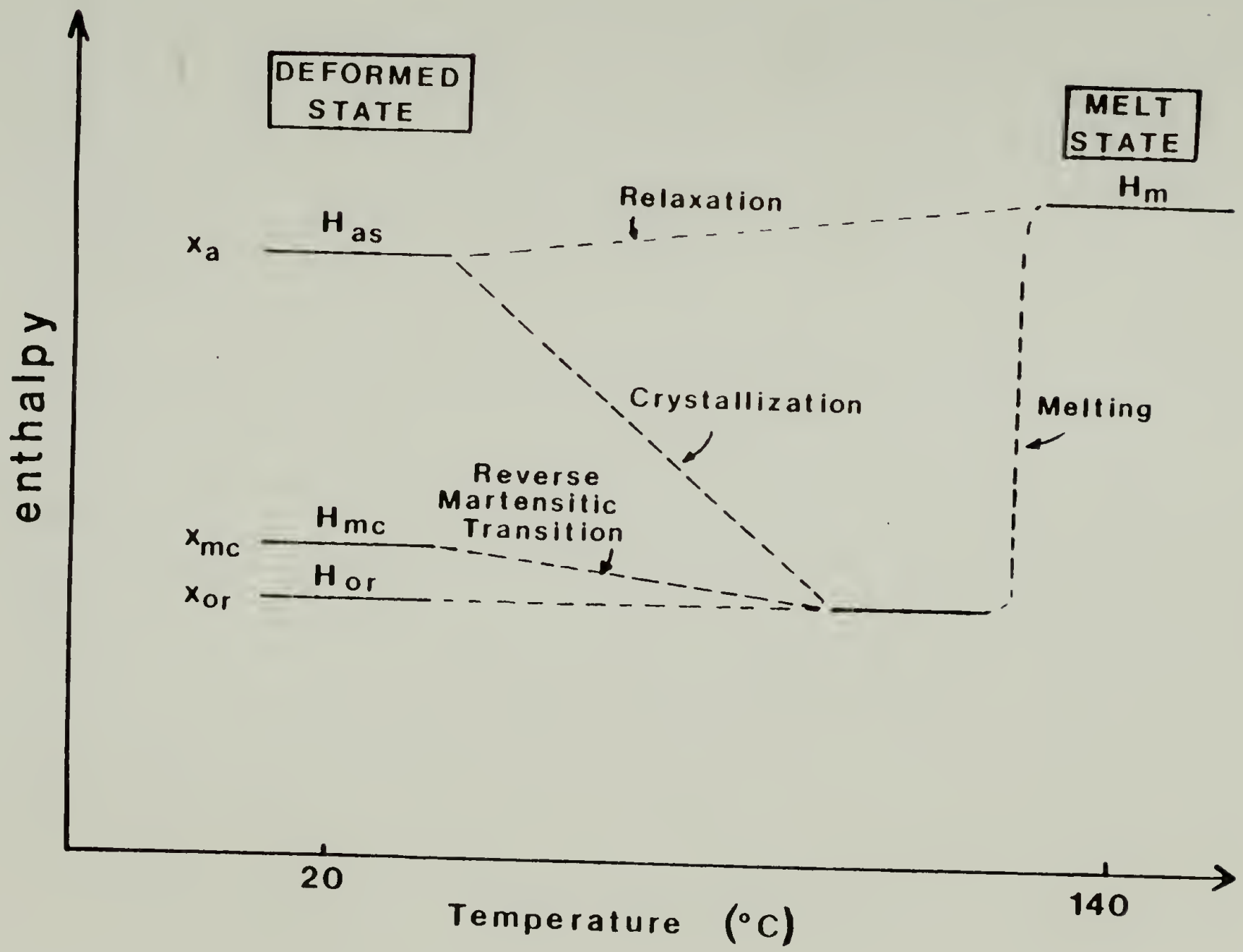

monoclinic back into the orthorhombic). These two might further on be distinguished by the temperature domain of their occurrence. In this regard, identical specimens of HDPE forged at room temperature were annealed at several intermediate temperatures between 24°C and 130°C and their density and heat of fusion measured. Results are shown in figure 6.13. The broken lines gives the initial values for density and heat of fusion prior to deformation. The data suggests two regimes in the increase of heat of fusion and density with increasing annealing temperature. The second one at about 70°C (which can be expected to represent the reversed martensitic transition) appears to be superimposed to the main one at 100°C which undoubtedly represents recrystallization. Thus, we can conclude that the decrease in density and heat of fusion for polyethylene forged at low temperatures are the result of both martensitic transition and decrystallization.

e) Tensile Modulus Measurements.

The in-plane tensile moduli were measured at room temperature using an Instron tensile machine for the series of forged HDPE. Dogbone shaped specimens were cut in the radial direction of the forged samples and their dimensions were accurately measured. Because each specimen represents the highest level of compression which can be achieved without breaking the specimens for each set of deformation investigated, the moduli are expected to reflect the optimal tensile properties for each of these forging conditions. Results are plotted in figure 6.14 as

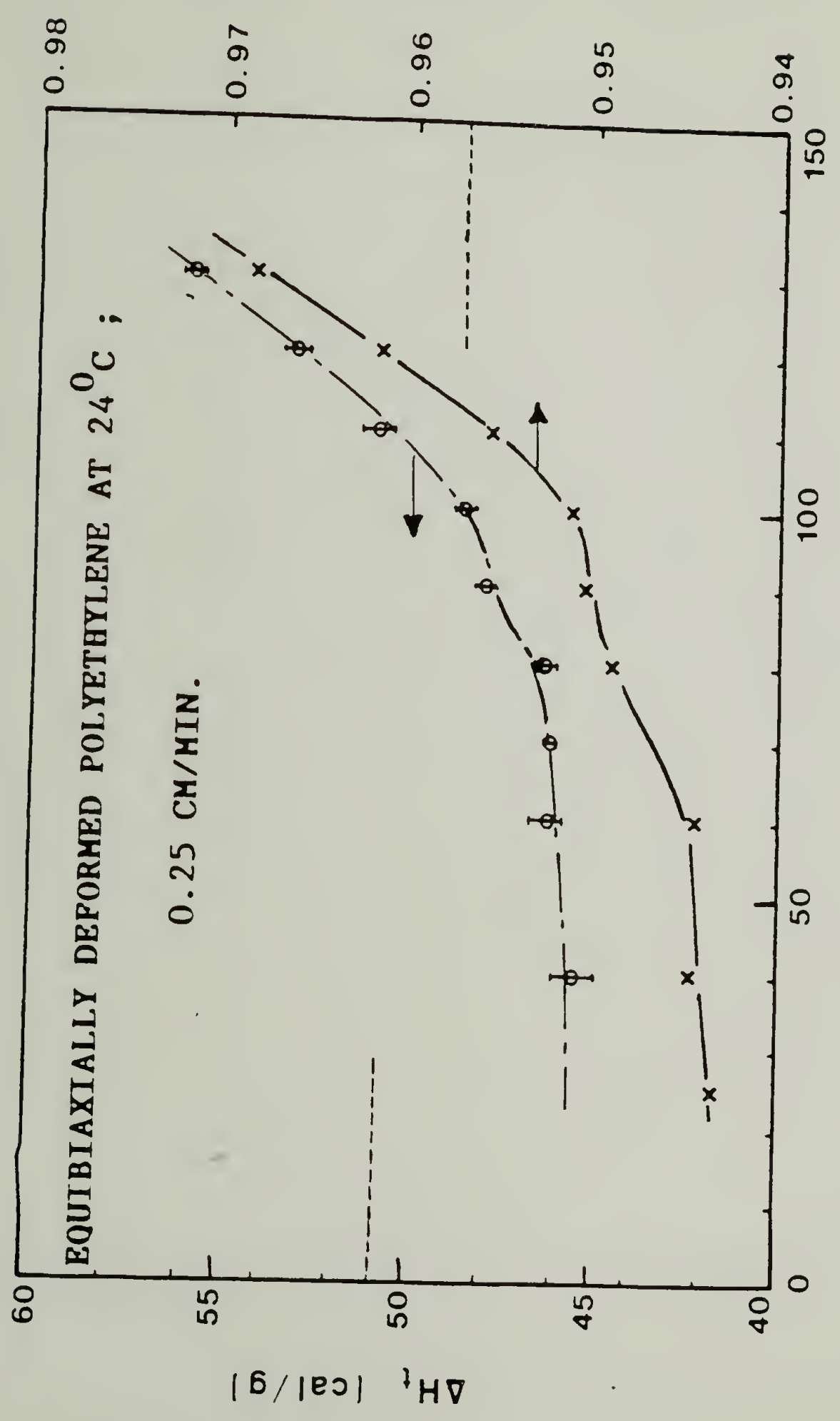

Figure 6.13. Total heat of transition (as measured from the difference with the baseline in a heating run) and density as a function of annealing temperature (30 min) for HDPE forged at 24°C and 0.25 cm/min. Broken lines indicate the initial values for HDPE prior to deformation.

a function of maximum compression ratio (MCR) for each specified forging temperature. The plot allows to compare the optimal moduli for varying forging temperatures. Globally, the data reveal a steady increase in tensile modulus with compression ratio for HDPE forged at low temperatures below 100^{o}C, but no further enhancement for the larger compression ratios obtained at higher temperatures. Interestingly, the change in tensile behavior correlates with the change in the deformation mechanism for the crystalline phase noticed above. According to the simple derivation given in the Introduction Chapter, a theoretical evaluation of the tensile modulus in equibiaxially deformed can be made by assimilating the system to a planar composite composed of randomly oriented fibers. A uppervalue for the tensile and transverse moduli of the composite fibers may be determined by assuming the fiber to be drawn in a plane to a draw ratio DR=$\sqrt{CR}$ (in the case of constant density). The change of modulus in HDPE in uniaxial deformation can then be found in the literature and be used for our purpose. Published values of the tensile modulus variations versus draw ratio are also indicated in figure 6.14 and set the upperlimit for the tensile moduli of forged specimens. The moduli obtained at low temperatures are comparatively to the expected value larger than the ones obtained for high temperatures forging. It confirms once more that low temperatures appears to set the optimal deformation conditions in equibiaxial deformation.

Figure 6.14. Experimental in-plane tensile modulus versus compression ratio for HDPE forged at several temperatures between 24°C and 120°C up to their Maximum Compression Ratio at a rate of 0.023 cm/min. Results are compared with published variations of tensile modulus of HDPE fibers with draw ratio.

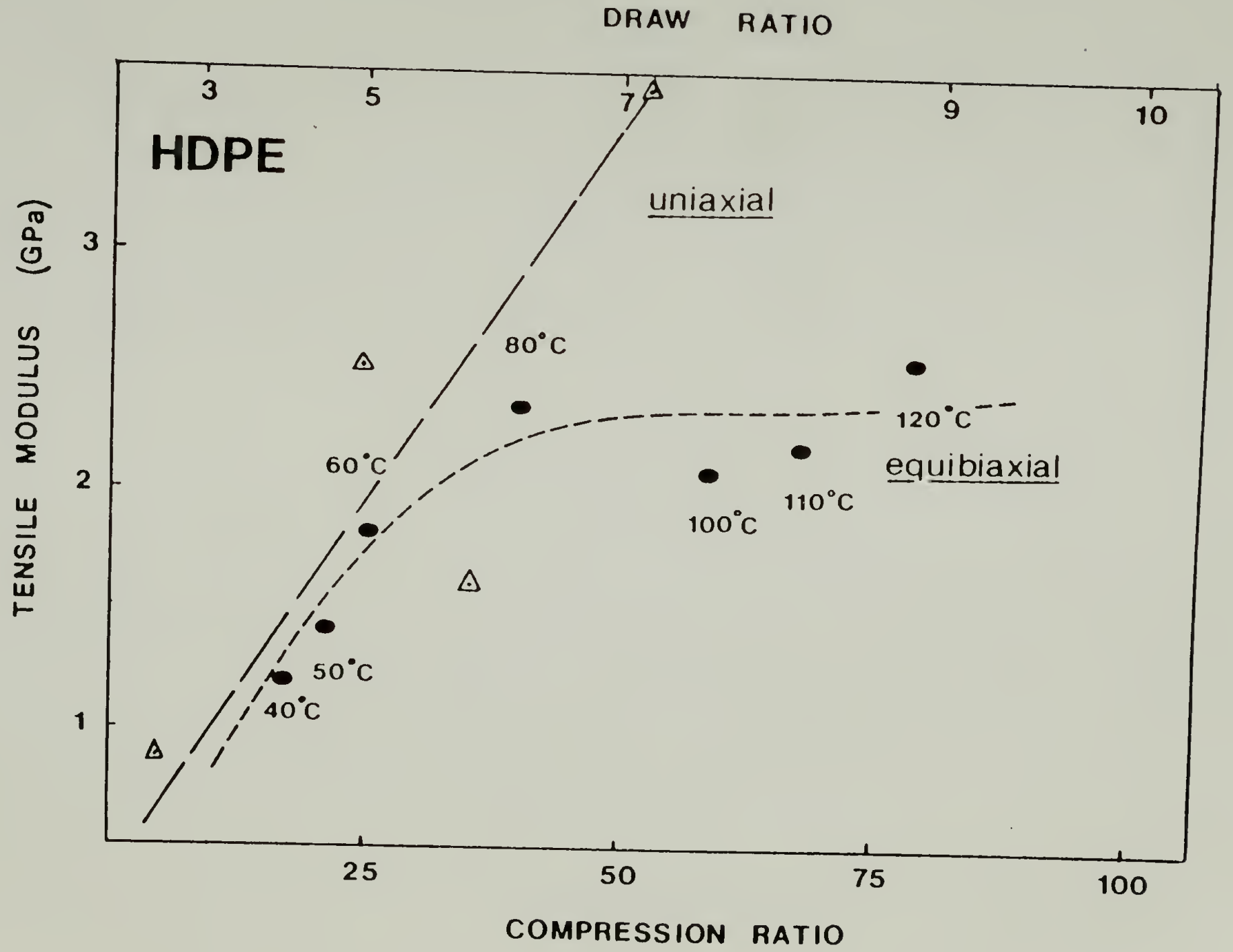
DRAW RATIO
3
5
7
9
10
HDPE
uniaxial
equibiaxial
80°C
60°C
120°C
100°C
110°C
50°C
40°C
TENSILE MODULUS (GPa)
3
2
1
25
50
75
100
COMPRESSION RATIO

4) Conclusions.

Equibiaxial deformation of high density polyethylene in the solid state can be readily achieved by forging. Our study provides evidence for two alternate deformation mechanisms which compete during the forging of HDPE to the largest achievable compression ratios. Each mechanism leads to different final crystalline textures (symmetry and orientation). The stability of the stress-induced monoclinic form during the deformation at a given temperature is what determines the relative contribution of each mechanism during the compression at this temperature. At relatively low temperatures, the monoclinic structure partially forms during the process and controls the deformation mode as indicated by the resultant Fiber texture. At temperatures above 100°C, on the other hand, the orthorhombic form remains stable during the entire process. As a result, the biaxial texture of the crystals becomes Planar. These textures reflect differences in the crystallography of deformation (by slip) between the two forms. Our X-ray analysis of the reversible martensitic transition permits the determination of the geometrical relationship between the two forms and our results agree with the one recently proposed by Takahashi[127]. On-line measurements of the compressive yield stress of PE samples deformed at various temperatures implement our conjecture by confirming the existence of two different regimes in the deformation process with approximately the same threshold temperature of 100°C. A higher ductility is found over the domain of stability of the monoclinic phase.

By thermal analysis and density measurements, the threshold for the monoclinic to orthorhombic transformation upon heating is characterized as 70^{o}C. Finally, in-plane modulus measurements shows a linear increase of the tensile modulus versus compression ratio over the low temperature regime. No further enhancement of the tensile modulus is achieved for deformations above 100^{o}C despite larger compression ratios. therefore, the study demonstrates that low temperatures provide the most ideal conditions for forging. This reveals a major discrepancy with uniaxial deformation processes in the preparation of highly oriented high modulus sheets. The result is explained in terms of difference in the deformation mechanisms in the crystalline phase between uniaxial and biaxial processes.

C H A P T E R VII

GENERAL CONCLUSIONS AND SUGGESTIONS FOR FUTURE WORK

1) Phase Behavior in Melt-crystallized Nylon 11.

The variety of structures present in nylon 11 crystallized from the melt has been reconsidered in the first part of this study. Thermal analysis was found to be able to differentiate between the different phases and could be use to provide essential information on the thermodynamics and kinetics of melting and crystallization of each particular species. During melt-crystallization, the smectic δ'-form is found to be kinetically favored, but transforms into the thermodynamically preferred α-form for longer crystallization times or during heat treatment. The smectic form exhibit a broad melting endotherm with its melting at 187°C (at 10°C/min), a higher value than for the crystal form, when the two species coexist. The α-form crystals exhibit double melting behavior, which is highly dependent upon thermal history. Thermal analysis alone, however, cannot resolve between the melting-recrystallization-remelting and the double morphology models to

explain the dual melting of the α-crystals. Finally, significant superheating effects are observed in the melting of α-form crystals.

Thermal analysis was also applied to reexamine the nature of the very peculiar α--δ transition in the crystal phase. Structural similarities between this transition and the Brill transition found in some even-even nylons (Nylon 66, Nylon 610) had been reported on the basis of WAXD studies. Enthalpic changes associated to the transition were determined and provided new information regarding its domain of occurrence. The extent of the transition on heating and cooling follows an hysteretic behavior, the transition being much faster on cooling than on heating. Solid state ^{15}N NMR spectroscopy and refractive index measurements confirm the broad temperature range for this transition. The crystal-condis crystal transition model developed by Wunderlich et al.[102] was found to describe the α--δ transition satisfactorily on the basis of the existence of different conformational isomers for the crystalline molecules at different temperatures. A difference in cooperativity (or tendency of aggregation) during conformational changes can serve explain the difference in behavior upon heating and cooling. At the molecular level, the transition is said to describe the progressive randomization of the hydrogen bonds between amide groups from the layerlike arrangement of the α-form to an hexagonally packed network. Finally, this mechanism might also explain in a similar way the origin of the Brill transition in even-even nylons.

Structural investigations of all the different forms were carried out on uniaxially stretched films. They were aimed at reviewing the

mode of molecular packing in the different crystal forms mentionned earlier. Hydrogen bonding between antiparallel molecular segments is found to be the thermodynamically most stable configuration for nylon 11. Molecules tend to pack in H-bonded layers in the α-form, which exhibits some disorder in the lateral arrangement of these layers. The smectic δ'-form exhibits "smectic-like" order. Disorder is found in the lateral packing of the chains which however are found to be in registry along the chain axis, likely because of hydrogen bonding interactions.

2) Behavior of Nylon 11 and HDPE during Equibiaxial Deformation by Forging.

Our study has focused on the characterization of the changes in structure and properties in Nylon 11 and HDPE during forging under various conditions of deformation. Highest compression ratios for each set of deformation conditions were achieved so that optimal structure, properties and deformation conditions could be assessed. For both polymers, deformation temperature was found to largely affect the deformation mechanism and the subsequent properties. Two alternate regimes were characterized in the forging process of both nylon 11 and HDPE and occur over different temperature domains. These were found to reflect changes in the crystalline phase during the process.

The nylon 11 smectic form was found to be favored for forging at low temperatures, whereas the α-form was stable during forging at high temperatures. Our results indicate that the α-form provides the most

ideal conditions for forging and yields the largest in-plane stiffness in forged nylon 11. Despite the relatively low crystallinity in Nylon 11, such argument based on mechanisms in the crystal phase seemed to be relevant. For HDPE, the orthorhombic to monoclinic transition has been shown to partially take place during forging below 100°C and to drastically modify the mechanism of crystal deformation. Texture analysis by WAXD clearly reveals the difference, and suggest an explanation of the overall deformation mechanism . In contrast to nylon 11, the stress-induced monoclinic form enhances the forging process of HDPE by promoting ductility, favoring crystal orientation in Fiber texture (as opposed to the orthorhombic, which form Planar texture), and enhancing tensile properties.

An absolute comparison of tensile moduli between forged nylon 11 and HDPE indicates how nylon 11 forged under optimal conditions (high temperatures) is a better material for tensile properties in biaxial. This is contrary to the tensile properties found in uniaxial.

The criteria proposed to select the optimal deformations conditions for any polymer on the basis of its deformation-induced crystal changes and the ability of the crystals to deform have been verified for the two polymers under investigation.

3) Future Work.

First, it would be of interest to carry out a complete kinetic study of the crystallization behavior of nylon 11 in parallel with a

morphological study. At high crystallization temperatures, an Avrami analysis of the kinetics of crystallization of the α-form should provide information on nucleation and growth process (from the Avrami exponent). Morphological differences for crystallization at high and low undercoolings may be monitored by inducing crystallization of thin films in a light scattering apparatus or a optical microscope. This may solve our uncertainty on the origin of the α-form double melting behavior. Also it may allow to discriminate between the crystallization of both smectic and crystal forms.

A major implication of the first chapters of this thesis is the essential role played by hydrogen bonding in the structure and properties of nylon 11, and likely of other nylons as well. Therefore, their existence, energy and energy distribution should strongly control the nature of both amorphous and ordered phases and all structural phenomena related to them. ^{15}N NMR appears to be a good technique to create a general database for nylons and provide a measure of the characteristics of the hydrogen bonded network.

Finally, new applications for the forging process can be considered. Some of them being presently carried out in our laboratory such as forging of LCPs or UHMWPE sintered powders. Other properties of forged specimens might be of interest such as optical or electrical ones.

APPENDIX A

GENERAL DERIVATION OF THE AZIMUTHAL ANGLES AND FOR ANY (hkl) REFLECTION IN FIBER AND PLANAR TEXTURES FROM UNIT CELL PARAMETERS.

Consider (hkl) reflection described by the reciprocal vector $\underset{\sim}{R}(hkl)$:

In the case of Fiber texture with $\underset{\sim}{F}^*$ aligned parallel to the compression axis (normal direction), ϕ_f for (hkl) is given by:

$$\cos\phi_f = \frac{\underset{\sim}{R}(hkl).\underset{\sim}{F}^*}{|\underset{\sim}{R}(hkl)|F^*} ;$$

In the case of Planar texture with $\underset{\sim}{c}$ oriented in the compression plane, ϕ_p for (hkl) is given by:

$$\cos\phi_p = \frac{\underset{\sim}{R}(hkl).\underset{\sim}{c}}{|\underset{\sim}{R}(hkl)|c} ;$$

These expressions are used to calculate the values reported in Tables 5.2, 6.2 and 6.3.

APPENDIX B

STRUCTURAL PREDICTIONS FOR NYLON 11 α-FORM.

From the diffraction patterns of the single textured film of nylon 11 shown in figure 4.3, the unit cell dimensions were derived as follows:

d_{001}, d_{010} and d_{200} were directly evaluated on the patterns and used to determine c^*, b^* and a^* respectively with the following relationships:

$$c^* = \frac{1}{d_{001}} \; ; \; b^* = \frac{1}{d_{010}} \; ; \; a^* = \frac{1}{2d_{200}} \; ;$$

The angles α^* and γ^* were directly approximated from the patterns shown in figures 4.3 and 4.2, since in both cases, the corresponding reciprocal vectors were located in the plane perpendicular to the incident X-ray beam.

β^* was subsequently determined using the relationship:

$$a^* c^* \cos\beta^* = \underset{\sim}{a}^* . \underset{\sim}{c}^* \; ;$$

Other (hkl) reflections were then calculated by:

$$d_{hkl}=(h^2a^{*2}+k^2b^{*2}+l^2c^{*2}+2hk\cos\gamma^{*}+2hl\cos\beta^{*}+2kl\cos\alpha^{*})^{-1/2};$$

For the reflections $(hkl)_c$ attributed to the subcell and seen along the chain axis, the spacings were calculated from the projections of d_{C-C} along the chain axis. The length of the C-C bond projected along the chain axis is:

$$d_{C-C}\cos 35.25=1.26\ \text{Å};$$

Since the hydrocarbon segments are slightly apart from the ideal extended conformation, with would give c=14.92 Å (instead of 14.45 Å), the calculated values need be corrected by the following compression factor:

$$c_f=14.45/14.92=0.97;$$

Subsequently, for the subcell:

$$d_{(00n)_c}=n\ d_{C-C}=n\ \ 1.26\ \ c_f\ ;$$

REFERENCES

1. A. Peterlin, a) J. Mater. Sci, 6, 490 (1971).
   b) Polym. Eng. Sci., 18, 488 (1978).

2. R.S. Porter, Amer. Chem. Soc., Polym. Prepr., 12(2) (1971).

3. A.G. Gibson, G.R. Darres and I.M. Ward, Polymer, 19, 683 (1971).

4. E.W. Fisher and H. Goddar, J. Polym. Sci., C16, 4405 (1969).

5. E.S. Clark and L.S. Scott, Polym. Eng. Sci., 14, 682 (1974).

6. D.C. Prevorsek, P.J. Harget, R.K. Sharma and A.C. Reimscheussel, J. Macromol. Sci. Phys., B-8, 127 (1973).

7. R.G.C. Arridge, P.J. Barham, and A. Keller, J. Polym. Sci.: Polym. Phys. Ed., 15, 389 (1977).

8. M. Takayanagi, K. Imada, T. Kajiyama, J. Polym. Sci., C15, 263 (1966)

9. A.J. Pennings and A.M. Kiel, Kolloid Z., 205, 160 (1965).

10. P. Smith and P.J. Lemstra, J. Mater. Sci., 15, 505 (1980).

11. T. Kanamoto, E.S. Sherman and R.S. Porter, Polymer J., 11, 497 (1979).

12. G.T. Paulikowski, D.J. Mitchell, J. Polym. Sci.: Polym. Phys. Ed., 26, 1865 (1988).

    T. Kanamoto, A. Tsuruta, K. Tanaka, M. Takeda and R.S. Porter, Polymer J., 15, 327 (1983).

13. A.E. Zachariades and R.S. Porter, "The Strength and Stiffness of Polymers, Dekker, NY (1983).

14. M.J. Shankernarayanan, D.C. Sun, M. Kojima and J.H. Magill, Intern. Polymer Processing, 1, 2 (1987).

15. G. Cappacio and I.M. Ward, Polymer, 15, 233 (1974).

16. J.H. Southern and R.S. Porter, J. Appl. Poly. Sci., 14, 2305 (1970).

17. A.J. Gibson, I.M. Ward, B.N. Cole and B. Parsons, J. Mater. Sci., 9, 1193 (1974).

18. A. Richardson, P.S. Hope and I.M. Ward, J. Polym. Sci.: Polym. Phys Ed., 21, 2525 (1983).

19. D.M. Bigg, E.G. Smith, M.M. Epstein and R.J. Fiorentino, Polym. Proc. Soc. Proceedings, 6/7, 35 (1986).

20. I. Matsubara and J.H. Magill, J. Polym. Sci.: Polym. Phys. Ed., 11, 1173 (1973).

21. A. Kaito, K. Nakayama and H. Kanetsuna, J. Appl. Polym. Sci., 30, 1241 (1985).

22. I.M. Ward, "Structure and Properties of Oriented Polymers", Applied Science Publishers Ldt, London, (1975).

23. R.J. Samuels, Structured Polymer Properties, J. Wiley & Sons, NY (1973).

24. C.J. Heffelfinger and R.L. Burton, J. Polym. Sci., 47, 289 (1960).

25. a) W.T. Stephensen (to Dow Co.), U.S. Patent 2, 453,080 (1940), British Patent, 656,735 (1951). b) J.W. McIntyer (to Dow Co.), U.S. Patent 2,688,773 (1954).

26. J. Jack, British Plastic, 34, 312 and 391 (1961).

27. Z. Tadmor and C.G. Gogos, Principles of Polymer Processing, SPE Monographs, John Wiley and Sons Inc., NY (1979).

28. a) M.O. Longstretch, et al, U.S> Patents 2,695,420 (1954), 2,697248 (1955) and 2,779,007 (1956). b) A.R. Austen and D.V. Humphries, (to Bethlehem steel Co.), U.S. Patent 4,282,277 (1981).

29. R.F. Saraf, Ph.D. Dissertation, University of Massachusetts, (1987).

30. R.F. Saraf and R.S. Porter, J. of Rheol., 31(1), 59 (1987).

31. J.Y. Guan, S.G. Liu, S.L. Wang, and M. Xu, Polym. Commun., 1, 57 (1984).

32. J.Y. Guan, R.F. Saraf, and R.S. Porter, J. Appl. Polym. Sci., 33, 1517 (1987).

33. R.F. Saraf and R.S. Porter, Pol. Eng. Sci., 28, 842 (1988).

34. L.S. Thomas, SPE J., 28, 39 June (1972).

35. K.J. Cleereman, SPE J., 28, 61 April (1972).

36. A.J. De Vries, C. Bonnebat, and J. Beautemps, J. Polym. Sci., 58C, 109 (1977).

37. J.L. White and J.E. Spruiell, Polym. Eng. Sci., 21(13), 859 (1981).

38. C.R. Desper, J. Appl. Polym. Sci., 13, 169 (1969).

39. W.F. Maddams and J.F. Preedy, J. Appl. Polym. Sci., 22, 2721 (1978).

40. Y. Sasaki and K. Miyasaka, IUPAC Macro-88, Kyoto, Japan (1988).

41. D. Hull, "Introduction to dislocations", Pergamon Press, Oxford (1965).

42. J.P. Hirth and J. Lothe, "Theory of dislocations", Second edition, Mc Graw-Hill Inc., New York (1982).

43. A. Kelly and G.W. Groves, "Crystallography of Crystals Defects", Longman, London (1970).

44. R. Hill, "The Mathematical Theory of Plasticity", Clarendon press, Oxford (1965).

45. J Petermann and H. Gleiter, J. Mater. Sci., 8, 673 (1973).

46. J.M. Peterson, J. Appl. Phys., 37, 4047 (1966).

47. P.B. Bowden, R.J. Young, J. Mater. Sci., 9, 2034 (1974).

48. R.F. Saraf and R.S. Porter, J. Polym. Sci.: Polym. Phys. Ed., 26, 1049 (1988).

49. J. Brady and E.L. Thomas, J. Mater. Sci., __, (1989).

50. J.H. Magill, J. Polym. Sci.: Part A-2, 7, 123 (1969).

51. M.G. Norhtolt, J. Polym. Sci.: Part C, 38, 205 (1972).

52. M.G. Northolt, B.J. Tabor, J.J. Van Aarsten, Prog. Colloid Polym. Sci., 57, 225 (1975).

53. C.W. Bunn, Trans. Faraday Soc., 35, 482 (1939).

54. T. Seto, T. Hara, and K. Tanaka, Japan. J. Appl. Phys., 7, 31 (1968).

55. W.R. Sorenson and T.W. Campbell, "Preparative Methods of polymer Chemistry", 2nd Ed.; Interscience; NY, 81 (1968).

56. M. Genas, Angew. Chem., 74, 535 (1962).

57. W.P. Slichter, J. Polym. Sci., 35, 77 (1958).

W.P. Slichter, J. Polym. Sci., 36, 259 (1959).

58. R. Aelion, Ann., 3, 5 (1948).

59. Y. Kinoshita, Makromol. Chem, 33, 1 (1959).

60. F.W. Lord, Polymer, 15, 42 (1974).

61. D. C. Vogelsong, J. Polym. Sci.: part A, 1, 1055 (1963).

62. A. Kawaguchi, T. Ikawa, Y. Fujiwara, J. Macrom. Sci. Phys., B20, 1 (1981).

63. B.A. Newman, T.P. Sham, K.D. Pae, J. Appl. Phys., 48, 4092 (1977).

64. G.F. Schmidt, H.Z. Stuart, Z. Naturgorsch, 13, 222 (1958).

65. K. Little, Brit. J. Appl. Phys., 10, 225 (1959).

66. A.G. Gordon, J. Polym. Sci.: part A-2, 9, 1693 (1971).

67. R. Greco, L. Nicolais, Polymer, 17, 1049 (1976).

68. S. Gogolewski, Colloid Polym. Sci., 257, 811 (1979)

69. P.K. Chen, B.A. Newman, J.I. Scheinbeim, J. Mater. Sci., 20, 1753 (1985)

70. D. Strovanek,P.P. Painteŕ,M.M. Coleman, Macromolecules, 18, 1676 (1985).

71. J.P. Bell, P.E. Slade, J.H. Dumbleton, J. Polym. Sci., 6, 1773 (1968).

72. K.H. Illers, H Haberkorn, Macromol. Chem., 142, 31 (1971).

73. G. Hinrichsen, Makromol. Chem., 166, 291 (1973).

74. P. Holdsworth, A. Turner-Jones, Polymer, 12, 195 (1971).

75. G. C. Alfonso, E. Pedemonte, L. Ponzetti, Polymer, 20, 104 (1979).

76. P.J. Lemstra, T .Kooistra, G.J. Challa, J. Polym. Sci.: Phys. Ed., 10, 823 (1972).

77. Y.C. Lee, R.S. Porter, Macromolecules, 20, 1336 (1987).

78. P.B. Rim, J.P. Runt, Macromolecules, 16, 1662 (1983).

79. D.C. Bassett, R.H. Olley, I.A.M. Al Raheil, Polymer, 29, 1745 (1988).

80. M. Inoue, J. Polym. Sci.: part A, 1, 2697 (1963).

81. Any Textbook on Polymer Crystallization. See for ex. B. Wunderlich

82. K. G. Kim, B.A. Newman, J.I. Scheinbeim, J. Polym. Sci.: Phys. Ed., 23, 2477 (1985).

83. V. Gelfandbein and D. Katz, Ferroelectrics, 33, 111 (1981).

84. D. Katz and V. Gelfandbein, J. Phys. D:Appl. Phys., 15, L115 (1982).

85. R. Brill, Makromol. Chem., 28/29, 294 (1956).

86. T. Itoh, Jap. J. Appl. Phys., 12, 2295 (1976).

87. H.G. Olf and A. Peterlin, J. Polym. Sci.: Part A-2, 9, 1449 (1971).

88. A.D. English, Polym. Preprints, 30(1), 312 (1989).

89. D.G. Powell, A.M. Sikes and L.J. Mathias, Macromolecules, 21, 1533 (1988).

90. J.H. Magill, J. Polym. Sci.: Part A-2, 4, 243 (1966).

W. Breshende, Kolloid Z., 15, 35 (1959).

91. J.I. Scheinbeim, J. Appl. Phys., 51, 5161 (1980).

92. J.I. Scheinbeim, J. Appl. Phys., 52, 5939 (1981).

J.I. Scheinbeim, J. Polym. Sci., 23, 2477 (1985).

93. J.I. Scheinbeim, S.C. Mathur, and B.A. Newman, J. Polym. Sci.: Polym. Polym. Ed., 24, 1791 (1986).

S.C. Mathur, B.A. Newman, and J.I. Scheinbeim, J. Polym. Sci.: Polym. Phys. Ed., 26, 447 (1988).

S.C. Mathur, J.I. Scheinbeim, and B.A. Newman, J. Appl. Phys., 56, 2419 (1984).

94. M.L. Colclough and R. Baker, J. Mater. Sci., 13, 2531 (1978).

95. H.W. Starkweather, Jr and G.A. Jones, J. Polym. Sci.: Polym. Phys. Ed, 19, 467 (1981).

96. J.S. Samuels, J. Appl. polym. Sci., 26, 1383 (1981).

97. D.M. Gezovich and P.H. Geil, J. mater. Sci., 6, 531 (1971).

98. M. Dosiere, J.J. Point, J. Polym. Sci.: Phys. Ed., 21, 625 (1983).

M. Dosiere, J. Mater. Sci., 18, 1941 (1983).

M. Dosiere and J.J. Point, J. Polym. Sci.: Polym. Phys. Ed., 22, 1383 (1984).

99. D. Strovanek, P. C. Painter and M.M. Coleman, Macromolecules, 19, 699 (1986).

100. L.J. Mathias, D.G. Powell and A.M. Sikes, Polym. Commun., 29, 192 (1988).

101. L.J. Mathias, D.G. Powell, J.P. Autran and R.S. Porter, Macromolecules, 23(4), 963 (1990).

102. B. Wunderlich, M. Möller, J. Grebowicz and H. Baur, Advances in Polym. Sci., 87, (1987).

104. I.L. Hay, and A. Keller, J. Polym. Sci., C30, 289 (1970).

105. G.A. Gordon, J. Polym. Sci.: Part A-2, 9, 1693 (1971).

106. K. Ishikawa, K. Miyasaka, M. Maeda and M. Yamada, J. Polym. Sci.: Part A-2, 7, 1259 (1969).

107. K. Ishikawa, K. Miyasaka and T. Okabe, Makromol. Chem., 122, 123 (1969).

A. Keller, J. Polym. Sci., 15, 31 (1955).
17, 351 (1955).

108. H. Arimoto, M. Ishibashi, M. Hirai and Y. Chatani, J. Polym. Sci.: Part A, 3, 317 (1965).

D.R. Holmes, C.W. Bunn and D.J. Smith, J. Polym. Sci., 17, 159 (1955).

109. D.G. Vogelsong, J. Polym. Sci.: Part A, 1, 1055 (1963).

110. M.G. Northolt, B.J. Tabor and J.J. Van Aarsten, J. Polym. Sci.: Part A-2, 10, 191 (1972).

111. A. Martorana, V. Malta, G. Cojazzi, A. Fichera, A. Marigo and R. Zannetti, Eur. Polym. J., 23(11), 839 (1987).

112. G. Cojazzi, A. Fichera, V. malta and R. Zannetti, Eur. Polym. J., 21(3), 309 (1985).

113. N. Hiramatsu, S. hashida and S. Hirakawa, Jap. J. Appl. Phys., 21(4), 651 (1982).

114. M.G. Northolt, B.J. Tabor and J.J. Van Aarsten, Prog. Colloid and Polym. Sci, 57, 225 (1975).

115. M. Dosiere and J.J. Point, J. Polym. Sci.: Polym. Phys Ed., 22, 749 (1984).

116. I.M. Ward, "Review: The Yield Behavior of Polymers," J. Mater. Sci, 6, 1397 (1971).

117. H. Tresca, Compt. Rend. Acad. Sci. Paris, 59, 754 (1864), 64, 809 (1867).

118. R. Von Mises, Gottinger Nachrichten, Math-Phys. Klasse, 582 (1913).

119. S. Rabinowitz, I.M. Ward and J.S.C. Parry, J. Mater. Sci., 5, 29 (1970).

120. F.C. Frank, A. Keller, and A. O'Connor, A., Phil. Mag., 8, 64 (1958).

121. H. Kiho, A. Peterlin, and P.H. Geil, J. Polym. Sci., B3, 157 (1965).

H. Kiho, A. Peterlin, and P.H. Geil, J. Polym. Sci., B3, 263 (1965).

122. I.L. Hay and A. Keller, J. mater. Sci., 2, 538 (1967).

123. H. Gleiter and A. Argon, Phil. Mag., 24, 71 (1971).

124. R.J. Young, Ph.D. Dissertation, "Deformation Mechanisms in Semicrystalline Polymers," University of Cambridge, (1972).

125. J. Petermann and J. Gleiter, J. Mater. Sci., 8, 673 (1973).

126. T. Kanamoto, M. Nakanishi, K. Tanaka, M. Takeda and R.S. Porter, Rept. prog. Polym. Phys., Japan, 29, 185 (1985).

127. Y. Takahashi, T. Ishida, and M. Furusaka, J. Polym. Sci.: Polym. Phys. Ed., 26, 2267 (1988).

128. T. Seto, T. Hara and K. Tanaka, Jap. J. Appl. Phys., 7, 31 (1968).

129. L.E. Alexander, "X-Ray Diffraction Methods in Polymer Science", John Wiley and Sons Inc., New York (1969).

129. M. Takayanagi and T. Kajiyama, J, Macromol. Sci.-Phys., B8, 1 (1973).

130. R.C. Wilhoit and M. Dole, J, Phys. Chem., 57, 14 (1953).

131. A. Peterlin and G. Meinel, J. Appl. Phys., 36, 3028 (1965).

G. Meinel and A. Peterlin, J. Polym. Sci., B5, 613 (1967).

BIBLIOGRAPHY

Aelion, R., Ann., 3, 5 (1948).

Alexander, L.E., "X-ray Diffraction methods in Polymer Science", John Wiley and Sons Inc., New York (1969).

Alfonso, G.C., Pedemonte, E., and Ponzetti, L., Polymer, 20, 104 (1979).

Arimoto, H., Ishibashi, M., Hirai, M., and Chatani, Y., J. Polym. Sci.,Part A, 3, 317 (1965).

Arridge, R.G.C., Barham, P.J., and Keller, A., J. Polym. Sci.: Polym. Phys. Ed., 15, 389 (1973).

Bassett, D.C., Olley, R.H., and Al Raheil, I.A.M., Polymer, 29, 1745 (1988).

Bell, J.P., Slade, P.E., and Dumbleton, J.H., J. Polym. Sci.; Part A, 6, 1773 (1968).

Bigg, D.M., Smith, E.G., Epstein, M.M., and Fiorentino, R.J., Polym. Proc. Soc. Proceedings, 6/7, 35 (1986).

Bowden, P.B. and Young, R.J., J. Mater. ci., 9, 2034 (1974).

Breschende, W., Kolloid. Z., 15, 35 (1959).

Brill, R., J. Prakt. Chem., 161, 49 (1942).

Brill, R., Makromol. Chem., 28/29, 294 (1956).

Bunn, C.W., J. Polym. Sci., 16, 323 (1955).

Cappacio, G., and Ward, I.M., Polymer, 15, 233 (1974).

Chen, P.K., Newman, B.A., and Scheinbeim, J.I., J. Mater. Sci., 20, 1753 (1985).

Clark, E.S. and Scott, L.S., Polym. Eng. Sci., 14, 682 (1974).

Cleereman, K.J., SPE J., 28, 61, April (1972).

Cojazzi, G., Fichera, A., Malta., V., and Zannetti, R., Eur. Polym. J., 21(3), 309 (1985).

Colclough, M.L. and Baker, R., J. Mater. Sci., 13, 2531 (1978).

Desper, C.R., J. Appl. Polym. Sci., 13, 169 (1969).

De Vries, A.J., Bonnebat, C., and Beautemps, J., J. Polym. Sci., 58C, 109 (1977).

Dosiere, M., J. Mater. Sci., 18, 1941 (1983).

Dosiere, M. and Point, J.J., J. Polym. Sci.; Polym. Phys. Ed., 21, 625 (1983).

Dosiere, M. and Point, J.J., J. Polym. Sci.: Polym. Phys Ed., 22, 1383 (1984).

English, A.D., Polym. Preprints, 30(1), 312 (1989).

Fisher, E.W. and Goddar, H., J. Polym. Sci., C16, 4405 (1969).

Frank, F.C., Keller A., and O'Connor, A., phil. Mag., 8, 64 (1958).

Gelfandbein, V. and Katz, D., Ferroelectrics, 33, 111 (1981).

Genas, M., Angew. Chem., 74, 535 (1962).

Gezovich, D.M. and Geil, P.H., J. Mater. Sci., 6, 531 (1971).

Gibson, A.G., Darres, G.R., and Ward, I.M., Polymer, 19, 683 (1978).Gleiter, H. and Argon, A., Phil. Mag., 24, 71 (1971).

Gogolewski, S., Colloid Polym. Sci., 257, 811 (1979).

Gordon, G.A., J. Polym. Sci.: Part A-2, 9, 1693 (1971).

Grego, R. and Nicolais, L., Polymer, 17, 1049 (1976).

Guan, J.Y., Liu, S.G., Wang, S.L., and Xu, M., Polym. Commun., 1, 57 (1984).

Guan, J.Y., Saraf, R.F., and Porter, R.S., J. Appl. Polym. Sci., 33, 1517 (1987).

Hay, I.L. and Keller, A., J. mater. Sci, 2, 538 (1967).

Hay, I.L. and Keller, A., J. Polym. Sci., C30, 289 (1970).

Heffelfinger, C.J. and Burton, R.L., J. Polym Sci., 47, 289 (1960).

Hill, R., "The Mathematical teoryy of Plasticity", Clarendon Press, Oxford (1950).

Hinrichsen, G., Makromol. Chem., 166, 291 (1973).

Hirth, J.P. and Lothe, J., "Theory of dislocations", Second Edition, Mc Graw-Hill Inc., New York (1982).

Holdsworth, P. and Turner-Jones, A., Polymer, 12, 195 (1971).

Holmes, D.R., Bunn, C.W., and Smith, D.J., J. Polym. Sci., 17, 159 (1955).

Hull, D., "Introduction to Dislocations", Pergamon Press, Oxford (1965).

Illers, K.H. and Haberkorn, H., Makromol. Chem., 142, 31 (1971).

Inoue, M., J. Polym. Sci.: Part A, 1, 2697 (1963).

Ishikawa, K., Miyasaka, K., Maeda, M., and Yamada, M., J. Polym. Sci.: Part A-2, 7, 1259 (1969).

Itoh, T., J. Appl. Phys., 12, 2295 (1976).

Jack, J., British plastic, 34, 312 and 391 (1961).

Kaito, A., Nakayama, K., Kanetsuna, H., J. Appl. Polym. Sci, 30, 1241 (1985).

Kanamoto, T., Sherman, E.S., and Porter, R.S., Polymer J., 11, 497 (1979).

Kanamoto, T., Nakanishi, M., Tanaka, K., Takeda, M., and Porter, R.S., Rept. Prog. Polym. Phys., Japan, 29, 185 (1985).

Kanamoto, T., Tsuruta, A., Tanaka, K., Takeda, M., and Porter, R.S., Polymer J., 15, 327 (1983).

Katz, D. and Gelfandbein, V., J. Phys. D: Appl. Phys., 15, L115 (1982).

Kawaguchi, A., Ikawa, T., and Fujiwara, Y., J. Macromol. Sci.-Phys., B20, 1 (1981).

Keller, A., a) J. polym. Sci., 15, 31 (1955). b) J. Polym. Sci., 21, 363 (1956).

Kelly, A. and Groves, G.W., "Crystallography of Crystals Defects", Longman, London (1970).

Kiho, H., Peterlin, A., and Geil, P.H., J. Polym. Sci., B3, 157 (1965).

Kiho, H., Peterlin, A., and Geil, P.H., J. Polym. Sci., B3, 263 (1965).

Kim, K.G., Newman, B.A., and Scheinbeim, J.I., J. Polym. Sci,: Polym. Phys. Ed., 23, 2477 (1985).

Kinoshita, Y., Makromol. Chem., 33, 1 (1959).

Lee, Y.C. and Porter, R.S., Macromolecules, 20, 1336 (1987).

Lemstra, P.J., Kooistra, T., and Challa, G.J., J. Polym. Sci.; Polym. Phys. Ed., 10, 823 (1972).

Little, K., Brit. J. Appl. Phys., 10, 225 (1959).

Lord, F.W., Polymer, 15, 42 (1974).

Maddams, W.F. and Preedy, J.F., J. Appl. Polym. Sci., 22, 2721 (1978).

Magill, J.H., J. Polym. Sci.: Part A-2, 7, 123 (1969).

Mathias, L.J., Powell, D.G., Autran, J.-P., and Porter, R.S., Macromolecules, 23(4), 963 (1990).

Mathias, L.J., Powell, D.G., and Sikes, A.M., Polym. Commun., 29, 192 (1988).

Mathur, S.C., Newman, B.A., and Scheinbeim, J.I., J. Polym. Sci.: Polym. Phys. Ed., 26, 447 (1988).

Mathur, S.C., Scheinbeim, J.I., and Newman, B.A., J. Appl. Phys., 56, 2419 (1984).

Matsubara, I., and Magill, J.H., J. Polym Sci.: Polym. Phys Ed., 11, 1173 (1973).

Meinel, G. and Peterlin, A., J. Polym. Sci., B5, 613 (1967).

Newman, B.A., Chen, P., Pae, K.D., and Scheinbeim, J.I., J. Appl. Phys., 51, (1980).

Newman, B.A., Sham, T.P., and Pae, K.D., J. Appl. Phys., 48, 4092 (1977).

Norhtolt, M.G., J. Polym. Sci.: Part C, 38, 205 (1972).

Northolt, M.G., Tabor, B.J., and Van Aarsten, J.J., Prog. Colloid Polym. Sci., 57, 225 (1975).

Olf, H.G. and Peterlin, A., J. Polym. Sci.:Part A-2, 9, 1449 (1971).

Parker, J.P. and Lindenmeyer, P.H., J. Appl. polym. Sci., 21, 821 (1977).

Paulikowski, G.T., Mitchell, D.J., J. Polym. Sci.: Polym. Phys. Ed., 26, 1865 (1988).

Pennings, A.J., Kiel A.M., Kolloid Z., 205, 160 (1965).

Peterlin, A., Polym. Eng. Sci., 18, 488 (1978).

Peterlin, A., J. Mater. Sci., 6, 490 (1971).

Peterlin, A. and Meinel, G., J. Appl. Phys., 36, 3028 (1965).

Petermann, J. and Gleiter, J., J. Mater. Sci., 8, 673 (1973).

Peterson, J.M., J. Appl. Phys., 37, 4047 (1966).

Pimentel, G.C. and Mc Clellan, A.L., "The Hydrogen Bond", W.H. Freeman and Co., San Francisco and London (1960).

Porter, R.S., J. Polym. Sci., 16, 1134 (1981).

Porter, R.S., Amer. Chem. Soc., Polym. Prepr., 12(2), (1971).

Prevorsek, D.C., Harget, P.J., Sharma, R.K., and Reimscheussel, J., J. Macromol. Sci. Phys., B-8, 127 (1973).

Richardson, A., Hope, P.S., and Ward, I.M., J. Polym. Sci.: Polym. Phys. Ed., 21, 2525 (1983).

Rim, P.B. and Runt, J.P., Macromolecules, 16, 1662 (1983).

Samuels, J.S., J. Appl. Polym. Sci., 26, 1383 (1981).

Saraf, R.F., Ph.D. Dissertation, University of Massachusetts, (1987).

Saraf, R.F., and Porter, R.S., J. of Rheol., 31(1), 59 (1987).

Saraf, R.F., and Porter, R.S., Pol. Eng. Sci., 28, 842 (1988).

Sasaki, Y. and Miyasaka, K., IUPAC Macro-88, Kyoto, Japan, August (1988).

Scheinbeim, J.I., J. Appl. Phys., 51, 5161 (1980).

Scheinbeim, J.I., J. Appl. Phys., 52, 5939 (1981).

Scheinbeim, J.I., J. Polym. Sci.; Polym. Phys. Ed., 23, 2477 (1985).

Scheinbeim, J.I., Mathur, S.C., and Newman, B.A., J. Polym. Sci.: Polym. Polym. Ed., 24, 1791 (1986).

Schmidt, G.F. and Stuart, H.Z., Z. Naturgorsch, 13, 222 (1958).

Seto, T., Hara, T., and Tanaka, K., Japan. J. Appl. Phys., 7, 31 (1968).

Shankernarayanan, M.J., Sun, D.C., Kojima, M., and Magill, J.H., Intern. Polymer Processing, 1, 2 (1987).

Slichter, W.P., J. Polym. Sci., 35, 77 (1958).

Slichter, W.P., J. Polym. Sci., 36, 259 (1959).

Smith, P. and Lemstra, P.J., J. Mater. Sci., 15, 505 (1980).

Southern, J.H., and Porter, R.S., J. Appl. Poly. Sci., 14, 2305 (1970).

Starkweather, Jr, H.W. and Jones, G.A., J. Polym. Sci,: Polym. Phys Ed., 19, 467 (1981).

Strovanek, D., Painter, P.C., and Coleman, M.M., Macromolecules, 18, 1676 (1985).

Strovanek, D., Painter, P.C., and Coleman, M.M., Macromolecules, 19, 699 (1986).

Takahashi, Y., Ishida, T., and Furusaka, M., J. Polym. Sci.: Polym. Phys. Ed., 26, 2267 (1988).

Takayanagi, M. and Kajiyama, T., J. Macromol. Sci.-Phys., B8, 1 (1973).

Takayanagi, M., Imada, K., and Kajiyama, T., J. Polym. Sci., C15, 263 (1966).

Thomas, L.S., SPE J., 28, 39 June (1972).

Tresca, H., Compt. Rend. Acad. Sci. Paris, 59, 754 (1864), 64, 809 (1867).

Vogelsong, D.C., J. Polym. Sci.: Part A, 1, 1055 (1963).

Von Mises, R., Gottinger Nachrichten, Math-Phys. Klasse, 582 (1913).

Ward, I.M., Structure and Properties of Oriented Polymers, Applied Science Publishers Ldt, London (1975).

Ward, I.M., "Review: The Yield Behavior of Polymers," J. Mater. Sci, 6, 1397 (1971).

White, J.L. and Spruiell, J.E., Polym. Eng. Sci., 21(13), 859 (1981).

Wilchinsky, Z.W., Advances in X-ray Analysis, Vol 6, Plenum press, New York (1963)

Wilhoit, R.C. and Dole, M., J. Phys. Chem., 57, 14 (1953).

Young, R.J., Ph.D. Dissertation, "Deformation Mechanisms in Semicrystalline Polymers," University of Cambridge, 1972.

Young, R.J. and Bowden, P.B., Phil. Mag.. 29, 1061 (1974).

Zaukelies, D.A., J. Appl. Phys., 33, 2797 (1962).